METHODS FOR LOCALIZATION OF ELECTRICAL SOURCES IN THE HUMAN BRAIN AND APPLICATIONS TO THE VISUAL SYSTEM

Thesis by

Terrance Michael Darcey

In Partial Fulfillment of the Requirements

for the Degree of

Doctor of Philosophy

California Institute of Technology

Pasadena, California

1979

(Submitted January 26, 1979)

ACKNOWLEDGEMENTS

Many people provided me with both direct and indirect support in the course of my stay at Caltech and have helped to make this work possible. My advisor, Dr. Derek H. Fender, suggested many of the ideas pursued in this thesis, provided excellent research facilities and participated in numerous helpful discussions, for which I am very grateful. His encouragement, infinite patience and understanding made him more than just an advisor to me. I also wish to thank Dr. Stan Klein, whose insight and enthusiasm was an inspiration to me and with whom I had many enlightening discussions. I am indebted to Dr. J. P. Ary in many ways, for his electronic wizardry and for the numerous times that he unselfishly put aside his own work to assist me with mine. I also wish to acknowledge Dr. Norbert Bischof, who provided me with my first real exposure to the joy and frustration of experimental research.

A number of other people should be acknowledged for their contributions: Rinus Dekker (massive amounts of technical assistance), Evelyn Johnson (much help in coping with academic and financial matters), Dale Knutsen (programming assistance), Shirley Lucas (technical assistance) and Mark Webster (technical assistance). I would also like to express my appreciation to Dr. Mike Hyson, Raymond Hou, Rick Williams, Tom Santoro and Ross Larkin for helpful discussions and encouragement.

I am grateful to Caltech and the citizens of the United States (through the National Institutes of Health) for providing financial aid and research facilities throughout my graduate years.

Finally, I wish to thank my entire family, without whose love, encouragement and assistance this work would not have been done. In particular, I must give special thanks to my wife, Candis, and my

daughter, Lauren, who provided me with a happy home life, and very often subordinated their needs to the production of this thesis. For my wife and myself, this has been a team effort in many respects, even to the extent that it was my wife who typed this manuscript.

ABSTRACT

Multichannel human visual evoked scalp potential (VESP) recording was combined with results from electric field theory and the methods of non-linear parameter estimation to see if it was possible to infer the general spatio-temporal course of brain excitation in the processing of a visual stimulus. To do this, various models of the head and underlying sources were tested. Head models included a simple homogeneous and 2 different piecewise homogeneous volume-conducting spheres, the latter of which were designed to account for the known electrical inhomogeneity and anisotropy provided by the skull and scalp. Source models studied were single and multiple electrostatic dipoles and two simple types of extended sources, radial cap and annular sector dipole layers. Equivalent sources for the experimental data were found by taking least-squares estimates of model parameters, minimizing the sum of the squared deviations between the actual scalp potentials and the scalp potentials computed by the model. Since these models were parameterized for both location and source characteristics (e.g. orientation and magnitude), one could attempt to relate them to the topography and functional anatomy of the brain. A working assumption in relating these was that active cortex could be modeled to a first approximation as a neuronal layer wherein the neurons are treated as discrete current sources oriented normal or at right-angles to the cortical surface. Thus, it was assumed that VESP's reflect the topography of the tissues that produce them.

40-channel VESP measurements were made to briefly appearing checkerboard patterns placed in various areas of the visual field. These data were analyzed in terms of underlying equivalent sources in

the brain. Although there were some variations present in the 3 subjects studied, these may be consistent with known variations in cortical topography. The measured potential distributions showed a radical dependence of VESP topography on stimulus locus and indicated that these VESP's are probably volume-conducted field effects arising from a small number of fairly localized sources in the brain. Equivalent dipoles in general give excellent fits to the measured data and the mapping between the visual field and these equivalent sources is similar to the commonly accepted mapping between the visual field and visual cortex. As such, it appears that evoked potentials may be used as a crude tool for defining the anatomical projection of localized sensory fields onto the cortical surface in humans.

TABLE OF CONTENTS

1. INTRODUCTION

1.1 The Big Picture

Consider the following problem: a given system is to be analyzed. It is an intimately familiar system in some ways, but for the most part nothing is known about it. It contains some 10^{10} discrete but highly interconnected elements which together have extraordinary capabilities. Some of the characteristics of these elements are known but this information is based on the analysis of similar systems. The system has many inputs and outputs. There are certain parts of this system which, if removed or damaged cause the system to lose its capabilities. At the same time there are other parts of the system which reveal an amazing plasticity. In general, however, it is an extremely delicate system which cannot be dismantled without destroying or changing it. It is enclosed in a hard shell which shields its inner workings and which cannot be opened under ordinary circumstances. Many have said that the study of this system is central to Man's understanding of himself. The best efforts for a lifetime will not solve the problem. Indeed, it is unlikely that this system will ever be completely understood.

The problem is to understand the workings of the human brain. The preceding is not intended to impress a sense of smallness or impotence in considering the problem of studying the human brain, but instead to convey that the author is aware of the limitations of such research and thus has tried to keep his attempts as simple and clear as possible.

1.2 The Little Picture

Now let me tell how I have tried to reduce the problem of studying the brain to something manageable. First, I have chosen to study the visual system, because it is relatively easy to stimulate and because more is already known about it than any other sensory system. Since I wish to learn something about the intact, functioning human brain and in particular something about its inner workings or physiology, I have chosen to utilize the only available electrophysiological measure which reflects what is going on in an intact brain[1], the electroencephalogram (EEG) or scalp potential measurement.[2] There are alternative ways of getting information about the human brain, but these other methods are often too indirect and complicated to tell one anything more than rules concerning what the brain or sensory system does.[3] At their worst they are forms of the so-called "black box" approach and are mostly inappropriate to the task of opening the "black box" and learning how the brain

---

[1] It is possible to question whether the EEG represents anything physiologically significant, or is a mere epiphenomenon of no scientific value. While under some circumstances the latter may be the case, this thesis defends the physiological significance of the EEG under a special set of circumstances.

[2] An exception is the magnetoencephalogram (MEG) which senses the magnetic field at the surface of the head. This technology is, however, still in its formative stages and relies on fairly sophisticated equipment {1}.

[3] One very fruitful approach has been in the use of a certain class of psychophysical experiment where an essential part of the result is a subject's report of his own sensations. This type of experiment can be used to test physiological hypotheses if they are made in terms of indistinguishability of two stimuli {2}. Examples of this are matching experiments and threshold determinations. Psychophysical results in general may provide important clues to the physiologist and anatomist as to what types of mechanisms to look for. In some cases they may be used in conjunction with anatomical or physiological information to infer possible sites of information processing (e.g. the work of Julesz {3} using cyclopean stimuli).

does what it does. A seemingly modest approach at the outset then would be to attempt to learn the when and where, that is, what is the general spatio-temporal course of brain excitation in the processing of a visual stimulus? I will try to show in this thesis that the EEG is an indicator of this information if analyzed properly.

1.3 The Evoked Potential (EP)

One problem with an approach using scalp potentials is that they reflect many things going on in the head electrically. This means that if the brain is busy there will be a considerable mixture of information. This is compounded by the possibility of excitation of non-neural cranial tissues such as muscle. This difficulty is, however, somewhat alleviated by the restriction of study to what is called the evoked potential (EP), which extracts that part of the EEG signal which is related to or time-locked to a stimulus or other time reference event. One way in which this can be accomplished is by the technique of signal-averaging with respect to the time-marks defined by the repeated occurrence of the stimulus. This technique is a special case of the more general method of crosscorrelation between system input and output. In the case of signal averaging to get the impulse response, the input is a series of impulse functions defined by the stimulus events. For certain stimuli the method of signal averaging gives highly stable and clearcut response waveforms which are stimulus specific, i.e. variations in the response characteristics result from specific variations in the stimulus.

1.4 Purpose of this Study

The purpose of this dissertation is to measure the specific variations of average scalp potentials to variations of stimulus locus in

the visual field and to analyze these data in terms of their underlying sources in the brain. The characteristics of these sources will then be related to the topography and functional anatomy of the brain. It will be shown that the mapping between the visual field and these underlying brain wave sources is strikingly similar to the commonly accepted mapping between the visual field and visual cortex. As a result, evoked scalp potentials may be used as a tool, albeit a crude one, for defining the anatomical projection of localized sensory fields onto the cortical surface.

2. BACKGROUND

2.1 The Source Localization Problem

2.1.1 The Inverse Problem

Assuming that evoked potentials reflect at least some aspects of the macroscopic electrophysiology of the brain and that some reasonable assumptions may be made about the form of neural activity leading to evoked potentials, let us consider the problem of how evoked potentials might be used to determine the spatio-temporal course of brain information processing. The objective is to use electric field theory to trace the internal neuroelectric sources which give rise to scalp potentials. A problem of this sort is referred to as an inverse or backward problem. At the outset it should be emphasized that the general inverse source problem, in the absence of any knowledge of the basic form of internal electrical sources, is ill-posed and thus has no unique solution. There is in effect an infinite number of possible source configurations which could give rise to the same surface measurements. This may be seen by considering Helmholtz's equivalent dipole layer principle [4,5], which states that for a conductor containing arbitrary electrical sources, there exists a non-uniform dipole layer for any surface bounding the sources (but within the conductor), which produces the same external field as the sources themselves. The equivalent dipole layer is the three-dimensional analogue of that guaranteed in circuit theory by Thevenin's theorem [6].

Plonsey [7] discusses the limitations of the inverse problem in terms of the multipole expansion, which is a concise and fundamental method of calculating surface potentials resulting from an arbitrary distribution of electrical sources.

He notes that the coefficients of the multipole expansion are always calculable when the potential is specified on the surface, but that there is an infinite number of source distributions which have the same multipole expansion. This, of course, precludes the possibility of converting surface potential information alone into information concerning the actual distribution of sources. He {7} also discusses the fact that in practice there is an even greater indeterminacy. This arises from the fact that since higher order multipoles depend on successively larger inverse powers of distance, the effects of higher order multipoles will eventually be obscured as a result of the finite signal-to-noise ratio inherent to potential measurements. This means that different sources with only a finite number of similar multipole coefficients will appear equivalent for practical purposes.

If reasonable assumptions can be used to restrict the possible sources to a particular class, then it is often possible to determine so-called equivalent model sources uniquely from surface potential measurements[4]. The word equivalent is used because such sources are chosen because they accurately duplicate the measured data, while the word model reflects the fact that a particular parametric model is assumed. As discussed above, there is an infinite number of different equivalent model sources which are equally effective in duplicating the measured data. However, some model sources are obviously more realistic than others in terms of conforming to available physiological and anatomical knowledge of the brain tissues in question,

---

[4]For example, a unique equivalent solution is theoretically possible if one can restrict the possible generators to a finite number of discrete sources {8}.

while retaining sufficient generality to accurately predict scalp potential data over a wide variety of different stimulus conditions. A model source of adequate generality ought to include as free parameters such source characteristics as location, magnitude, orientation and extent. A priori, the location and extent parameters would appear to be the most important to determine in achieving the stated goal of this thesis, which is to determine the when and where of brain information processing in a macroscopic sense. As will be seen, however, in this work the orientation parameters take on paramount importance because of the extreme sensitivity of surface potentials to source orientation, coupled with a radical dependence of cortical topography on stimulus parameters.

The forward or direct problem, i.e. the calculation of surface potentials from known source characteristics, is a well-posed problem and has been solved for many geometries and source configurations. Once an appropriate model has been chosen, one procedure for utilizing it is first to determine its forward solution by one of the standard methods {9,10}. Inverse solutions can then be derived by taking least-squares estimates of model parameters, which are optimal in that the sum of the squared deviations of the actual scalp potentials from the scalp potentials computed by the model is minimized. A single model may not work well in all instances. If, however, the set of reasonable alternative models can be reduced to a small number, it is possible to compare their performance and make inferences as to the most likely source configuration. In this thesis, a small set of hypothetical models will be considered and defended on the basis of their generality,

ability to duplicate experimental data and conformity to ancillary physiological and anatomical knowledge {11}. Due to the limitations imposed by theoretical non-uniqueness, the ultimate test of a model's correctness must await direct measurements of source characteristics.

2.1.2 Volume Conduction

It is intuitive that when depth recordings are not possible, the best knowledge of internal bioelectric sources will be determined from the most detailed possible knowledge of their field effects at the surface of the head. This is so because the media making up the head are conductive and even very localized sources can produce currents everywhere in the head. Although the current density will be highest in the vicinity of the source, the potential differences that characterize a current field may be recorded with electrodes which are a considerable distance from neural generators. The topography of and form of activation of the various brain tissues and the electrical and geometrical characteristics of the head will determine the scalp potentials.

Historically, these facts have been largely ignored and many investigators have tacitly assumed that scalp-recorded EEG or evoked potential signals represent bioelectric activity immediately below or in very close proximity to the recording site. Obviously, all that is necessary for a potential difference to be recorded is that the "active" and reference electrodes be on disparate isopotential lines. In addition to the theoretical facts supporting the possibility of widespread volume conducted currents, there exists experimental evidence which shows that subcortical, in-depth sources as well as sources located in the contralateral hemisphere can contribute to scalp potential

recordings {12-16}.

An important question in this context is whether or not evoked potential surface fields are synchronous with their sources. In other words, can the head be treated as a volume conductor with propagation through cranial tissues essentially instantaneous? This will not be the case unless the media of the brain, skull and scalp can be accurately approximated as being purely resistive, or typically having reactive currents which are negligible compared to resistive currents. If the media were not purely resistive, then surface measurements could be reflections of source activity at many different (past) times, the most recent values being at those surface positions closest to the source. This would make the source identification problem considerably more complex. As will be seen, the resistive assumption allows one to proceed as if steady-state conditions exist at any instant. Consequently, the problem is then a quasi-static one, and Laplace's equation applies.

Although the theory of volume conduction has been questioned for some types of brain wave activity {17,18}, most investigators agree that the media making up the head are purely resistive in the range of frequencies to which they are subjected by the EEG (0.5-1000 Hz)[5] and that reactive effects are negligible {19-22}. Plonsey and Heppner {20}, in particular, consider the conditions under which the general time-varying electromagnetic problem may be reduced to a quasi-static problem

---

[5]The upper limit of 1000 Hz is presumably related to the fact that the most rapid known neuroelectric activity occurs with action potentials which have a minimum rise time of about 1 msec.

and conclude that these conditions are probably met for all known electrophysiological systems. Gerlernter and Swihart {23} estimate that the decay time of transients related to conduction within the human body are at least an order of magnitude below 10^{-4} seconds, so that steady-state boundary conditions are instantaneously satisfied in any real physiological case. This notion has also been supported by investigators who have introduced artificial electrical sources into animal brains and subsequently measured surface signals {16,24}. One investigator {25} has proposed that potentials mostly reach the surface by propagation through active neuronal pathways. Although this proposal has not been discounted, little evidence has been put forth to support it.

2.1.3 Governing Equations

In deriving the appropriate equations, let us follow the line of Freeman {26}:

The current density $\vec{j}$ is a vector quantity representing the current (di) which flows perpendicular to a specified surface area (dA)

$$\vec{j} \equiv \frac{di}{dA} \cdot \hat{j}$$

where $\hat{j}$ is a unit vector perpendicular to dA. In the nervous system, currents originate in the electrochemical activity of individual cells and involve the movement of ions in closed loops which originate and end at individual neural membranes. For an individual neuron the total current in will always equal the current out. However, the region at which current exits from a cell need not be the same as the region where current enters, and different regions of a single neuron's membrane may

form effective[6] sources (areas of current exit) and sinks (areas of current entry) for the production of external currents. The different exit and entry points arise by virtue of differences in local membrane state. Membrane state differences may result from an active process (as in the case of membrane activation in the course of action potential propagation) or a passive process (as in the case of the electrotonic spread of postsynaptic potentials along the dendritic tree to the soma). The distribution of external current produced by an individual neuron will be determined by the distribution of the effective sources and sinks on the cell membrane, as well as the characteristics of the medium surrounding the cell. One highly active cell may produce little net current beyond a short distance by virture of far field cancellation effects arising from a symmetrical source and sink distribution. Another active cell may produce a considerable far field current by virtue of asymmetry in its source and sink distribution. The same considerations apply to active neural masses, which may give more or less external current, depending on the overall distribution of sources and sinks.

Continuing with the derivation of the governing equations, we now note that in a source- (or sink-) free volume

$$\nabla \cdot \vec{j} = 0 \tag{1}$$

while in a volume containing a source (or sink)

---

[6]The word effective is used because there can be no true sources or sinks in the nervous system, since the nervous system can neither create nor destroy charge.

$$\nabla \cdot \vec{j} + \frac{d\xi}{dt} = 0 \tag{2}$$

where $\frac{d\xi}{dt}$ is the rate of change of charge density. Assuming that only electrostatic and resistive forces act on the ions in a volume which is source-free, the differential or local form of Ohm's law applies

$$\vec{j} = \rho^{-1}\vec{E} \tag{3}$$

where ρ is a resistance term (volume specific) and $\vec{E}$ is the electric field. Combining (1) and (2) with (3), we have

$$\nabla \cdot \vec{j} = \nabla \cdot (\rho^{-1}\vec{E}) = \vec{E}\nabla \cdot \rho^{-1} + \rho^{-1}\nabla \cdot \vec{E} = 0$$

and

$$\nabla \cdot \vec{j} = \vec{E}\nabla \cdot \rho^{-1} + \rho^{-1}\nabla \vec{E} = -\frac{d\xi}{dt}$$

For a homogeneous isotropic medium[7] we have

$$\nabla \cdot \rho^{-1} = 0$$

Now, since the electric field $\vec{E} = -\nabla V$ and $\nabla \vec{E} = -\nabla^2 V$, where V is the scalar potential, we have

$$\nabla^2 V = 0 \qquad \text{(Laplace's Equation)}$$

and

$$\nabla^2 V = \rho \frac{d\xi}{dt} \qquad \text{(Poisson's Equation)}$$

for source-free and source-containing volumes respectively. This shows that current sources in a medium which is a homogeneous isotropic volume conductor give rise to the same equations as fixed charges. Thus, the problem may be considered as a purely electrostatic one with lines of current replaced by electrostatic lines of force. The currents at any instant depend only on the sources at that instant and obey the principle

---

[7] A homogeneous medium has the same resistive properties throughout. An isotropic medium has the same resistive properties in all directions.

of superposition. For purposes of modeling brain activity, the potential V will satisfy Laplace's equation everywhere in the head except at a source, where it must have an appropriate singularity and there satisfy Poisson's equation. In addition, since the medium external to the head (air) is nonconducting and current cannot flow out of the head, the normal derivative of the potential must be equal to zero at the boundary.

Although the volume conduction assumption is probably valid, the assumptions of homogeneity and isotropy are obviously invalid. The equations may, however, be applied in an inhomogeneous medium if it consists of a finite number of homogeneous subregions which are considered separately with appropriate matching of boundary conditions {20}. In addition, the equations may be adapted for special forms of anisotropy which are simple in nature.

2.1.4 Relationship of Scalp Potentials to Brain Activities

A preliminary question for interpreting scalp potentials in terms of their underlying sources is whether or not scalp potentials reflect cortical potentials. This topic was once wrought with controversy, but there is now general experimental agreement that scalp electrodes record accurate but attenuated versions of potentials on the cortical surface immediately below them {11,27-33}. For example, Heath and Galbraith {31} found this when comparing direct cortical recordings of human flash VEP's with flash VEP's recorded by signal averaging of scalp potentials. The degree of this correspondence is related to the relative size of the cortical and scalp electrodes, an effect which is due to the integrating property of larger electrodes.

Theoretically, however, the scalp potential will be an attenuated and weighted average of the potentials on a finite region of the cortical surface below, with the weighting dependent on the smearing effects of the tissues between the cortex and scalp. As will be seen, the smearing and attenuation resulting from the alternating low and high conductivity layers of the skull and scalp have a dramatic effect on resulting scalp potentials.

A secondary question is how gross cortical potentials may be related to the electrical activities of individual neurons. Regan {34} discusses the difficulties of establishing this relationship. The comparison of gross cortical potentials and single cell potentials is further complicated by the fact that a single cell may not be representative of the population of cells which gives rise to the cortical potential. It is possible for a sampling of cells to be biased towards a particular cell type, such as cells which are very large. Indeed, the true relationship may be statistical, so that the activity of an individual cell may not be nearly as important as the global activity of populations of cells {35}. There is evidence, for example, that as one passes to higher and higher levels of the brain, the activities of transmitting neurons may show decreasing synchronization with one another {36,37}.[8]

Although there is not general agreement about the mechanism of cortical potential generation, most investigators believe that it in

---

[8]This would also have the unfortunate effect that one might have difficulty detecting the activity of high levels of the brain using time-locked averaging techniques.

some way directly or indirectly reflects the activity of cortical neurons. In theory {11,38} one can use electric field theory to predict gross cortical potentials from the activities of single neurons. This can be done if the geometry and distribution of the neurons are known as well as their degree of synchrony. However, such predictions are difficult to obtain in practice and have not been attempted at more than a primitive level {39}. In this study, models are presented which are intended to represent the macroscopic geometrical and electrical characteristics of the head and underlying sources. The detailed neuronal basis of cortical potentials is ignored. This is in conformity with the limited goals of this study, which mainly seeks to determine the when and where of brain excitation in human visual information processing.

2.1.5 The Normal Dipole Layer Approximation and the Cellular Basis of Cortical Potentials

One assumption regarding the cellular basis of cortical potentials will be made and will be based on overall neuronal geometry in cortex. This assumption will be that active cortex may be modeled to a first approximation as a neuronal layer wherein the neurons are treated as discrete dipole current sources oriented normal or at right angles to the cortical surface. It will be shown that this first approximation is more than adequate for the modeling of the far field (scalp) potential measurements which are the data upon which this thesis is based. This assumption forms the basis for an underlying hypothesis of this thesis, which is that variations in the surface (scalp) distributions of EP components with variations of stimulus parameters often result from differences in the topography and location of different brain areas

which respond to the stimulus, rather than from variations in forms of cortical activity.

The above assumption may be defended on theoretical grounds {40}. In considering this, it is useful to contrast the roles which two different idealized neuron types might play in the production of the EP, i.e. neurons with axial symmetry (e.g. cortical pyramidal cells having long apical dendrites and long axons, etc.), as opposed to neurons having radial symmetry (e.g. granular, stellate or cells with short axons). This is illustrated in Fig. 1 in which excitatory input to a particular branch of the dendritic tree is assummed to produce a source-sink relationship between the dendrite and soma, while inhibitory input is assummed to produce a sink-source relationship. A preponderance of either excitatory or inhibitory inputs to an axially symmetric cell will tend to give an axially symmetric mass of paired sources and sinks, while a radially symmetric cell with similar inputs will tend to give a radially symmetric mass of paired sources and sinks. At a distance, the potential field produced by either of these cell types will to a first approximation[9] be that of a current dipole coincident with and of the same magnitude and orientation as the resultant of all the source-sink pairs. This apparent dipole source will obviously tend to be much larger for the axially symmetric cell than for the radially symmetric cell which suffers cancellation effects. The orientation of the

---

[9]This approximation is very good, when the maximum distance between the sources and sinks is small compared to the distance at which the potential field is being scrutinized. Specifically the soma to dendrite distances must be small compared to the distance between the neuron and the scalp.

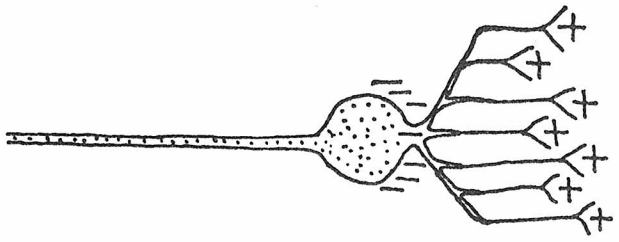

AXIALLY
SYMMETRIC

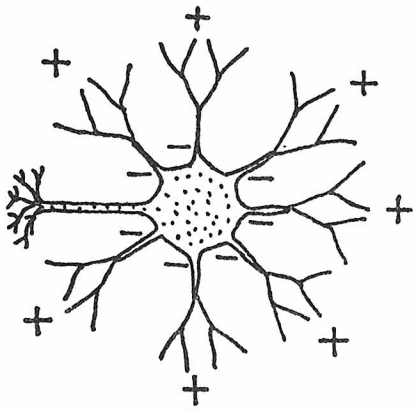

RADIALLY
SYMMETRIC

Fig. 1 - Two idealized cells illustrating symmetry types.

apparent dipole will be parallel to an axially symmetric cell's axis of symmetry but may be indeterminate for radially symmetric cells. Due to irregularities in the distribution of the dendritic branches of neurons and active sites in the membrane, real neurons do not conform precisely to the idealized axially symmetric or radially symmetric models. This classification is not essential. Indeed, most cells could probably be considered as hybrids of these two types. What is essential is that no matter what the actual case is, to a first approximation only the resultant dipole will be sensed in the far field. Thus, for far field purposes, it is sensible to use a current dipole model of neural activity, with the axis of the dipole oriented parallel to the axis of symmetry of the neuron.

The normal dipole layer approximation then has its basis in the above theory and in the fact that neurons in most parts of cortex have a common orientation {41} which is vertical or at right angles to the cortical surface. In addition, the connective pathways within cortex are largely normal to the surface {42} and thalamocortical afferents ascend vertically in cortex.[10] In paleocortex the positions (in depth) and orientations of the neurons tend to be the same, while in neocortex the neurons have a common orientation but may be displaced vertically from one another.

A plane of dipole generators in parallel would have many of the general electrical characteristics of a single unit membrane

---

[10]These facts are reflected in the columnar structure which has been found in numerous cortical structures. These vertical columns of cells usually respond to the same modality and region of sensory stimulation.

itself, as if the giant squid axon membrane were spread out as a sheet. The layers of neurons in the nervous system usually occur in the form of curved surfaces. Freeman {40} has pointed out that one effect of curvature is to increase the amplitude of potential in the concavity and to decrease the amplitude in the convexity.

The normal dipole layer approximation has also been defended on experimental grounds. Landau {43} has analyzed evoked potentials at the cortical level and found that the evoked potential field across active cell layers appeared to be largely dipolar and vertically oriented and "essentially a standing wave for a given component distributed over a vertical depth in fractions of millimeters." He further states that the components of cortical EP's are such that they cannot be accounted for by an axonal model because spikes have such a high frequency and velocity relative to cortical waves. He also states that the vertically oriented field potentials probably arise from unequal postsynaptic activity in different regions of the soma-dendrite complexes which form most of (90% of surface area, on the average) the neural tissue in cortex. Here source-sink relationships will arise in the form of extracellular currents from inactive or less active regions towards more active regions. Creutzfeldt et al {44} have also studied the relationship between evoked potentials at the cortical level and single cell activity in cortex. They propose a similar origin to that of Landau {43} in terms of the complex pattern of excitatory and inhibitory postsynaptic potentials which act as inputs to the pyramidal cell of cortex. Freeman {40} has carried out detailed three-dimensional measurements of evoked potential fields within the cat brain using

electrode arrays and found many instances of dipolar fields. He also found instances of closed fields, i.e. fields which were for all practical purposes, limited to finite regions within the head and undetectable outside of these regions. He noted that for far field purposes, all the fields could be accurately modeled by current dipole sources.

In addition to the work involving direct measurement of cortical evoked potentials, there have been a number of investigations in which scalp EP fields were measured and found to have dipole-like characteristics. A discussion of this work will be deferred until a later section (2.3.5). Suffice it to say, however, that many of these studies support the notion of a dipole-like source with the dipole axis perpendicular to the cortical surface.

It is now well to consider what features ought to be included in an electrostatic model of the head for the purposes of source localization. Many of these features have been proposed by previous investigators and fall into three categories: (1) properties of the media making up the head, (2) properties of the geometry of the head and (3) properties of the source(s).

2.1.6 Head Media Properties

As previously discussed, the media making up the head are generally considered to exhibit volume conduction with propagation of potential through cranial tissues essentially instantaneous. Further, it is usually assumed that the brain, cerebrospinal fluid, skull and scalp can be separately regarded as homogeneous, isotropic conductors. There are two strong objections to this idealized scheme. The first is the fact that the brain is really inhomogeneous and composed of gray and

white matter, and cerebrospinal fluid, which have different conductive properties. To answer this, Witwer et al {45} used a finite-difference scheme to solve Laplace's Equation for an irregular head with a realistically inhomogeneous brain. They concluded that predicted scalp potentials are not significantly changed when one goes from a homogeneous brain to one which includes brain inhomogeneities. The second strong objection is to the assumption of the skull being isotropic.[11] One investigator {48} has reported that skull is 5 to 40 times more resistive to current normal to its surface than to current parallel to its surface, but that its equivalent isotropic resistivity is about 80 times that of the scalp and brain. This may be explained by considering the structure of the skull and noticing that it is really made up of three relatively homogeneous and isotropic layers, i.e. two high resistivity calcified layers sandwiching a low resistivity sponge-like material called diploe. This study will subscribe to the assumption of an isotropic and piecewise homogeneous head, with 5 separate regions of different conductivity representing the brain, 3 skull elements and scalp, respectively. The importance of accounting for the layering of the surroundings of the brain is well established. There is general agreement that the overall effect is to attenuate and smear the pattern

---

[11] The brain is also somewhat anisotropic {46,47}. This may be found in fiber tracts or other areas where fibers run parallel to one another. Areas of cortex containing axially symmetric cells may exhibit an anisotropy with conductivity greater in the direction normal to the cortical surface than in the direction tangential to its surface. This could actually enhance the dipole-like nature of some neurons owing to more resultant current flow in the normal direction. However, since the cortex is so thin (1-3 mm), this effect is probably negligible.

of scalp potentials {49-52}. Ignoring these aspects tends to make underlying sources appear more centric and of lower magnitude than they really are.

2.1.7 Head Geometry

Most investigators have approximated the geometry of the head by a sphere. A more accurate model approximates the brain as a sphere or ellipsoid (Fig. 2) surrounded by four concentric shells comprising the three skull layers and the scalp. This model is inaccurate to the extent that the brain departs from a spherical or elliptical configuration and that its coverings are irregular in shape and thickness. Such considerations are relatively insignificant for the upper half of the brain, but render inferences concerning lower portions less satisfactory. The spherical and ellipsoidal concentric shell models are the most complicated models which are potentially useful and for which analytic forward solutions to Laplace's equation are presently obtainable. Passing from a spherical model to an ellipsoidal model of the head is quite simple and basically involves a change of coordinates in which spherical locations are converted to ellipsoidal locations by multiplying each cartesian coordinate by the corresponding semiaxis of the ellipsoid.

More accurate models are available if use is made of approximations such as those of finite difference methods {10}. The finite difference technique permits pointwise variation of conductivity coincident with various intracranial inhomogeneities, as well as arbitrary boundary characteristics. This approach has the limitation that a model with any spatial resolution involves the solution of a huge set of simultaneous equations. Witwer et al {45} have investigated forward

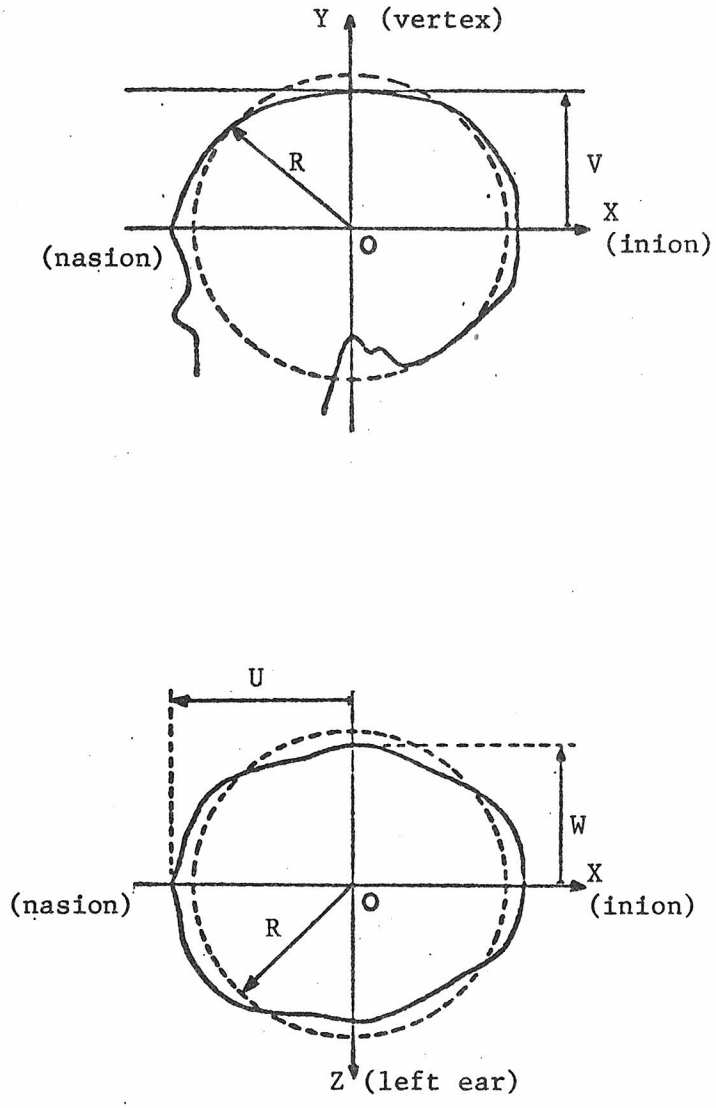

Fig. 2 - Two possible approximations to the geometry of the head: A sphere of radius R and an ellipsoid with semiaxes (U,V,W).

solutions using this method and conclude that accounting for boundary irregularities may be warranted in some regions where there are significant deviations from spherical. However, deviations from spherical are not so severe near many areas of interest, especially in the vicinity of visual areas. Therefore, spherical concentric shell models are used in this study to approximate the geometry of the head.

2.1.8 Source Properties

As discussed in section 2.1.5, active cortex might be modeled as a layer of dipole current sources oriented at right angles to the cortical surface. Historically, most efforts in modeling cortical sources have centered around a dipole model. A number of previous investigators have approximated the overall activity of large populations of neurons by a single equivalent dipole. Again, the motivation for this is that an exact expression for the potential due to a volume of discrete current sources in an infinite series whose successively higher order terms decrease more rapidly for points distant from the sources. Since bioelectric current sources have a zero algebraic sum by considerations of charge conservation, the first or monopolar term does not occur. Then as a first approximation, the second term, the dipole term, suffices to determine the potential field at distances large compared to the maximum distance between sources producing the field (i.e. far field). By the same token, the single dipole model may serve as an adequate approximation for a region of active cortex, if that region's extent is small compared to the distance at which the potential is being measured. This may be seen {6 } by noting that the individual dipoles making up such a surface may be moved to a common

central point and summed with negligible effect on the potential they produce remotely. The validity of such a transformation is increased by the smearing and attenuation effects of the skull and scalp, which have the effect of shielding underlying activity, so that a source in the head can be displaced somewhat without making significant changes in scalp potentials.

In situations where the single dipole model is not adequate, the sources must be modeled either by a number of dipoles or by extended 2-dimensional dipole sheets which conceivably may have highly irregular surfaces. The details of these surfaces must reflect anatomical knowledge which specifies the geometry of both individual neurons and populations thereof. The angular extent of a dipole sheet affects the surface distribution of potential {53}. A sheet of small angular extent gives rise to surface potentials that attenuate rapidly with distance from the points of maximum amplitude, while larger angular subtense produces potentials that are larger and attenuate somewhat more slowly with distance. Vaughan {53} has proposed a scheme wherein most cortical sources might be represented by one of two simple dipole layer representations which conform to the geometry of cortex (Fig. 3). The first is a dipole layer in the shape of a circular segment or cap concentric with the surface of the sphere representing the head (radial cap). This could model cortex on the outermost surface of the brain or elsewhere where the tissue is concentric with the skull. An example of this would be cortex on the exterior surface of the occipital lobe. The second is a dipole layer shaped like a plane annular sector bounded by two concentric arcs (annular sector). This could be used to model cortex

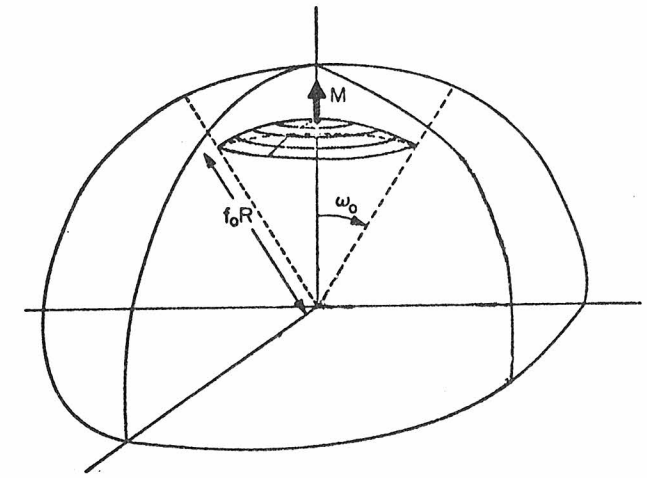

RADIAL CAP

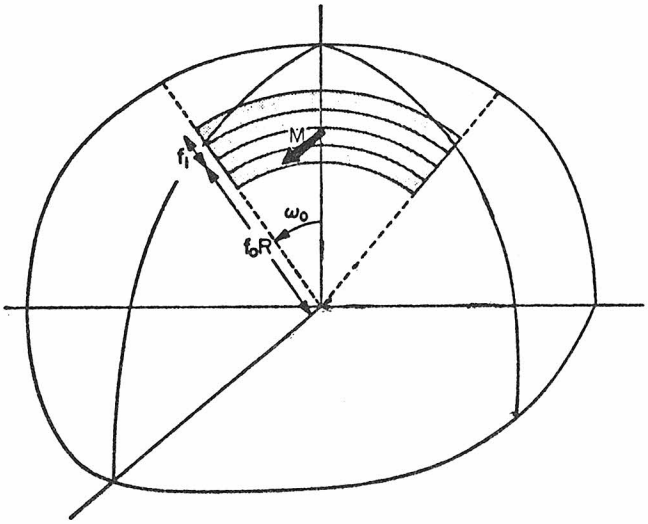

ANNULAR SECTOR

Fig. 3 - Two geometries may be used to model cortex as a normal dipole layer. A radial cap of eccentricity f_0 and angular extent $2\omega_0$, and an annular sector of eccentricity f_0, angular extent $2\omega_0$ and eccentric extent $2f_1$. In the limit of small extents these layers become single (M) radially and tangentially directed dipoles, respectively.

perpendicular to the skull surface, e.g. sulcal cortex in the region of the calcarine fissure. Analogous single dipole equivalents of radial cap and annular sector dipole layers are radially directed and tangentially directed unit dipoles respectively (Fig. 3). As for analytic solutions to Laplace's Equation with extended sources, they are available only for a few very regular and symmetric surfaces. In practice, one can resolve any extended source geometry into a summation of individual dipole elements and determine the resultant field by superposition.

2.1.9 Previous Attempts at Source Localization

Most previous attempts at cortical source localization on the basis of scalp potentials were qualitative studies. The procedure in these studies was to make a qualitative comparison between model and measured potential distributions. Several investigators {54-59} have considered dipoles as comparable generators of certain scalp potentials and have drawn conclusions concerning the feasibility of such modeling on the basis of the similarity between real data and the potential distributions of dipoles with various orientations. Similarly, others {60-68} have made qualitative comparisions between pattern-evoked potentials elicited from specific regions of the visual field and potentials generated by hypothetical dipole sources. One investigator {69} has compared potential distributions elicited by patterns of different colors with those given by various dipole sources.

The first really quantitative results were obtained by Schneider and Gerin {70}, who used certain features of the electrical field to localize equivalent dipoles below a plane surface representing artificial sources in live animals as well as certain types of epileptic

discharges in humans. Schneider {71} proposed a computational approach for doing inverse fits of model parameters to EEG data utilizing a standard nonlinear least-squares parameter estimation algorithm, and reported on attempts at applying it to the localization of epileptic foci. More recently, Henderson et al {52} have used a model consisting of a dipole in a homogeneous conducting sphere to localize an equivalent source for each of various types of bioelectric phenomena in humans. They found that the source locations agreed more or less with their expectations, but admitted that the model was limited by the fact that only one locus could be found in situations where multiple sources were expected. Even more recently, Henderson et al {72} claimed to have tested a model which included either two independent dipoles in a homogeneous sphere or a rectangular sheet of 4 or 9 dipoles of common orientation in a homogeneous sphere. The details of this work are yet to be published, but they note a successful application of the two dipole model to the localization of eye movement sources and an unsuccessful application to localizing cortical generators. They described the application of the dipole sheet model to the localization of alpha rhythm and VER's due to central field stimulation, but were not very specific about their procedures or results. To date only one investigator has given a complete report on attempts at inverse fits of model parameters to evoked potential data with other than the simplest of modeling assumptions. Kavanagh {73} developed and tested algorithms for inverse solutions in terms of single and paired dipoles imbedded in homogeneous and inhomogeneous spherical head models. He applied these algorithms to human flash evoked potential data with mixed results, probably due to the choice of

inappropriate stimuli. This thesis began with the intent of extending Kavanagh's {73} methods and applying them to data derived from more physiologically meaningful stimuli. The aim was to establish the inverse localization technique as a tool for studying the intact human brain.

2.2 Relevant Visual System Structure and Function

2.2.1 Subcortical Elements

The gross anatomy of the visual system up to the initial cortical level is well established (Fig. 4). Although direct experimental evidence on humans is relatively sparse, most studies have indicated that the human visual system is similar in many respects to that of monkeys and other primates. There are, however, some differences. These will be noted, as will extrapolations from non-human primates which are not established beyond a reasonable doubt.

In all primates there is one major pathway from the retina to primary visual cortex (also called striate cortex or area 17) via the lateral geniculate nucleus (LGN) of the thalamus. The thalamus lies near the center of the brain, while primary visual cortex lies in and around the medial surface of the occipital lobe. Some 70 to 80% of all retinal fibers subserve this pathway. These fibers reach the LGN by a decussation at the optic chiasm of fibers from the nasal half of each retina (or the contralateral half of the visual field). The precision of splitting the visual field in humans is somewhat controversial due to the phenomenon of macular sparing.[12]

The anatomy and projections of the human LGN do not appear to differ significantly from those of other primates {75}. When the retinal fibers reach the LGN, they terminate in a number of laminae, each of

---

[12] Macular sparing refers to the frequent survival in humans of all of the very center of the visual field (macular area) following extensive injury to one occipital lobe or optic radiation {74}. This has led some investigators to believe that there is bilateral representation of the macula in humans.

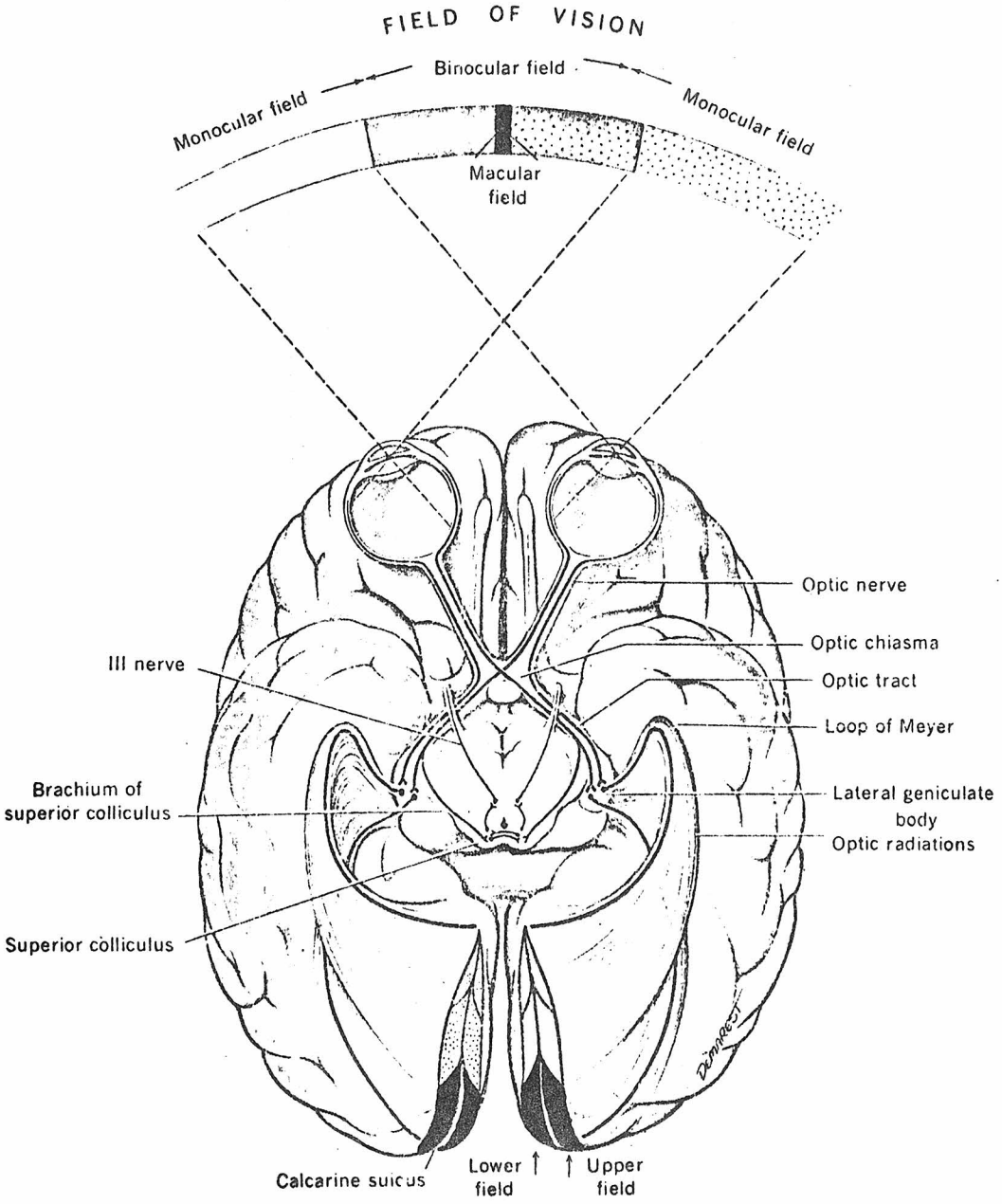

Fig. 4 - The geniculo-cortical pathway of the human visual system.

which received a topographic projection from a hemiretina and project to the cerebral cortex. The laminae are stacked in visuotopic[13] register so that there is a direct continuity of visual field between adjacent laminae {76}. It appears that in primates nearly all the cells leaving the LGN project directly to striate cortex {77}. The precise function of the LGN has yet to be illuminated, although it is fairly clear that it is more than a mere relay station. It has, for instance, been implicated as performing a gain control function on the transfer of information to visual cortex, owing to the fact that the excitability of various LGN cells is influenced by projections from cortical and brainstem areas {78}.

As the visual field projects to cortex, the proportion of cells representing areas in the center of the visual field is considerably larger than would be expected on the basis of relative numbers of retinal fibers (ganglion cells). This reflects a tremendous bias of the visual system towards the center of the visual field {76}.

2.2.2 Non-geniculate Optic Tracts

The retina also has several other projections. The most notable of these is the projection to the optic tectum (superior colliculus and pretectal nucleus). The role of the non-geniculate tracts in vision is often discounted or ignored. In mammals the projections to the optic tectum are known to play a role in eye movement control

[13] The term visuotopic refers to a continuous form of mapping between the visual field and a brain area. In other words, a visuotopic mapping is a geographic or point-to-point mapping in which neighboring points in the visual field are for the most part neighboring points in the brain area. The term retinotopic is an equivalent description for the same type of mapping when considered between the retina and brain.

as well as pupillary control and visual grasp reflexes {79}. Other functions have not been proved as yet, but a number of possibilities are open, owing to the rich interconnections of the midbrain areas with thalamic and cortical areas. There is a visuotopic projection of the contralateral visual field onto the tectum {79}. The superior colliculus has a widespread cortical projection via thalamic relays and the pulvinar, while the colliculus and its thalamic relays receive projections from many parts of cortex. Also, some collicular inputs are collaterals of fibers which are inputs to the thalamus {79}. The important point for the purpose of this study is that anatomy does support the existence of at least two separate retino-cortical pathways. A number of speculations have been offered as to their respective purposes. Most of the discussion has centered around the geniculo-striate-circumstriate and colliculo-pulvinar-temporal neocortex pathways. One suggestion is that the striate pathway is concerned with the detailed analysis of visual pattern, while the tectal pathways are concerned with spatial orientation functions and have only crude discrimination capabilities {80}. This issue is relevant to the origin of various types of visual evoked potentials, and will be discussed at length in a later section (2.3.2).

2.2.3 Striate Cortex

Although it has not been verified directly in man, it is fairly certain that the laminae of the LGN project via the optic radiations exclusively to layer IV of striate cortex {77}, having fanned out and entered the cortex perpendicular to its surface. Striate cortex, which has seven cell layers, is distinguished by a

horizontal band of myelinated fibers and occupies that portion of the cortex in and around the calcarine fissure (Fig. 5a). The calcarine fissure is a long, deep horizontal fold in the cortex of the medial wall of the occipital lobe. In the striate cortex of each occipital lobe there is a visuotopic mapping of the contralateral half of the visual field. This particular mapping is the most detailed known map of the visual field in the primate visual system {81}. Its general characteristics are known in all primates, including man (Figs. 5b,5c). The perimeter of striate cortex represents the vertical meridian of the visual field, with center to periphery going posterior to anterior. The representation of the horizontal meridian of the visual field follows the length of the calcarine fissure in a similar posterior to anterior fashion. The more peripheral areas along the horizontal meridian project to the depths of the calcarine fissure. The most central part of the contralateral hemifield is represented on the posteriolateral surface of the occipital lobe. The intermediate and peripheral parts of the visual field are represented on the medial wall of the hemisphere and within the calcarine fissure.

As previously mentioned, the center of the visual field has a much magnified representation in visual cortex (Figs. 5b, 5c). Schwartz {82} has proposed that this and the other aspects of the primary spatial mapping between visual field and cortex may be described by a complex logarithmic conformal mapping of the retinal surface on layer IV of striate cortex (Fig. 6). He also suggests that other receptor surfaces have similar orderly spatial maps in sensory cortex (receptotopic maps). On the basis of primate single cell recordings

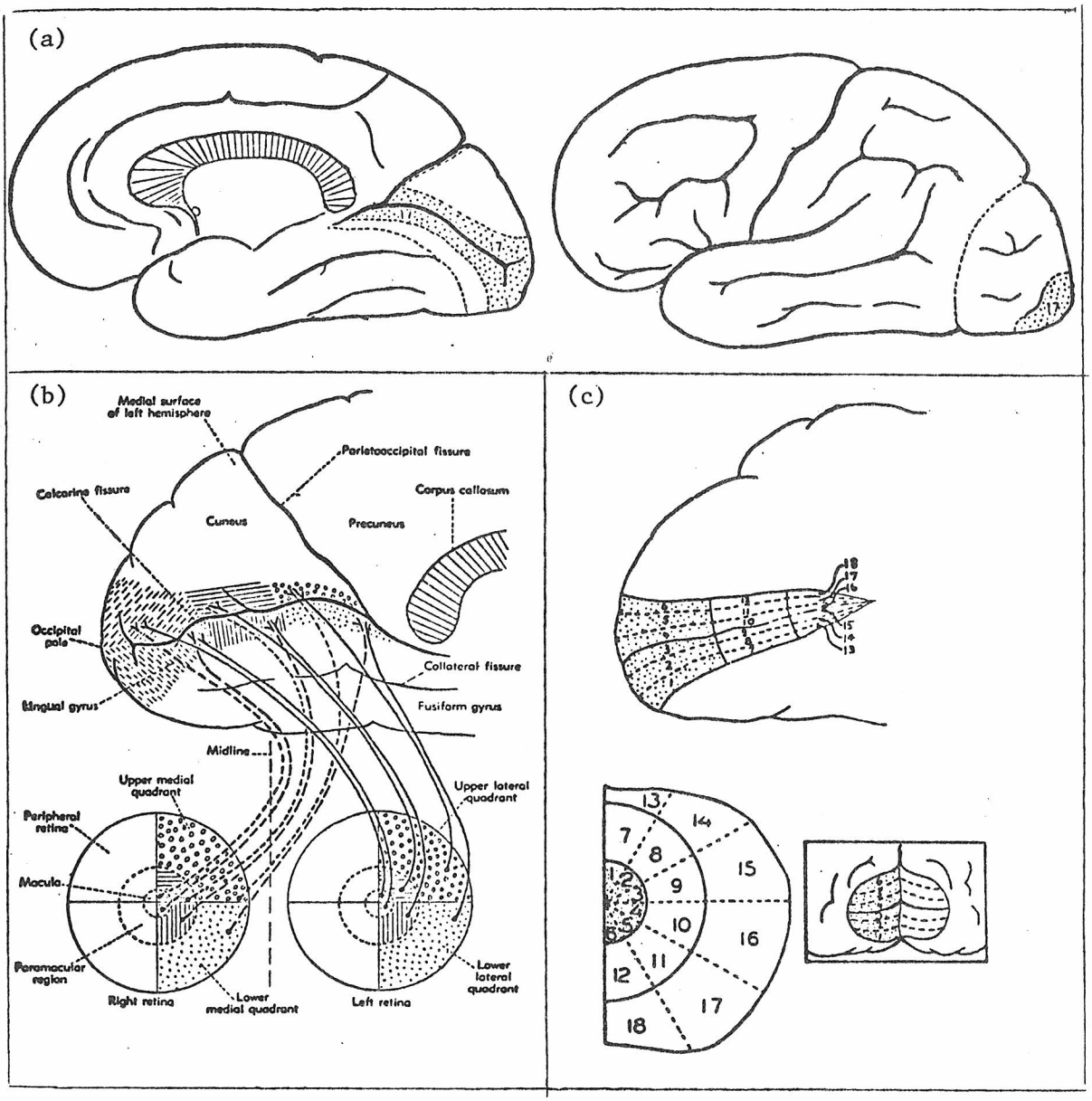

Fig. 5 - (a) Medial view of right hemisphere and lateral view of left hemisphere showing striate cortex (17) and surrounding extrastriate area.

(b) Medial view of left hemisphere showing projections of visual field on striate cortex.

(c) Medial and rear views of occipital pole showing additional detail of projections of visual field on striate cortex.

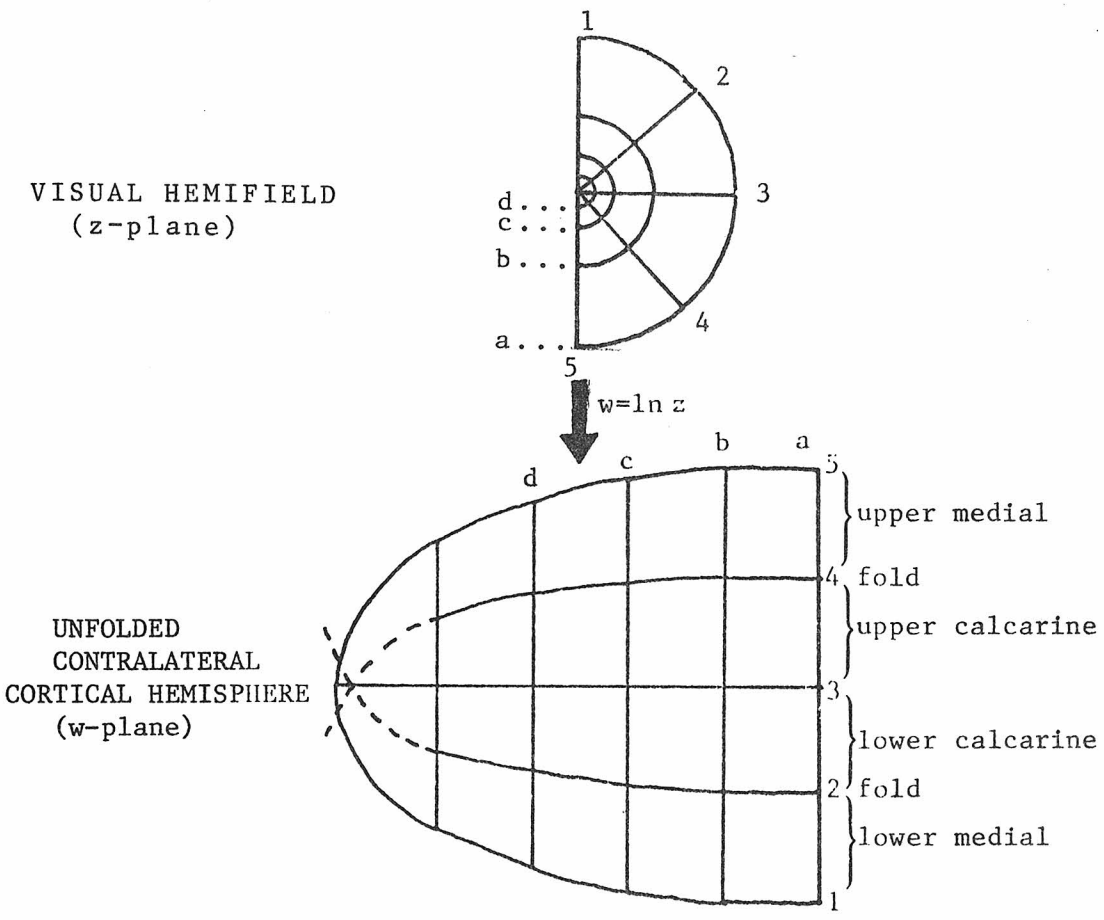

Fig. 6 - A complex logarithmic conformal mapping accounts for most aspects of the spatial maps between receptor surfaces and sensory cortex. This figure shows how this principle applies to the mapping between the visual field and striate cortex {82}.

{83}, the locus of precise topographical representation in striate cortex appears to be limited to layer IVc. It is in layer IVc that the receptive fields are predominantly small and circularly symmetric and the cortical afferents from the LGN arrive and terminate. On a local (single cell) level, neurons in other layers appear to represent random interspersed regions in the visual field distributed over some small region {83,84}. These regions generally get larger as one moves to striate cortical regions representing the peripheral visual field. The mapping appears rather orderly in all layers if one uses large enough electrodes to integrate away the distributional effects seen on the microscopically local level.

Striate cortex appears to have at least two important functions. The first {85} is to bring the inputs from the two eyes together for the first time, as evidenced by the fact that most of its cells are influenced by stimulation of either eye (although they tend to respond better to stimulation of one eye or the other). The second {85} is the detailed analysis of contour, as evidenced by the fact that most striate cortical cells respond to contours of specific orientation.

2.2.4 Extrastriate Cortical Areas

Surrounding striate cortex is prestriate cortex (Fig. 5a), which receives systematic projections from striate cortex and appears to contain several separate visual areas which possess different mappings of the contralateral hemifield {76,85}. Extensive mapping experiments {85} have been performed on a number of species of monkey (no direct work yet on humans). These have revealed that the various

prestriate mappings each have their own special characteristics, which are likely determined by their physiological function in terms of analyzing different aspects of visual field {85}.[14] As such, the maps are not necessarily the same in terms of magnification factors, for instance, which appear to be distorted in accordance with an area's function. In spite of these distortions, continuity is maintained in the sense that adjacent points in the visual field are generally represented by adjacent points in cortex. There are numerous connections between visual areas in the two hemispheres via the corpus callosum, especially between regions where the vertical meridian of the visual field is represented {85}.

One of the larger prestriate areas, which is thought by some to be involved in producing EPs, is known as V-II, and is directly adjacent to and surrounding striate cortex (V-I). This area contains an even larger proportional representation of the central visual field than striate cortex and is a mirror image mapping thereof {76}. In area V-II, the representation of the horizontal meridian forms the outer border. The vertical meridian forms the inner border of area V-II adjacent to the vertical meridian representation in striate cortex. As in striate cortex, the foveal or most central part of the contralateral hemifield is represented on the posteriolateral surface of the occipital lobe. There exist reciprocal interconnections between representations of the same localities in visual space in striate cortex and V-II {76}.

---

[14] The specific physiological functions of these visual areas are yet to be determined.

The portion of striate cortex devoted to the horizontal meridian more than a few degrees eccentric projects to two loci in area V-II {76}. Also the vertical meridian representations in area V-II in each hemisphere are heavily interconnected via the corpus collosum {76}. Thus, while a striate cortical response in one hemisphere is only attributable to input arriving over visual radiations on that side, an area V-II response may be attributable to input via visual radiations on either side.

2.2.5 Some Direct Studies on Humans

Direct experimental evidence on the human visual system is sparse. However, indirect information regarding the geniculo-striate pathway in humans is extensive. Much of it has come from studies of the characteristic features of visual field defects after missile wounds to the brain. These features were pieced together to roughly characterize the geniculo-striate pathway and to make a crude map of the projection of the visual field on striate cortex. This information is in general conformity with that obtained by other methods and that obtained by extrapolation from other primates. This work has been summarized by Teuber et al {74} and the general results are depicted in Fig. 7.

One problem which arises from this work is that there are often slight departures from congruence {74}. In other words, the scotomas (visual field deficits) are not identical in the two eyes for a given cortical injury. Although the crossed and uncrossed projections reside in separate laminae in the LGN, they are thought to be highly aligned in visual cortex. However, there is evidence from

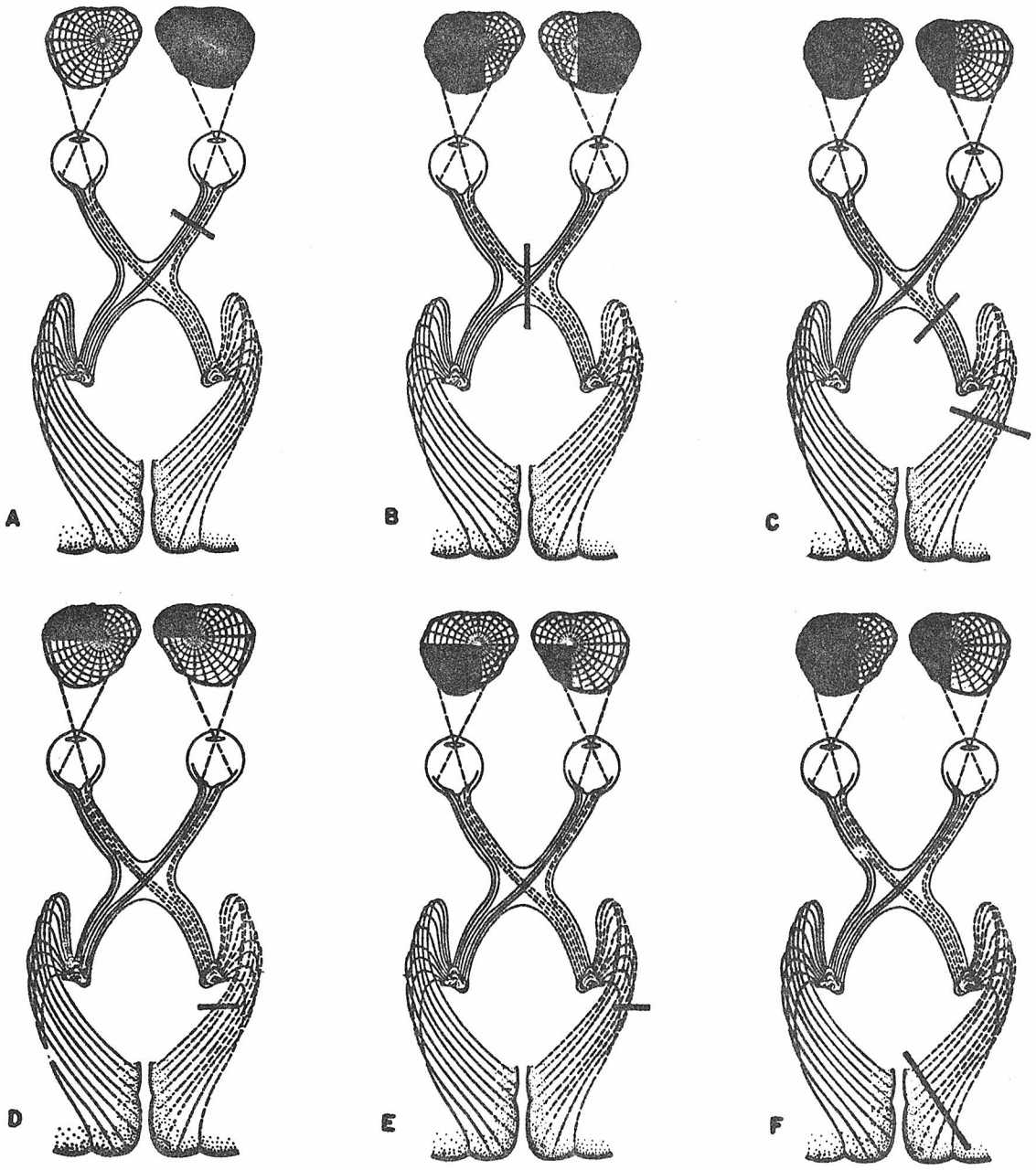

Fig. 7 - Some gross visual field defects caused by interuptions of the geniculo-striate pathway: A- severed optic nerve, B- split chiasm, C- optic tract or optic radiation section, D- section of lower optic radiation, E- section of upper optic radiation, F- destruction of occipital lobe in one hemisphere (from Teuber et al {74}).

studies in primates other than man that there is still a segregation of ipsilateral and contralateral eye projections within layer IV and that the degree of this segregation differs among various primate species {76}.

Another problem which has arisen is that of macular sparing.[12] This phenomenon may imply that the visuotopic principle does not apply to the macular region and that there is a bilateral projection of the macula on striate cortex. This is suprising since in all other primates studied there is evidence for bilateral representation of the vertical meridian in higher visual areas (via the corpus callosum), but not in striate cortex {77}. Indeed, at least one investigator {86} has claimed on the basis of missile wound studies that macular vision is unilaterally represented. However, macular sparing has other possible explanations {74}, owing in general to the fact that such experiments are obviously not very precisely controlled. For instance, there may be fixation problems in performing tests for visual field defects. There may be plasticity in cortical representation or the forming of a pseudo-fovea by eccentric fixation. A likely explanation is that cortex representing the center of the visual field is less vulnerable to injury than cortex representing the periphery of the visual field. Indeed, central areas are much magnified to start out with and have a more profuse blood supply as well.

The existence of an orderly visuotopic mapping to striate cortex in humans has also been corroborated by cortical stimulation studies {87}. This involved the placement of an electrode or array of electrodes over calcarine cortex in a blind subject and delivering

electrical stimuli to the cortical surface. This procedure evokes subjective phosphenes (or flashes of light) which the subject perceives in different locations in the visual field depending on the cortical location stimulated. This method has so far produced results which are for the most part consistent with the established visual map. These studies also support the claim that macular vision is unilaterally represented in striate cortex. Brindley et al {88}, however, have questioned the notion of an orderly mapping in humans on the basis of one one of these studies. In this subject the phosphenes were in a random order. Some adjacent electrodes gave disparate phosphenes and some adjacent phosphenes resulted from disparate electrodes. The latter result is difficult to explain, but may be related to the size of the electrodes used in stimulating and the uncertainty of which cortical cells they are activating. Disparate phosphenes resulting from adjacent electrodes may be due to intervening sulci (fissures).

In addition, the visual fields of a few cells in human visual cortex have been plotted {89}. As yet this approach has failed to yield any useful results, since only 9 cells in 5 subjects have been studied and no verification of their location is available.

2.2.6 Variable Cortical Topography - Modified Cruciform Model of Striate Cortex

The details of cortical topography in humans is known to be variable {90}. Cortex is a highly complex surface, with convoluted, double curved surfaces whose folding pattern varies among individuals. Details aside, the appearance of the calcarine fissure in man is somewhat variable {90,91}, and one may find a large vertical fold in about one brain in four. Also the representation of the upper field on the

floor of the calcarine fissure may extend further forward than the lower field on the roof. Thus, it is probable that the horizontal meridian does not always lie exactly at the furthest depth of the calcarine fissure {92}. In addition, the relationship of cortical areas to fissural landmarks is not reliable in detail. However, the inversion of the upper and lower visual fields to lower and upper striate cortex relative to the calcarine fissure is undisputed. Neither is the fact that the right and left visual field project to the left and right hemispheres, respectively, disputed. There is also general agreement that the mapping from fovea to periphery goes from posterior to anterior striate cortex. These undisputed facts are the only ones required for the purposes of this thesis.

Fig. 8 illustrates a crude model of the conformation of human striate cortex. The data and analysis of results of this thesis will be discussed in terms of this model and its variations. It is similar to the so-called "cruciform model" of Jeffreys and Axford {64} and Ristanovic {58,59} modified to include the posteriolateral representation of the very center (0°-2°) of the visual field. Cortex in the posteriolateral portions is roughly parallel to the surface of the skull while all other portions are roughly tangential to the surface of the skull. Basically it is assumed {64} that striate cortex around the calcarine fissures and interhemispheric gap is near symmetrical and that the fissures are single furrows perpendicular to the (vertical) medial surfaces. Each quadrant of the visual field is then represented by a portion of striate cortex of right-angled transverse

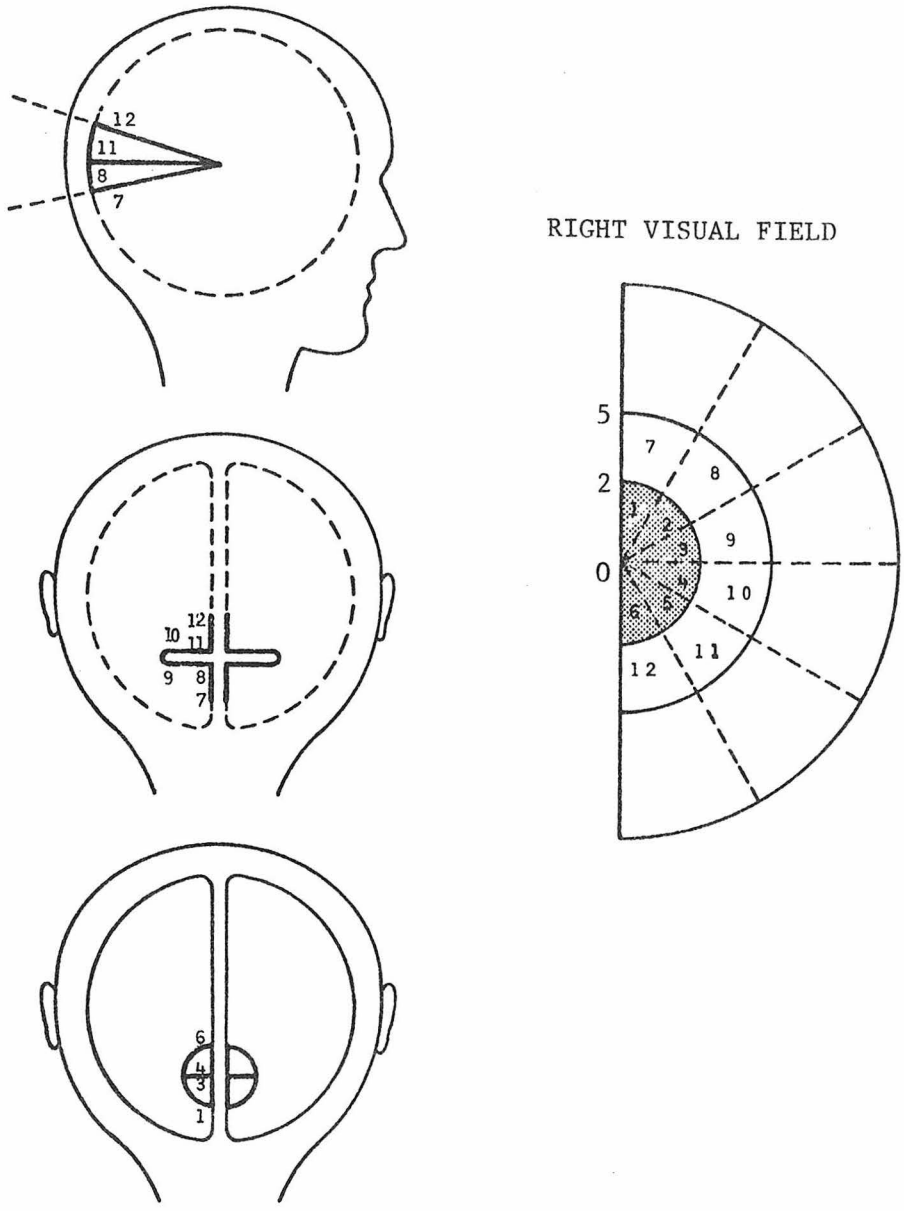

Fig. 8 - The cruciform model of human striate cortex

cross-section, whose horizontal and vertical 'arms' respectively represent the horizontal and vertical octants of the visual field beyond about 2° eccentricity. The portions of the visual field from 0° - 2° eccentricity are represented by appropriate sectors of the posteriolateral striate cortex. The relative contributions of calcarine and posteriolateral tissues will be assumed to be as shown in Fig. 5c.

This idealized model predicts that various half field and quadrant stimuli will each activate surfaces of different orientations in the head and that complementary stimuli (e.g. left vs. right half field, upper vs. lower half field, upper left vs. lower right quadrant) will activate surfaces of opposite orientation. A lateral half field (e.g. 5° radius) would activate all of posteriolateral and portions of medial and intracalcarine striate cortex in the contralateral hemisphere. Using the normal dipole layer approximation to active cortex (section 2.1.5), one would expect the intracalcarine portions to cancel electrically, leaving the posteriolateral and medial portions. A vertical half field stimulus, on the other hand, would activate posteriolateral, medial and intracalcarine striate cortex bilaterally either above (lower half field) or below (upper half field) the level of the calcarine fissure. Here one would expect the medial portions to cancel electrically, leaving the intracalcarine and posteriolateral portions. A quadrant stimulus would be expected to activate posteriolateral, medial and intracalcarine cortex unilaterally either above (lower quadrant) or below (upper quadrant) the level of the calcarine fissure.

2.3 The Origin and Topography of VEP's

2.3.1 Direct Cortical Measurements

Visual studies utilizing direct cortical recording on humans are sparse and in most cases have been done using macroscopic electrodes in conjunction with blank flash or other spatially unstructured stimulation.[15] For instance, Morrell {93} has carried out cortical recording in humans and observed localized desynchronization of ongoing (alpha) activity in striate cortex in the region of the calcarine fissure when various sectors of the visual field are illuminated. These were consistent with the visuotopic mapping between the visual field and striate cortex. Using full field stimulation and multielectrode depth recordings in humans, Chatrian et al {94} and Perez-Borja et al {95} found that responses to light in the occipital lobe were focused in the calcarine region. This held true for patterned stimulation, steady illumination, single flashes of light and repetitive flashes of light. Although the form of the response to each of these forms of stimulation was somewhat different, nevertheless the focus of the response was limited to discrete areas in and around the calcarine fissure. Hirsch et al {96} found similar results using the same methods, but also noted visual evoked potentials on the external surface of the occipital lobe. However, the responses had their greatest amplitude opposite the calcarine fissure. Corletto et al {32} measured flash-evoked potentials on the scalp and in visual cortex below and found that they had the same waveshape. When flash evoked scalp potentials were again

---

[15] This is unfortunate since there is abundant evidence that such stimuli are not appropriate to the majority of primary cortical neurons (see section 2.3.3).

measured following removal of the occipital lobe, initial and late components of the response were not affected, while components between 50 and 110 msec latency were greatly diminished.

In non-human primates, it has been found that if cortical VEP's are elicited by shining small spots of light (about 1°) on the retina, the initial response is a potential with a prominent positivity focused within a restricted field of striate cortex {33}. Using this method, the mapping of cortical VEP's with respect to stimulus locus has been plotted for various primate species. These mappings were for the most part in conformity with a striate cortical origin of this component {33}. However, the waveforms of cortical VEP's in humans often differ from those of animals and show dependence on such parameters as level of anesthesia (if used) and states of attentiveness {33}. Thus, results in animals may be extrapolated to humans only with extreme caution. Furthermore, animals often show high frequency oscillatory activity on the cortex which does not appear at the scalp, while humans show no such activity at either the scalp or cortical level.

2.3.2 The Effect of Lesions on Vision and VEP's

A number of studies have been done on the effect of lesions on human vision and scalp VEP's. As with the direct cortical studies, most of these have utilized flash stimuli. Vaughan {97} reported that subcortical geniculo-cortical lesions resulting in homonymous visual field defects abolished the initial surface positive component (40-80 ms) in response to flash stimulation in the affected half-field, but did not affect the response in the other half field. The concomitant negative deflection and subsequent waves for stimulation of either half

field were unaffected. From this he inferred that the initial component of the scalp EP was due to the geniculo-calcarine input to cortex. Lehmann et al {14} plotted VEP fields due to monocular full field flash stimulation in a subject with a split chiasm. Such a subject has his only direct input to visual cortex via ipsilateral routing. They found equivalent dipole sources which were located exclusively on the side of the head ipsilateral to the stimulated eye.

Vaughan and Katzman {98} have studied scalp EP effects due to retinal, optic nerve, optic chiasm, optic radiation and visual cortex lesions. They found in all instances that the flash EP was absent when a visual stimulus was placed in a retinal area which had to project through one of these lesions. They also reported that complete blindness associated with pregeniculate lesions produces complete loss of all responses to flash stimulation, whereas with bilateral geniculo-cortical lesions the initial surface postive component is lost, while later peaks persist. Kooi et al {99} gave similar results supporting the importance of the primary visual pathway in the production of early components of flash-evoked scalp potentials.

Some evidence as to the origin of scalp VEP's has come from investigations in which residual discrimination abilities following the ablation of striate and circumstriate cortical areas were studied. This presumably destroys the geniculo-striate-circumstriate pathway while leaving the colliculo-pulvinar-temporal neocortex pathway intact. For all mammals but man it is clear that gross differences in the intensity of illumination can still be distinguished after such ablation. Further, in monkeys with only circumstriate areas removed and striate cortex

intact, visual acuity and the ability to sort objects is preserved {100}. In addition, such a monkey will respond to moving objects, but is apparently blind to static objects. Brindley et al {101} have claimed that in humans who are considered to be cortically blind as a result of nearly total ablation of occipital lobe, only sudden changes in light level can be sensed. This observation would have the implication {69} that non-geniculate pathways are unlikely sources of cortical responses to constant luminance stimuli.[16] This is an important implication because constant luminance stimuli are used in the experiments presented in this thesis. However, Doty {80} has questioned this result on a number of grounds, the most important of which is that Brindley et al {101} did not properly test their subjects for their ability to distinguish simultaneous stimuli differing in luminosity. Also, the possibility remains that the conflict between human and monkey may be due to incomplete or diffuse brain damage in the human patients, rather than reflective of genuine interspecies differences {102}.

Additional evidence in this area comes from studies of visual evoked potentials in cases of complete blindness due to cerebral lesions. A number of investigators have been able to record evoked potentials to diffuse light stimuli in cortically blind subjects {103-105}. Although there is agreement that flash-evoked potentials can be recorded, there are contradictory results as to their nature and distribution over the scalp. Kooi and Sharbrough {103} found a response

---

[16] A constant luminance (or luminance-balanced) stimulus is one in which the stimulus event involves no change in overall luminance in spite of local luminance changes. This type of stimulus will be discussed in the next section (2.3.3).

in the region of the vertex, but were unable to find any response in the occipital region, while Spehlmann et al {104} found responses of long latency in the occipital region. Bodis-Wollner et al {105} recorded an essentially normal flash response in the occipital region. These discrepancies are probably due to the differences in the cortical lesions producing the blindnesses. Spehlmann et al {104} reported post-mortem findings showing bilateral damage to the optic radiations and postulated a non-geniculostriate origin for the responses that they recorded. Bodis-Wollner et al {105} estimated where the lesions were by performing computerized tomography (CT Scan) on their subject and concluded that there was extensive and perhaps complete destruction of the occipital lobes except for parts of the striate cortex. Although the accuracy of their interpretation of the CT Scan might be questionable, there is the implication that flash responses to diffuse light stimuli can arise from striate cortex and/or the accessory pathway. Bodis-Wollner et al {105} also recorded occipital potentials of normal amplitude and waveform from reversing sinusoidal gratings of low spatial frequency. This might have implications for the role of striate cortex in the production of evoked potentials by constant luminance stimuli. Since their subject was completely blind to the extent that he had no behavioral response whatever to visual stimuli, this may also speak for the role of striate cortex in the production of behavioral responses. However, since there is not hard evidence that the striate cortex of the subject was functional, a non-striate origin is not eliminated. In fact, such an origin might explain their observation that there is no response to patterns of spatial frequency greater than about 4 cycles per degree.

Alternating patterns of low spatial frequency cease to be luminance balanced stimuli at some unknown point when local luminance imbalances become significant. Thus, coarser patterns may be treated as flash stimuli locally.

There has also been a considerable number of experiments on animals which may be useful for comparative purposes. For instance, Vaughan and Gross {106} have studied the effects of various selective lesions on cortical VEP's in monkeys. They found that their form was similar to that recorded cortically in humans {97} and concluded that the wavelets recorded in striate cortex reflected the geniculo-calcarine input, but that some of the slower components were derived from a contralateral input (possible cortico-cortical via prestriate cortices and corpus callosum). On the other hand, Cohn {107} found in monkeys that almost normal visual evoked potentials could be recorded following various injuries to visual cortex and the geniculo-cortical optic tract. From this he concluded that the visual EP to flash in the intact animal does not reflect the classical anatomical visual pathway to striate cortex via the LGN. In man, however, Corletto et al {32} reported that total ablation of the occipital pole in man caused greatly diminished amplitudes in certain early components of the scalp and cortical flash EP.

Although lesion studies have generally supported the geniculo-cortical pathway as the primary source of early componenets of flash-evoked scalp EP's in humans, much of the data is only suggestive and sometimes difficult to interpret. One reason that the story remains inconclusive is that few studies have shed any light on which cortical area or areas (e.g. striate cortex or extrastriate cortex or both) is

producing the response. Some investigators (e.g. {99}) have pointed to extrastriate cortical areas, largely due to their more extensive lateral representation in the brain and proximity to the scalp, indicating that contributions of striate cortex are dependent on the area of striate cortex which has lateral exposure (as opposed to medial or intracalcarine). Others have pointed to striate cortex (e.g. {53}), invoking volume conduction and other arguments, or (e.g. {64,65}) have theorized that striate cortex and extrastriate area 18 produce the first two components of the response, respectively. In any case, it is likely that the relative contribution of these areas would be different for responses due to patterned stimuli as opposed to responses due to flash stimuli. In fact, there has been a number of qualitative studies using luminance-balanced pattern stimuli (mostly in normal subjects), which have attempted to compare the topography of the response with the topography of striate and extrastriate cortex in an effort to tie these areas with specific components of the response. These studies will be discussed in section 2.3.5. This thesis follows a similar approach, but is designed to be more comprehensive and to make judgments on a much firmer quantitative basis.

2.3.3 The Stimulation of Specific Areas of the Visual Field - Patterned Stimuli

One goal of this thesis is to study the mapping between the visual field and visual cortex in the intact human. Local stimuli are required for this task. In other words, stimuli are needed which selectively stimulate specific areas of the visual field. This is not a trivial task, because any light passing into the eye is scattered to

a significant degree before reaching the photoreceptors {108}, thus making the precise location of a stimulus hard to define. Compelling evidence of this has been provided by investigators (e.g. Jacobson et al {109}) who have flashed spots of light on the blind spot and obtained VEP's and ERG's (electroretinograms) within the criteria for normality.

One method of surmounting this difficulty is to provide an adapting field along with the stimulus which is being presented, choosing the adapting field so that the areas of the visual field surrounding the stimulus are rendered insensitive to scattered light. This technique may be used successfully with either unstructured (diffuse) {109} or patterned stimuli {67,69}. Such a stimulus should give no response when presented to the blind spot.

The use of patterned stimuli in lieu of unstructured or diffuse stimuli has come to the forefront in recent years (reviewed by Regan {110}) and some striking differences between these two types of stimulation have become apparent. These differences will be discussed at length in the following two sections. It seems that patterned stimuli are much more potent stimuli to the visual system. This is in conformity with the single cell work of many investigators {89,111-113}, who stress that diffuse stimuli are effective in stimulating a very small proportion of cortical cells. Most cortical units investigated do not respond at all to this form of stimulus, and those that do respond only weakly.

The needs for patterned stimulation and stray light control have led to the use of constant luminance stimuli, in which the stimulus event is a change in the stimulus other than its luminance. The typical stimulus paradigm is to produce changes in pattern rather

than changes in overall luminous flux. One variant of this is the pattern reversal stimulus, in which the stimulus event consists in the exchange of two patterns which are negatives or complements of one another and have equal areas of light and dark patches. If the two patterns are balanced for equal average luminance and have a reasonably small patch size, there is a constant average amount of scattered light delivered to the retina. Thus, if the pattern to be reversed is located in a particular area of the visual field, its time-locked effects can be expected to arise from there. Another variant is the so-called pattern appearance/disappearance stimulus in which a pattern is exchanged with a uniform field or mask of the same size, shape and overall luminous flux. For example, a pattern of a specified luminance with equal areas of light and dark patches might be exchanged with a uniform mask of one-half that specified luminance. The exchange of the two patterns is typically performed in either a continuous fashion (e.g. sinusoidally) or in a stepwise fashion. The use of a continuously modulated stimulus involves the use of synchronous detection to extract the response, while stepwise stimuli utilize conventional time-locked averaging. Only the latter stimulation mode is use in this thesis, although the former may prove fruitful in future investigations.

2.3.4 The Dependence of Human VESP's on Retinal Region Stimulated - Unstructured Stimulus Fields

A number of investigators have shown changes in human VESP's for blank-field flash stimulation of different retinal fields. The claim has been made, but not completely supported, that the distribution of early components is consistent with their originating in striate

cortex {17}. Some discrepancies have been reported on the relative contributions of foveal and extrafoveal regions {109,114-118}. Some of these discrepancies can be related to scattered light problems resulting from the lack of an adapting surround {17}. Other discrepancies can be related to the cancellation of components resulting from symmetric stimuli, in conformity with the so-called 'cruciform model' (see section 2.2.6) of striate cortex. The most difficult results to reconcile are those of Jacobson et al {109} and Eason and White {117}. Jacobson et al {109} explored the horizontal meridian of the visual field using one degree spots of light on an adapting surround carefully selected to minimize stray light effects. They found that the response is at about 50% full amplitude at 5° eccentricity and negligible beyond 10° eccentricity. In contrast, Eason and White {117} also explored the horizontal meridian using one degree spots and similar background illumination, but found that the response was still at 50% full amplitude at 50° eccentricity. The striking difference in these results may be due to some subtleties of the stimulus used (Jacobson et al {109} used a white stimulus on a white background, while Eason and White {117} used red and blue stimulation on a white background) or the fact that recordings of Eason and White {117} were done in conjunction with the subject's performing a reaction time task, while the subjects of Jacobson et al {109} did not perform a task. It is more likely due to the different recording conventions used (Jacobson et al {109} placed an electrode on the midline 2 cm above the inion and referenced to linked earlobes, while Eason and White {117} placed an electrode 2.5 cm above and 2.5 cm lateral to the inion and referenced to the earlobe on that side). A resolution of this

controversy will likely await experiments that are similar, but which involve measurement of scalp potential distributions.

Studies involving flash stimulation of lateral and vertical half-fields and quadrants have also yielded some confusing results. Most of these studies again suffer for lack of more widespread electrode placements which might yield more definitive results. In addition, some investigators have not adequately controlled for stray light effects. Jeffreys {119} has found differences between some early components of upper and lower half field (9^{o} diameter) flash EP's. He also measured whole field EP's, noting that the waveshape was similar at all electrodes (there were 4 electrodes each 3 cm to the right of the inion and at 0, 3, 6 and 9 cm above the inion respectively) and showed no close correspondence with the sum of the half-field EP's. Using small test flashes in different retinal locations with the rest of the retina carefully adapted to avoid stray light effects, Schreinemachers and Henkes {120} report a polarity reversal of early VEP components for upper and lower half field stimulation. Reitveld et al {121} have performed experiments using flash stimulation of quadrants and half-fields while recording 2 cm above the inion referenced to the right mastoid. They found that both upper quadrants give roughly the same response, as do both of the lower quadrants, but that the upper and lower quadrants (or half fields) give very different responses in terms of latencies of early components. Nagata and Jacobson {122} have also reported that component latencies vary with retinal position of the stimulus. In flash stimulating lateral half fields, the response has usually but not always been found to be maximal over the contralateral hemisphere {123, 124}. Probably the most

definitive work along these lines was carried out by Nakamura and Biersdorf {67-69}, who studied polarity reversals associated with left and right half and quadrant blank field stimulation via an equipotential contour mapping technique. They found a strong contralateral component only during the early part of the response (before 100 ms) and noted that the potential distributions resulting from blank field stimuli were more skewed and asymmetric with respect to the midline than those resulting from patterned stimuli.

2.3.5 The Dependence of Human VESP's on Retinal Region Stimulated - Spatially Structured Stimulus Fields

The results are much clearer when spatially structured or patterned stimuli are used in lieu of blank flash stimuli. Although a number of studies investigating the dependence of the VESP on the retinal region stimulated have been done using patterned stimulation, only those which utilize some technique for control of scattered light will be considered here. Only by using such controls will the locus of the stimulus be definable. As will be seen, however, there can be substantial differences in responses to stimuli encompassing the same retina region but utilizing different stimulus modulation modes (e.g. reversal as opposed to appearance/disappearance stimulation or flash with adapting surround).

The issue of the contribution of the fovea, parafovea and periphery to visual evoked potentials is somewhat clearer for patterned stimulation than for blank flash stimulation. While blank field EP's may have appreciable extrafoveal contributions, pattern EP's are believed to be almost entirely due to stimulation of the central 6°

(radius) or so of the visual field {63-65,67,125}. This applies generally to pattern reversal, pattern appearance/disappearance and pattern flash (with adapting surround) stimulation schemes. The exploration of this question is aided by the use of asymmetric stimuli (e.g. sectors of circles or of rings), since radially symmetric stimuli (e.g. circles or rings) may invoke cancellation phenomena when expanded into peripheral areas of the visual field {17}. Some investigators (e.g. {126} have not accounted for this possibility.

Using patterned stimuli with stray light control procedures, it has been clearly demonstrated {62-69,125,127-130} that the polarity and magnitude of early EP components can change with the retinal locus of stimulation. These studies have also shown that the spatial distribution (over the scalp) of early EP components varies with retinal locus. These observations lend credence to the suggestion that changes observed in the EP reflect changes in the cerebral location and orientation of its source(s), rather than changes in the generative process at fixed source(s). In other words, it is suggested that changes in the EP are mainly a reflection of the topography of the mapping between the visual field and visual cortex. Polarity reversal effects and radical distributional effects often can be produced by a change in retinal locus amounting to only a few degrees, and are most often associated with reflections of the stimulus about the center of the visual field (e.g. left half field to right half field or upper half field to lower half field). It is indeed unlikely that two areas of the visual field which are identical in their relationship to the macula (i.e. same eccentricity), which are stimulated with the same pattern and which

are only a few degrees apart, would cause cortex to respond with processes of opposite polarity or radically different distribution. It is more likely that the two areas of tissue corresponding to these retinal areas respond with processes of the same polarity and that the two areas are oriented in different directions. As will be seen, the topography of the 'modified cruciform' model (presented in section 2.2.6) may provide an explanation for the polarity and distribution effects of stimulating different areas of the visual field with pattern.

There have been a number of studies using partial field pattern stimulation. Most have utilized vertical and lateral half-field stimuli {58,59,62-69,125,127-130}, but some have used quadrant and octant stimuli {58,59,62-65,68}. Some have varied the radius (both inside and outside) of these stimuli in an attempt to estimate the relative contribution of central and peripheral areas of the visual field {63-65, 67,125}. Many of these have made qualitative comparisions between potentials elicited by these stimuli and potentials generated by hypothetical dipole sources {57-66,125}. Unfortunately, none of the above investigators made quantitative estimates of their hypothetical sources, owing in part to the fact that they have not recorded from sufficient electrode positions to make such estimates {131}. A few have visualized potential distributions resulting from partial field pattern stimulation by a contour mapping technique {66-69,130}, but only one investigator {130} recorded from a sufficient number of electrode positions to get a reasonably complete description of the potential distributions. This investigator {130} made no attempt to estimate hypothetical sources. This thesis project combines many of the

features of the above investigators in the choice of stimuli, but potentials are recorded from a much larger number of electrodes than most previous investigators. In addition, a quantitative source localization scheme is tested and applied to these data.

Among the more complete of the previous studies are those of Jeffreys and Axford {64,65}. They obtained longitudinal and transverse cross-sections of the potential distributions (up to 16 electrodes) on the back of the head resulting from partial field pattern appearance/disappearance stimulation of 25 msec duration between appearance and disappearance. Utilizing a checkerboard pattern (14' check size) filling the halves, quadrants and octants of a 6° field, they identified two distinct and differently distributed components, both of which reverse polarity with upper and lower field stimulation. The first component (80 ms latency) shows a midline polarity reversal for left and right half-field stimulation and also shows consistent differences between adjacent upper and lower quadrants and between adjacent vertical and horizontal octants. In addition, the central and peripheral parts of these patterns were found to differ in their contributions to each of the two components. They suggested that the first component originates in striate cortex in and adjacent to the calcarine fissure, while the second component originates in extrastriate cortex. They based this interpretation on the relationship between cortical topography and the orientations of dipoles which might generate distributional cross-sections such as those which are measured. They also found that EP's due to full-field stimulation appeared to be roughly similar to the sum of the EP's to separate stimulation of upper and lower half-

fields. In general, the results obtained using patterned stimulation were found to be quite different from those obtained using blank-flash stimulation.[17] One subject of the four used showed a systematic departure from the others. They explained this in terms of the well-known {90} intersubject variability of calcarine cortex. Ristanovic {58,59} has obtained similar results using virtually identical methods.

Both Halliday and Michael {62} and Michael and Halliday {63} obtained differing results using partial field pattern reversal stimulation. Using 10 electrodes and a checkerboard pattern (50' check size) filling the halves, quadrants and octants of a 14° to 18° field, they confirmed the polarity reversal for upper and lower half and quadrant fields. However, they did not confirm a result of Jeffreys and Axford {64,65}, who found that adjacent horizontal octants gave a clear polarity reversal with respect to one another. They {62,63} instead found that vertical octants from the same half-field gave strong polarity reversals, a result which is unexpected since the striate cortical representations of such octants are roughly parallel to one another. As a result they suggest that both components originate in extrastriate cortex. Since extrastriate cortex does not include opposing surfaces, an explanation of the remaining polarity reversal results was required. They suggested two possibilities. The first invoked the fact that the extrastriate cortical representations of the upper and lower visual field are on the undersurface and upper convexity of the occipital lobe,

---

[17] On the other hand, Nakamura and Biersdörf {67-69} claim that the responses to blank field stimuli are not radically different from those to patterned stimuli when an adapting surround is used.

respectively. The second invoked processes of opposite polarity in the same regions of extrastriate cortex. The first hypothesis found the most support in their latest study {63}. In further conflict with Jeffreys and Axford {64,65}, they found a general agreement of results obtained using patterned stimulation and those obtained using blank-flash stimulation. Also, they explain their intersubject variability in terms of referencing problems, as opposed to variable cortical topography.

It is difficult to compare the data and conclusions of Jeffreys and Axford {64,65} with that of Halliday and Michael {62} and Michael and Halliday {63} as they present it. However, there are a number of differences between the two experiments and their analysis methods which may help account for the discrepancies. As previously mentioned, they used different check and pattern sizes and different stimulus paradigms. In the former {64,65} EP amplitudes were measured from a baseline, while in the latter {62,63} EP amplitudes were derived from a peak-to-peak measure between succeeding peaks. Ary {69} has pointed out that the second difference may be crucial, noting that it appears that Halliday and Michael {62} used both of Jeffreys and Axford's {64,65} peaks to locate one source in extrastriate cortex. Estevez and Spekreijse {132} have forwarded another explanation based on the intrinsically different nature of pattern appearance/disappearance and pattern reversal stimuli. They note that the pattern appearance/disappearance stimulus is dominated by contrast increase, while the pattern reversal stimulus is dominated by contrast decrease.

The work of Nakamura and Biersdorf {66}, Biersdorf and

Nakamura {67} and Biersdorf {68} embodies the combination of partial field pattern stimulation (pattern flash on adapted surround) and potential distribution analysis (via equipotential contour mapping). The maps were used to infer possible sites and orientations of hypothetical dipole sources. They used both hemifield and quadrant stimuli and reported results which were in substantial agreement with Jeffreys and Axford {64,65} with respect to the first EP component. The mapping technique allowed a much less ambiguous interpretation of the results in terms of inferring their sources, but these interpretations remained crude and qualitative due to the relatively small number of electrodes (16) used in deriving the maps. Ary {69} and Lehmann et al {130} also have combined partial field stimulation with equipotential contour mapping. Ary {69} studied distributions due to lateral half field stimulation (pattern flash on adapted surround) using 28 electrodes, while Lehmann et al {130} studied distributions due to reversing vertical half fields using 48 electrodes. Their results do not conflict significantly with those of the previous investigators.

3. METHODS

3.1 Stimuli

A stimulation system (Fig. 9) was constructed for these experiments which could provide either appearance/disappearance or reversal stimuli in a sharply stepped fashion. This apparatus was basically a two channel Maxwellian viewing system {133} with the light in each of the two channels being modulated in antiphase. The modulation was accomplished by the use of two linear motion vibrators (C_1,C_2) which carried knife-edges and which were driven 180° out of phase with one another. These knife-edges traveled over small (1 mm) pinholes (PH), on which were imaged, in reduced form (via L_1), the filament of a high intensity quartz-halogen lamp. The lamp was powered by a highly regulated d.c. power supply. Diffusers (D) were placed on the lamp side of the pinholes to remove any remnants of the filament structure from the image. Collimating lenses (L_2) were placed one focal length from the pinholes to produce beams of parallel light. The intensities of these beams were uniform across about two-thirds their radius, which was sufficient, since only about one-half of their radius was used in producing the stimulus. The intensity of each beam was proportional to the area of its pinhole which was open at any particular time, so that by driving the two knife-edges in antiphase, the total luminance of the two beams could be held constant. The intensity of each beam could be adjusted using iris diaphragms (ID_1, ID_2) and neutral density filters (F_1,F_2). The color of the two beams was matched using color-compensating filters (CF_1,CF_2).

Each channel of parallel light was incident on a separate slide

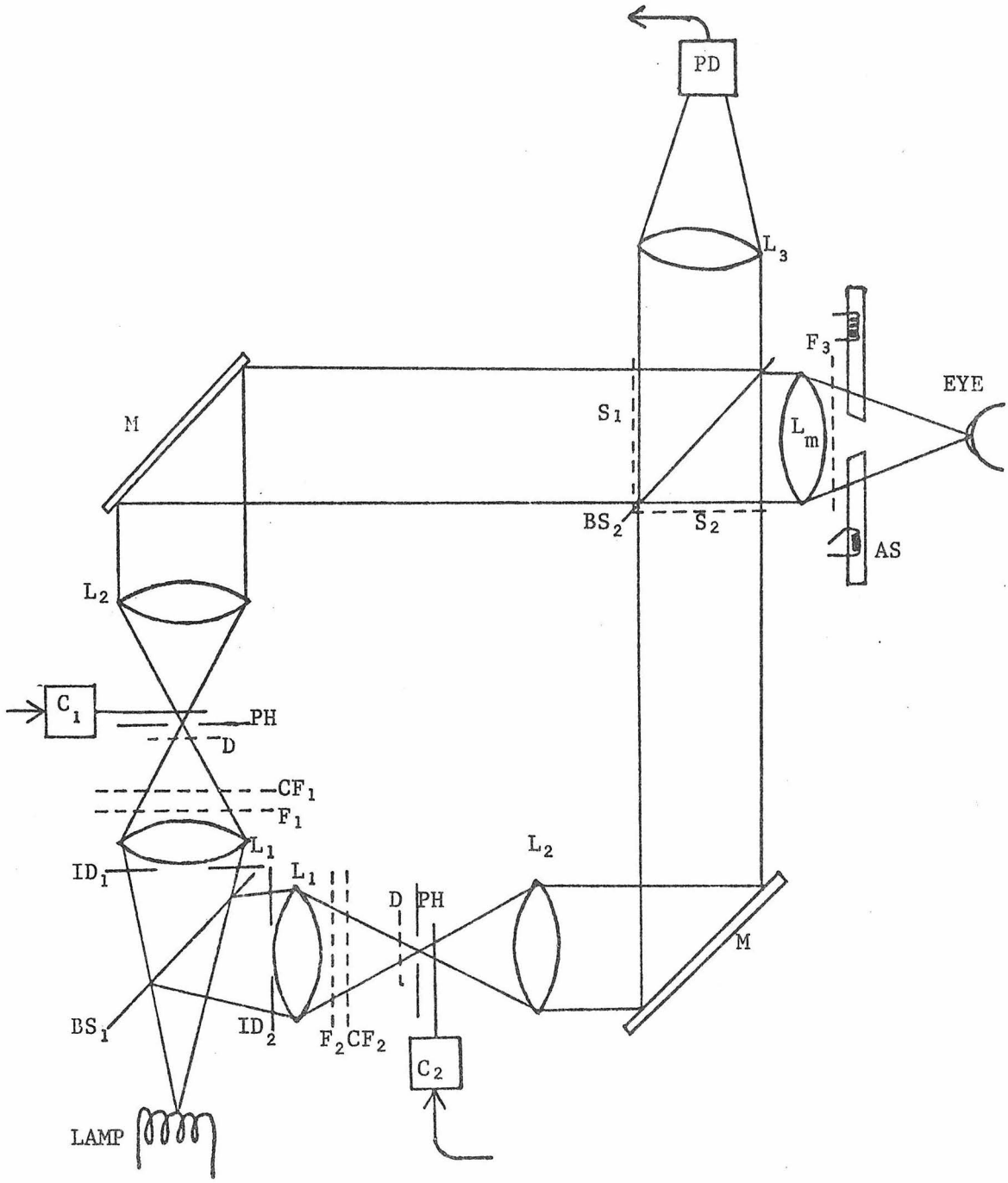

Fig. 9 - Stimulation system

(S_1,S_2), which was mounted on a movement for alignment purposes. The two images were then joined by a pellicle beamsplitter (BS_2) and presented in Maxwellian view (at infinity) to one eye[18] of the subject by use of an intervening lens (L_m) placed at its own focal length from the pupil of the eye and the slides (S_1,S_2). Color filters (F_3) could be placed between the Maxwellian lens (L_m) and the eye. The subject's eye was held in position through the use of a bite board. The system had a 20° diameter clear aperture and, due to the high efficiency inherent in Maxwellian viewing systems {133}, could be operated over a very large range of luminances. A 20° inside diameter and 120° outside diameter diffuse adapting surround (AS) was also provided (d.c. powered), since there were plans to investigate the effects of adaptive state.

The luminance balance of the two channels was very carefully adjusted and maintained. This had to be done in both a static and dynamic fashion, since a luminance artifact associated with the stepwise change of the two channels would have been unacceptable. This could be done very precisely by placing a Gamma Scientific (Model 2000) wide angle telephotometer in the same place as the subject's eye would be and alternating the stimulus. Later, a lens (L_3) and PIN diode (PD) were permanently placed in the system for continous balance monitoring. Balance could also be checked psychophysically by having the subject defocus the stimulus pattern with a diffuser and adjust the beams

---

[18] Monocular stimulation was used here because little difference is seen between VEP's obtained from left and right eye stimulation of subjects with normal vision. Responses to binocular stimulation are usually larger in amplitude, but similar in form and distribution {44,115}.

for a brightness match with the stimulus alternating. The psychophysical check could be done very quickly and was nearly as accurate as the electronic method. As such, the psychophysical procedure was carried out periodically and whenever any changes were made in the stimulus. Adjustments were seldom necessary except when the stimulus was changed.

The pattern appearance/disappearance stimuli used in these experiments were light[19] and dark checkerboards (S_1) which were alternated with a uniform (light) mask (S_2). These patterns (Fig. 10) occupied either the whole of a 10° area in the center of the visual field or one of its constituent halves, quadrants or octants (see section 2.3.5). Each check subtended an 18' arc. Each light check had luminance L, while each dark check had luminance ε. The mask (S_2) had luminance $(L + \varepsilon)/2$. Except as otherwise noted, the value of L was always adjusted to be 20 footlamberts and ε .5 footlamberts, making for a contrast of 95%. The checksize of the stimulus was chosen in accordance with the knowledge that the largest responses are obtained for checksizes between 10' and 20' of arc {135}. Color was introduced because response distributions are known to depend on stimulus color {69}. Both the pattern and mask contained a fixation target consisting of cross-hairs and two concentric rings (½° and 1° diameter, respectively). Fig. 11a shows the time course of the stimulus event, which lasted 30 msec in most of the experiments reported here. The switching

---

[19]The light checks were red in most of the experiments reported here. This was done by making F_3 (see Fig. 9) a Kodak #25 Wratten Filter. The blue checks used in some of the experiments were produced using a Kodak #48 Wratten Filter.

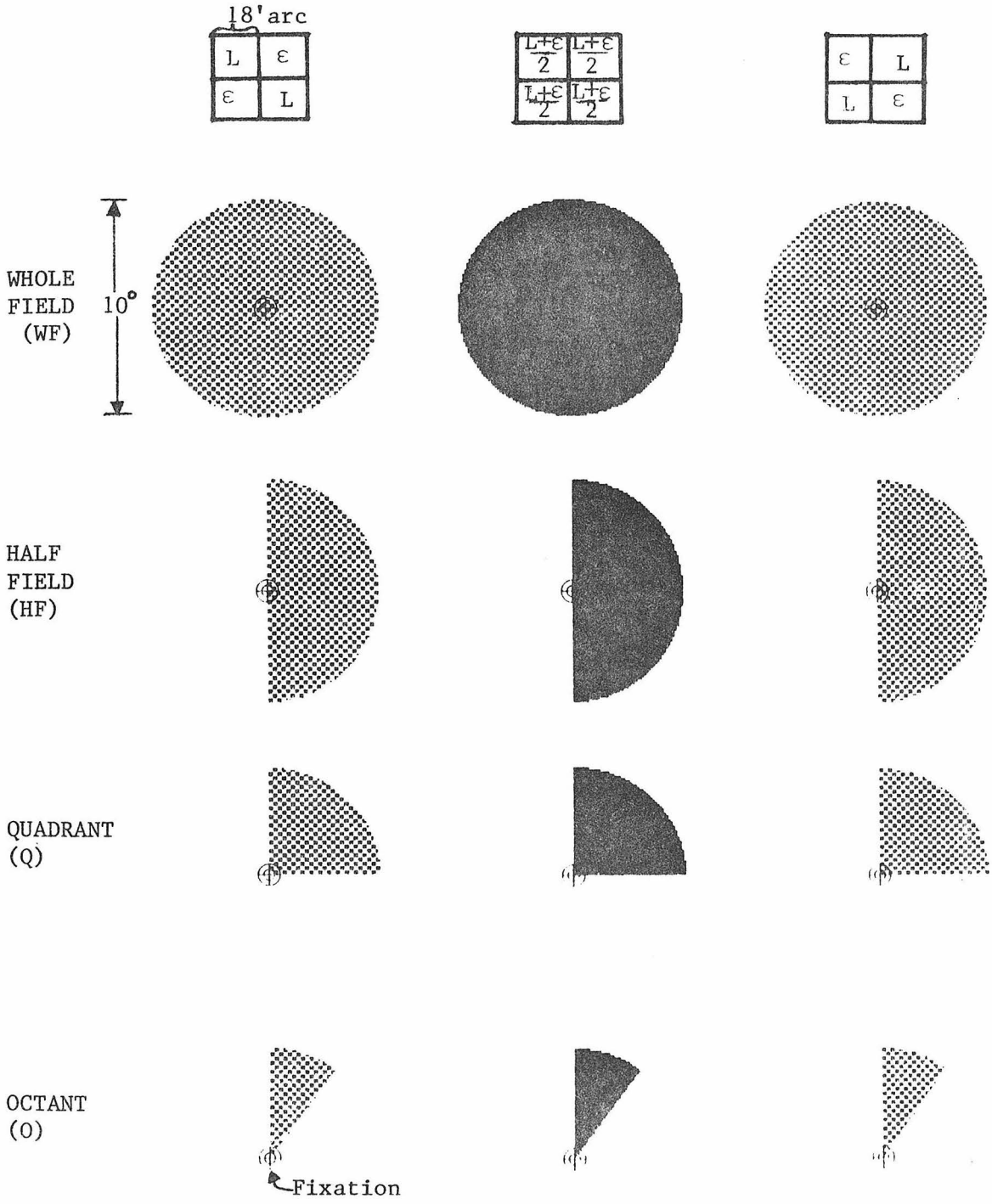

Fig. 10 - Partial field pattern stimuli.

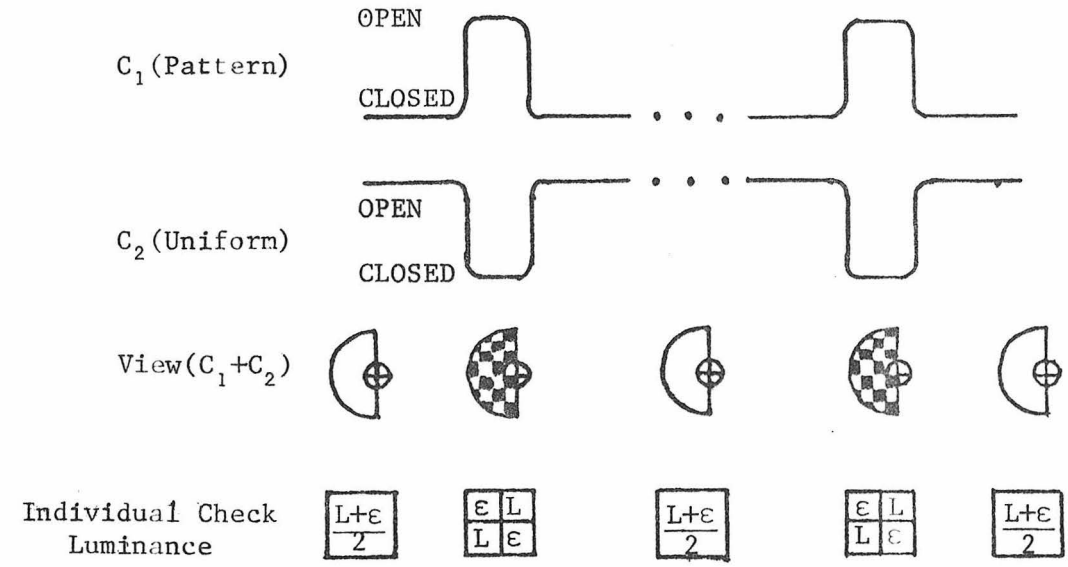

Fig. 11a - Pattern Appearance/Disappearance Stimulus

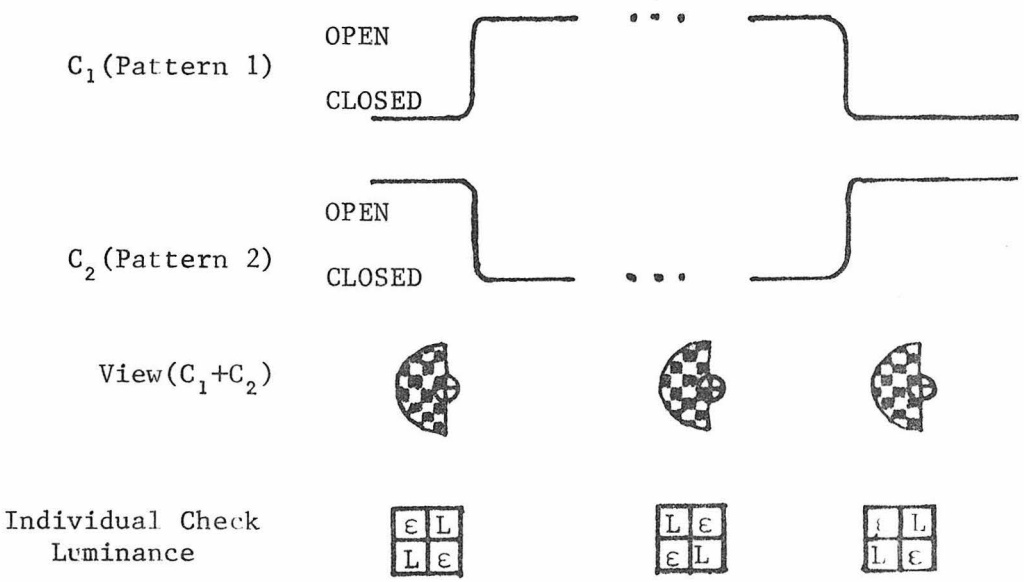

Fig. 11b - Pattern Reversal Stimulus

time of the stimulus was 3 msec. The stimulus events had a random spacing to minimize rhythmic and carry-over effects (see section 3.3.2).

The pattern reversal stimuli used in these experiments were light and dark checkerboards (S_1) that were alternated with other light and dark checkerboards (S_2). The second checkerboard (S_2) was the complement of the first checkerboard (S_1) in that all checks which were light in the first (S_1) were dark in the second (S_2) and vice versa (Fig. 10). The two checkerboards were identical to each other in all other respects. As a result of their equal areas of light and dark checks, luminance balance could be achieved by setting the check luminance in both patterns equal to L. All other characteristics of the two patterns were identical to those of the pattern (S_1) used in the appearance/disappearance stimulus. Fig. 11b shows the time course of the stimulus event, which was sharply stepped and had a random spacing.

3.2 Data Collection

3.2.1 Helmets and Electrode Placements

Scalp potentials evoked by the previously described stimuli were measured using a large number of electrodes placed on the scalp. To facilitate rapid and repeatable placement of electrodes, custom-fitted plexiglass helmets were made for each subject (Fig. 12). Holes were cut in these helmets in many positions so as to encompass most conceivable electrode placements. Only a portion of these were used in a particular experiment; the rest were left open for ventilation purposes.

The electrode layout on each subject was designed so as to be

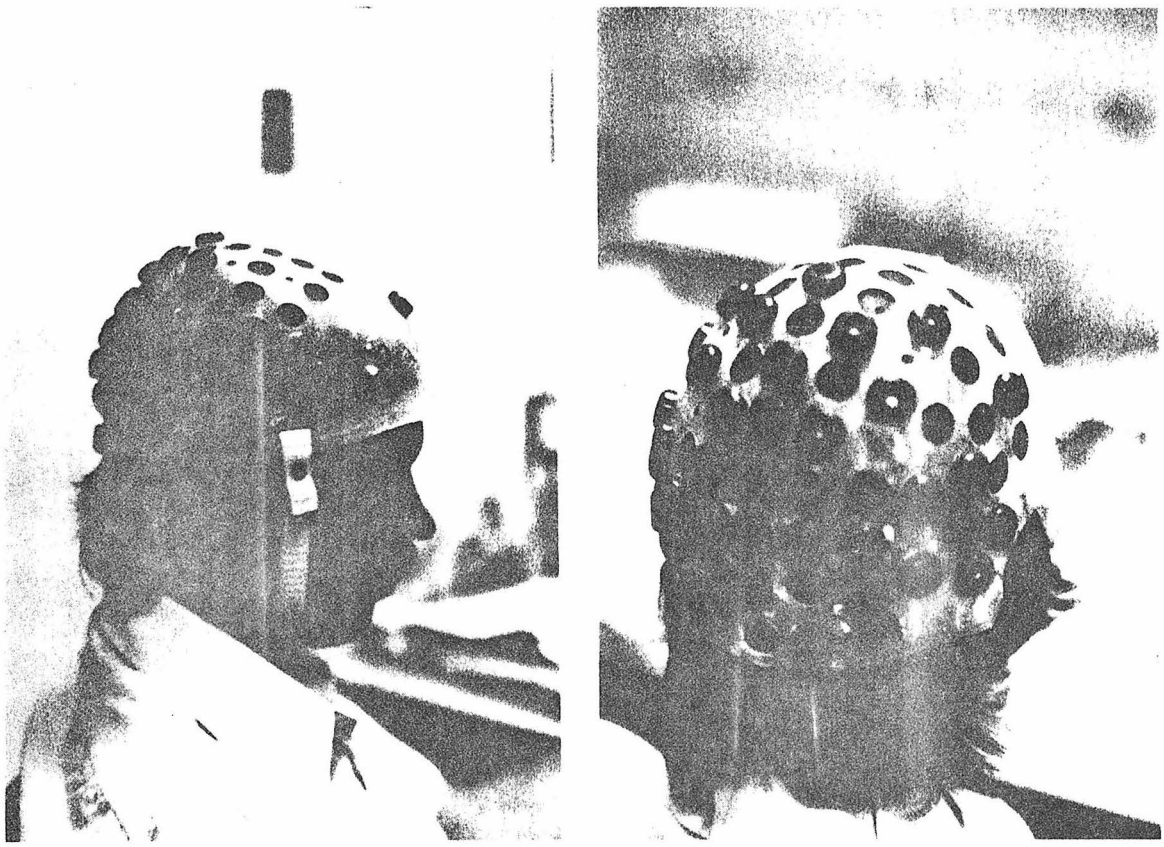

Fig. 12 - Helmet and electrode holders

in conformity with that sphere that best approximated the back of his head. This was done because a spherical model of the head was to be used in the data analysis, and it was thought that the model ought to be most accurate on the back of the head, where most of the responses to visual stimulation occur. To find the hypothetical sphere which best approximated the back of the head, a center-finding device was constructed. This consisted of a telescoping shaft with a ball on one end and a universal joint at the other end. The universal joint was clamped in place, but its position could be changed by means of a 3-D micromovement. This device was used on the inverted helmet mold, and radii and centers could be repeatably found to within a few millimeters. Once the center and radius were found, they were projected out the sides and rear of the helmet and used to lay out on the helmet an equiangularly spaced array of electrode holes (Fig. 13). The positions of these holes were repeatable to well within the size of an electrode and made up a globe-like spherical coordinate system with the 'north pole' near the right ear and the 'equator' corresponding to the midline (i.e. the locus of points midway between the ears). This coordinate system was convenient for modeling purposes and gave a fairly uniform layout in the occipital region. The electrode spacing (Fig. 14) used was 15° and angles measured ear-to-ear designated θ(θ negative towards the left ear and positive towards the right ear), while angles measured along the midline were designated ϕ($\phi=0^{\circ}$ at the inion level and ϕ positive above the inion level). On the helmet were also marked various landmarks of the head (inion, nasion, vertex), so that the helmet could be placed in the same position

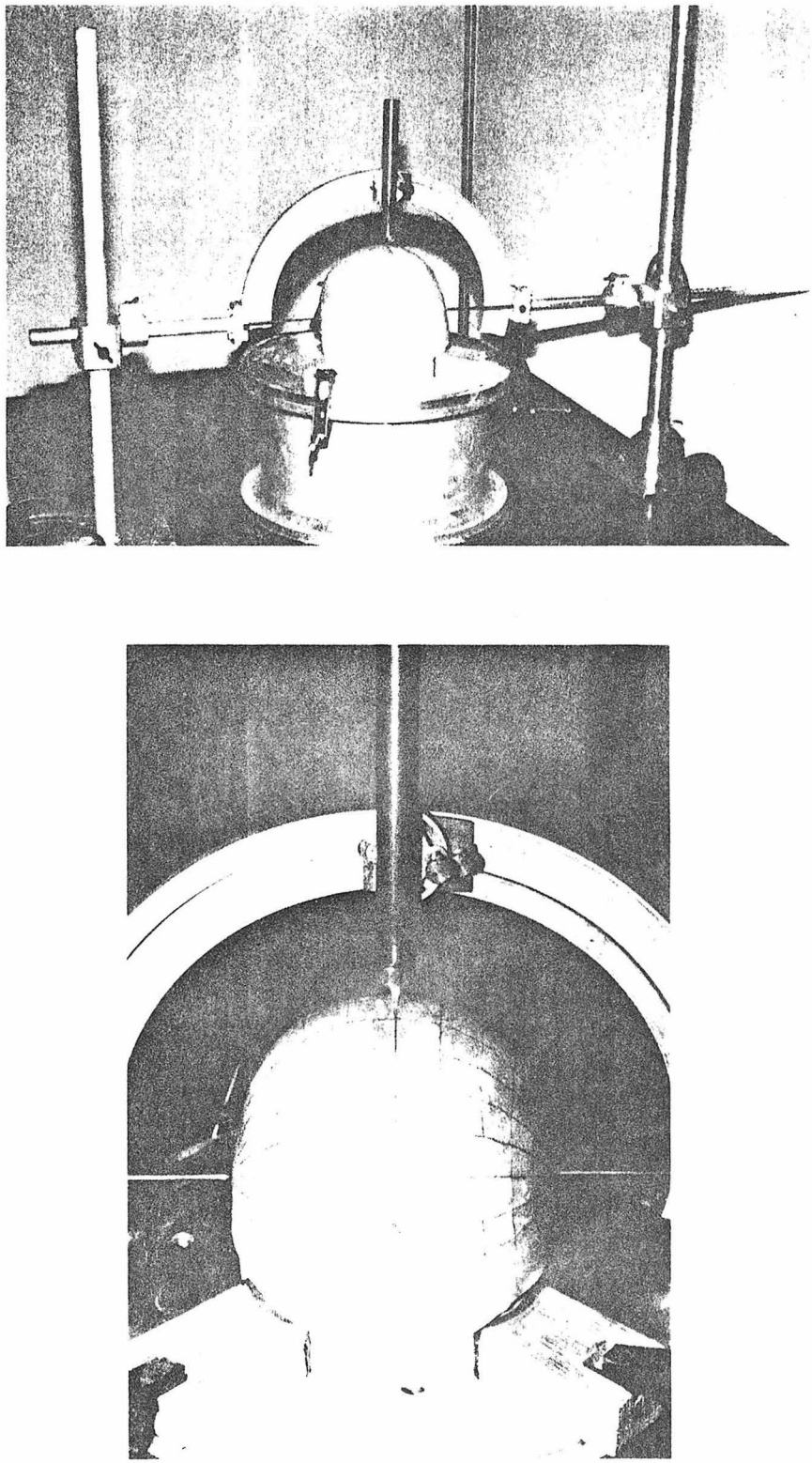

Fig. 13 - Apparatus for laying out electrode arrays

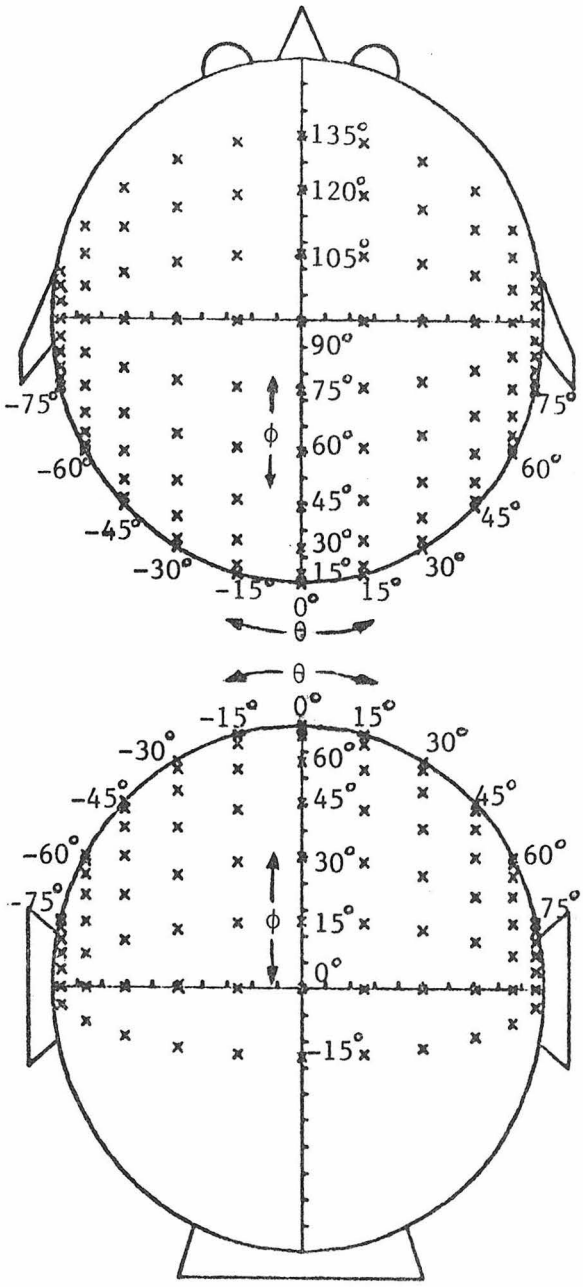

Fig. 14 - Equiangular electrode layout (15° spacing)

each time. The helmet was held in place by an elastic chin strap and also by virtue of its having a close fit to the subject's head.

The helmets served not only as a template for electrode layout, but also as a structural element whereby electrodes could be held stably in position. The latter was accomplished by the use of flanged rubber plugs which could be inserted into selected holes (Fig. 12). In the center of each of these plugs was a hole into which an electrode could be pressed and held in place by friction between the rubber and electrode. The electrodes used were silverplated brass cylinders with cups on one end and solder joints on the other (Fig. 15). They were silver/silver chlorided. Wires ran from each of these to an amplifier system (Fig. 16).

Electrode sites were prepared with the helmet in place, using HP Redux Paste as an abrasive to break down skin resistance and Grass Type EC-2 electrode paste to achieve electrical contact between electrode and scalp. Once all electrodes had been placed, the impedance of each was measured using a Grass Model EZM1D Electrode Impedance Meter. If an electrode read greater than 10 KΩ, the site was cleaned out and prepared again. Impedances were often rechecked after an experiment was complete and somtimes during an experiment if a particular electrode was exhibiting unusual activity. Data taken from a rare bad electrode were rejected.

Forty electrodes were used in the experiments presented here, with most electrodes placed on the back of the head. At various times two different electrode arrays were used on each of the three subjects (JPA, PDP, and RML) as illustrated in Figs. 17 and 18.

Fig. 15 - Electrodes used for these experiments

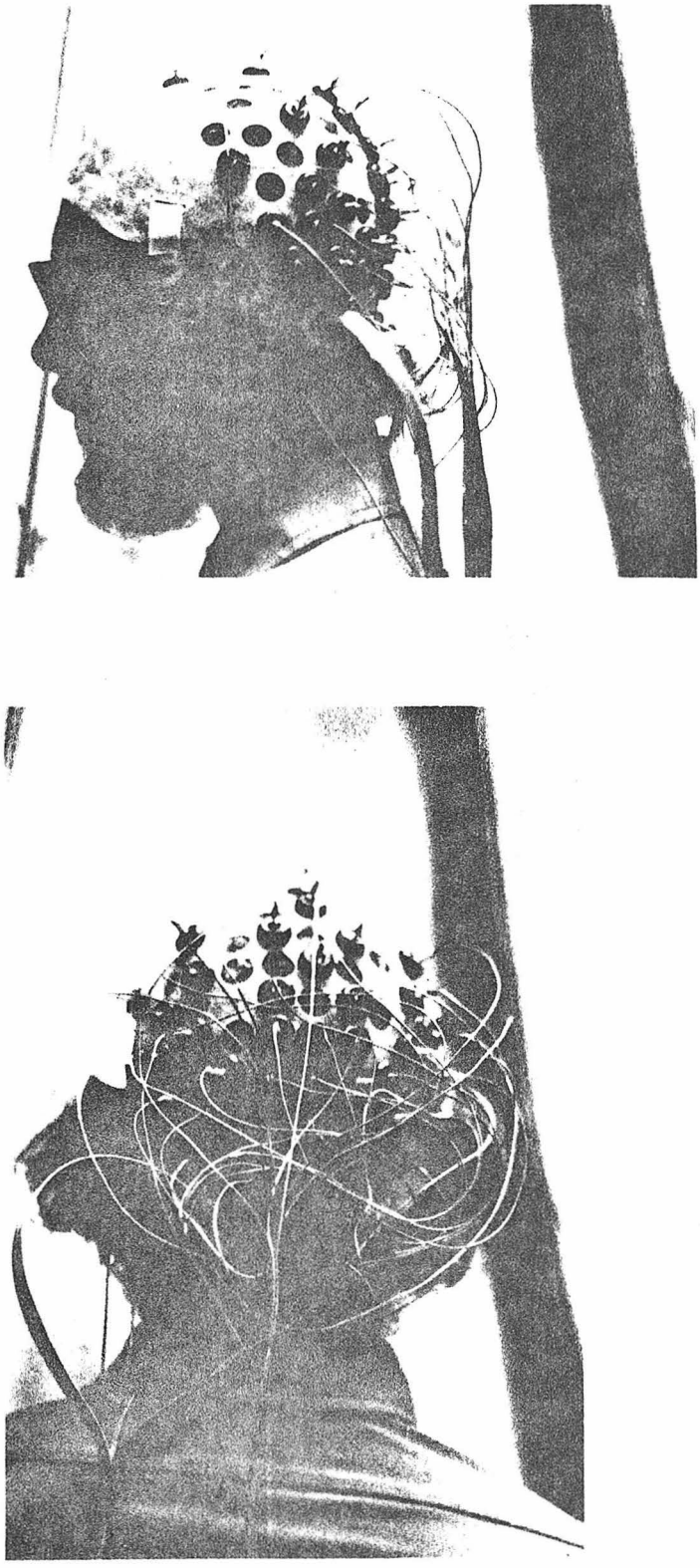

Fig. 16 - Helmet and electrodes in place

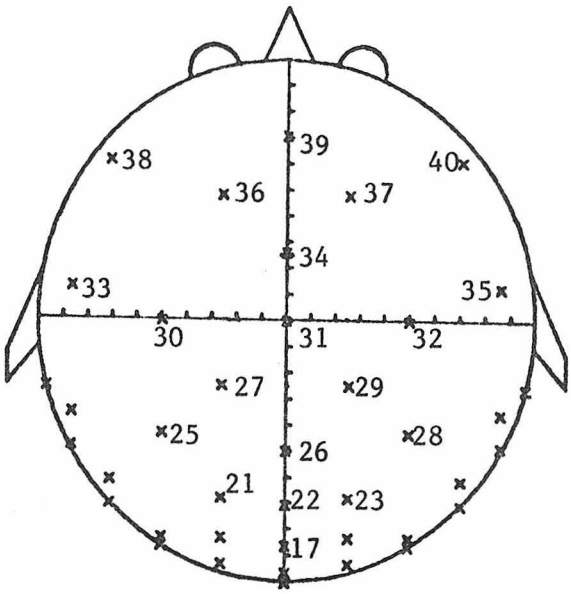

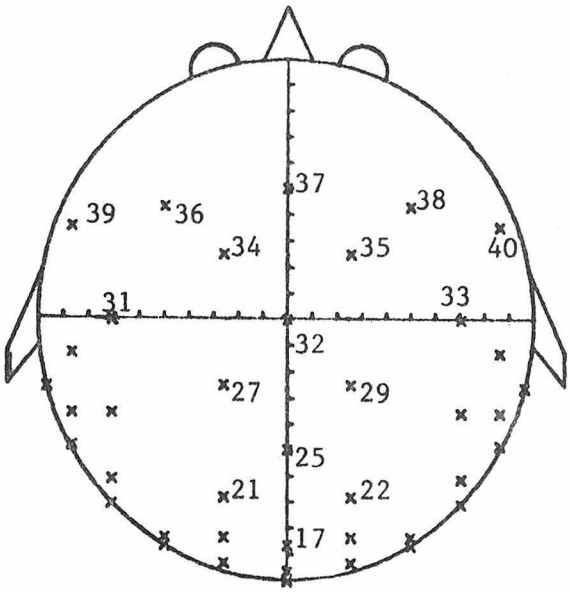

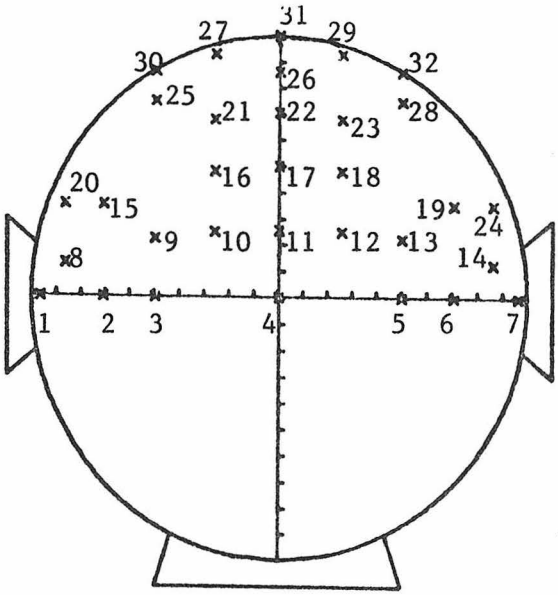

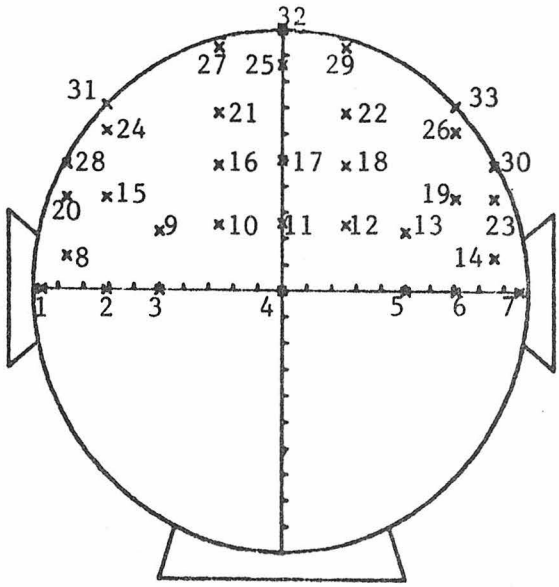

Fig. 17 - Subject JPA electrode layout 1

Subjects PDP, RML electrode layout 1

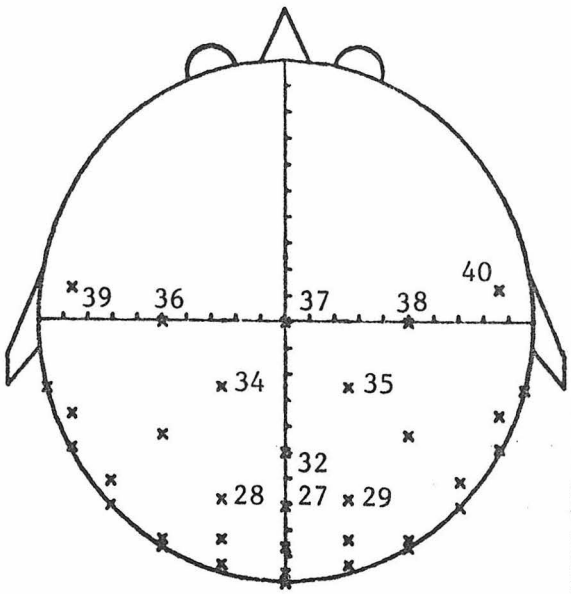

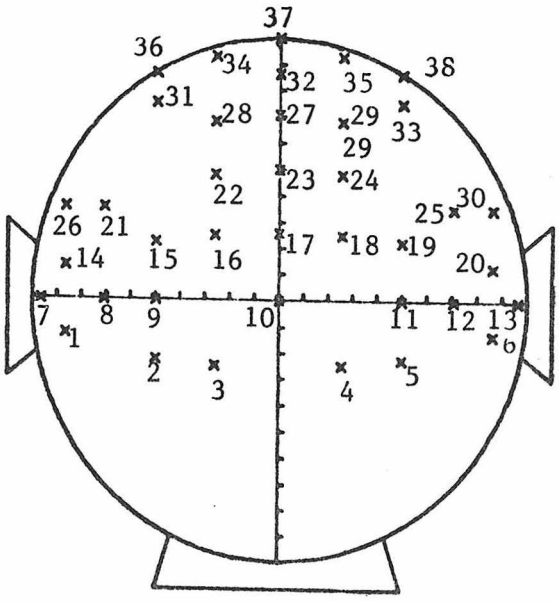

Fig. 18 - Subject JPA electrode layout 2

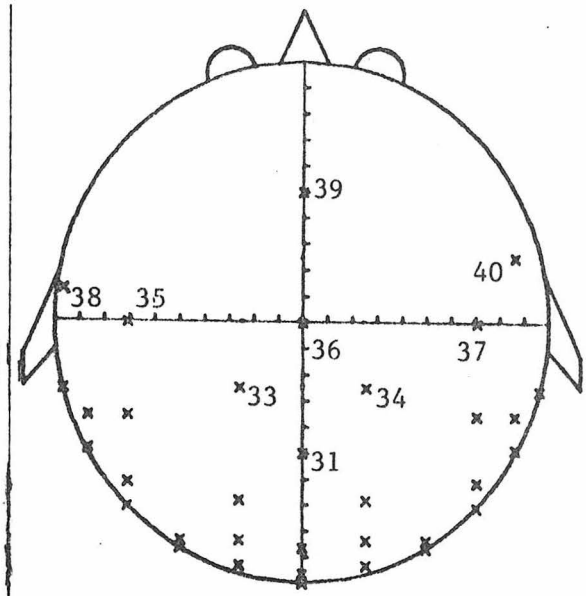

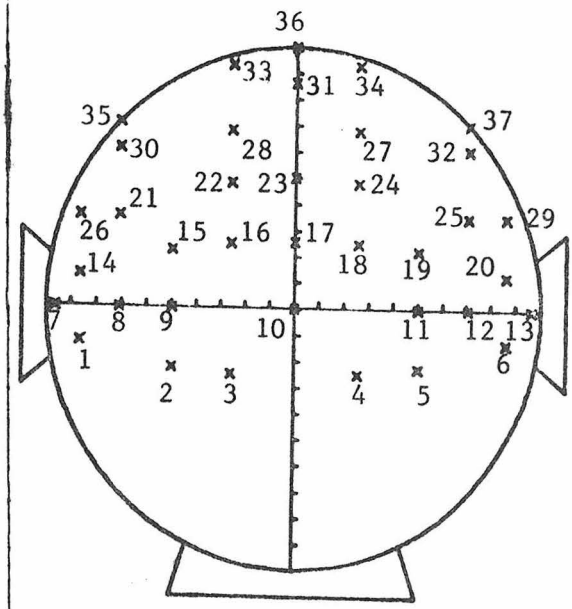

Subjects PDP, RML electrode layout 2

3.2.2 Referencing

Because potentials are really potential differences, measurements at each electrode must be referred to some reference or reference electrode. The choice of a reference for evoked potential recording has been the subject of much discussion, but to date no completely satisfactory solution has been agreed upon. Thus, this problem will be discussed at some length here.

Ideally, one would like to find a reference which allows measurements to be taken in the absence of excessive noise and which is indifferent in that its value is relatively unchanged by the stimulus event. It will be seen that these are competing objectives, which are difficult to achieve simultaneously. The amplification process must somehow reject the very large extraneous potentials[20] which exist at each electrode. Among these are fluctuations caused by physiological signals such as the EKG (Electrocardiogram) and electrical interference caused by line voltage (60 Hz). If these signals are nearly identical at the reference and the active electrode, then the common mode rejection property of the differential amplifier will be utilized fully and the signals of interest will not be obscured by noise. Thus, the choice of a reference which is as far from the active electrode as possible (e.g. somewhere on the body other than the head) to insure indifference, is not acceptable in most cases because the likelihood of large extraneous signals being identical at the active and reference electrodes decreases as their spacing increases. On the other hand, a reference electrode

---

[20] These extraneous potentials may often be 100 to 1000 times the size of the EEG.

placed as close as possible to the active electrode is most often not indifferent.

Note that the selection of a reference is different from the selection of a zero potential point. This can be illustrated {136} by recalling that the potential at the surface of a volume conductor containing a known distribution of current sources can be found only to within an additive constant. Thus, the question of choosing a zero potential point is equivalent to the choice of this constant and there is no fundamental advantage of one choice over another {136}. On the other hand, the selection of an indifferent reference will depend on the geometrical and electrical characteristics of the volume conductor and the source or sources within it.

The fact that the choice of a zero potential point is arbitrary, leads to the point that, in theory, any referencing scheme is adequate for the determination of model source locations and orientations. The essential information for estimating these parameters is a knowledge of the shape or topography of the potential distribution, not its absolute values. Thus, potential gradient information or, more particularly, the zeros and turning points of the potential gradient are sufficient {55,71}. The locations on the head of these features are independent of the behavior of the reference electrode. Measurements of the potential difference between any pair of electrodes gives information about the gradient of potential between them, or in other words, that component of the electric field vector which lies along the line between the two electrodes.

However, if one wishes to compare the relative magnitude of

activity at successive times, an indifferent reference is desirable. A reference which varies with time may cause errors in the estimation of relative magnitude. For example, a reference which itself responds to the stimulus may diminish or enhance measured values, making temporal comparisons unreliable. Another motivation, but from a practical point of view, is that measurements relative to an indifferent reference are much easier to interpret intuitively.

In theory, the rejection of large extraneous potentials in the amplification process is unnecessary, since these may be removed in the averaging process. However, from a practical point of view, they must be removed by the common mode rejection property of the amplifier. This is so because of their size is often huge[20] relative to the EEG, making it difficult to amplify the signal enough to extract evoked potentials, while using the amplifier in its linear operating range.

In the face of these considerations, three referencing schemes have come into general use in the measurement of evoked potentials {137}. These are: (1) bipolar referencing, (2) monopolar referencing, and (3) average referencing.

The bipolar method bypasses the problem of an indifferent reference by taking as signal the difference between a pair of (usually) adjacent electrodes. If the two electrodes are close together, this approach gives a direct approximation of the gradient of potential in the region between the two electrodes. The advantage of this method is that, if the two electrodes are sufficiently close together, optimal advantage is taken of the common mode rejection property of the differential amplifier. This method has the disadvantages that potentials between closely space electrodes may be quite small and difficult

to amplify cleanly, and that bipolarly recorded waveforms are not easy to interpret intuitively.

Monopolar referencing seeks to find one site which is inactive with respect to stimulus evoked activity, but is so selected as to be equipotential to the active electrode with respect to non-stimulus-related activity. An ideal monopolar reference placement will be stable with time and have small potential gradients in its vicinity. In practice, there is no single location which adequately possesses these characteristics in the general instance. Usually, a particular placement will only work adequately for the subject being studied and the special circumstances of the experiment. There are a number of sites in general use which are relatively indifferent to most forms of visual stimulation. However, one can almost always demonstrate that some small potentials ascribed to the stimulus are present, and most sites are susceptible to the pickup of unbalanced common mode signals between the active and reference electrodes. Examples of these are the cheek, nose, earlobe and linked earlobe references. Unfortunately, both cheek and nose referencing are very susceptible to the unbalanced pickup of potentials due to eye and facial movements, while all of these sites can be affected by extraneous myogenic activity. Despite these considerations, monopolar referencing remains the most popular method for use with small numbers of electrodes. In practice, the adequacy of a particular placement must be checked carefully by experiment.

From the above descriptions, it is clear that the distinction between bipolar and monopolar references is somewhat arbitrary, since both electrode configurations are essentially bipolar in that they involve

one electrode being referenced against another {137,138}. Whether rightfully or not, it is assumed that a bipolar scheme records the difference in potential between two 'active' regions, while a monopolar scheme records the difference in potential between one 'active' and another 'inactive' region. Indeed, it is possible to convert back and forth between the two schemes by taking linear combinations of various channels {137}.

Average referencing {137,139,140} takes as reference the average of all active electrodes. This method may be appropriate when a large number of electrodes is being used, since it is based on the assumption that the activity which gives rise to the scalp potentials involves electronic charges which sum to zero (or at least a constant). This involves the invocation of Gauss's law, which states that the sum of potentials over a closed surface bounding a fixed number of charges is zero or some constant. One might expect that an average reference derived from a reasonable sampling over the surface of the head would be stable. The objection to this idealized scenario is that in practice there is no systematic way of ensuring that the sampling is adequate in all instances, especially where the potential distributions vary radically with time. This objection is not too serious because, for this theory to be applicable to a reasonable approximation, only sites which exhibit stimulus-related activity above the inherent noise level need to be sampled. Fortunately, these sites are almost always on the scalp, so that a reasonable distribution of electrodes over the scalp is sufficient. Further, for responses derived from a specific sense modality, active sites tend to be concentrated over a restricted region of the scalp.

The basic drawback of the average reference is that it may pick up time-locked activity due to the fact that the average is a linear combination of active channels and hence will be related to them to the extent that cancellation is incomplete. Kavanagh {73} has shown an instance of a 41 channel average reference which was correlated with active channels in a case of visual stimulation. However, the actual levels of the reference swings compared to the active channel swings were quite small. As will be seen in Chapter 4, in this study it was found that the use of a frontal monopolar reference and average reference were interchangeable to the extent that the measured distributions were substantially the same in both cases. However, it was also found that the average reference gave results which were superior to those of a frontal monopolar reference with respect to signal-to-noise ratio. The reason for this is undoubtedly the fact that the average reference takes advantage of the common mode rejection property, especially in the area of alpha wave rejection. This is so because alpha activity is more closely equipotential between locations on the scalp in the vicinity of visually active areas, than between visually active areas and a frontal reference {141}. In this sense, the average reference is a compromise between the competing problems of achieving noise rejection and reference indifference. The average reference also has the advantage that it provides negative feedback, which is useful in stabilizing multichannel amplifier systems {142}. An average reference scheme was used for nearly all of the data presented in this thesis.

3.2.3 Amplifier System

A multichannel amplifier system was constructed to provide appropriate amplification and referencing for the signals on each of the 40 electrodes.[21] The difficulties in building a multichannel system which works satisfactorily are replete {142}. This situation is frustrating in view of the fact that designing and implementing a system with one or a few amplifiers is very simple. The basic problem is in coping with the inherent interaction in a multichannel EEG system, which must measure from many places on the same head using the same reference and which must operate at high gains, thereby allowing small effects at the input to create large effects at the output. Basically, to be useful for EEG work, each amplifier in such a system must be stable, operate independently of the others (amplifier crosstalk down greater than 40 dB at 100 Hz and lower), have a high gain (10,000 to 100,000), have a high common mode rejection ratio or CMRR (greater than 60 dB down at 60 Hz with a 20 KΩ source imbalance), have a high input impedance (greater than 10 MΩ at 100 Hz), and have a roughly uniform band pass between say 1 Hz and 50 Hz. The system described here has these characteristics.

A schematic of the amplifier system is shown in Fig. 19. Each amplifier has several stages and the purposes of each will be briefly described:

(1) This is the front-end preamplifier stage, where dual-FET input instrumentation amplifiers are used. These provide the necessary input impedance, draw

---

[21] I am indebted to Dr. J. P. Ary for the design and implementation of the amplifier system described here.

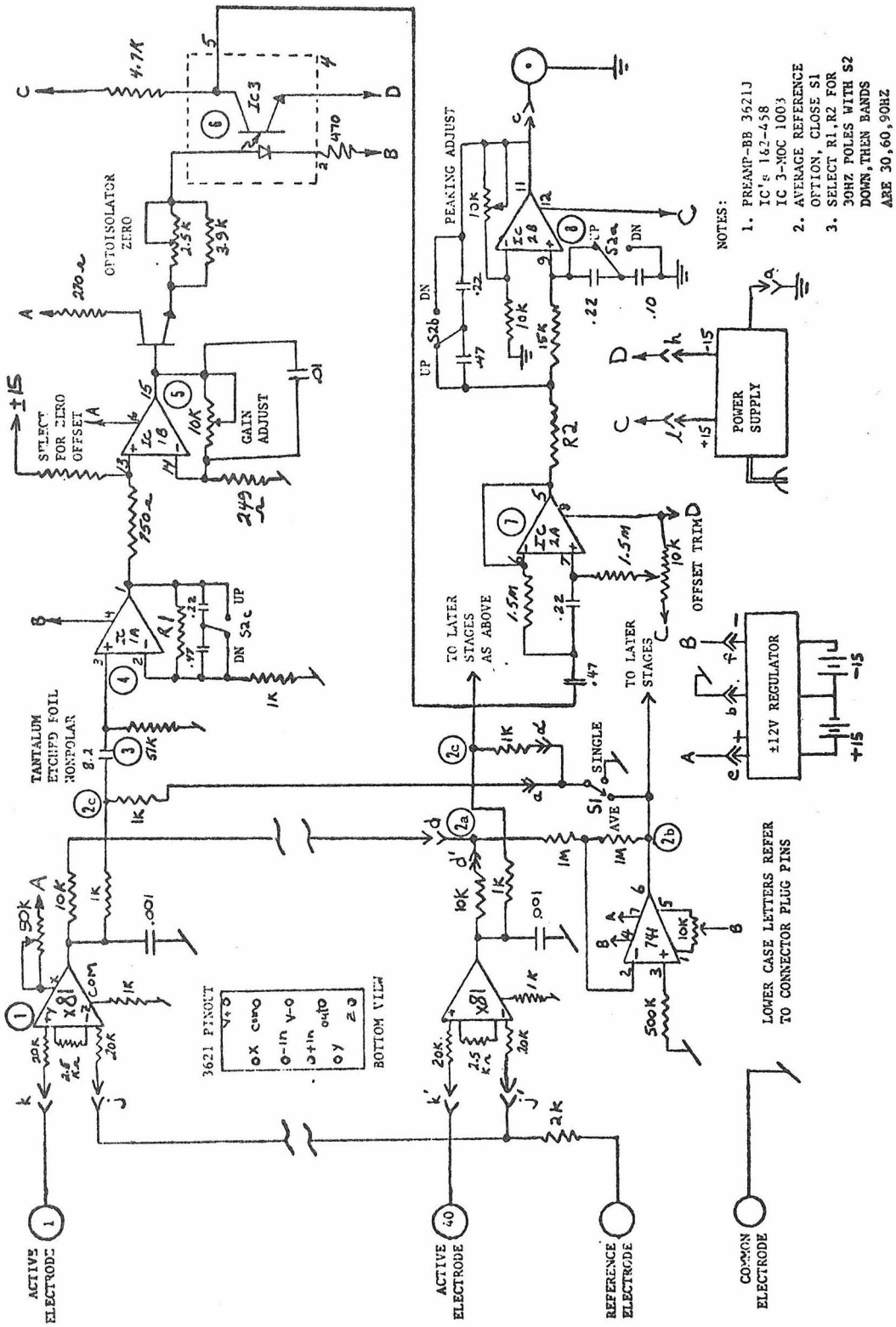

Fig. 19 - 40 Channel EEG Amplifier

very low bias current, have a CMRR with a 20 KΩ source imbalance of greater than 60 dB in the frequency band of interest, have an adequate linear frequency range and provide an initial gain of 81. These amplifiers are referenced to an electrode placed somewhere on the head.

(2) This provides for switching (via S1) between a monopolar reference and an average reference. The average of all the preamplifier outputs appears at 2a. Its inverted value appears at 2b. If S1 is switched to the averaging mode, then the value appearing at locations 2c is one-half the difference between the output of the preamplifier and the average of the outputs of all the preamplifiers. The summing reference is placed here to isolate its resistor network from the preamplifier stage, thus allowing for the preamplifiers to operate with their maximum input impedance.

(3) This is a high-pass filter or capactive coupler which consists of a simple RC network with C=8.2μF and R=51KΩ.

(4) This is a one-pole passive filter and is the first of two stages which provide for a three-pole low-pass filter. It also provides some additional gain (≃14).

(5) This is the variable gain stage, at which the gain of the amplifier system is adjusted. The range of this gain is from 1 to 41.

(6) This stage provides optoisolation to protect the subject from electrocution in case of failure of line-powered equipment. Everything to this point is powered by batteries (Nickel/Cadmium), while all successive stages are powered by a regulated supply connected to line power. The resistance to power supply grounds through the optoisolator is greater than 1000 MΩ. The maximum current that could be provided to the subject by the batteries is about .75mA per electrode (15 V battery voltage/20 KΩ minimum source impedance), which is well below the danger level.

(7) This is an unpeaked 2-pole high-pass filtering stage with a low frequency cutoff at approximately 0.5 Hz.

(8) This is the second low-pass filtering stage, which is a two-pole active filter and also provides some additional gain. The gain is varied to achieve an α-factor of 1, which determines peaking in the neighborhood of the corner frequency {143}. The entire low-pass filtering system (stages (4) and (8) together) is switchable via S2 to one of three upper 3dB points: 30 Hz, 60 Hz or 90 Hz.

The overall gain of each amplifier was set at approximately 60,000. Bode plots of typical amplifier characteristics are shown in Figs. 20 and 21. Individual amplifiers were stable in their characteristics, but separate amplifiers could vary 2 Hz in the frequency of the upper 3dB point and up to .5dB in the amount of peaking. These variations were not large enough to cause a significant distortion of the results, as evidenced by tests involving random sorting of the amplifiers and repetition of experiments.

3.2.4 Experimental Procedures and Data Collection System

The three subjects used in these experiments were all right-handed males corrected for normal vision.[22] These subjects were designated JPA, PDP, and RML.

Figs. 22 and 23 show the overall experimental layout which was used. The subject, amplifiers and batteries were placed in an electrically screened (double Faraday cage) and nominally soundproof room, which was connected to a special earth ground. This ground was also used for the data collection system and the post-optoisolator power supply. All other electronics were outside the screened room. The light for the stimulus passed through two small holes in the room. The light modulators were under the control of a minicomputer (PDP-11/20), which also controlled multichannel data collection and performed various bookkeeping procedures. The computer was programmed to interact with the experimenter and effect the required number of stimulus events with an aperiodic spacing specified by the experimenter (specified average

---

[22] It was later discovered that subject RML was color anomalous (see Chapter 4).

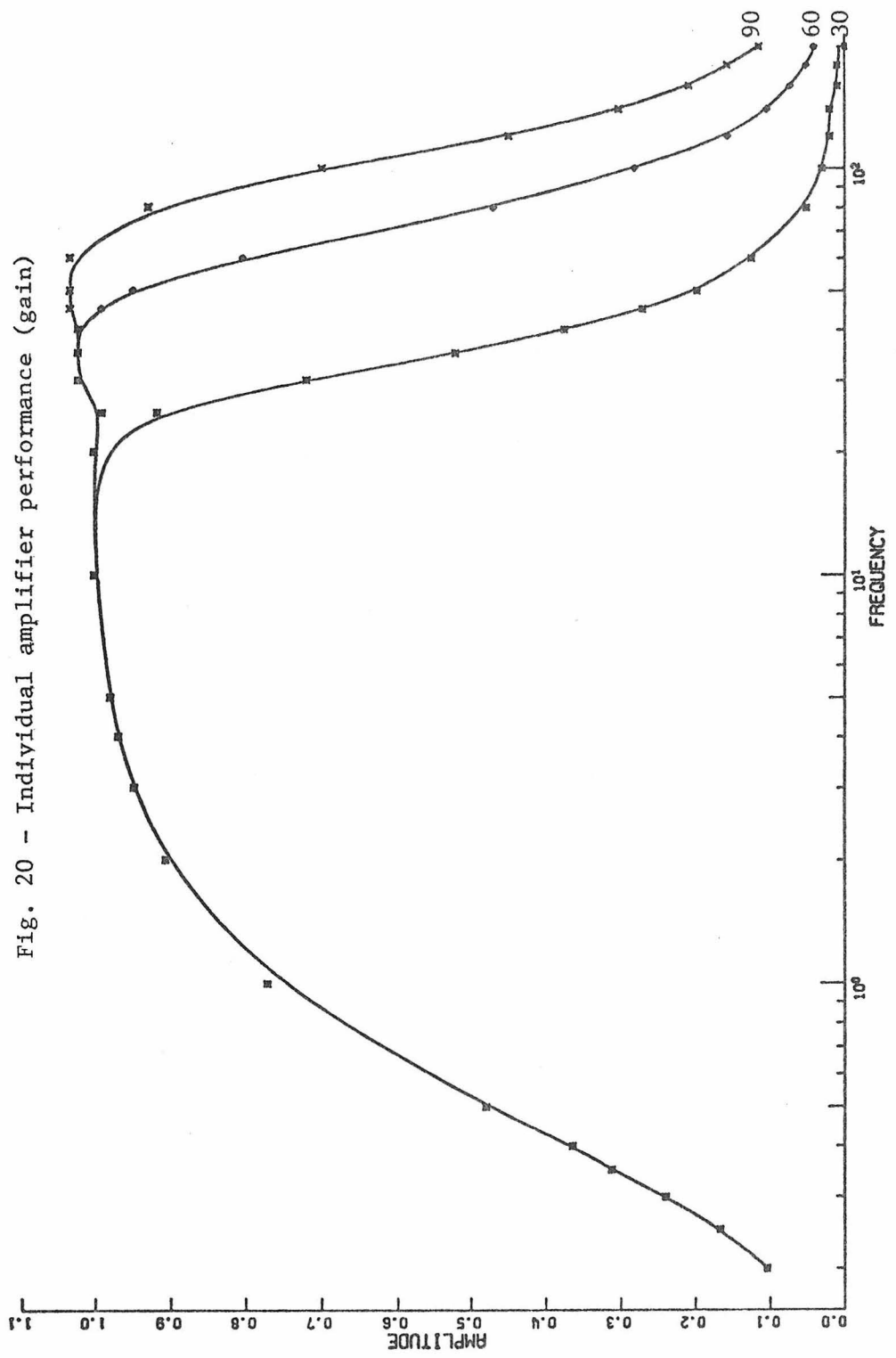

Fig. 20 - Individual amplifier performance (gain)

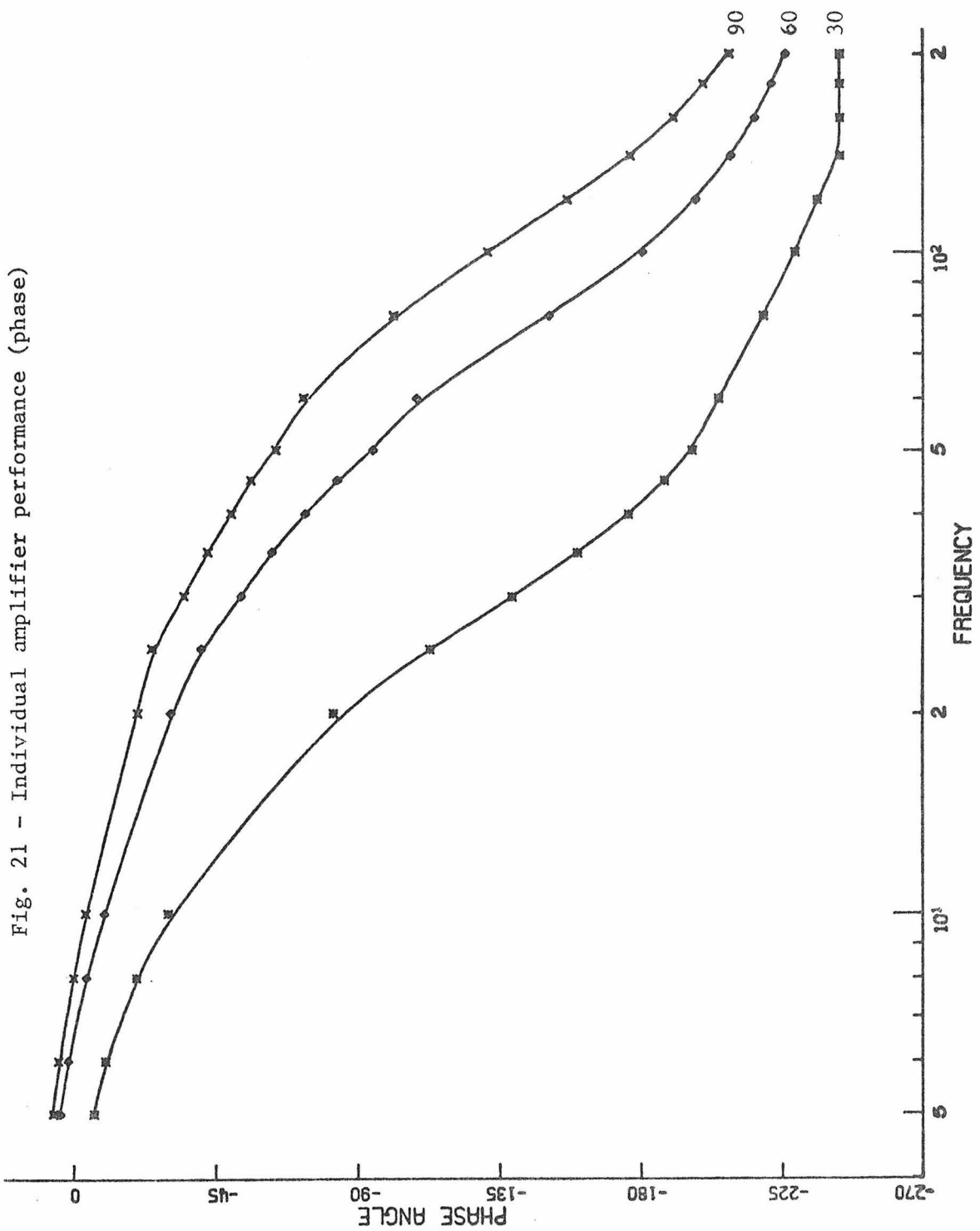

Fig. 21 - Individual amplifier performance (phase)

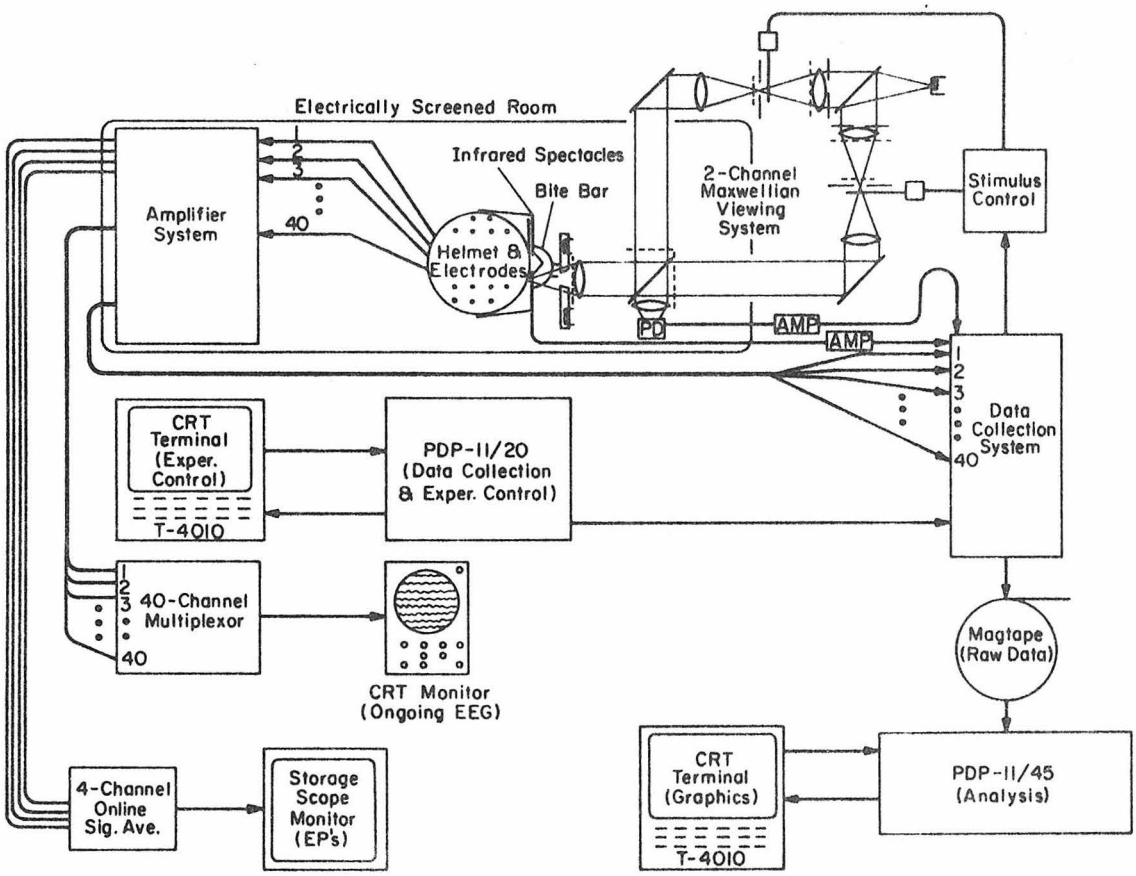

Fig. 22 - Overall experimental layout (schematic)

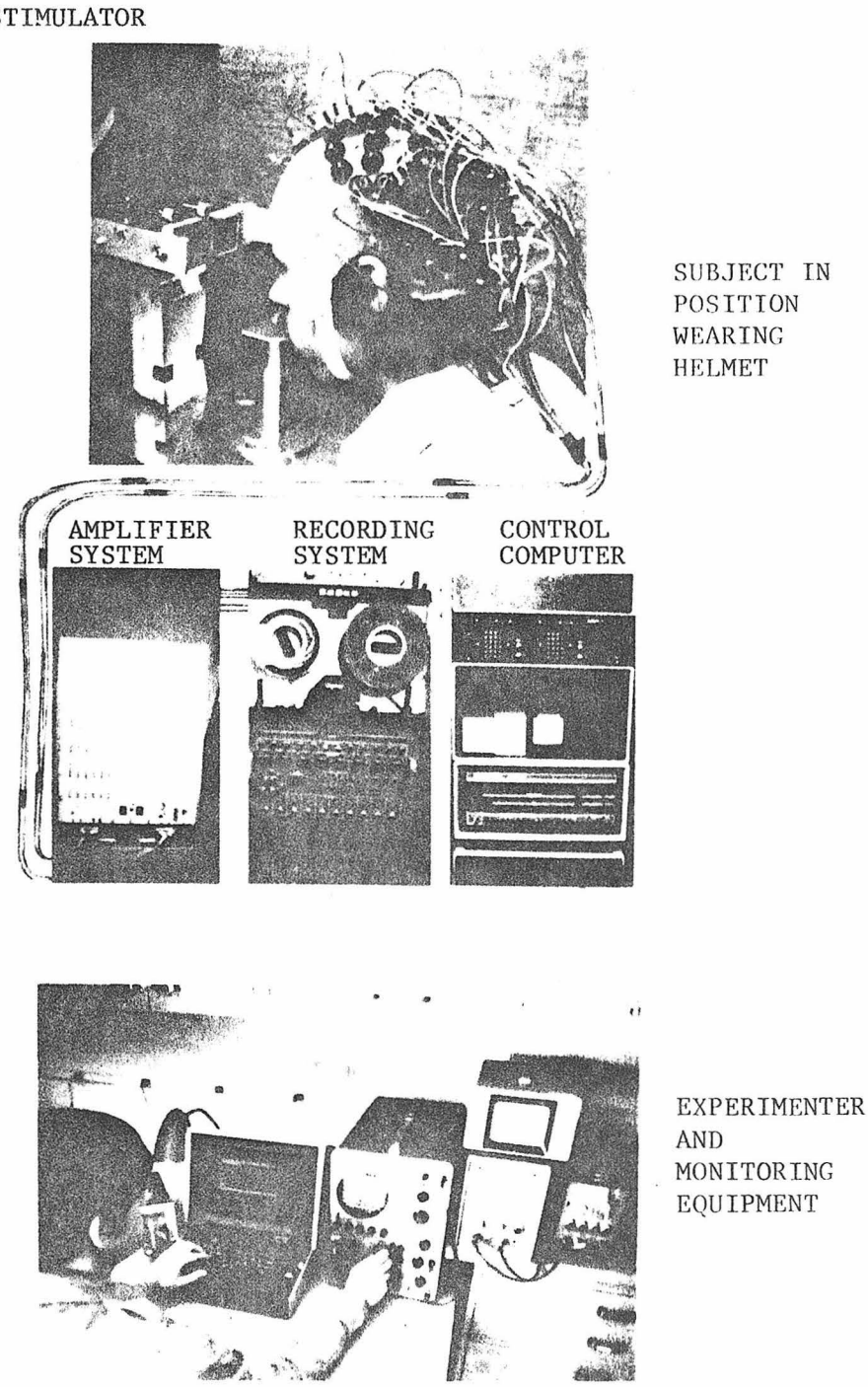

Fig. 23 - Overall experimental layout (pictorial)

interstimulus interval ± random times taken from a uniform distribution of specified width).

The data collection system and stimulus sequencing system consisted of a 100 KHz multiplexer, A/D converter and dual buffered digital tape recording system, along with associated data collection and stimulus control hardware. For these experiments, data were recorded at 250 Hz per channel (every 4 msec) for 400 msec for each stimulus event, including 125 msec before the stimulus and 275 msec during and following the stimulus event. Stimulus timing and data synchronization channels were recorded in addition to the 40 active electrode channels.

A typical experimental session consisted of one to two dozen runs. A run was defined as 150 repetitions of a selected stimulus. The experimenter would warn the subject when a run was to begin and then direct the computer to carry out the run. A given stimulus was usually repeated for 3 or 4 runs to help assess repeatability of the evoked potentials.

Two additional systems were used to allow the experimenter to monitor the data as it was being collected. The first was a multichannel CRT monitor which displayed all 40 electrode channels. This was used to check electrode behavior and determine whether a run was proceeding properly. Unstable, noisy or disconnected electrodes were easy to spot, as were runs in which an excessive number of artifacts (e.g. eye blinks, eye movements, head movements) were occuring. The second monitoring system was a 4 channel real-time signal averager (Nuclear Data Model ND-801 Enhancetron), which displayed approximate evoked responses from selected channels on a storage oscilloscope. Thus, as an experiment

progressed, the experimenter could assess the repeatability of evoked responses on subsequent runs and also ascertain the number of repetitions necessary to extract the evoked potential (the experimenter could watch the response grow and stabilize as the run progressed). 150 repetitions were used for extracting the evoked potentials presented in this thesis.

3.3 Preliminary Data Analysis

3.3.1 Averaging and Signal-to-Noise

Following an experimental session, the recorded data were taken to a PDP-11/45 computer for analysis (Figs. 22,23). The first analysis step was to perform signal averaging on the data, so as to extract evoked potentials. At this point, we will digress briefly to consider some simple theoretical points about signal averaging and the EEG.

In measuring evoked potentials, one must extract these weak but repetitive signals from an uncorrelated background (ongoing EEG, etc.). It is intuitive that signal averaging will enhance activity which is correlated in time with the stimulus and average to zero activity which is non-correlated. This amounts to a signal-to-noise improvement process. To estimate how many stimulus repetitions might be needed to extract an evoked potential, consider the following argument [73,144]:

> Assume that the raw waveform f(t) is the sum of two independent waveforms, s(t) the signal and n(t) the noise. If we assume that the noise is gaussian with zero mean and variance σ^2 , then the expected value of f(t) is s(t). Moreover, if we define the signal-to-noise ratio as the expected value of the signal divided by the standard deviation of the noise, then on this basis the signal-to-noise ratio for some sample time t_i is $s(t_i)/\sigma(t_i)$ and for the average of N samples $s(t_i)/\sigma(t_i)\sqrt{N}$. This means that averaging N samples improves the signal-to-noise ratio by a factor $\sqrt{N}$.

The above analysis is idealized, since the noise is not truly gaussian[23] and may be correlated with the stimulus for some short intervals {144}. However, over long intervals the assumption of uncorrelated noise is more acceptable, since the central limit theorem of statistics {145} is applicable if enough short intervals are uncorrelated. At any rate, small departures from the ideal case lessen, but do not negate the signal-to-noise enhancement capability of the signal averaging technique. In practice, the event-related signal is at best only about one-third of the size of the raw EEG signal. Thus, one must average at least 100 stimulus repetitions to get a reasonable signal-to-noise ratio (3:1). For the experiments reported here, 150 stimulus repetitions were used in each run.

The averaging process has an inherent weakness {146,147} that the experimenter must be wary of. This is the fact that an average calculation does not reveal when a system is non-stationary, i.e. varying in response from sample to sample. This is illustrated in Fig. 24, which shows that an average response may be unrepresentative of individual responses. Among possible causes of non-stationarity are habituation, drowsiness, shifts of attention and boredom, to mention a few {147}. With noisy data such as the EEG, it is difficult to convince oneself that such variations are not present, since one usually must average to see any stimulus-related response at all. However, a crude indication can be derived from breaking the data into smaller sections and looking for

---

[23] Spontaneous EEG {144} is considered by some to be describable as band-filtered gaussian noise, while others prefer to describe it as selectively filtered gaussian noise (at or around the alpha frequency).

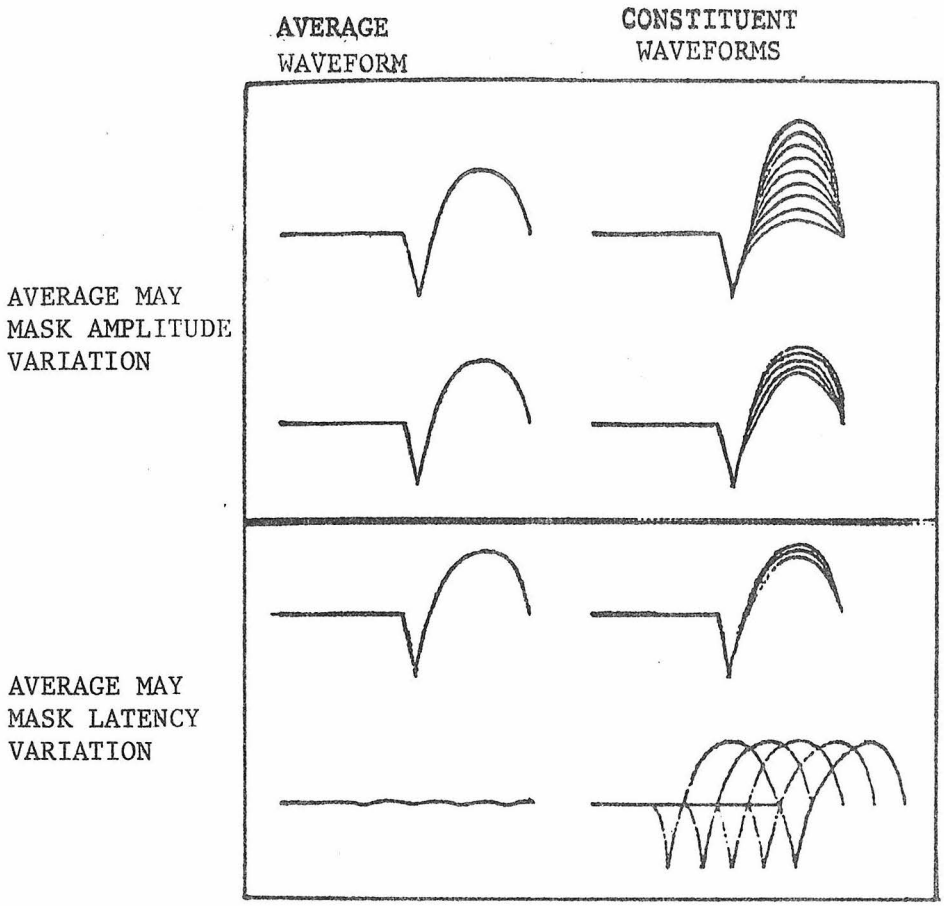

Fig. 24 - Illustration of two classes of ambiguity present in averaged response records (from Brazier [146]).

significant differences in evoked potentials derived from different sections. For instance, the average response from the last 50 of 150 repetitions of the stimulus may be compared with the average response from the first 50 repetitions. Such tests were carried out on some of the data presented in this thesis and no systematic variations were apparent. As a precautionary measure, however, the data from the first few repetitions of the stimulus were dropped from subsequent averaging. This was to preclude any transient effects related to the starting of the stimulus procedure.

3.3.2 Artifacts

Since one is defining as signal those components time-locked to the stimulus, it is clear that difficulties might arise when time-locked artifacts are included in the EEG signal. Some of these might be responses arising from sense modalities other than that which one wishes to stimulate. For example, an auditory artifact might result from the click of a shutter producing a visual stimulus. It is also possible for scalp responses to be contaminated by responses from the same sense modality. Two examples of this are the electroretinogram (ERG) picked up by scalp electrodes and contamination of averages due to overlapping of successive responses when the interstimulus interval is smaller than the duration of the response. The latter often occurs when periodic or near periodic stimuli are used. In addition, there is the possibility of drivable brain rhythms affecting the response. The prime example of this is the so-called alpha rhythm which may phase lock to periodic or near periodic stimuli at or near the alpha characteristic frequency of 8-12 Hz.

Artifacts which are not time-locked to the stimulus may be a problem if their amplitudes are sufficiently large. Examples of these are potentials due to changes in the direction of the steady corneo-retinal field during blinks and eye movements, and movements of the subject. These phenomena often produce such large potentials that even rare occurrence can be disastrous for the averaging process. Increasing the number of stimulus repetitions included in the averaging process does not necessarily alleviate the problem.

There are a number of methods available for coping with the aforementioned artifacts. Some of these artifacts are measureable in themselves and their occurrence easily detected. Ideally one could note their occurrence and delete from the averaging any repetitions containing them. This removal technique can work well for eye blinks, eye movements and subject movements which do not occur often. It can also work for alpha rhythm removal provided the alpha rhythm comes in rather infrequent bursts. However, repetition removal is difficult to carry out in real time, and is most easily carried out off-line using a digital computer. It is impractical if the artifact occurs often or in every repetition. On the other hand, if it can be demonstrated that the artifact in question is repeatable and independent of the phenomenon of interest, its effects may be calibrated by measuring it alone. Then, when this artifact occurs, its effects may legitimately be removed by subtracting them from the composite response.

Another major artifact control technique is the use of aperiodic stimuli, i.e. the provision of an interstimulus interval which has a random distribution. As previously mentioned, this method was used in collecting the data in this thesis. This is particularly important when

the response persists beyond the time when a subsequent stimulus is applied. If a periodic or near periodic stimulus is used, it may not be possible to separate unequivocally the average waveform into those components which are due to overlap and those components which constitute the initial response to the stimulus. Intuitively, the use of a random interstimulus interval will remove this problem because the amount of overlap will be different for each repetition. Ruchkin {148} worked out the mathematical details of this method and concluded that the average response is a biased estimate of the evoked potential, with the amount of biasing dependent on the form of the overlap and the chosen probability distribution for the interstimulus interval. For most applications, a flat symmetric distribution about some average interstimulus interval seems appropriate.

It is also possible to control artifacts by the use of signal enhancement algorithms other than signal averaging. Principal among these other algorithms are median computations {149}, median approximation computations {150} and zero-crossing computations {151}. The principal advantage of the median and zero-crossing analysis over averaging is that they are less sensitive to occasional large artifacts. This is so because in these algorithms each sample has an equal weight in the computation of the response, whereas with averaging each sample has a contribution proportional to its size. Another advantage is that the responses may be extracted without a requirement for large storage or computation facilities.[24] The principal disadvantage of these methods involves their somewhat slower enhancement of the signal-to-noise ratio

---

[24] This advantage does not apply to exact median computation schemes.

{152,153}. In addition, there is distortion of small sample medians when the noise consists predominantly of quasi-sinusoidal waves {154}. After some experimentation with alternative algorithms, a standard averaging algorithm was settled on for this thesis project. The effects of large artifacts were handled by a clipping technique. This was accomplished by running the measurement system so that the A/D converter would saturate at a value which was not far above the level of expected ongoing EEG. This gave results essentially identical to the other methods, but was simpler to use and more efficient. In addition, the experimenter rejected runs which contained excessive amounts of visible artifacts (eyeblinks, alpha rhythm etc.).

Finally, there are a number of other artifact removal methods, which are simple but often prove effective. These include providing comfortable conditions for the subject so that, for example, he is less likely to move or blink his eyes. Undesired modality responses may be eliminated by keeping them from reaching the subject. For example, ear plugs can be used to attenuate or random noise used to mask extraneous sounds, thus precluding auditory artifacts. Another possibility is to only consider that part of the response which is within a certain time window. This only works when the artifact is outside of the time window in question. Some artifacts such as alpha wave contamination can be diminished or eliminated by inducing the subject to concentrate on the experimental task. The aforementioned methods were all used to various extents in the experiments performed for this thesis.

There are also many potential problems related to non-biological or equipmental sources of interference. These may involve instrumental

noise and electromagnetic or radiation interference. A treatment of these problems is beyond the scope of this thesis, but extensive discussions are to be found elsewhere [155,156].

3.3.3 Evoked Potential Handling and Display

Once evoked potentials were obtained for each channel in each experimental run, those which resulted from the same stimulus condition were gathered together and statistics computed. Principal among these was the mean evoked potential on each electrode:

$$\bar{V}_i(t_j) \equiv \frac{1}{NRUNS} \sum_{k=1}^{NRUNS} V_i^k(t_j)$$

where NRUNS is the number of runs performed (on the order of 10 for each stimulus condition), i is an electrode index, j a time index and k a run index. Also computed were two measures of variance. The first was the instantaneous variance on each electrode as a function of time:

$$\sigma_i^2(t_j) \equiv \frac{1}{NRUNS-1} \sum_{k=1}^{NRUNS} \{V_i^k(t_j) - \bar{V}_i(t_j)\}^2$$

The second was the average prestimulus variance on each electrode:

$$\sigma_i^2 \equiv \frac{1}{NRUNS} \sum_{k=1}^{NRUNS} \frac{1}{NVALB-1} \sum_{j=1}^{NVALB} \{V_i^k(t_j) - \bar{V}_i(t_j)\}^2$$

where NVALB is the number of samples before the stimulus (25 such values were used). As will be seen, the mean evoked potentials and average prestimulus variance values were used most extensively in the further analysis of the data. Instantaneous variances were not used for weighting schemes because of the relatively small number of runs which were done for each stimulus condition on each subject. Average prestimulus values were preferred for this purpose because they reflect the inherent noise level and reliability of data taken from a given electrode and, unlike poststimulus values, their value could not be influenced by variability in the response itself. Electrodes with zero or small values could be

given a weight equal to or greater than electrodes with large values. This is in accordance with the fact that electrodes with small values may signal the locations of zeros and turning points in the potential gradient, and are thus quite important to the determination of underlying sources {55,71}.

Although the above simple quantitative statistics could be used, the reliability and stability of the responses were generally assessed by graphical means. This was done, among other ways, on a CRT graphics terminal (Figs. 22,23), on which either evoked potentials from separate runs were plotted simultaneously, or mean evoked potentials plotted ± one standard deviation. Examples of these forms of display will be seen in later sections. Viewing the prestimulus values was useful in helping the experimenter to assure himself that the waveforms were stimulus-related, to estimate the inherent noise level and to identify the latencies of various components of the response.

Large numbers of evoked potential waveforms were mostly inconvenient for further analysis, so reliable data sets were plotted in the alternative format of time series of equipotential maps on the surface of the head. These are in effect 'snapshots' of the spatial distribution of potential at each time sample. They are much more appropriate to comprehending the relationship between electrodes than the comparison of evoked potential waveforms. In view of the results, they are also much more interpretable in terms of underlying brain sources, since in certain time periods the maps were especially coherent, stable and simple. A series of these maps (or indeed a slow motion movie) is a very concise display of the complete spatio-temporal course of evoked potential activity on the scalp. Fig. 25 illustrates how the maps were formed.

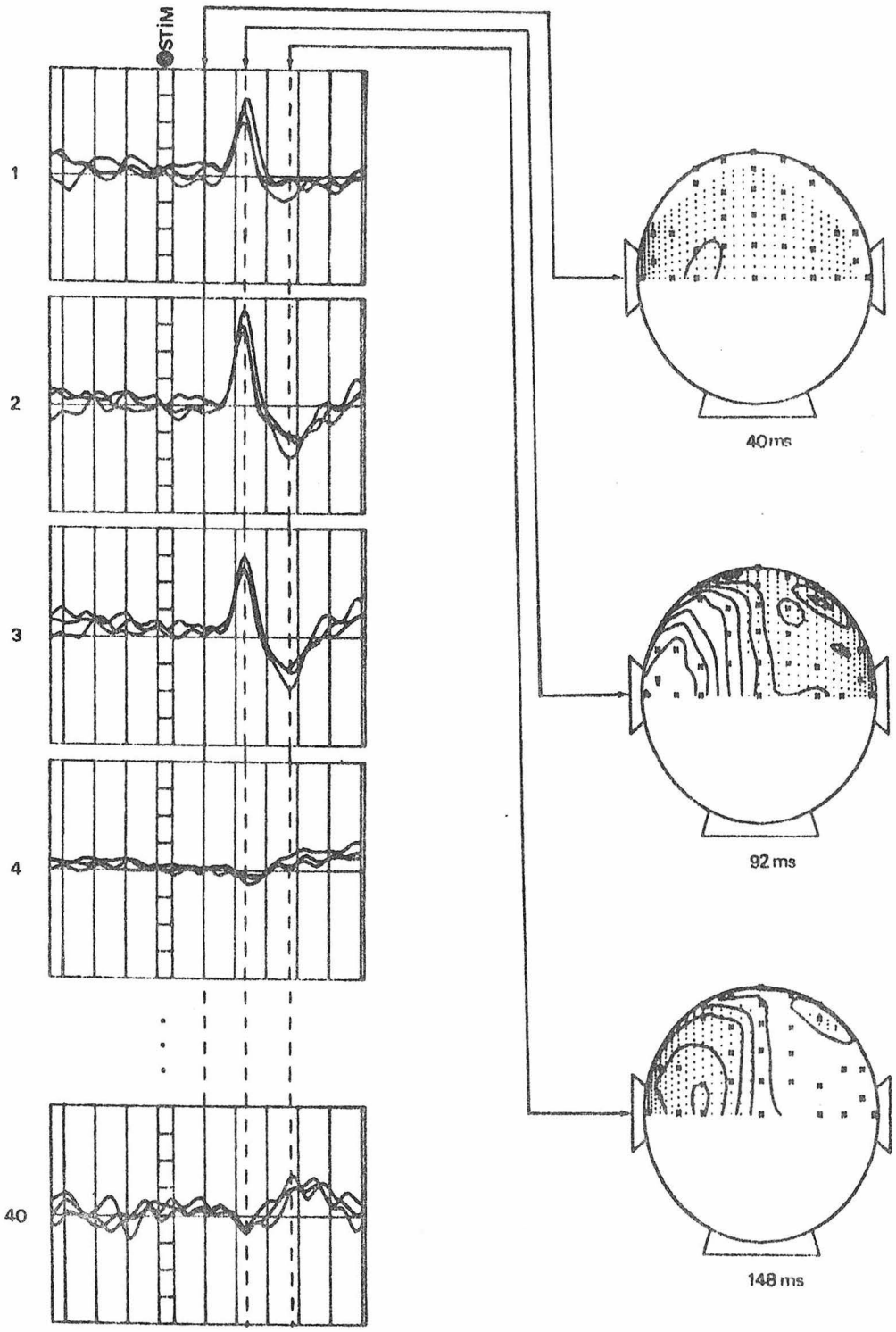

Fig. 25 - How equipotential maps are made. Each map is a 'snapshot' of the potential distribution at a given latency from the stimulus event. The X's indicate electrode positions. Regions of negative potential are dotted.

A computer program sorted the channels out according to their locations on the head, calculated[25] contours of constant potential on the head at each instant of time, and then projected these contours down to a perpendicular plane passing through the center of the head for 2-dimensional plotting. The contours were at 10 equally spaced intervals between the minimum and maximum of the evoked potentials at all electrodes. Negative values were identified by dotted regions. X's indicated electrode positions. All maps were centered on the inion.

Equipotential maps were done on mean evoked potentials whose reliabilities had been assessed by studying waveforms resulting from several runs of the same stimulus. Reliability could also be assessed by comparing maps plotted from different runs or by studying the effect of perturbing the mean equipotential map by adding to the potential at each electrode a sample from a random distribution of zero mean and with the standard deviation estimated for that electrode. It was also useful to look at prestimulus equipotential maps and maps from the control runs.

The final step in preliminary data analysis was to make reasonable guesses at the source parameters which might have given rise to the measured potential distributions. Although such guesses were not necessary, they usually make the modeling algorithms converge in fewer steps. Guesses were made by comparing maps from catalogs of model-generated equipotential maps with maps of the experimental data.

---

[25]The data were interpolated for graphical purposes. For this reason there were distortions in some of the maps. Fig. 26 illustrates the interpolation methods and some distortions. Since interpolation was only used for display purposes, it had no effect on the further results of this thesis. Whenever two equipotential maps were compared, they were always subjected to the same distortions.

Fig. 26 - Equipotential mapping interpolation and distortions.

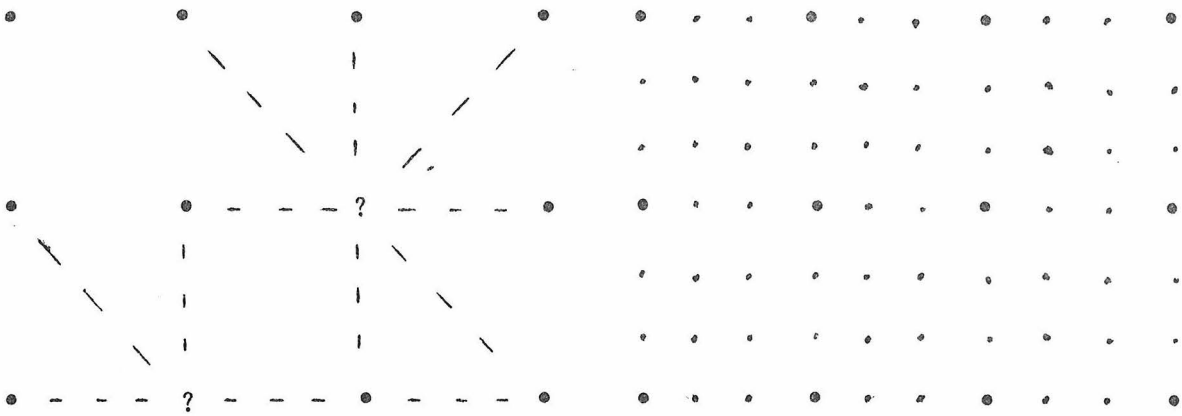

Step 1 - To make array uniform, fill in missing points by averaging neighboring points (weighted with inverse square of distance).

Step 2 - Use bicubic polynomial fit to expand further.

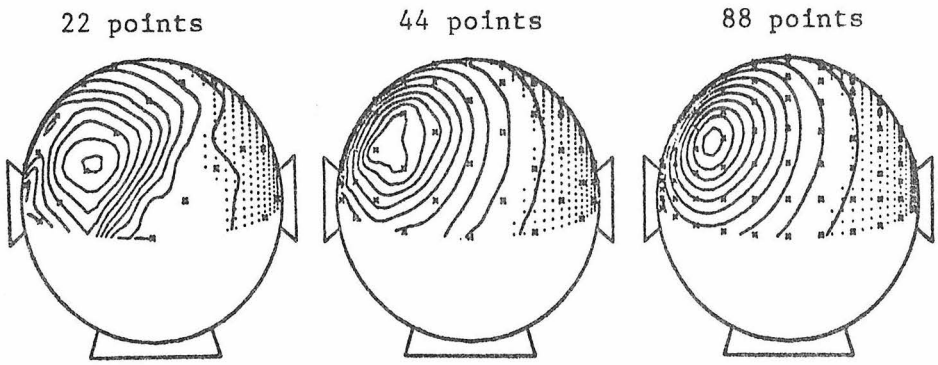

Equipotential maps of model generated data. Distortions may arise when a small number of electrodes are used.

Source parameters were chosen from the model maps which most closely resembled the experimental maps. There were catalogs for each head and source model. Examples from these are shown in section 3.4.

3.4 Modeling - Forward Solutions[26]

3.4.1 Dipole in Homogeneous Sphere

In this model, the head is represented by a homogeneous sphere of radius R and conductivity σ. The solution used here gives the potential at r=R for all θ and ϕ resulting from a dipole of moments (P_x, P_y, P_z) located along the z-axis at r=fR (Fig.27). For a sphere with an insulating boundary, the potential at the surface of the sphere is given by {157}:

$$V(\theta,\phi,f,P_x,P_y,P_z) = \frac{P_z}{4\pi\sigma f R^2}\cdot\left\{\frac{1-f^2}{(1+f^2-2f\mu)^{3/2}}-1\right\}+\frac{P_x\cos\phi+P_y\sin\phi}{4\pi\sigma f R^2\sin\theta}\cdot\left\{\frac{3f-3f^2\mu+f^3-\mu}{(1-f^2-2f\mu)^{3/2}}+\mu\right\}$$

where $\mu=\cos\theta$ and θ, ϕ are the azimuth and latitude in the coordinate system (r,θ,ϕ).

To be generally applicable, the coordinates of an arbitrary dipole must be rotated so that the z-axis passes through the center of the dipole. Doing this {73}, we have:

$$V(\theta,\phi;f,\alpha,\beta,P_x,P_y,P_z) = \frac{1}{4\pi\sigma R^2}\{V_1V_2+V_3V_4\}$$

where:

$$V_1 = \frac{P_x\sin\beta + (P_y\sin\alpha + P_z\cos\alpha)\cos\beta}{f}$$

$$V_2 = \frac{1-f^2}{(1+f^2-2f\mu)^{3/2}} - 1$$

$$V_3 = \frac{\{P_x\cos\beta - (P_y\sin\alpha + P_z\cos\alpha)\sin\beta\}C + \{P_y\cos\alpha - P_z\sin\alpha\}E}{fA}$$

$$V_4 = \frac{3f-3f^2\mu+f^3-\mu}{(1+f^2-2f\mu)^{3/2}} + \mu$$

---

[26] For an exposition of the techniques used in deriving the equations presented in this section, see Smythe {9}.

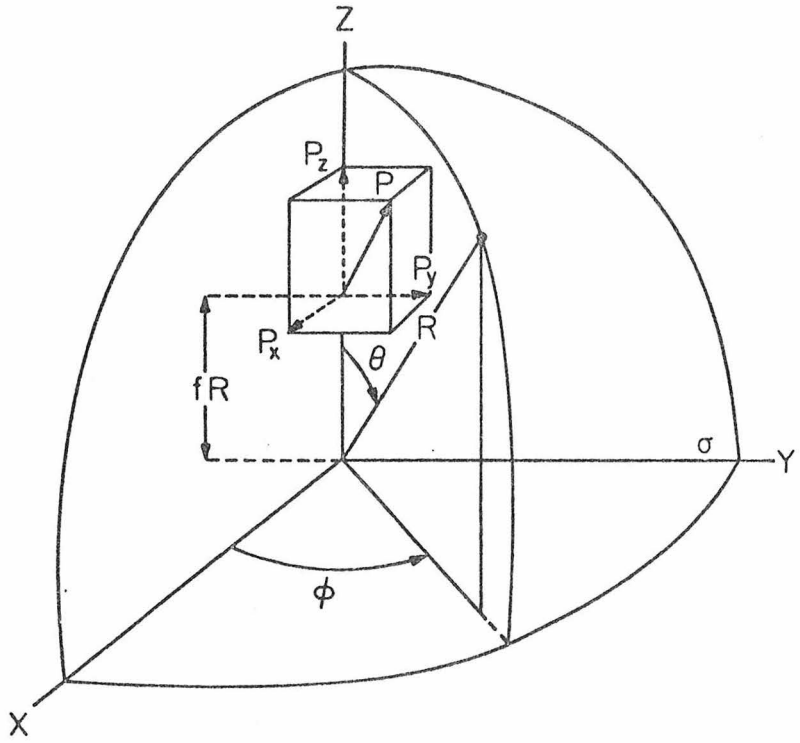

Fig. 27 - A dipole of components P_x, P_y and P_z located at r=fR along the z-axis, in a sphere of radius R and conductivity σ.

α = angle through which the coordinate system must be rotated about the x-axis in the clockwise direction to make the new z-axis colinear with the projection of the dipole position vector onto the y-z plane.

β = angle through which the coordinate system must be further rotated about the new y-axis is the counter-clockwise direction to make the dipole coincident with the z-axis.

μ = cos(azimuth in rotated coordinate system)

$$= \sin\theta \cos\phi \sin\beta + (\sin\theta \sin\phi \sin\alpha + \cos\theta \cos\alpha)\cos\beta$$

A = sin (azimuth in rotated coordinate system)

$$= \{1 - \mu^2\}^{\frac{1}{2}}$$

C = cos (latitude in rotated coordinate system)

$$= \frac{\sin\theta \cos\phi \cos\beta - (\sin\theta \sin\phi \sin\alpha + \cos\theta \cos\alpha)\sin\beta}{A}$$

E = sin (latitude in rotated coordinate system)

$$= \{1 - C^2\}^{\frac{1}{2}}$$

To express the location parameters in cartesian (x,y,z) coordinates we note that:

$$x = f \sin\beta$$

$$y = f \cos\beta \sin\alpha$$

$$z = f \cos\beta \cos\alpha$$

Figures 28, 29, and 30 show examples of potentials generated by various dipoles within the homogeneous sphere model. As seen in these figures and the above equations, the key parameters in determining distribution shapes are dipole orientation and eccentricity. Dipole

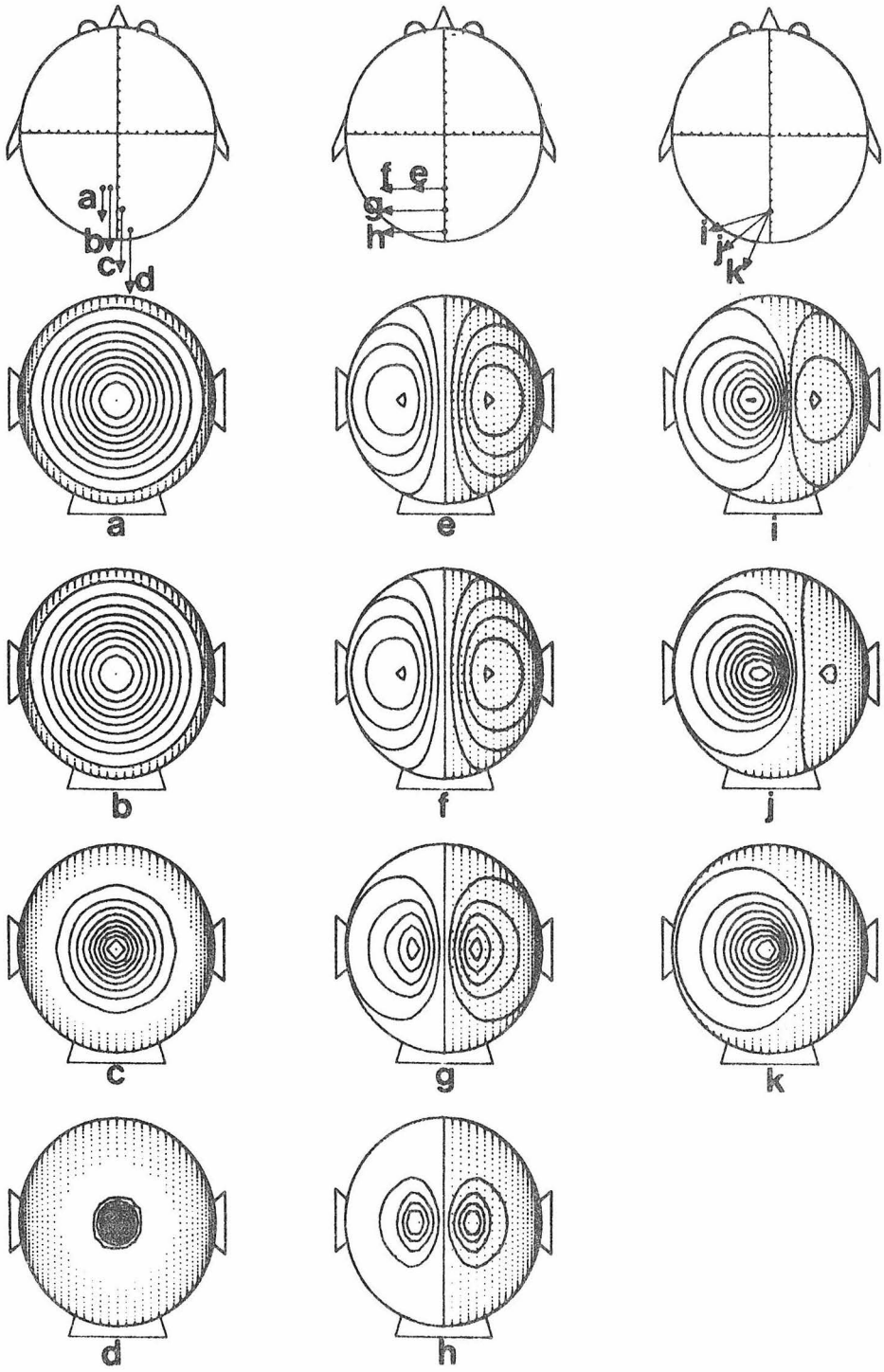

Fig. 28 - Model dipoles and corresponding distributions calculated for the homogeneous model of the head. a-d show various radial dipoles, while e-h show various tangential dipoles. i-k show various dipoles with radial and tangential components.

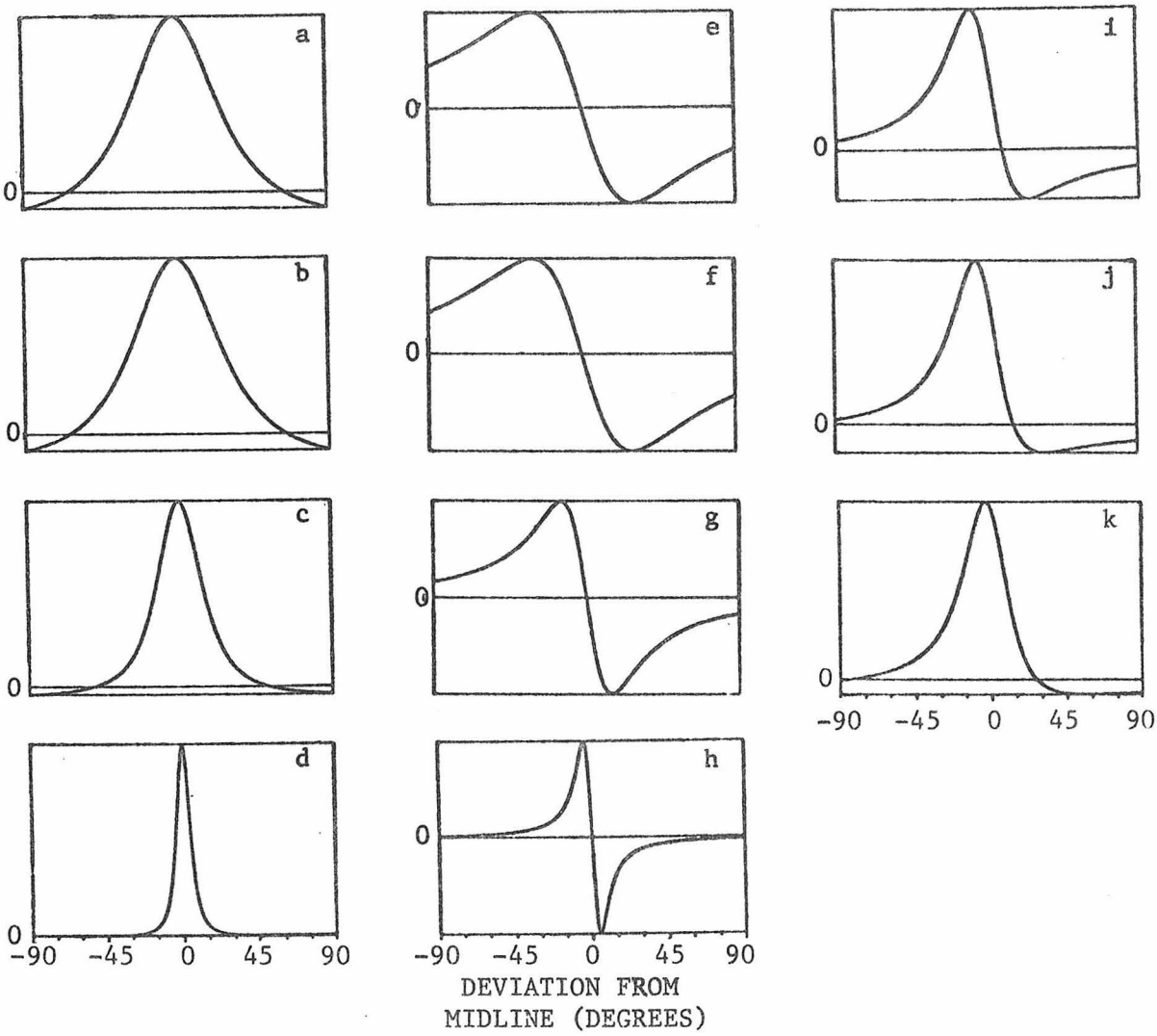

Fig. 29 - Cross-sections at the inion level of the potential distributions in the previous figure.

RADIAL
DIPOLES

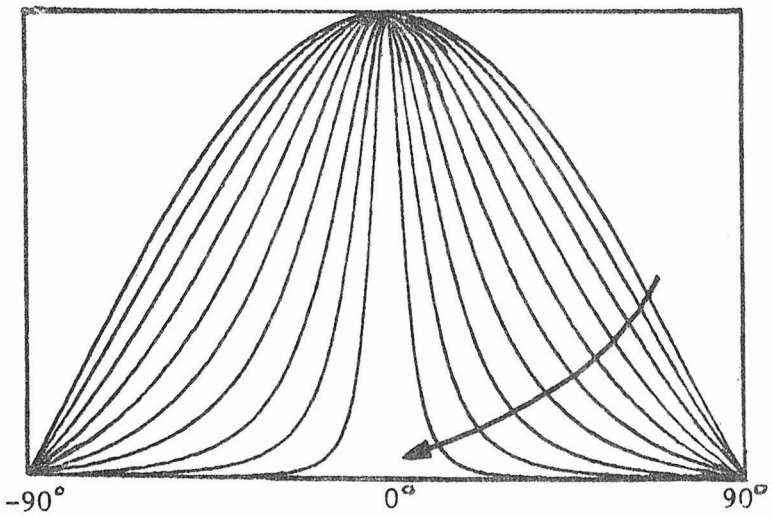

TANGENTIAL
DIPOLES

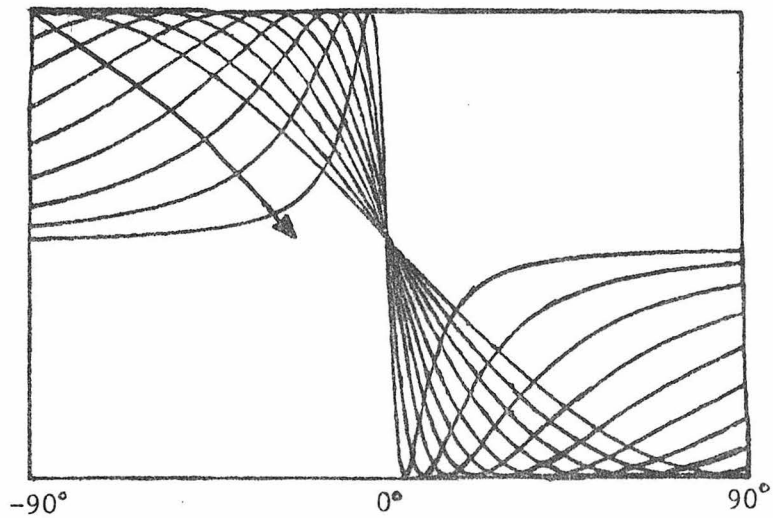

Fig. 30 - Potential distribution cross-sections at the inion level for two eccentricity series of dipoles in the homogeneous head model (f=0.01,0.1,0.2,0.3,0.4,0.5,0.6,0.7,0.8, 0.9). The arrows indicate increasing eccentricity.

magnitude ($\sqrt{P_x^2 + P_y^2 + P_z^2}$), head conductivity ($\sigma$) and head radius (R) are mere scale factors. Fig. 28 shows potential distributions plotted as equipotential maps, while Fig. 29 shows cross-sections of these same distributions at the inion level. Fig. 30 shows eccentricity series for radial and tangential dipoles.

3.4.2 Dipole in Inhomogeneous Sphere (3 Shell Model)

In this model, the brain and cerebrospinal fluid are approximated as shown in Fig. 31a by a spherical volume of radius r_1 and conductivity σ_1. The skull is a separate region of conductivity σ_2 and thickness $r_2 - r_1$, while the scalp is modeled as a layer of conductivity σ_3 and outer radius r_3. This model was suggested by Rush and Driscoll {49} and analyzed by Kavanagh {73}. The surface potential is the potential at the boundary r_3. Fig. 31b shows the dipole and coordinate system parameters. The solution used here gives the potential at r_3 for all θ and ϕ resulting from a dipole of moment M parallel to the z-axis (Fig. 31b) in the x-z plane ($r=b, \theta=\theta_0, \phi=0$). The solution is given by:

$$V(\theta,\phi;b,\theta_0,M) = \sum_{n=0}^{\infty} \sum_{m=0}^{n} M_{mn} K_n \, P_n^m(\mu) \cos m\phi$$

where:

$$M_{mn} = \frac{M}{4\pi\sigma_1} \cdot \frac{(2 - \delta_m^0)(n-m)!\, b^{n-1} P_{n-1}^m(\mu_0)}{(n+m-1)!}$$

$$K_n = \frac{K_1}{K_2 + K_3 K_4}$$

$$K_1 = (2n+1)^2 \left\{\frac{r_2}{r_1}\right\}^{2n+1} r_3^{-(n+1)}$$

$$K_2 = \left\{1 - \frac{\sigma_2}{\sigma_1}\right\} \cdot \left\{n^2 + n(n+1)\left\{\frac{r_2}{r_3}\right\}^{2n+1}\right\}$$

$$K_3 = \frac{n}{2n+1} \cdot \left\{\frac{\sigma_3}{\sigma_2}(n+1) + n\right\} + n\left\{\frac{n+1}{2n+1}\right\}\left\{1 - \frac{\sigma_3}{\sigma_2}\right\}\left\{\frac{r_2}{r_3}\right\}^{2n+1}$$

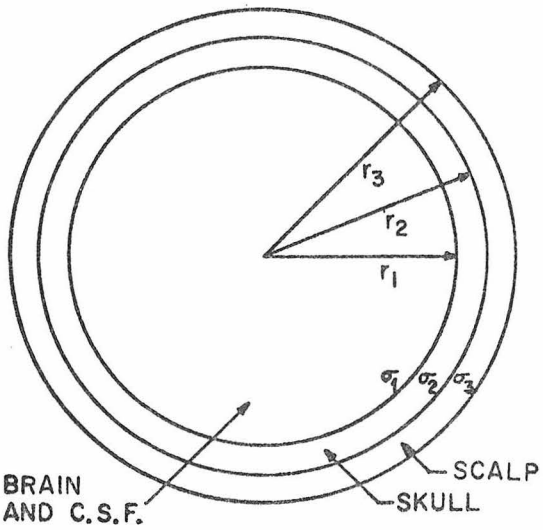

Fig. 31a - Concentric shell model of head (3 shell)

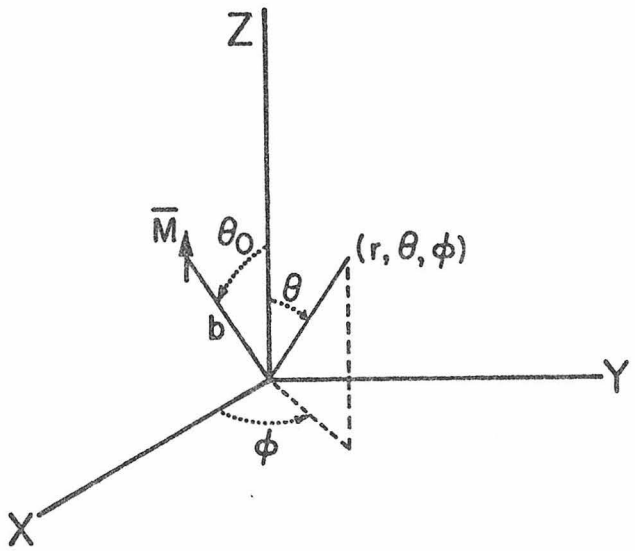

Fig. 31b - A dipole of moment M located at r=b, $\theta=\theta_0$, $\phi=0$ and parallel to the z-axis.

$$K_4 = \left(\frac{r_2}{r_1}\right)^{2n+1} \left\{\frac{\sigma_2}{\sigma_1}(n+1)+n\right\}+n\left\{\frac{\sigma_2}{\sigma_1}-1\right\}$$

$\mu = \cos\theta$

$\mu_0 = \cos\theta_0$

$P_n^m(\mu)$ = associated Legendre function of the first kind, with μ real and in the range $-1 \leq \mu \leq 1$

$$\delta_m^n = \begin{cases} 1 \text{ if } m=n \\ 0 \text{ if } m\neq n \end{cases}$$

To be generally applicable, the coordinates of an arbitrary dipole must be rotated so that the dipole is parallel to the z-axis in the x-z plane. When this is done [73], we have:

$$V(\theta,\phi;b,\theta_0,M,\alpha,\beta,\gamma) = V\{\theta^*(\theta,\phi,\alpha,\beta),\phi^*(\theta,\phi,\alpha,\beta,\gamma);b,\theta_0(\alpha,\beta,\gamma),M\}$$

$$=\sum_{n=0}^{\infty}\sum_{m=0}^{n} M_{mn}K_n P_n^m(\cos\theta^*)\cos m\phi^*$$

where all terms are as described above except:

α = angle through which the coordinate system must be rotated counterclockwise about the x-axis so that the projection of the dipole moment in the y-z plane is made parallel to the z-axis (y projection of dipole moment equal zero).

β = angle through which the coordinate system must be further rotated counterclockwise about the new y-axis so that the projection of the dipole moment in the new x-z plane is made parallel to the new z-axis (x projection of dipole moment equal zero).

γ = angle through which the coordinate system must be finally rotated counterclockwise about the new z-axis

to bring the dipole parallel to the z-axis in the x-z plane (ϕ=0).

$\theta^*(\theta,\phi,\alpha,\beta)$ = azimuth (θ) in rotated coordinate system.

$\phi^*(\theta,\phi,\alpha,\beta,\gamma)$ = latitude (ϕ) in rotated coordinate system.

Since these equations are in infinite series form, some convergence criteria must be set for the series. The criterion used was to stop summing the series at the point where three sucessive terms were smaller than some fraction δ of the current value of the series. A satisfactory value of δ was found to be 0.02 or 0.03. Figure 32 shows an example of the behavior of the series sum in the vicinity of where it was truncated.

Figures 33, 34, and 35 show examples of potentials generated by dipoles within the inhomogeneous sphere or 3 shell model. Here r_1=0.90, r_2=0.98 and r_3=1.0, while $\sigma_1=\sigma_3=80\sigma_2$ {48}. The dipoles are the same as those in Figures 28, 29, and 30. As before, the key parameters are dipole orientation and eccentricity. Note that distributions for dipoles in the homogeneous sphere model are of lower magnitude and less sharply peaked than distributions for corresponding dipoles in the shell model. This illustrates the attenuation and smearing effects introduced by the skull and scalp (see section 2.1.6).

3.4.3 Dipole in Inhomogeneous Sphere (5 shell Model)

In this model, the brain and cerebrospinal fluid are approximated as shown in Fig. 36 by a spherical volume of radius r_1 and conductivity σ_1. The skull is composed of three separate regions of conductivity σ_2, σ_3 and σ_4, with thicknesses r_2-r_1, r_3-r_2 and r_4-r_3, respectively. The regions of conductivity σ_2 and σ_4 represent the low conductivity inner and outer calcified layers of the skull, while the intervening region of conductivity σ_3 represents the highly conductive diploe. The

Fig. 32 - Behavior of Legendre series sums for radial and tangential dipoles located on the midline in the 3-shell model of the head (f=.7). Angles denote deviations from midline.

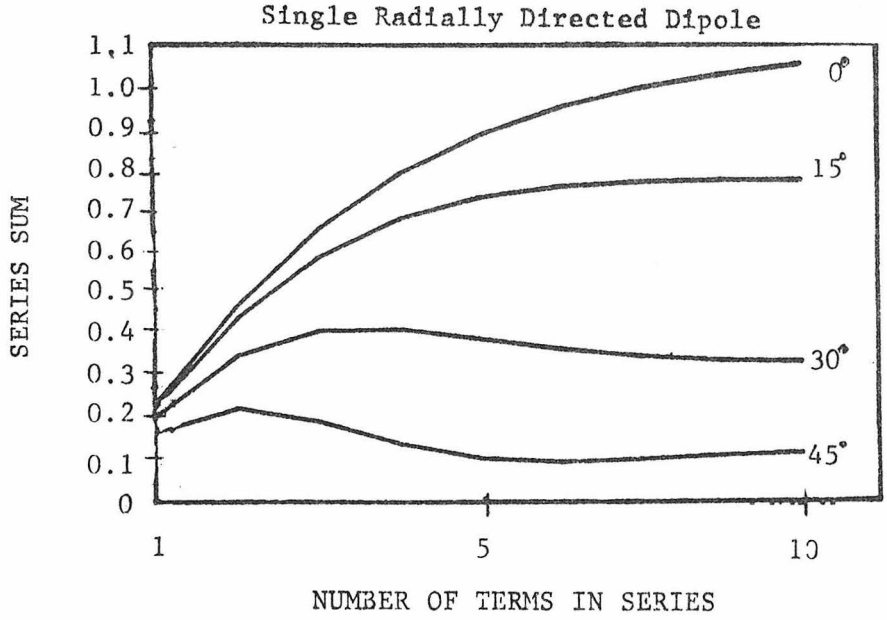

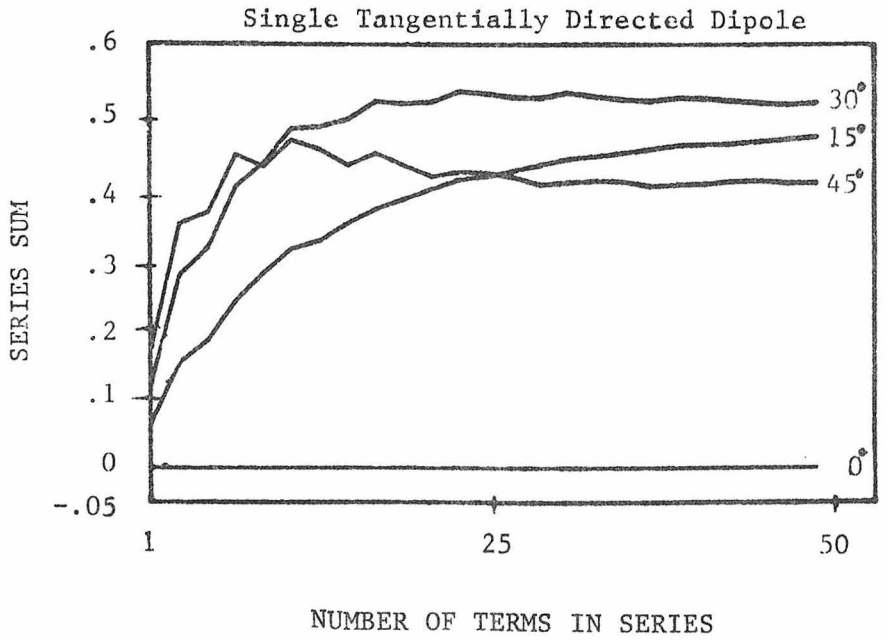

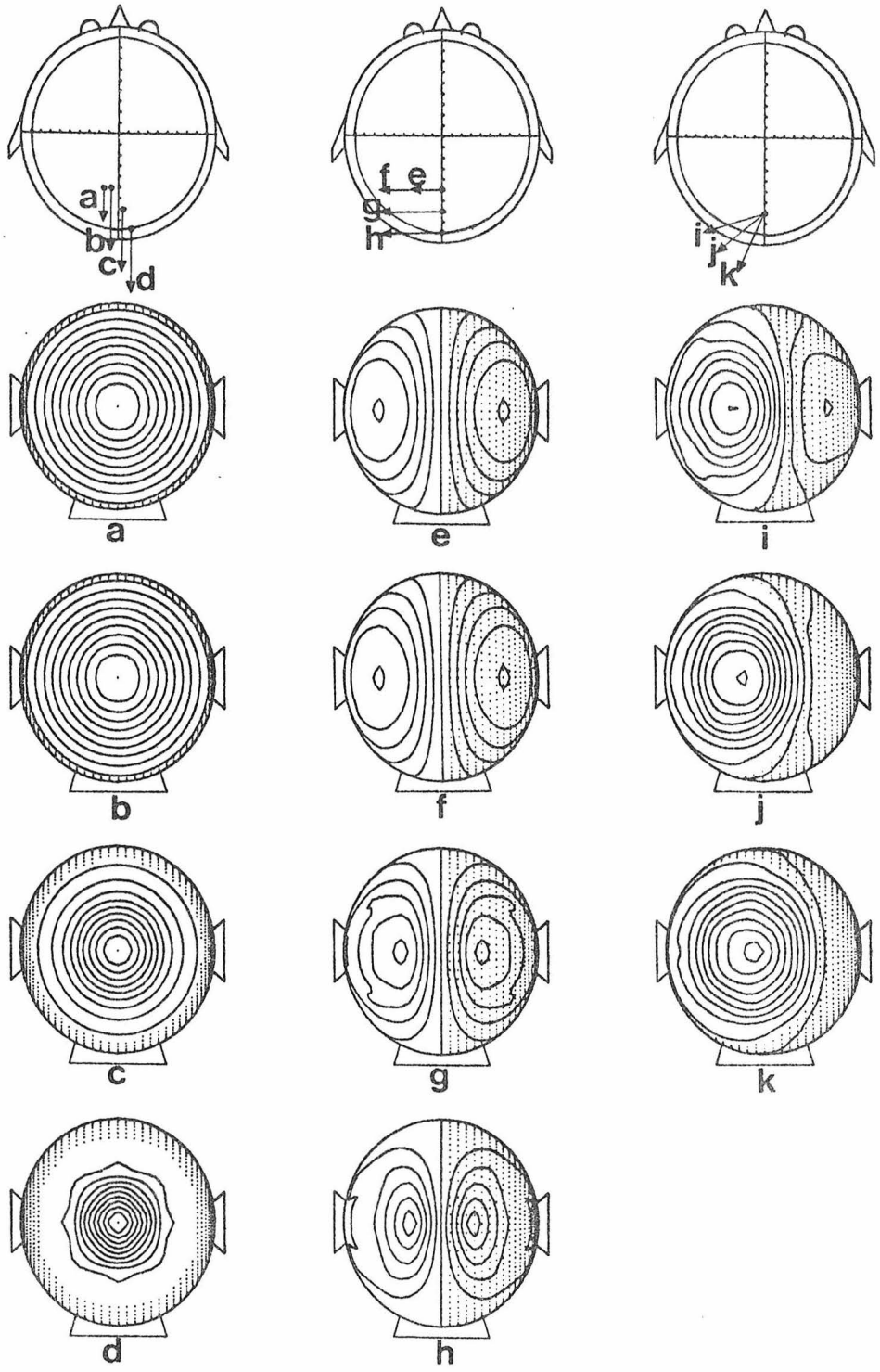

Fig. 33 - Model dipoles and corresponding distributions calculated for the 3-shell model of the head. a-d show various radial dipoles, while e-h show various tangential dipoles. i-k show various dipoles with radial and tangential components.

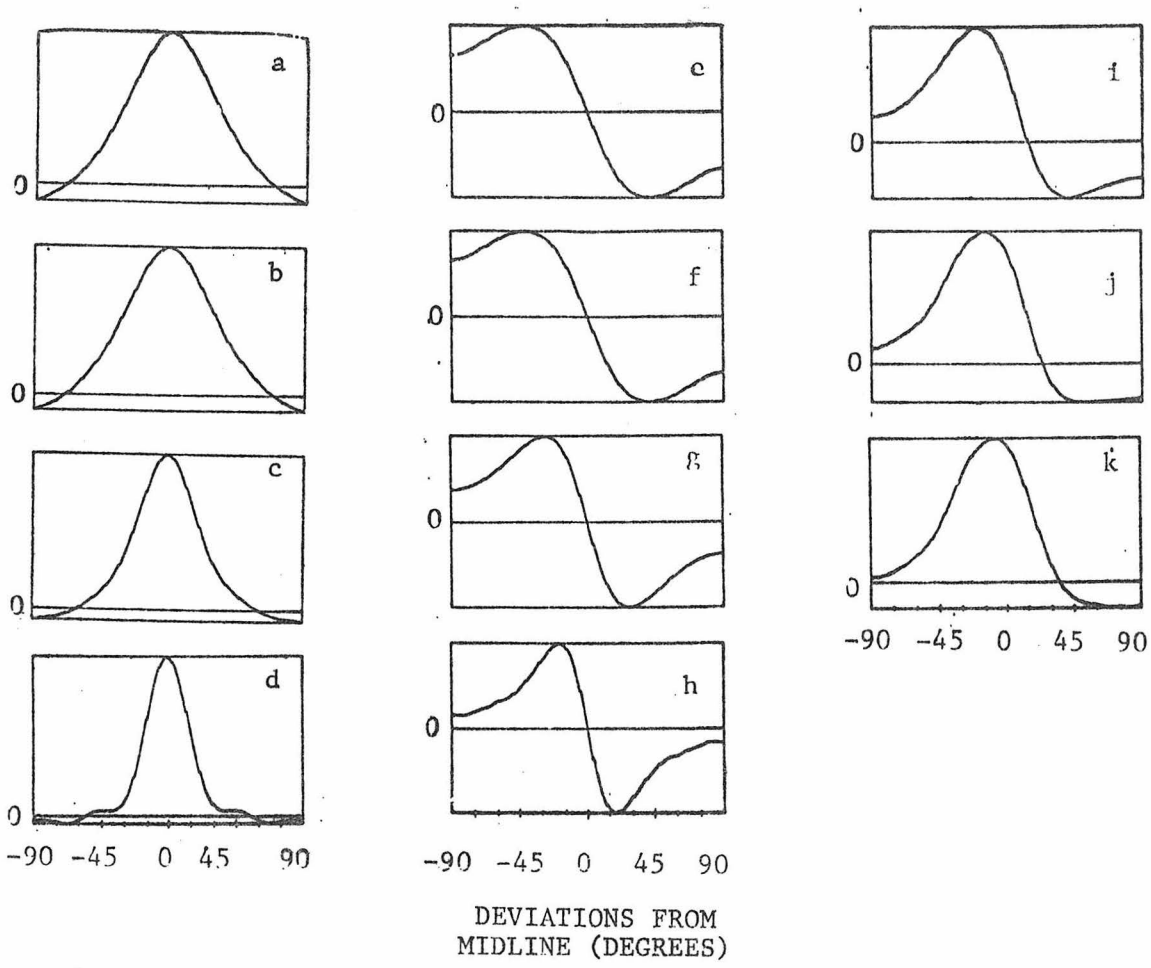

Fig. 34 - Cross-sections at the inion level of the potential distributions in the previous figure.

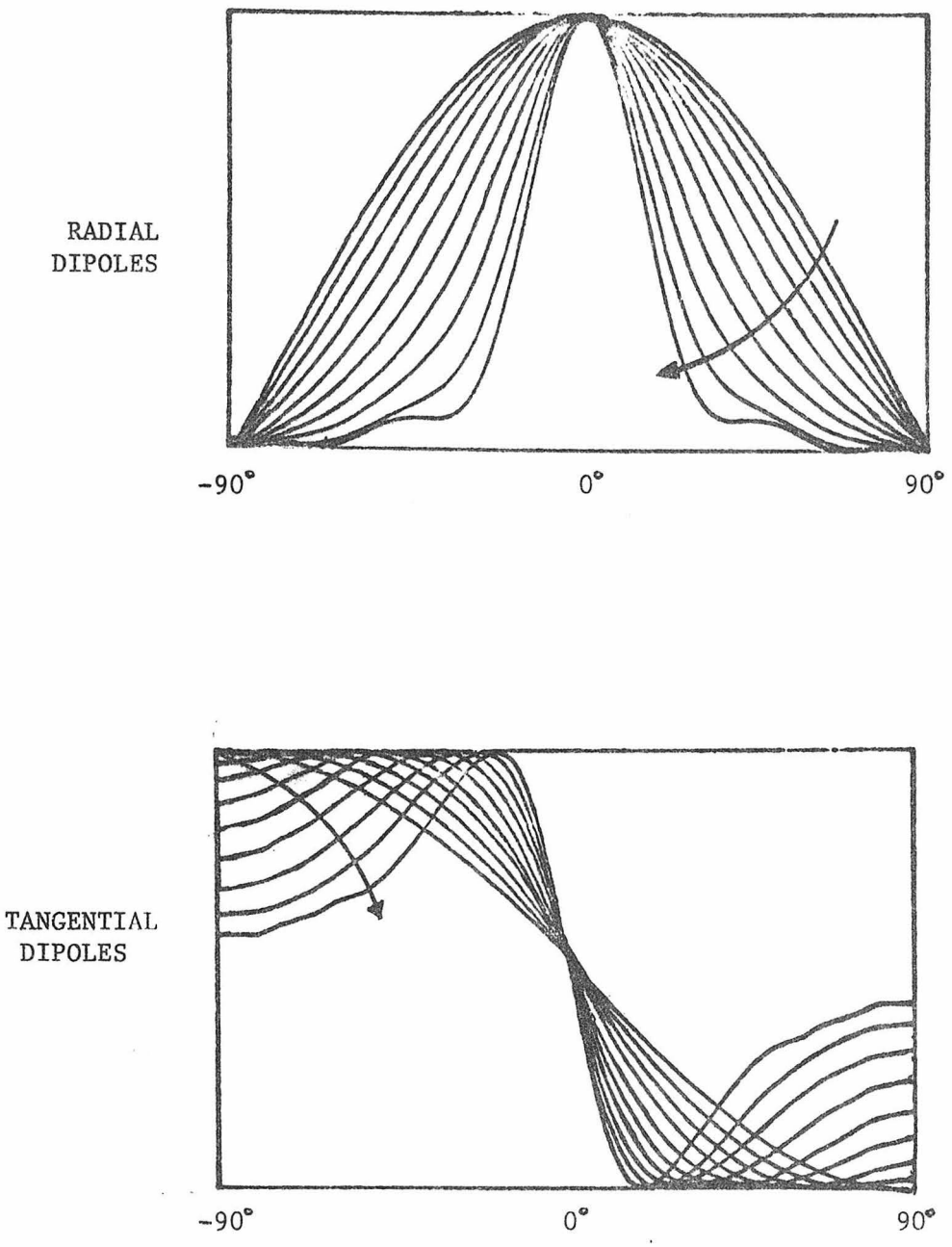

Fig. 35 - Potential distribution cross-sections at the inion level for two eccentricity series of dipoles in the 3-shell head model (f=0.01,0.1,0.2,0.3,0.4,0.5,0.6,0.7,0.8,0.9). The arrows indicate increasing eccentricity.

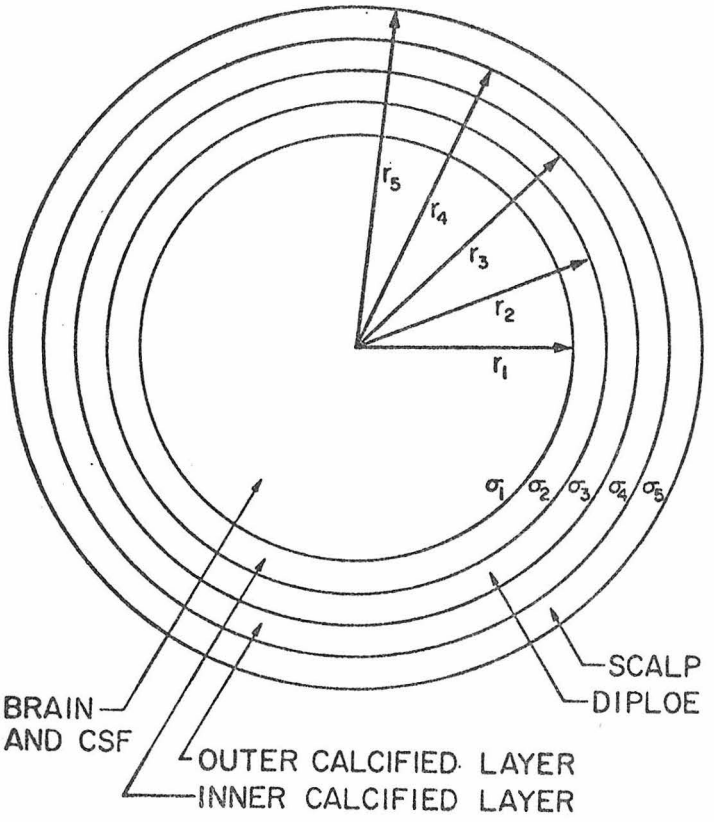

Fig. 36 - Concentric Shell Model of Head (5 shell)

scalp is modeled as a layer of conductivity σ_5 and outer radius r_5. The surface potential is the potential at the boundary r_5. The dipole and coordinate system parameters are the same those for the 3 shell model (Fig. 31b). To obtain the solution for this model, we will generalize the method of Kavanagh {73}:

The potential in region 1 due to dipole of moment M, located parallel to the z-axis in the x-z plane ($r=b$, $\theta=\theta_0$, $\phi=0$) is given by

$$\Phi_1 = \sum_{n=0}^{\infty} \sum_{m=0}^{n} \{ C_{mn_1} r^n + M_{mn} r^{-(n+1)} \} P_n^m(\mu) \cos m\phi \qquad b < r \leq r_1$$

where C_{mn_1} are undetermined constants and

$$M_{mn} = \frac{M}{4\pi\sigma_1} \cdot \frac{(2 - \delta_m^0)(n - m)!\, b^{n-1}\, P_{n-1}^m(\mu_0)}{(n + m - 1)!}$$

$\mu = \cos \theta$

$\mu_0 = \cos \theta_0$

$P_n^m(\mu)$ = associated Legendre function of the first kind with μ real and in the range $-1 \leq \mu \leq 1$.

$$\delta_m^n = \begin{cases} 1 \text{ if } m = n \\ 0 \text{ if } m \neq n \end{cases}$$

The potential in regions 2-5 are given by

$$\Phi_2 = \sum_{n=0}^{\infty} \sum_{m=0}^{n} \{ C_{mn_2} r^n + D_{mn_2} r^{-(n+1)} \} P_n^m(\mu) \cos m\phi \qquad r_1 \leq r \leq r_2$$

$$\Phi_3 = \sum_{n=0}^{\infty} \sum_{m=0}^{n} \{ C_{mn_3} r^n + D_{mn_3} r^{-(n+1)} \} P_n^m(\mu) \cos m\phi \qquad r_2 \leq r \leq r_3$$

$$\Phi_4 = \sum_{n=0}^{\infty} \sum_{m=0}^{n} \{ C_{mn_4} r^n + D_{mn_4} r^{-(n+1)} \} P_n^m(\mu) \cos m\phi \qquad r_3 \leq r \leq r_4$$

$$\Phi_5 = \sum_{n=0}^{\infty} \sum_{m=0}^{n} \{ C_{mn_5} r^n + D_{mn_5} r^{-(n+1)} \} P_n^m(\mu) \cos m\phi \qquad r_4 \leq r \leq r_5$$

In order to evaluate the unknown coefficients (C_{mn_1}, C_{mn_2}, C_{mn_3}, C_{mn_4}, C_{mn_5}, D_{mn_2}, D_{mn_3}, D_{mn_4}, D_{mn_5}) we must evaluate various boundary conditions. First of all, the potential must be continous at the boundaries between regions 1 and 2, 2 and 3, 3 and 4, and 4 and 5, i.e.

$$\Phi_1(r_1,\theta,\phi) = \Phi_2(r_1,\theta,\phi)$$

$$\Phi_2(r_2,\theta,\phi) = \Phi_3(r_2,\theta,\phi)$$

$$\Phi_3(r_3,\theta,\phi) = \Phi_4(r_3,\theta,\phi)$$

$$\Phi_4(r_4,\theta,\phi) = \Phi_5(r_4,\theta,\phi)$$

Secondly, the normal current must be continous at these same boundaries, i.e.

$$\sigma_1 \frac{\partial \Phi_1}{\partial r}(r_1,\theta,\phi) = \sigma_2 \frac{\partial \Phi_2}{\partial r}(r_1,\theta,\phi)$$

$$\sigma_2 \frac{\partial \Phi_2}{\partial r}(r_2,\theta,\phi) = \sigma_3 \frac{\partial \Phi_3}{\partial r}(r_2,\theta,\phi)$$

$$\sigma_3 \frac{\partial \Phi_3}{\partial r}(r_3,\theta,\phi) = \sigma_4 \frac{\partial \Phi_4}{\partial r}(r_3,\theta,\phi)$$

$$\sigma_4 \frac{\partial \Phi_4}{\partial r}(r_4,\theta,\phi) = \sigma_5 \frac{\partial \Phi_5}{\partial r}(r_4,\theta,\phi)$$

Also, the normal current at the outer surface of region 5 (scalp) must be zero

$$\sigma_5 \frac{\partial \Phi_5}{\partial r}(r_5,\theta,\phi) = 0$$

Evaluating these conditions gives 9 equations in 9 unknowns

$$
\begin{aligned}
&r_1^n C_{mn_1} - r_1^n C_{mn_2} && && - r_1^{-(n+1)} D_{mn_2} = - r_1^{-(n+1)} M_0 \\
&r_2^n C_{mn_2} - r_2^n C_{mn_3} && + r_2^{-(n+1)} D_{mn_2} && - r_2^{-(n+1)} D_{mn_3} = 0 \\
&r_3^n C_{mn_3} - r_3^n C_{mn_4} && + r_3^{-(n+1)} D_{mn_3} && - r_3^{-(n+1)} D_{mn_4} = 0 \\
&r_4^n C_{mn_4} - r_4^n C_{mn_5} && + r_4^{-(n+1)} D_{mn_4} && - r_4^{-(n+1)} D_{mn_5} = 0 \\
&\sigma_1 n r_1^{n-1} C_{mn_1} - \sigma_2 n r_1^{n-1} C_{mn_2} && && + \sigma_2 (n+1) r_1^{-(n+2)} D_{mn_2} = \sigma_1 (n+1) M_0 r_1^{-(n+2)} \\
&\sigma_2 n r_2^{n-1} C_{mn_2} - \sigma_3 n r_2^{n-1} C_{mn_3} && - \sigma_2 (n+1) r_2^{-(n+2)} D_{mn_2} && + \sigma_3 (n+1) r_2^{-(n+2)} D_{mn_3} = 0 \\
&\sigma_3 n r_3^{n-1} C_{mn_3} - \sigma_4 n r_3^{n-1} C_{mn_4} && - \sigma_3 (n+1) r_3^{-(n+2)} D_{mn_3} && + \sigma_4 (n+1) r_3^{-(n+2)} D_{mn_4} = 0 \\
&\sigma_4 n r_4^{n-1} C_{mn_4} - \sigma_5 n r_4^{n-1} C_{mn_5} && - \sigma_4 (n+1) r_4^{-(n+2)} D_{mn_4} && + \sigma_5 (n+1) r_4^{-(n+2)} D_{mn_5} = 0 \\
&n r_5^{n-1} C_{mn_5} && - (n+1) r_5^{-(n+2)} D_{mn_5} && = 0
\end{aligned}
$$

The coefficients can now be solved for algebraically. Since it is the solution at the scalp that is desired, we need only find C_{mn_5} and D_{mn_5}. This could be done explicitly or numerically. Since these constants depend only on the dipole parameters, the method chosen here was to evaluate the coefficients numerically using the Gauss-Jordan method of solving matrix equations. Once C_{mn_5} and D_{mn_5} are found, the series can be evaluated

$$V(\theta,\phi;b,\theta_0,M) = \sum_{n=0}^{\infty} \sum_{m=0}^{n} K_n(b,\theta_0,M) P_n^m(\cos\theta) \cos m\phi$$

where

$$K_n(b,\theta_0,M) = C_{mn_5} + D_{mn_5}$$

Once again, for these equations to be generally applicable, the coordinates of an arbitrary dipole must be rotated so that the dipole is parallel to the z-axis in the x-z plane, thus

$$
\begin{aligned}
V(\theta,\phi;b,\theta_0,M,\alpha,\beta,\gamma) &= V\{\theta^*(\theta,\phi,\alpha,\beta),\phi^*(\theta,\phi,\alpha,\beta,\gamma);b,\theta_0(\alpha,\beta,\gamma),M\} \\
&= \sum_{n=0}^{\infty} \sum_{m=0}^{n} K_n(b,\theta_0(\alpha,\beta,\gamma),M) P_n^m(\cos\theta^*) \cos m\phi^*
\end{aligned}
$$

with all terms defined as for the 3 shell model. Also, the same convergence criterion was used for this model as for the 3 shell model.

Figures 37, 38 and 39 show examples of potentials generated by dipoles in the 5 shell model of the head. Here $r_1=0.90$, $r_2=0.92$, $r_3=0.96$, $r_4=0.98$ and $r_5=1$, while $\sigma_1=\sigma_3=\sigma_5=80\sigma_2=80\sigma_4$. The dipoles are the same as those in Figures 28, 29 and 30 and Figures 33, 34 and 35. Note that the distributions of the 5 shell model do not differ greatly from those of the 3 shell model.

3.4.4 Relationship of Dipoles in Homogeneous and Shell Models

As mentioned in section 2.1.6 and illustrated in the figures of sections 3.4.1, 3.4.2 and 3.4.3, there are significant differences between potential fields of dipoles in the homogeneous and shell models. The shell models more realistically reflect the properties of the head and are therefore preferable. However, the shell models are more difficult computationally than the homogeneous model. As will be seen, there is a systematic difference between solutions based on the shell models and solutions based on the homogeneous model. This makes it possible to compute solutions using the simpler homogeneous model and subsequently transform the solutions to inhomogeneous model solutions.

Arthur and Geselowitz [50] and Schneider [51] have shown that when terms beyond quadrapolar are neglected, coefficients of multipole expansions of the potential on the surface of the homogeneous and 3 shell models may be compared. For surface potential distributions which are equal up to quadrapolar contributions (but in error for higher order terms), the following ratios [51] apply to the dipole parameters

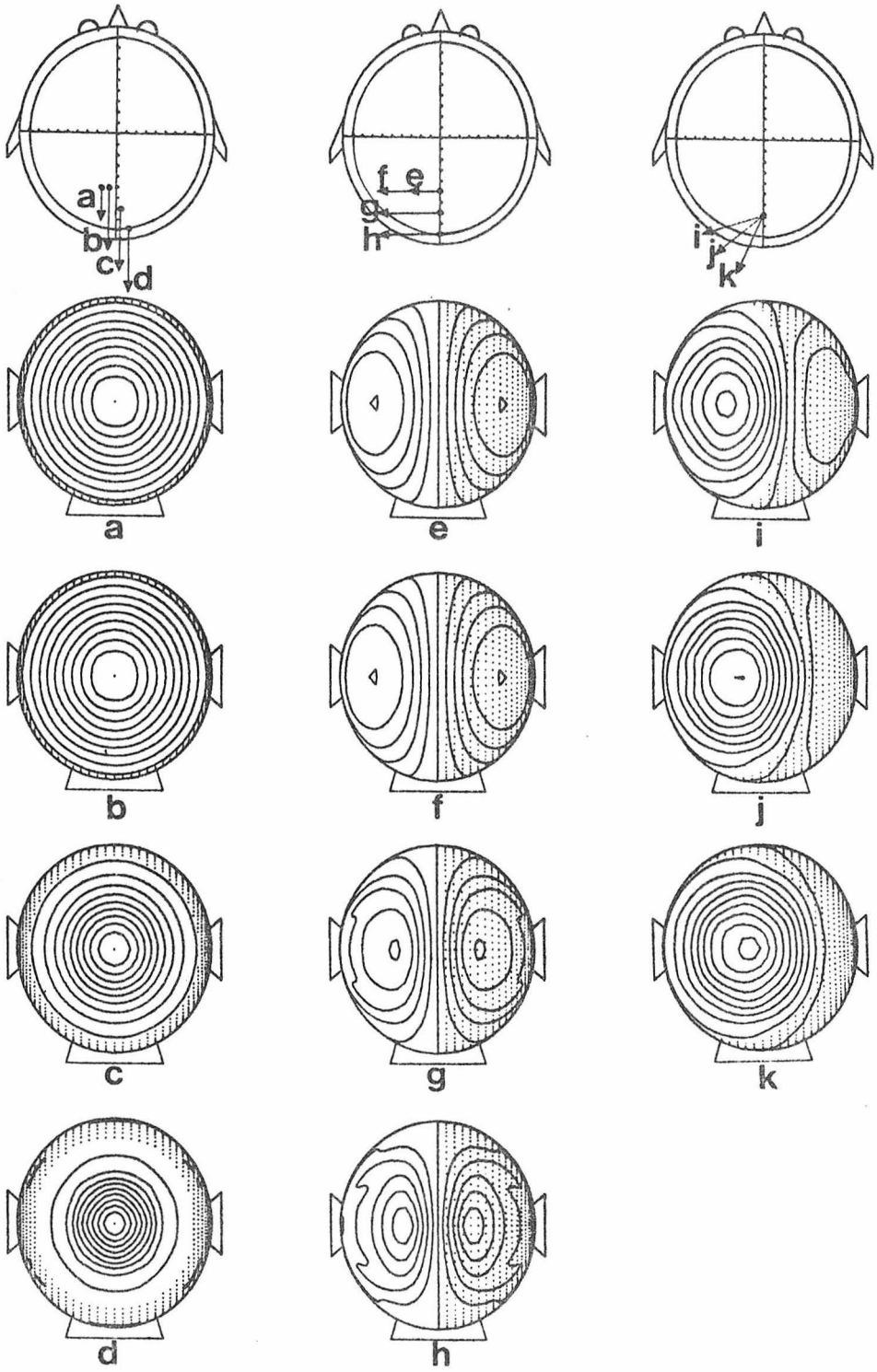

Fig. 28 - Model dipoles and corresponding distributions calculated for the 5-shell model of the head. a-d show various radial dipoles, while e-h show various tangential dipoles. i-k show various dipoles with radial and tangential components.

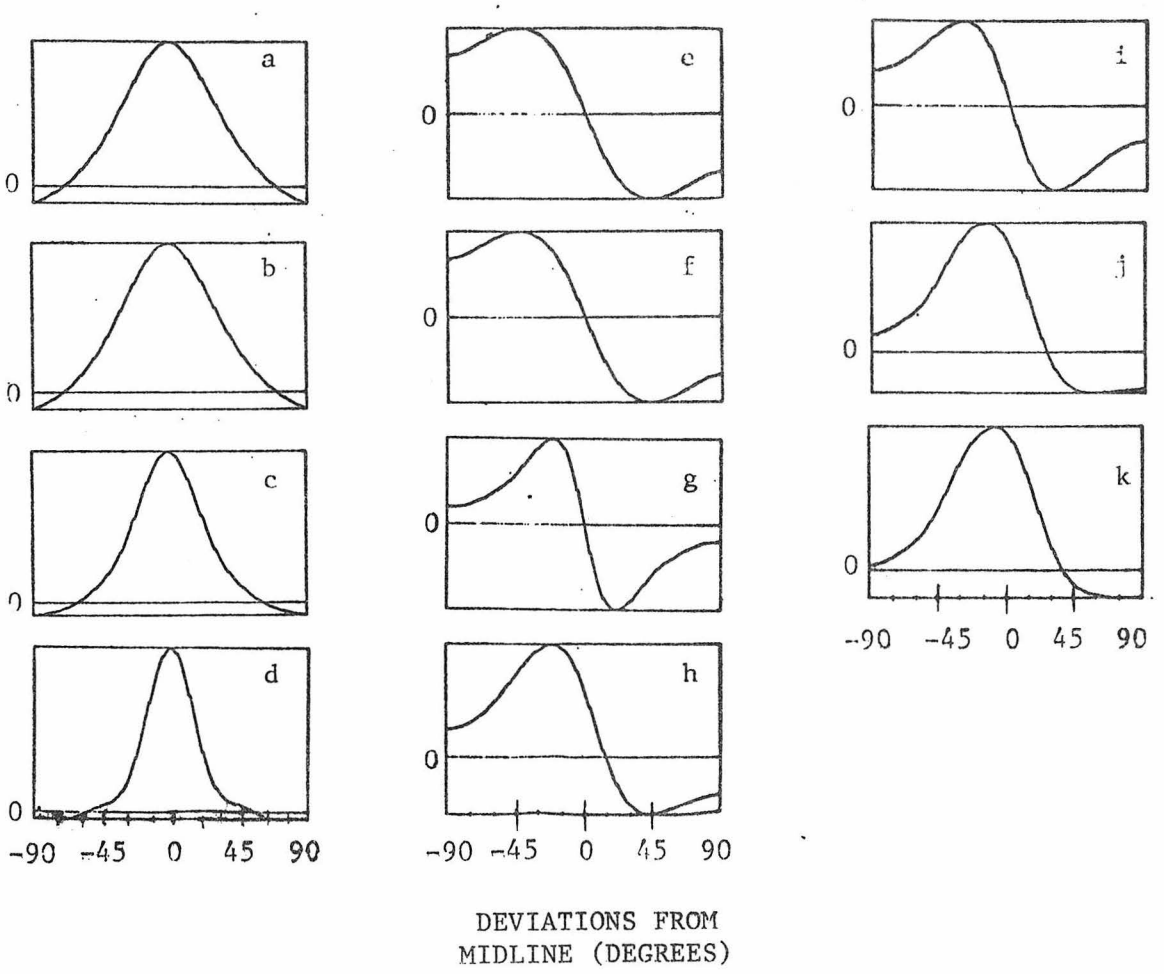

Fig. 38 - Cross-sections at the inion level of the potential distributions in the previous figure.

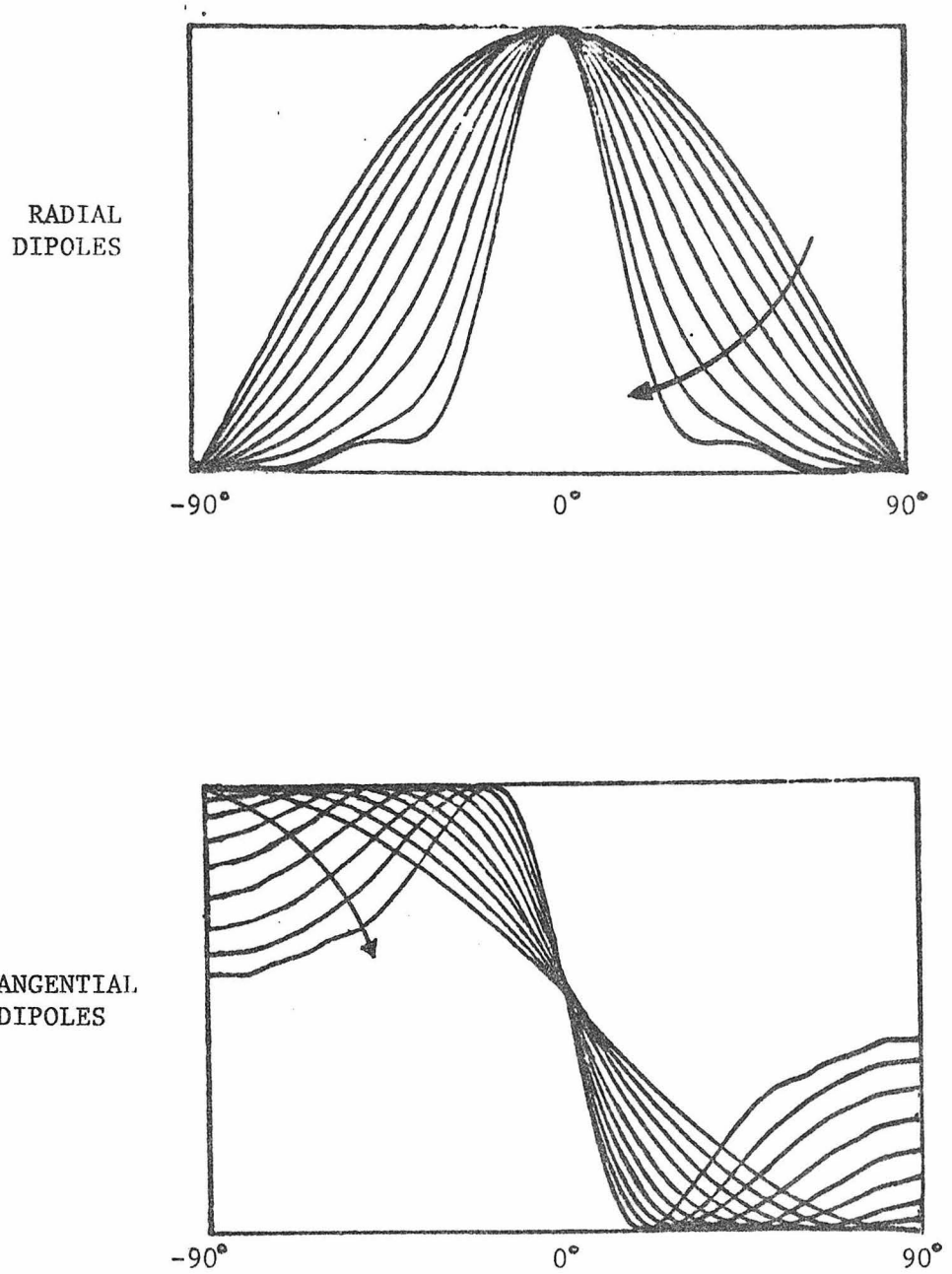

Fig. 39 - Potential distribution cross-sections at the inion level for two eccentricity series of dipoles in the 5-shell head model (f=0.01,0.1,0.2,0.3,0.4,0.5,0.6,0.7,0.8,0.9). The arrows indicate increasing eccentricity.

$$\frac{b_h}{b_s} = \frac{h(2)}{h(1)} \text{ and } \frac{M_h}{M_s} = h(1)$$

where b_h and M_h are the eccentricity and moment of the dipole in the homogeneous sphere, while b_s and M_s are the corresponding parameters in the 3 shell model, and

$$h(n) = \frac{(2n+1)^2 \cdot k}{(n+1) \cdot D_n}$$

where:

$$D_n = \frac{(kn + k + n)\left\{n \cdot \frac{k}{\ell} + n + 1\right\}}{n + 1}$$

$$-(kn + k + n)\left\{1 - \frac{k}{\ell}\right\} r_2^{2n+1}$$

$$+(1 - k)\left\{n + \frac{k}{\ell}(n + 1)\right\} r_1^{2n+1}$$

$$-n(1 - k)\left\{1 - \frac{k}{\ell}\right\}\left\{\frac{r_1}{r_2}\right\}^{2n+1}$$

and $k = \sigma_2/\sigma_1$ and $\ell = \sigma_3/\sigma_1$ with the σ_i and r_i as defined in Figure 31a. When $\sigma_1=\sigma_3=80\sigma_2$, and $r_1=0.90$ and $r_2=0.98$, we have:

$$\frac{b_h}{b_s} = 0.829 \text{ and } \frac{M_h}{M_s} = 0.338$$

These relationship are independent of dipole orientation. They indicate that the inhomogeneities of the 3 shell model tend to make a dipole's location appear more centric than if the case is analyzed as a homogeneous sphere. Similarly its magnitude appears to be reduced. These ratios may be used to make approximate conversions between the two models.

To check these ratios empirically in a practical situation and to estimate their value for the 5 shell model, computational tests were done. The method used was to calculate potential distributions for various dipole parameters in the 3 and 5 shell models and to find those dipole parameters in the homogeneous sphere model which gave the best

approximation to the inhomogeneous model distributions in the least-squares sense. This was done according to the methods described in section 3.5. Figs. 40 and 41 show the results for the two inhomogeneous models, where it can be seen that the eccentricity ratio (b_h/b_s) is substantially correct for the 3-shell model and modified slightly for the 5-shell model. The moment ratios (M_h/M_s) are also constant at 0.325 and 0.3 for the 3- and 5-shell models, respectively. These ratios are independent of dipole orientation. Figs. 42 and 43 show two other comparisons of the three models. Fig. 42 plots relative peak amplitudes of radial dipoles in each model as a function of dipole eccentricity, while Fig. 43 plots half-amplitude widths of radial dipoles as a function of eccentricity. These diagrams further point out the large differences between the homogeneous and shell models, and the insubstantial differences between the 3 and 5 shell models.

3.4.5 Multiple Sources and Source Distributions

There is no analytical difficulty in calculating surface potential distributions resulting from multiple sources in each model of the head. From considerations of linearity, results for a single dipole source can be generalized to multiple dipole source elements by the superposition principle. The potential at any point on the surface is merely the linear sum of the potentials from each individual source. This principle can be applied in a discrete fashion (summation) for distinct source elements or in a continuous fashion (integration) for source distributions.

As mentioned in Section 2.1.5, it is assumed that active cortex may be modeled to a good approximation as a layer of current dipoles with its constituent dipoles oriented at right angles to the cortical surface. Such dipole layers may be accurately approximated as continuous or by a

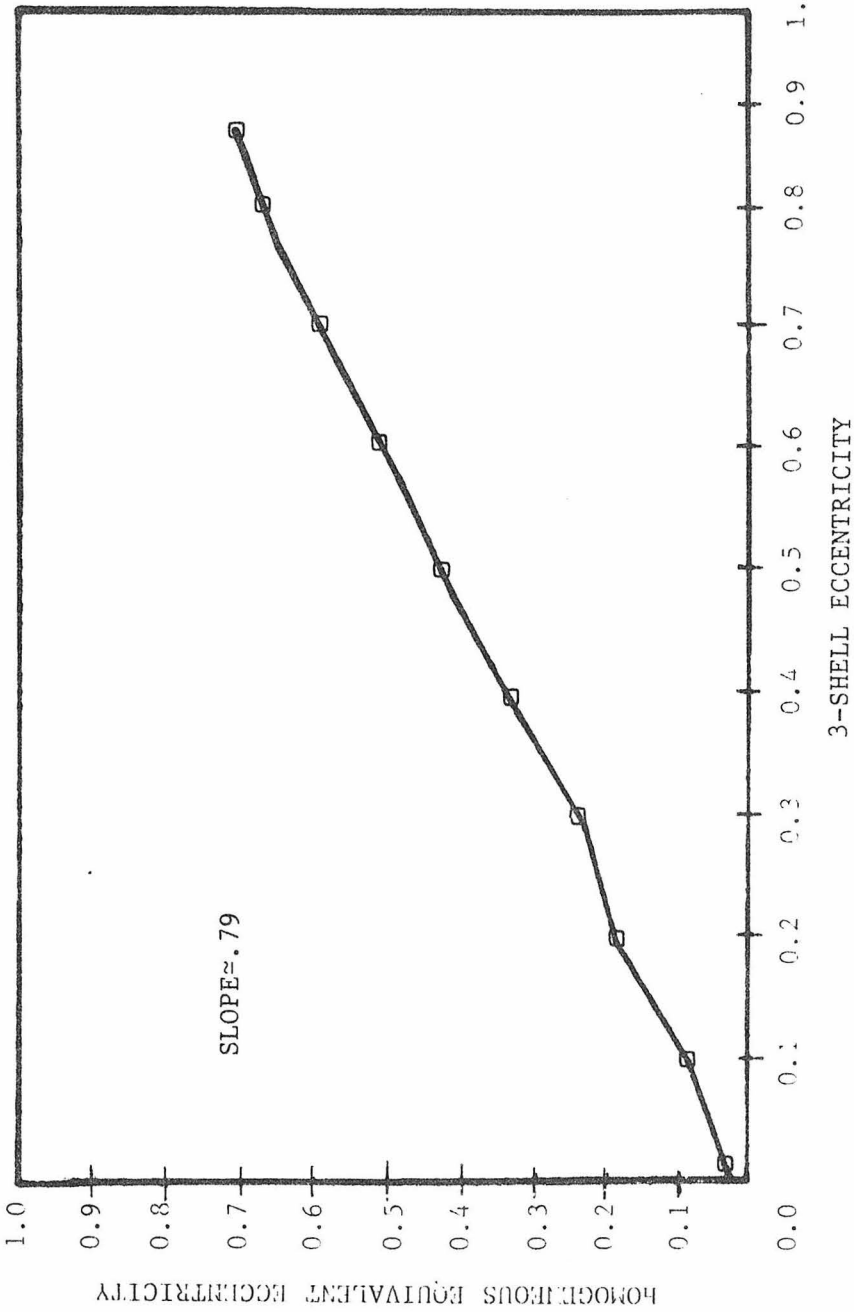

Fig. 40 - Eccentricity of homogeneous model dipoles which give optimal least-squares fits to various radially directed 3-shell model dipole fields.

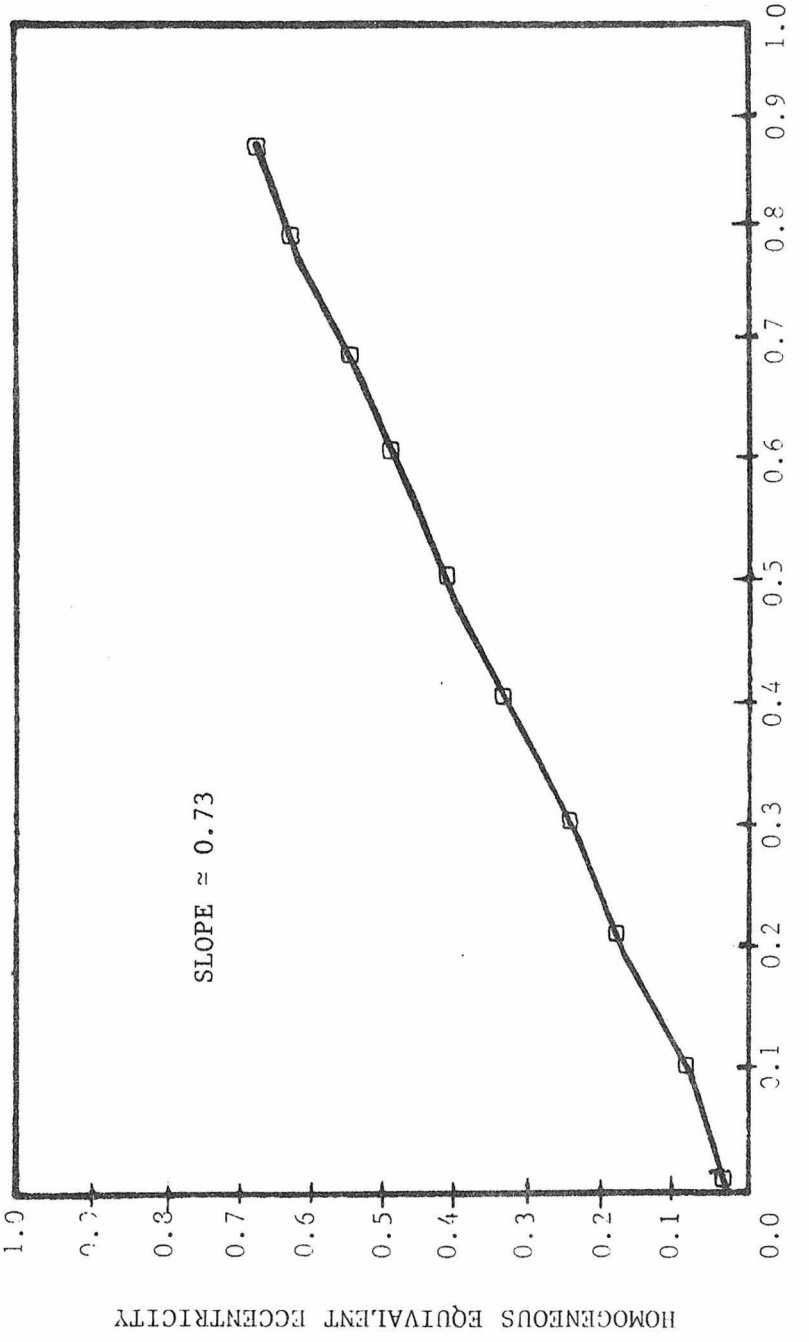

Fig. 41 - Eccentricity of homogeneous model dipoles which give optimal least-squares fits to various radially directed 5-shell model dipole fields.

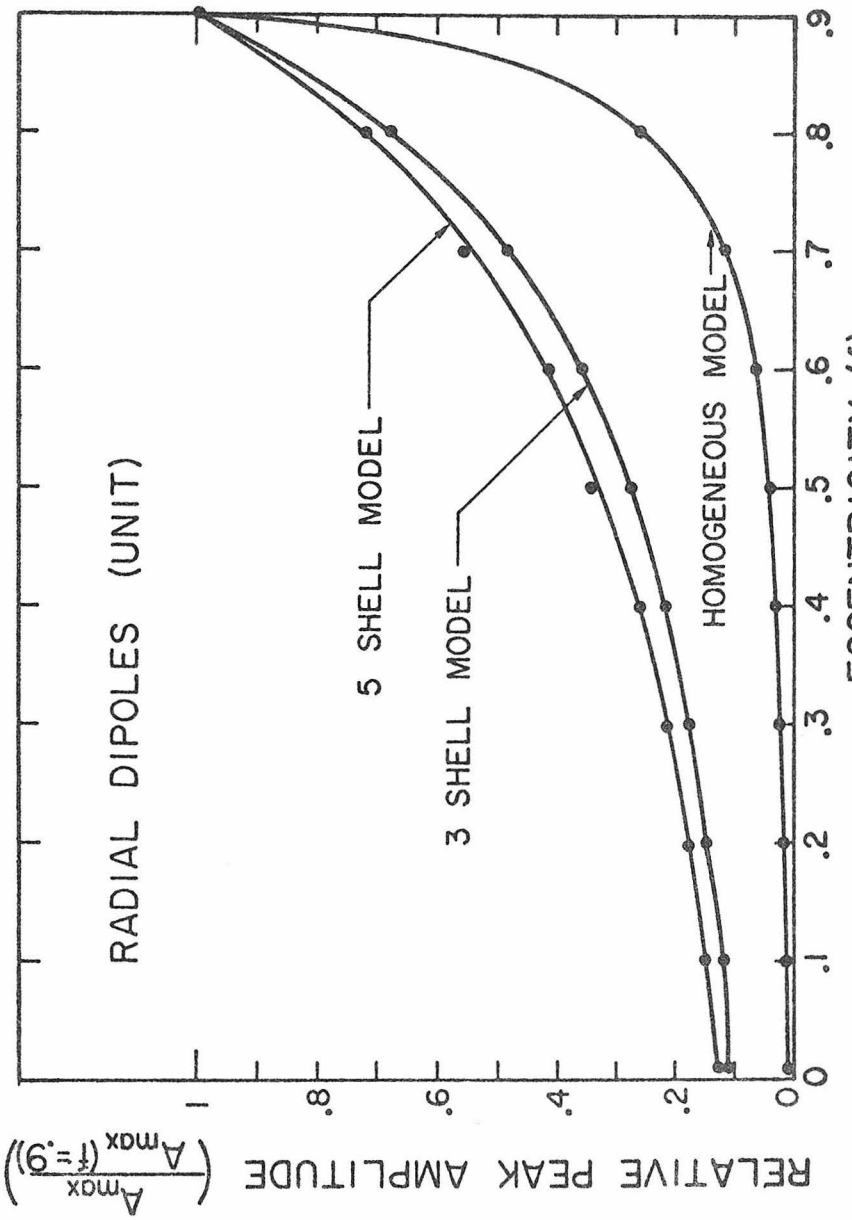

Fig. 42 - Dependence on eccentricity of peak amplitudes in potential distributions generated by radially directed dipoles in the three models of the head.

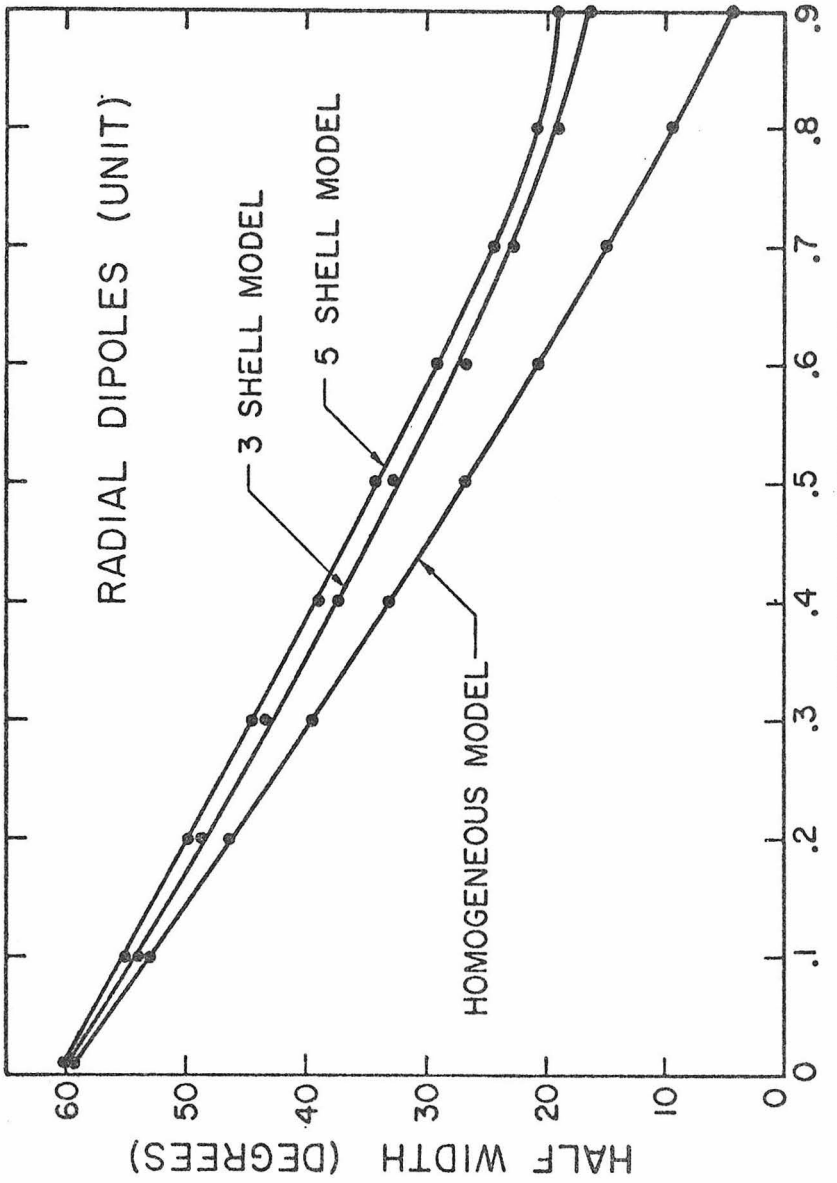

Fig. 43 - Dependence on eccentricity of half-amplitude widths of potential distributions generated by radially directed dipoles in the three models of the head.

number of discrete dipoles. For some continuous dipole layers with simple surfaces, exact solutions to Laplace's Equation are obtainable {158}. Other dipole layers must be discretely approximated. Discrete approximation is the method used here because of its general applicability.

3.4.6 Spherical Cap Dipole Layer

Here the head is represented by either the homogeneous sphere or one of the shell models. The solutions used here approximate the surface potential for all θ and ϕ resulting from a spherical cap dipole layer (constituent dipoles normal to cap surface) centered on the z-axis at $r=f_0 R$ and of angular extent $2\omega_0$ (Fig. 44a). Using superposition of discrete dipoles, we have:

$$V(\theta,\phi;f_0,\omega_0,M) = \sum_{\omega=0}^{\omega_0} \sum_{\mu=0}^{2\pi} V_1(\theta,\phi;f_0 x_{\omega\mu}, f_0 y_{\omega\mu}, f_0 z_{\omega\mu}, M_{\omega\mu}, My_{\omega\mu}, Mz_{\omega\mu})$$

where: V_1 = single radial dipole field prediction at (θ,ϕ),

$x_{\omega\mu}$ = sin ω cos μ,

$y_{\omega\mu}$ = sin ω sin μ,

$z_{\omega\mu}$ = cos ω,

ω = azimuth (θ coordinate) of given dipole equiangularly spaced between 0 and ω_0,

μ = latitude (ϕ coordinate) of given dipole with equiangular spacing between 0 and 2π.

The layout used for ω and μ is shown in Fig. 44b and was used to provide uniform dipole density. To be generally applicable, rotation parameters must be introduced so that the spherical cap may be centered on any radius of the sphere. Doing this, we have:

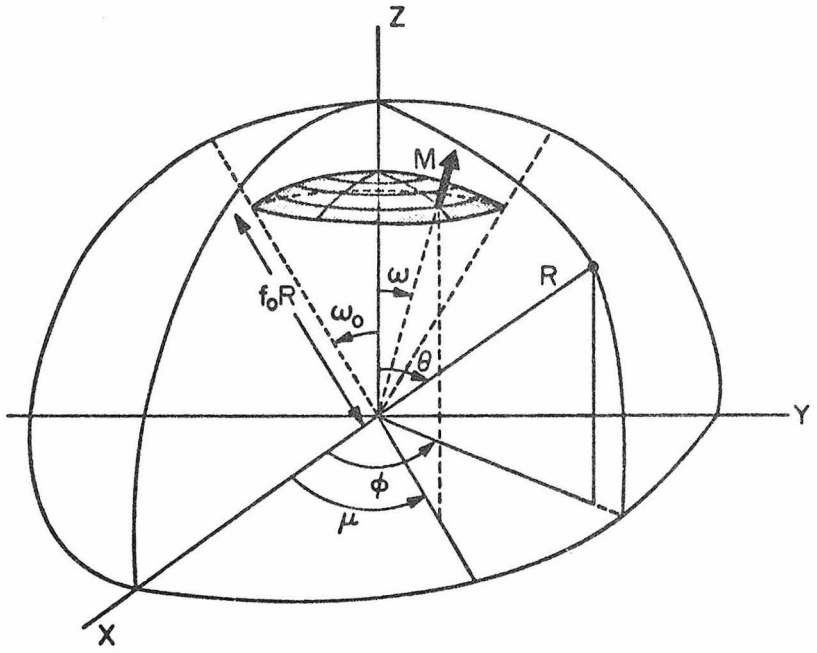

Fig. 44a - Coordinate system and parameters for radial cap dipole layer

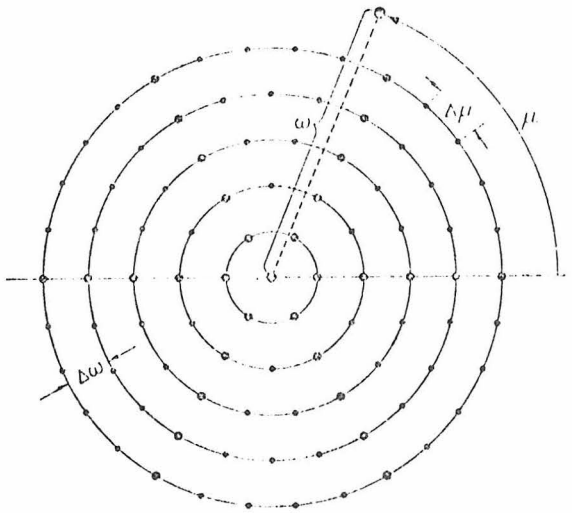

Fig. 44b - Spacing used in forming radial cap dipole layer

$$V(\theta,\phi;f_0,\omega_0,M,\theta^*,\phi^*) = \sum_{\omega=0}^{\omega_0} \sum_{\mu=0}^{2\pi} V_1(\theta',\phi';f_0x_{\omega\mu},f_0y_{\omega\mu},f_0z_{\omega\mu},Mx_{\omega\mu},My_{\omega\mu},Mz_{\omega\mu})$$

where: (θ^*, ϕ^*) = azimuth and latitude of spherical cap center

θ' = azimuth of surface point in rotated coordinate system

$= \cos^{-1}\{\cos\theta\cos\theta^* + \sin\theta\sin\theta^*\cos(\phi-\phi^*)\}$

ϕ' = latitude of surface point in rotated coordinate system

$= \sin^{-1}\{\sin\theta \cdot \sin(\phi-\phi^*) / \sin\theta'\}$

Fig. 45 illustrates the effects of dipole spacing ($\Delta\omega$) on potential distributions generated by spherical cap dipole layers in the homogeneous sphere model. These effects are much less noticeable in the shell models owing to the smearing effects of the skull and scalp. Figs. 46, 47 and 48 show examples of potential distributions generated by spherical caps of varying eccentricity (f_0) and angular extent (ω_0) in the homogeneous (Fig. 46), 3 shell (Fig. 47) and 5 shell (Fig. 48) models of the head. Note that the primary effect of angular extent is to flatten and extend the peak of the distribution and that this effect is less noticeable in the shell models.

The spherical cap dipole layer is intended to represent cortex parallel to the head's surface and is the extended source analogue of the single radially directed dipole. Fig. 49 illustrates the relationship between the radial cap model and a single radial dipole, by showing those single radial dipoles which give the best approximations in the least-squares sense to the fields of radial caps with various angular extents. Here it can be seen that a single radial dipole gives a good approximation to extended layers of up to 10° angular extent. For larger angular extents the single dipole model will underestimate the source's eccentricity and deviate significantly in its field predictions.

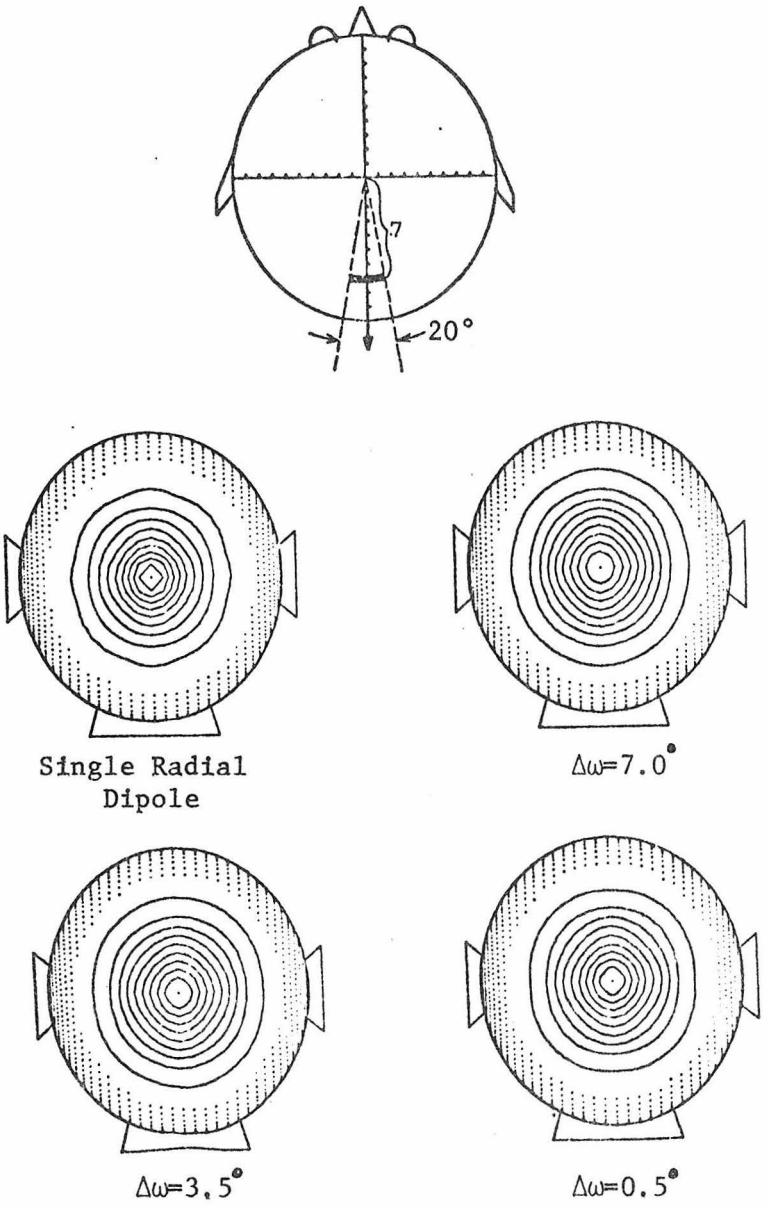

Fig. 45 - Effect of dipole spacing (Δω) on potential distributions generated by spherical cap dipole layers in the homogeneous sphere model of the head.

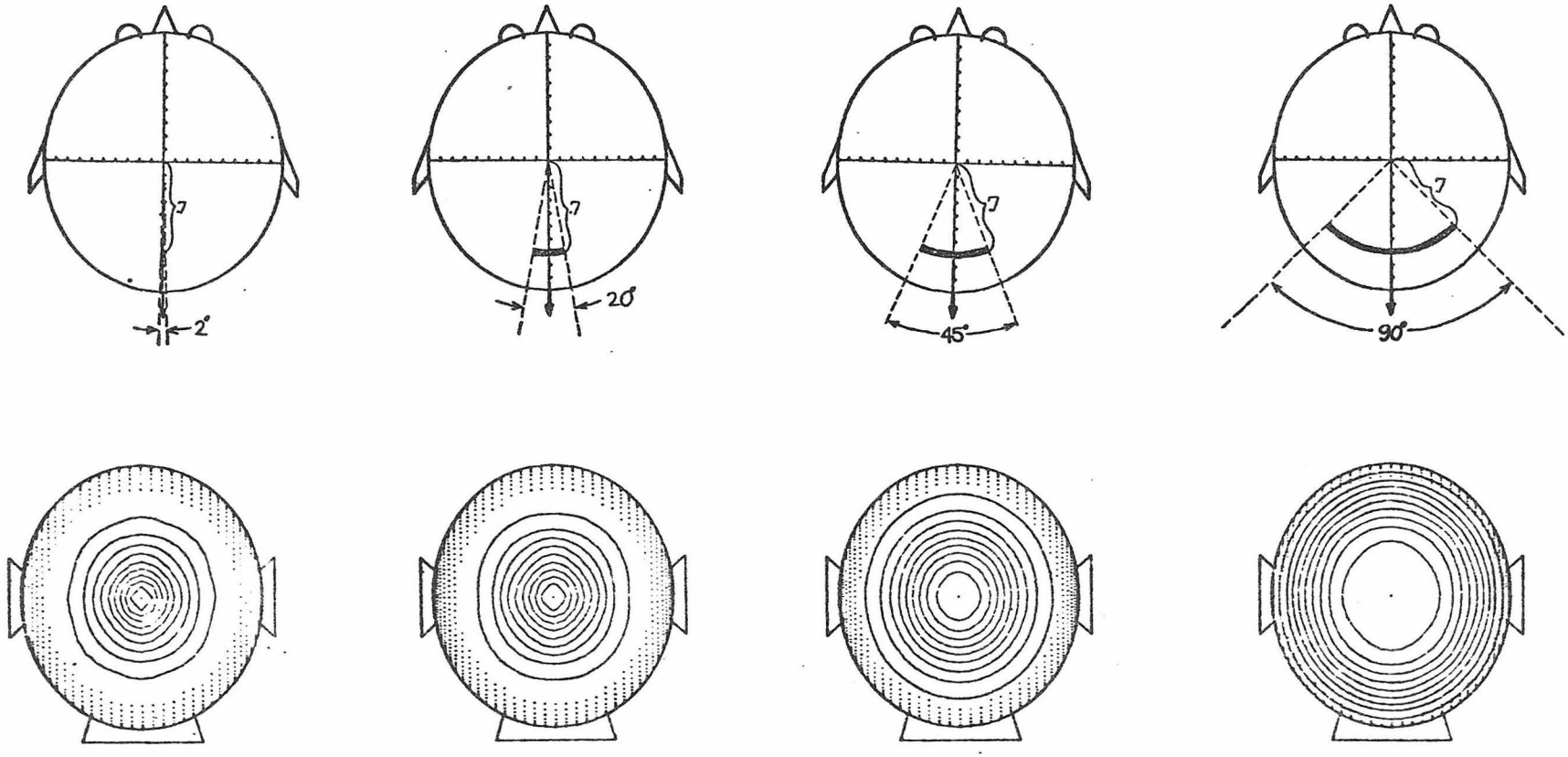

Fig. 46 - Examples of potential distributions generated by spherical caps of various angular extents (ω_0) in the homogeneous model of the head.

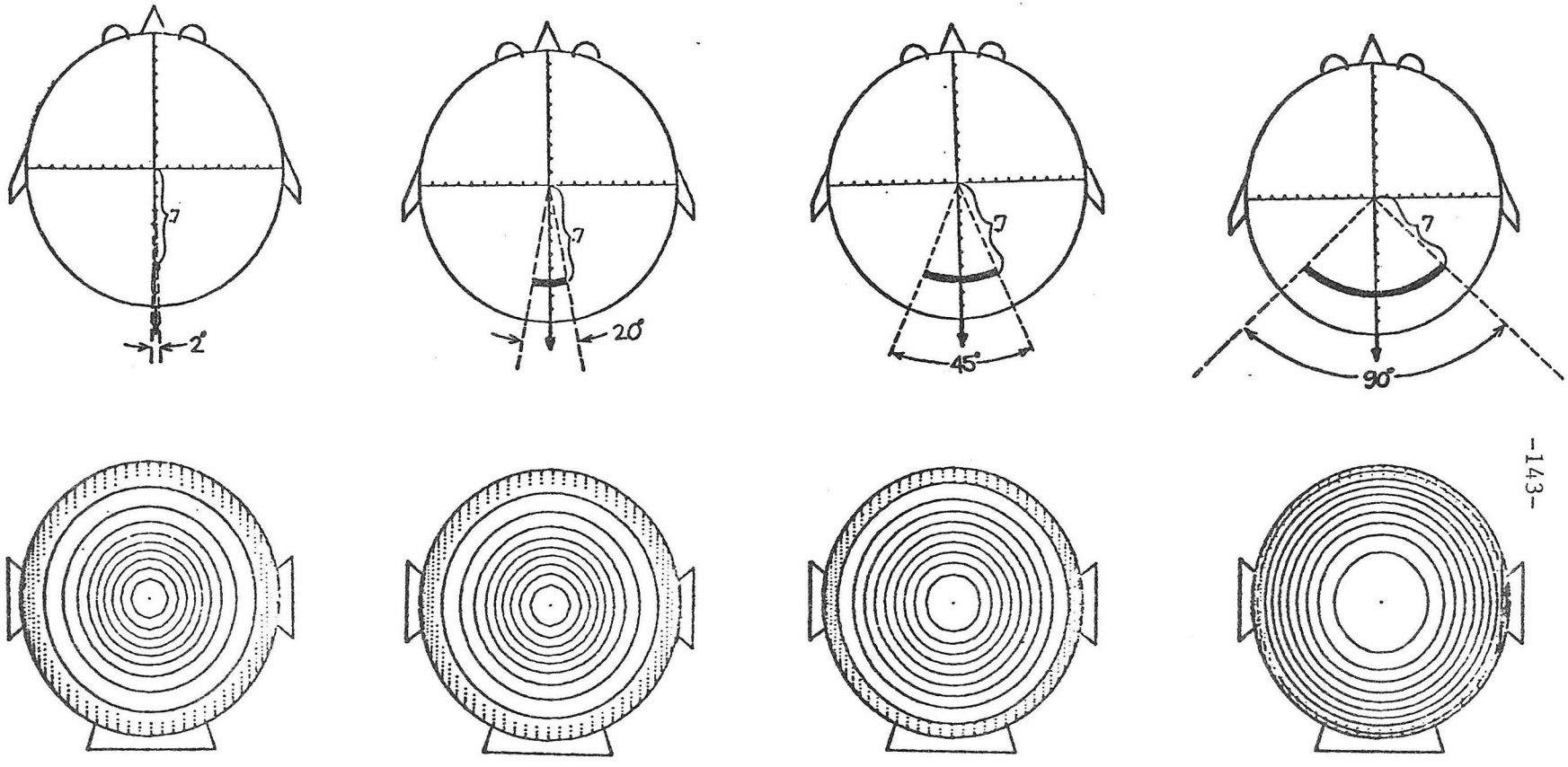

Fig. 47 - Examples of potential distributions generated by spherical caps of various angular extents (ω_0) in the 3-shell model of the head.

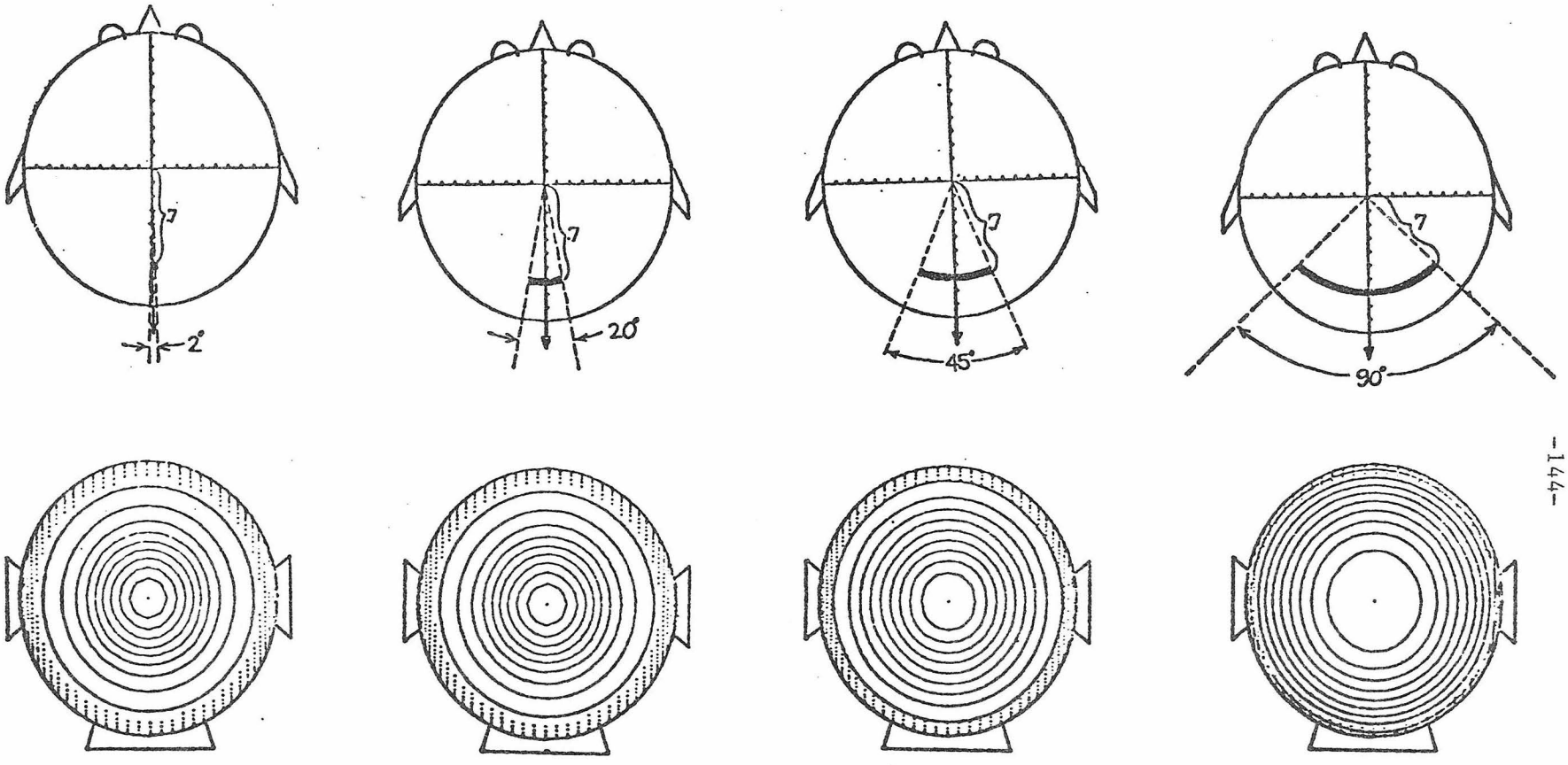

Fig. 48 - Examples of potential distributions generated by spherical caps of various angular extents (ω_0) in the 5-shell model of the head.

Fig. 49 - Comparison of radial cap dipole layers (f_0=0.7) with single radially directed dipoles

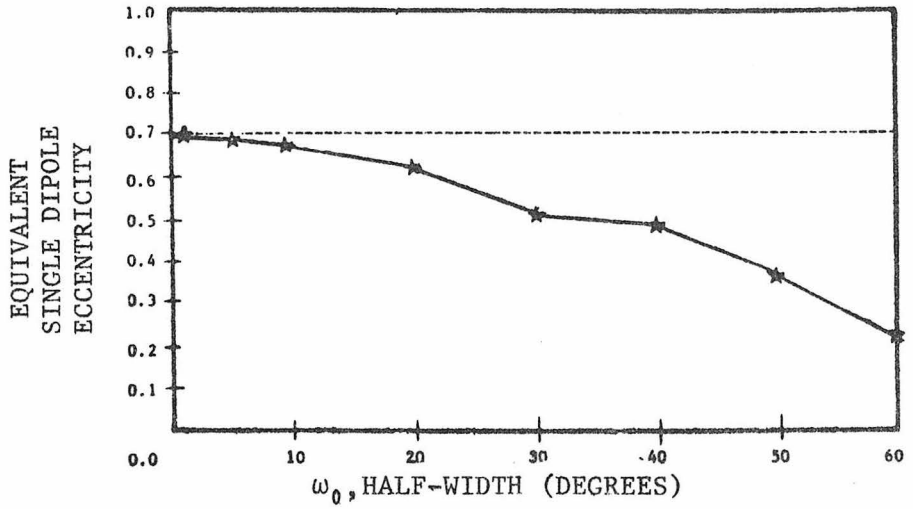

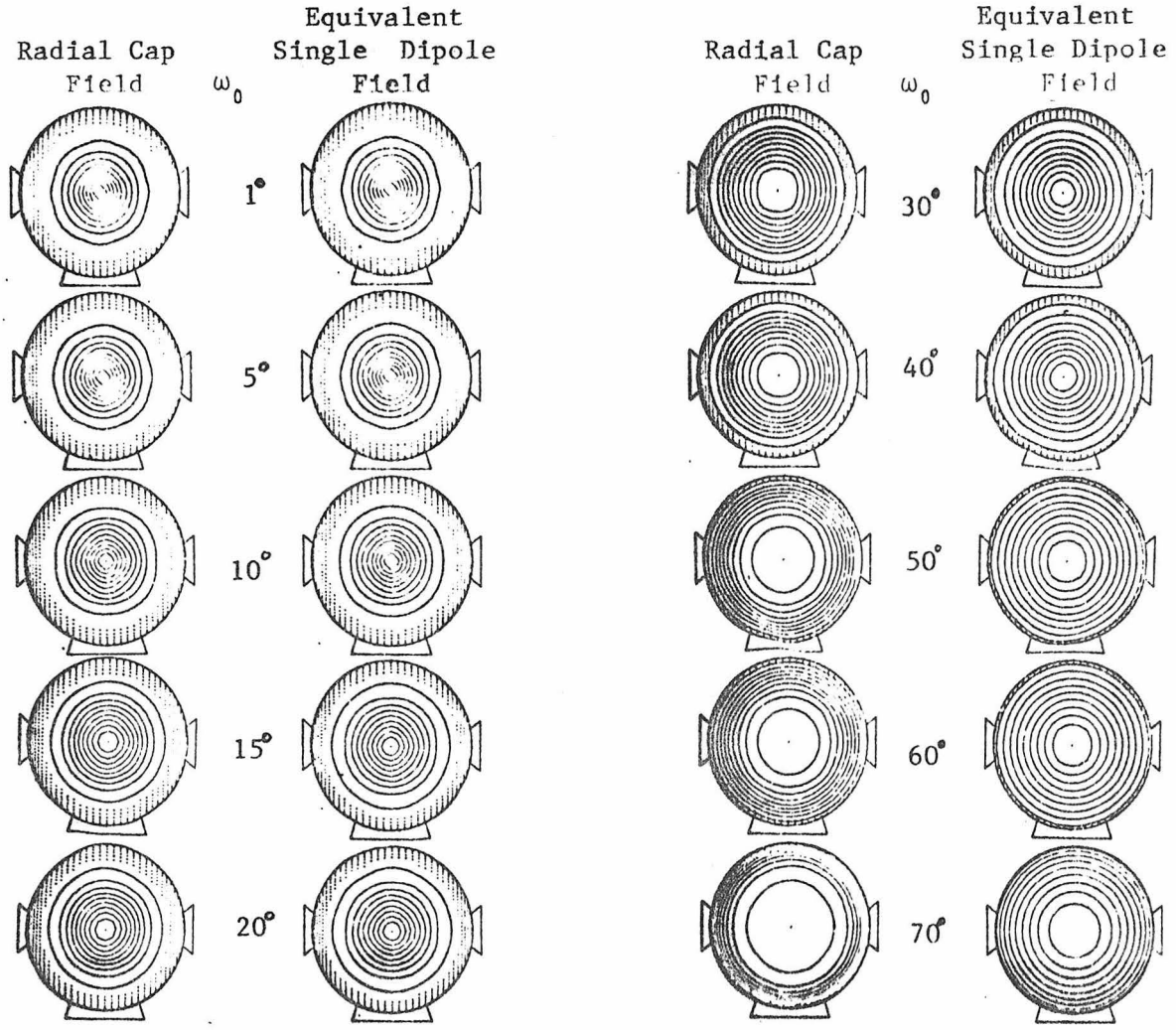

3.4.7 Annular Sector Dipole Layer

Again the head is represented by either the homogeneous sphere or one of the shell models. The solutions used here approximate the surface potential for all θ and ϕ resulting from a plane annular sector dipole layer (constituent dipoles normal to plane surface) centered on the z-axis between $r=f_0-f_1$ and $r=f_0+f_1$ in the y-z plane and of angular extent $2\omega_0$ (Fig. 50a). Using superposition of discrete dipoles, we have:

$$V(\theta,\phi;f_0,f_1,\omega_0,M) = \sum_{f=f_0-f_1}^{f_0+f_1} \sum_{\omega=-\omega_0}^{\omega_0} V_1(\theta,\phi;0,f\sin\omega,f\cos\omega,M,0,0)$$

where: V_1 = single tangential dipole field prediction at (θ,ϕ)

f = eccentricity of given dipole equally spaced between f_0-f_1 and f_0+f_1.

ω = azimuth (θ coordinate) of given dipole equiangularly spaced between $-\omega_0$ and ω_0

The layout used for f and ω is shown in Fig. 50b and was used to provide approximately uniform dipole density. Once again, rotation parameters must be introduced to allow arbitrary positioning of the dipole layer. Doing this, we have:

$$V(\theta,\phi;f_0,f_1,\omega_0,M,\theta^*,\phi^*,\gamma) = \sum_{f=f_0-f_1}^{f_0+f_1} \sum_{\omega=-\omega_0}^{\omega_0} V_1(\theta',\phi';0,f\sin\omega,f\cos\omega,M,0,0)$$

where: (θ^*,ϕ^*) = azimuth and latitude of annular sector center

γ = angle through which dipole layer must be rotated about z-axis counterclockwise to bring dipole layer into y-z plane

θ' = azimuth of surface point in rotated coordinate system

$= \cos^{-1}\{\cos\theta\cos\theta^* + \sin\theta\sin\theta^*\cos(\phi-\phi^*)\}$

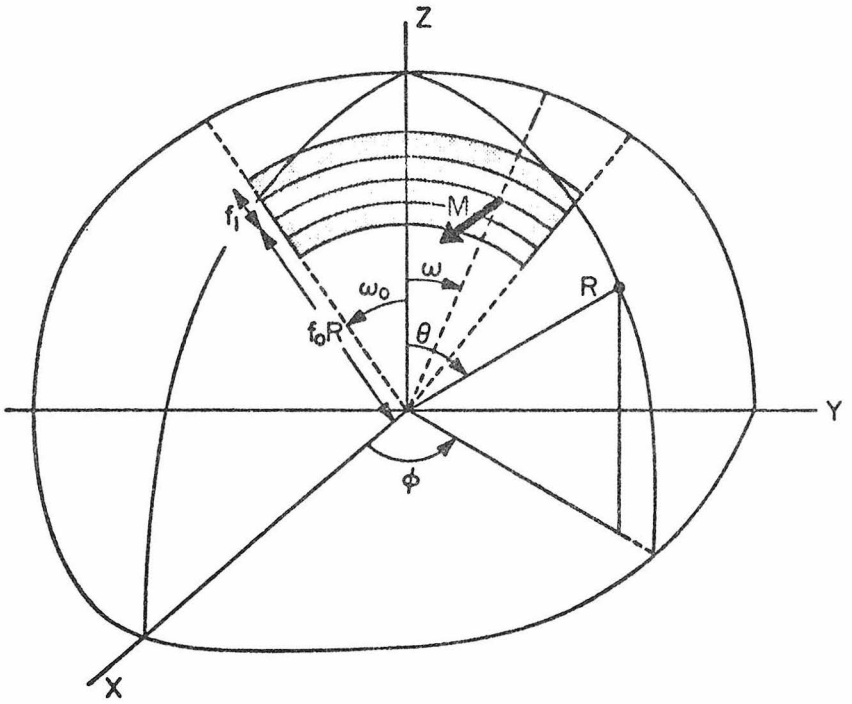

FIg. 50a - Coordinate system and parameters for annular sector dipole layer

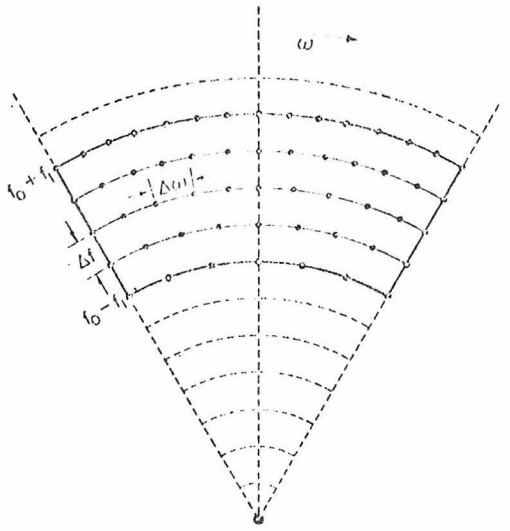

Fig. 50b - Spacing used in forming annular sector dipole layer

ϕ' = latitude of surface point in rotated coordinate system

$= \sin^{-1}\{\sin\theta \cdot \sin(\phi-\phi^*)/\sin\theta'\}-\gamma$

Fig. 51 illustrates the effects of dipole spacing (Δf) on potential distributions generated by plane annular sector dipole layers in the homogeneous sphere model. Again these effects are much less noticeable in the shell models. Figs. 52, 53 and 54 show examples of potential distributions generated by annular sectors of varying eccentric (f_1) and angular extent (ω_0) in the homogeneous (Fig. 52), 3 shell (Fig. 53) and 5 shell (Fig. 54) models of the head.

The annular sector dipole layer is intended to represent sulcal cortex perpendicular to the brain surface. It is the extended source analogue of a single tangentially directed dipole. Fig. 55 illustrates the relationship between the annular sector model and a single tangential dipole by showing those single tangential dipoles which give the best approximations in the least-squares sense (see section 3.5) to the fields of annular sectors with various angular and eccentric extents. Here it can be seen that a single tangential dipole gives a good approximation to extended layers of up to 20° angular extent and very large eccentric extent. However, it does appear to locate the centroid of the extended layer.

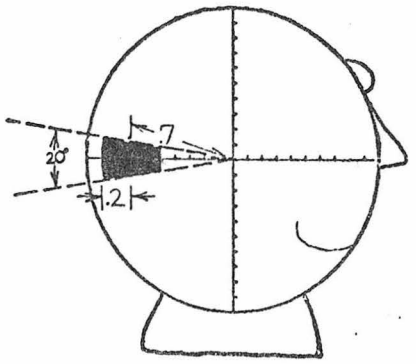

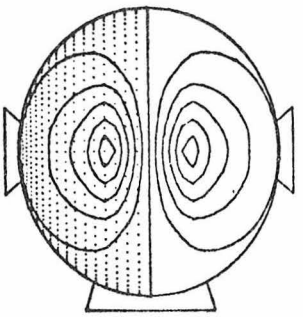

Single Tangential Dipole

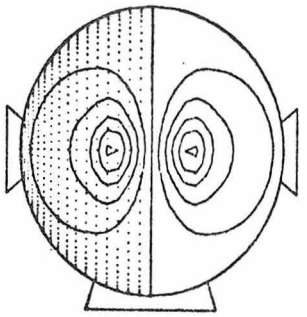

Δf=.2

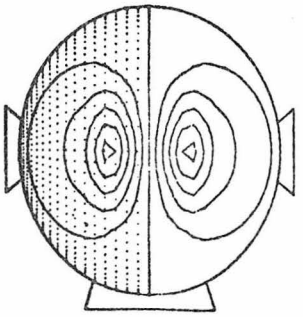

Δf=.1

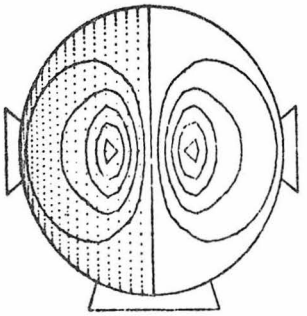

Δf=.01

Fig. 51 - Effect of dipole spacing (Δf) on potential distributions generated by annular sector dipole layers in the homogeneous sphere model of the head.

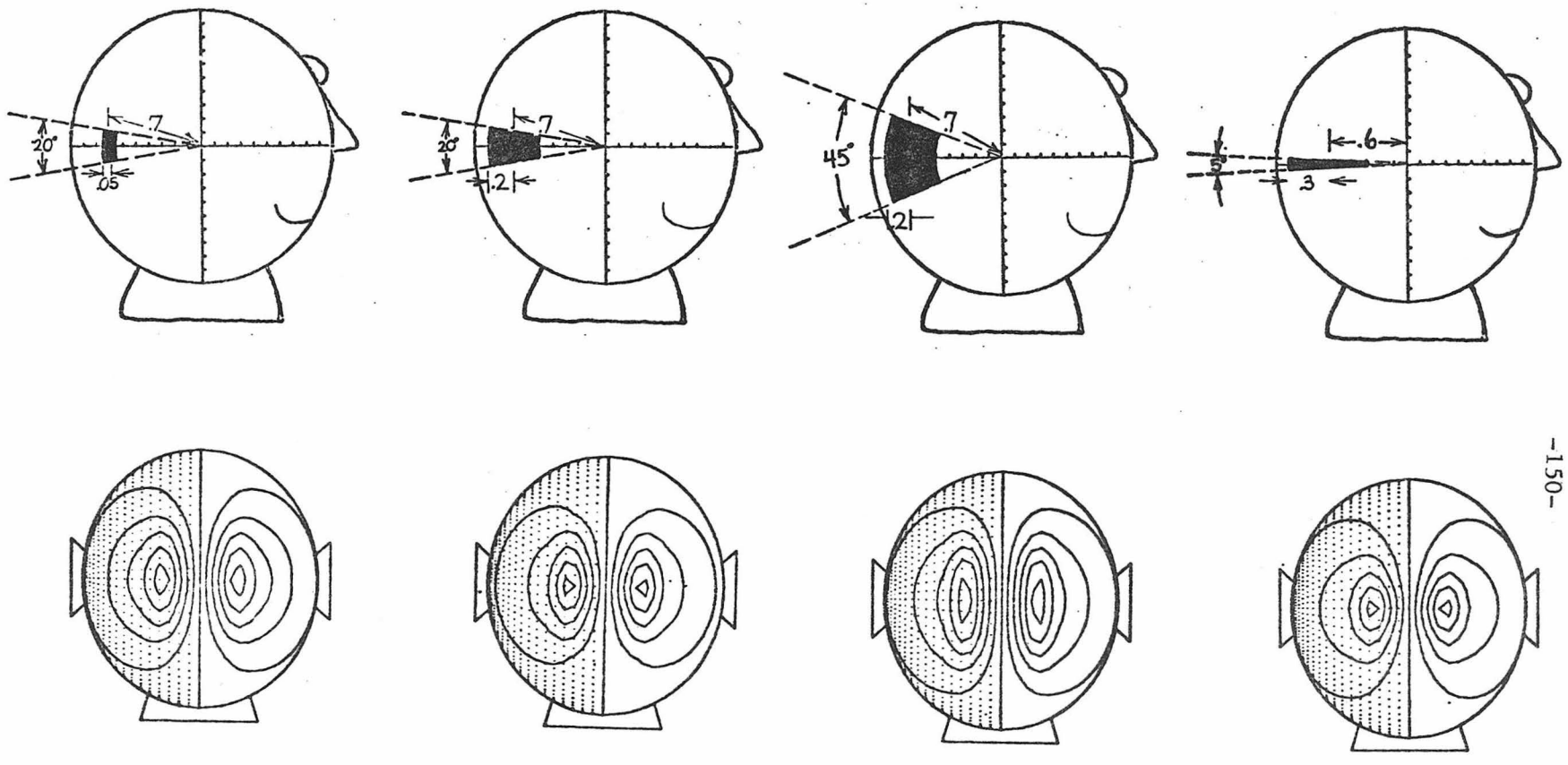

Fig. 52 - Examples of potential distributions generated by annular sector dipole layers of various eccentric (f_1) and angular extents (ω_0) in the homogeneous model of the head.

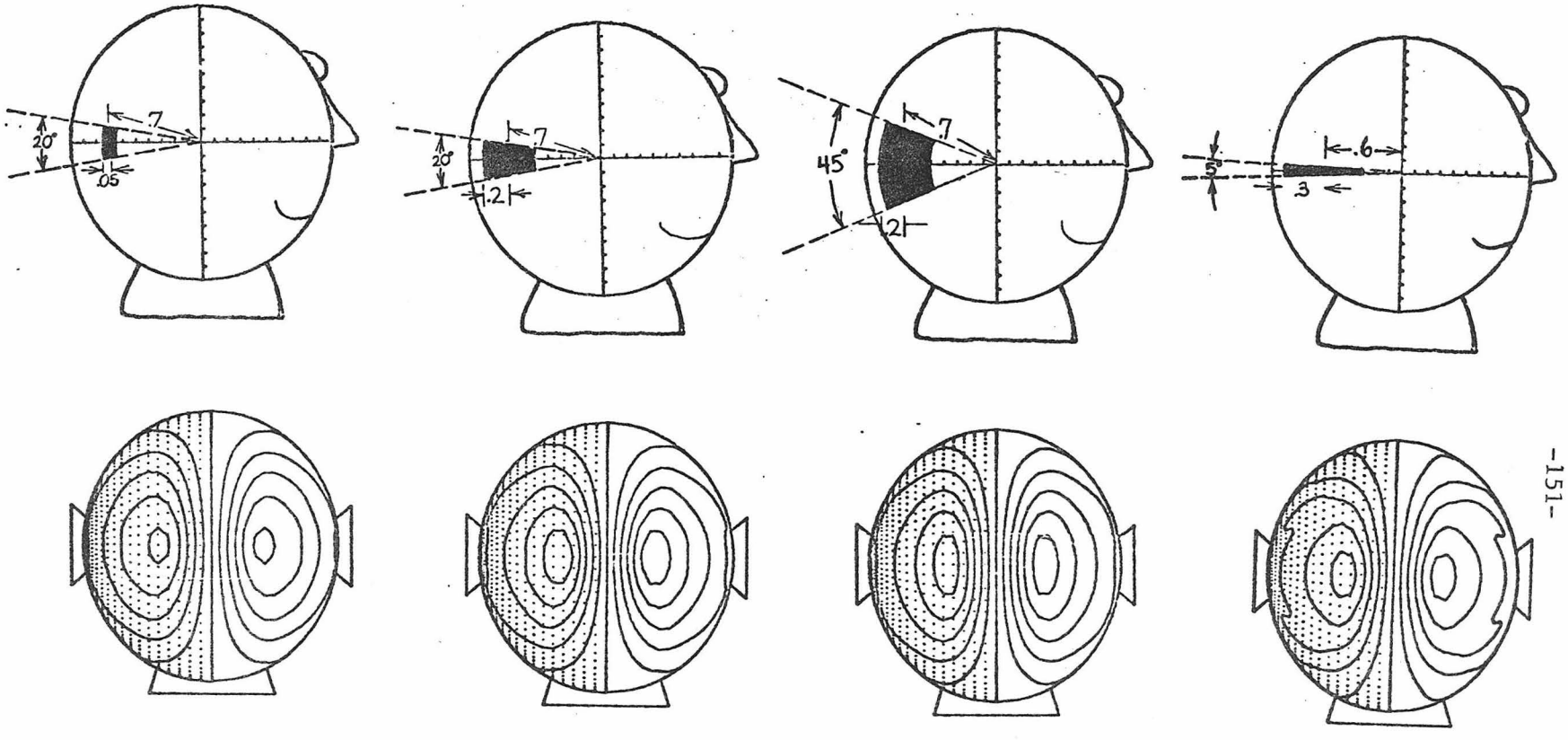

Fig. 53 - Examples of potential distributions generated by annular sector dipole layers of various eccentric (f_1) and angular extents (ω_0) in the 3-shell model of the head.

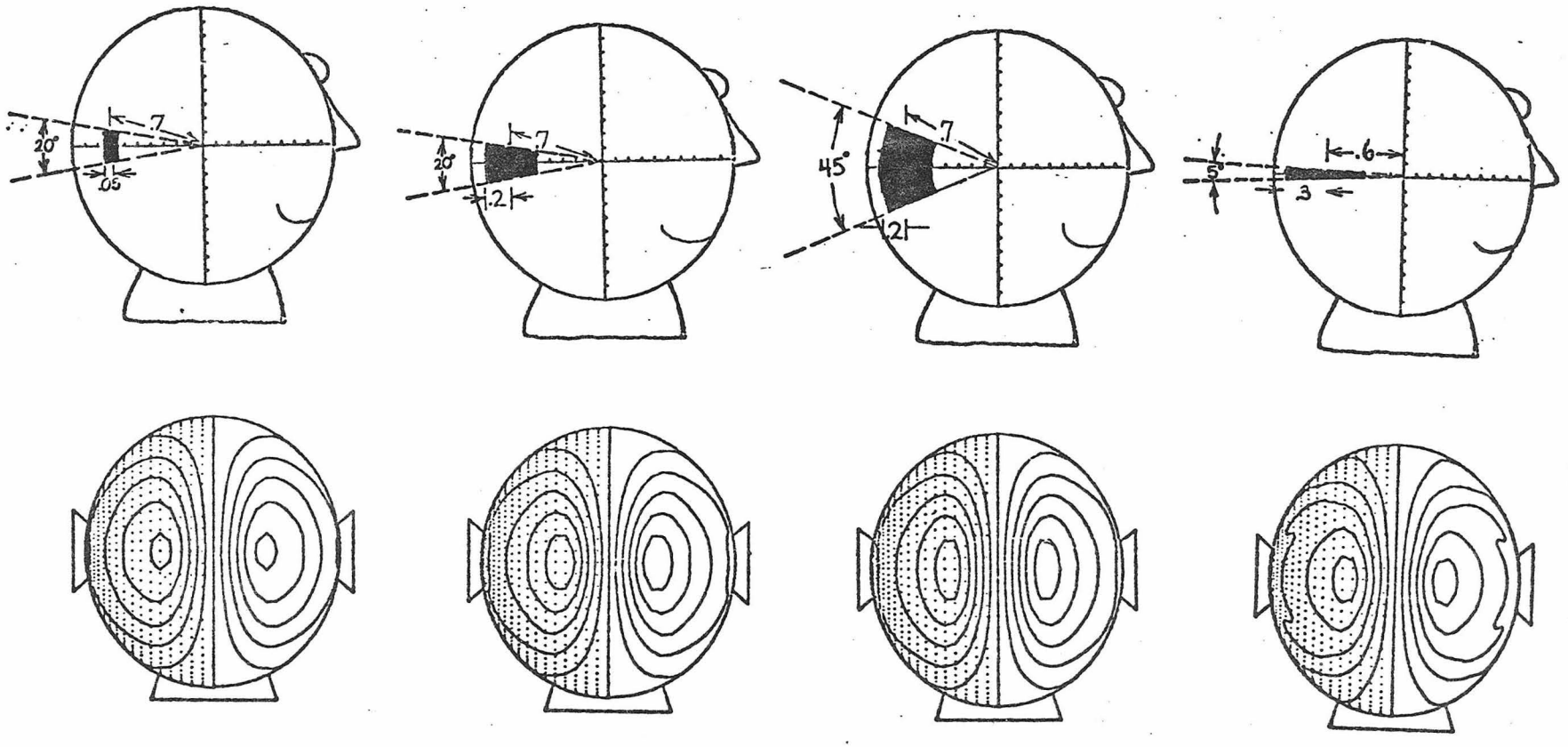

Fig. 54 - Examples of potential distributions generated by annular sector dipole layers of various eccentric (f_1) and angular extents (ω_0) in the 5-shell model of the head.

Fig. 55 - Comparison of annular sector dipole layers (f_0=0.7) with single tangentially directed dipoles.

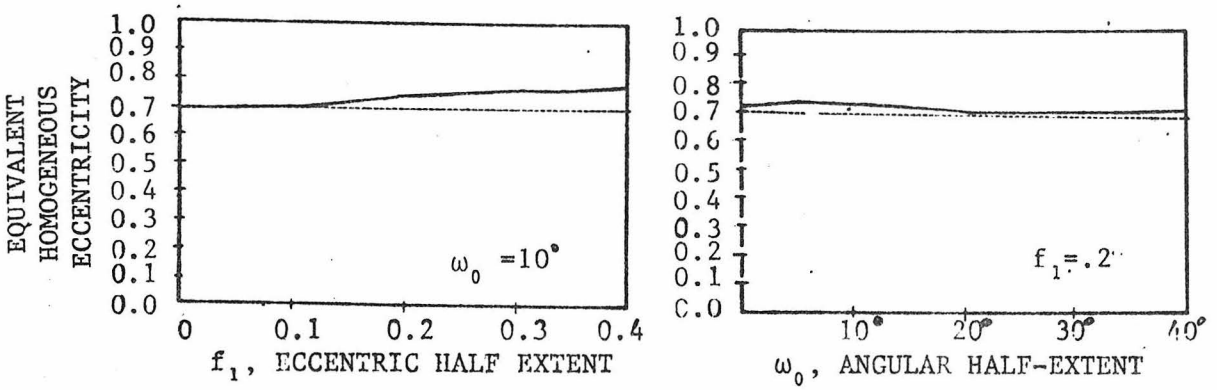

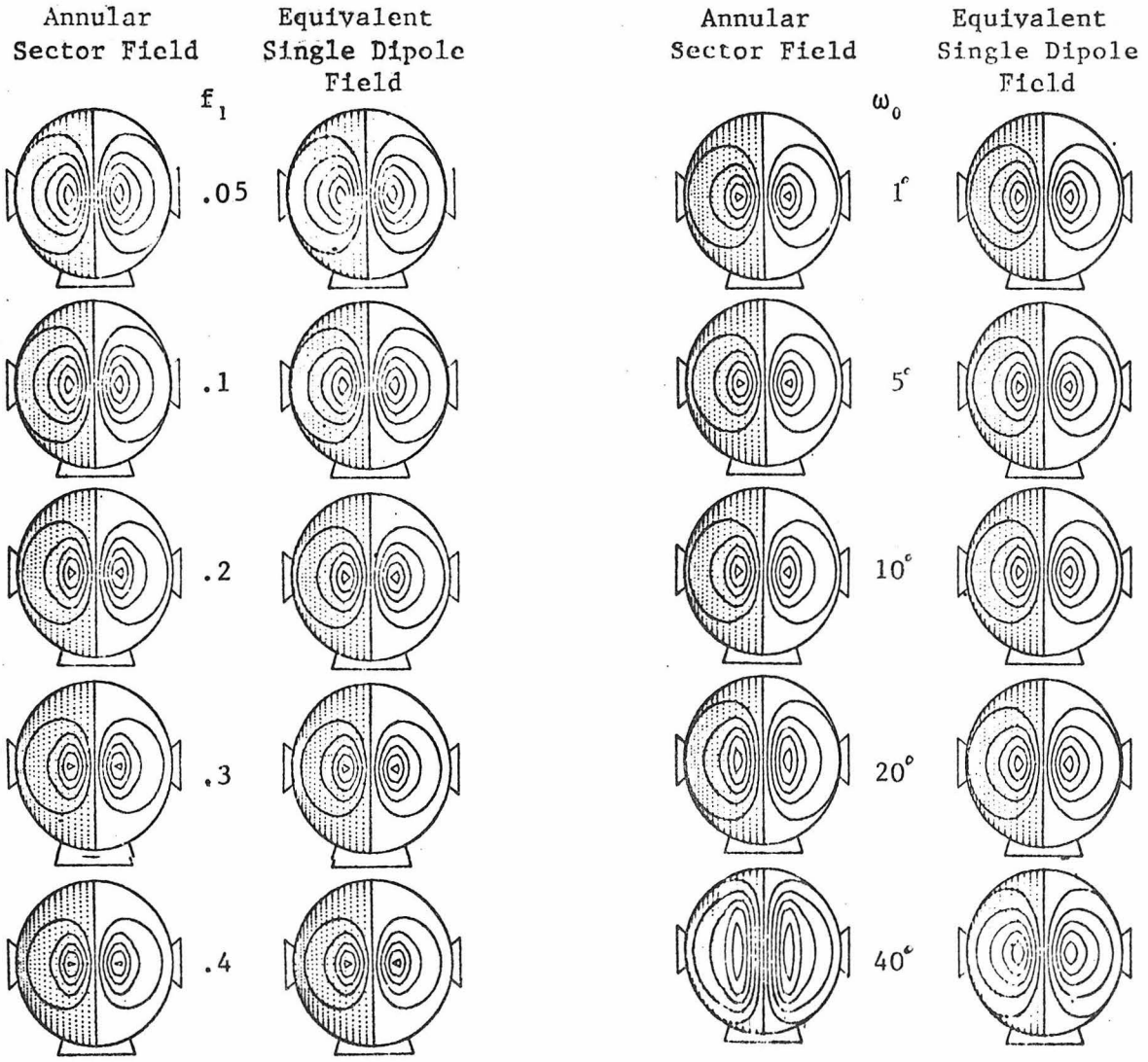

3.5 Modeling - Inverse Solutions

3.5.1 Nonlinear Least-Squares Parameter Estimation

Inverse solutions were calculated in the form of optimal source parameter estimates. These are found by adjusting model parameters to obtain those model scalp potential predictions that best match the experimentally measured scalp potentials in the least-squares sense. That is, the reduced chi-square function χ^2_ν is minimized with respect to the source parameters, a_j, where {159}:

$$\chi^2_\nu = \chi^2_\nu (a_1,\ldots,a_{NP}) = \sum_{i=1}^{NE} \frac{\frac{1}{\nu}\{V_i - \hat{V}_i(a_1,\ldots,a_{NP})\}^2}{\sigma_i^2}$$

NE = # electrodes,

NP = # source parameters,

ν = (NE-NP), the number of degrees of freedom left after fitting NE data points to NP source parameters,

V_i = measured scalp potential at electrode i,

$\hat{V}_i$ = model potential prediction at electrode i for source parameters $a_j, j=1,\ldots,NP$

σ_i = estimated uncertainty in measured scalp potential at electrode i.

χ^2_ν is in the form of the ratio of the variance of the model's fit to the data and the variance of the data itself. Thus, it is a convenient measure of the goodness of the fits. In addition, χ^2_ν has a well-known probability distribution {159}, which may be used to determine the χ^2_ν probability of χ^2_ν exceeding any particular value. For a good fit the probability of exceeding χ^2_ν should be approximately 0.5. For most purposes, the probability is reasonably close to 0.5 so long as χ^2_ν is reasonably close to 1, or more precisely $\chi^2_\nu \simeq 1 \pm \sqrt{\frac{1}{\nu}}$.

If $\hat{V}$ is a function which is linear in the source parameters, a_j, then a straightforward solution to the least-squares problem is easy to carry out. This is done by minimizing χ^2_ν with respect to each of the parameters simultaneously, solving the system of equations:

$$\frac{\partial}{\partial a_j} \chi^2_\nu = 0, \quad j=1,\ldots,NP$$

When $\hat{V}$ is a nonlinear function of the source parameters, the resulting equations are often difficult to solve explicitly. In this case it is more convenient to search parameter space for the appropriate minimum value of χ^2_ν. Since the models used in this thesis were complicated nonlinear functions of the source parameters, search algorithms were used to explore the parameter spaces of the chi-square functions. Two such algorithms were implemented on a digital computer.

The first approach minimized χ^2_ν using a simplex method for function minimization {160,161}. This method works with a simplex (or set of distinct points) in parameter space, i.e. NP+1 points for a parameter space of NP dimensions. New simplices are continually formed from previous ones by replacing the point with the highest function value by another point. The choice of the new point is made on the basis of the local landscape of the function, so that the simplex elongates when long inclined planes are encountered, changes directions on encountering a valley at an angle and contracts in the neighborhood of a minimum. Fig. 56 illustrates the method in a 2-dimensional parameter space.

The second approach minimized χ^2_ν using a method due to Marquardt {162}, which performs an optimal interpolation between the steepest-descent (or gradient) and Taylor Series expansion methods of function minimization. This combination utilizes the complementary facts that the steepest-descent method approaches a minimum quickly from far

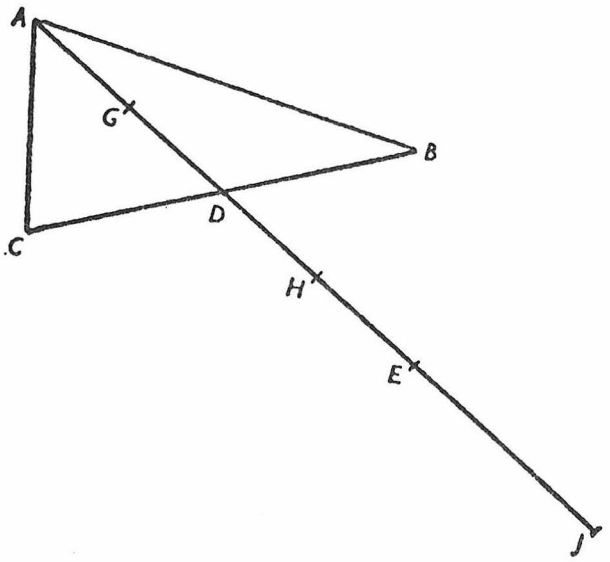

Fig. 56 - Illustration {161} of the simplex method of function minimization in 2-dimensional space. The algorithm proceeds as follows:

Let F(A) be the function value of the point $A=(X_A, Y_A)$ being a point in the space of the two variables.

Suppose F(A)>both F(B) and F(C) then we replace A by its reflection, E, in D, the centroid of B and C. If E is not successful, i.e. $F(E) \geq F(B)$ and F(C), then we contract to G or H depending whether F(A) or F(E) is lower. In the unusual case that F(G)>F(A) (or equivalently F(H)>F(E)) then the simplex is contracted around B or C according as F(B) or F(C) is lower.

If, however, E is successful and F(E)<F(B) and F(C) we extend to point J. We then keep E or J as a replacement for A according as F(E) or F(J) is lower.

If neither contraction nor extension is necessary we replace A by E.

Iteration then continues with B, C and the replacement for A, the simplex distorting in shape according to the slopes it encounters.

away, but converges slowly in the neighborhood of a minimum, while the Taylor Series expansion method converges rapidly near a minimum, but is unrealiable outside the region where a truncated Taylor Series expansion gives a reasonable approximation to the function.

3.5.2 Confidence Region Calculations

There is no general theory of confidence region estimation for least-squares parameters based on nonlinear models{ 163}. Most investigators have made approximations using the confidence region theory for linear models { 159,164}. Indeed, for most purposes the linear approximation is adequate. This is so because in the region of the minimum a nonlinear model will be approximately linear in its parameters. In fact, the assumption of linearity near the minimum is inherent to most nonlinear least-squares algorithms.

Linear confidence regions are related to the elements of the so-called error matrix of the model parameters at the minimum. This matrix is the inverse of the so-called curvature matrix, which is based on a linear expansion of the fitting function (model) in the neighborhood of the minimum. This expansion yields a parabolic approximation of the χ^2_ν hypersurface near the minimum. To see this, consider the following {159}:

> Let $\hat{V}_i(\vec{a}_0)$ be the value of the model prediction for electrode i at some point $\vec{a}_0 = (a_1^0, \ldots, a_{NP}^0)$ in the neighborhood of the minimum. A linear expansion of $\hat{V}_i(\vec{a})$, $\vec{a} = (a_1, \ldots, a_{NP})$ about $\vec{a}_0$ gives

$$\hat{V}_i(\vec{a}) \simeq \hat{V}_i(\vec{a}_0) + \sum_{j=1}^{NP} \left.\frac{\partial \hat{V}_i}{\partial a_j}\right|_{\vec{a}_0} \cdot (a_j - a_j^0) \quad .^{27}$$

Thus,

$$\chi_\nu^2 = \sum_{i=1}^{NE} \frac{1}{\nu\sigma_i^2} \left\{ V_i - \hat{V}_i(\vec{a}_0) - \sum_{j=1}^{NP} \left.\frac{\partial \hat{V}_i}{\partial a_j}\right|_{\vec{a}_0} \cdot (a_j - a_j^0) \right\}^2$$

To find $\vec{a}$ which minimizes χ_ν^2, we equate to zero the derivatives of χ_ν^2 with respect to each parameter a_k and obtain NP simultaneous equations called the normal equations

$$\sum_{i=1}^{NE} \frac{1}{\nu\sigma_i^2} \left\{ V_i - \hat{V}_i(\vec{a}_0) - \sum_{j=1}^{NP} \left.\frac{\partial V_i}{\partial a_j}\right|_{\vec{a}_0} \cdot (a_j - a_j^0) \right\} \cdot \left.\frac{\partial V_i}{\partial a_k}\right|_{\vec{a}_0} = 0 \quad , k = 1, \ldots, NP.$$

These equations are also expressible as

$$\vec{b} - C \cdot (\vec{a} - \vec{a}_0) = \vec{0}$$

where $\vec{0}$ is the zero vector and the components of $\vec{b}$ are

$$b_k = \sum_{i=1}^{NE} \frac{1}{\nu\sigma_i^2} \{ V_i - \hat{V}_i(\vec{a}_0) \} \cdot \left.\frac{\partial \hat{V}_i}{\partial a_k}\right|_{\vec{a}_0}$$

and C is the curvature matrix, with its elements

$$c_{jk} = \sum_{i=1}^{NE} \frac{1}{\nu\sigma_i^2} \left.\frac{\partial \hat{V}_i}{\partial a_j}\right|_{\vec{a}_0} \cdot \left.\frac{\partial \hat{V}_i}{\partial a_k}\right|_{\vec{a}_0}$$

Defining $E = C^{-1}$, we have

$$\vec{a} = E\vec{b} + \vec{a}_0 .$$

The relationship between the elements e_{jk} of E and the uncertainities of the parameters $\vec{a}$ is found by noting that each data point V_i contributes some fraction of its own uncertainty to the uncertainties in each parameter a_j i.e.

$$\sigma_{a_j}^2 = \sum_{i=1}^{NE} \sigma_i^2 \left\{ \frac{\partial a_j}{\partial V_i} \right\}^2 .$$

---

[27] The values of $\left.\frac{\partial V_i}{\partial a_j}\right|_{\vec{a}_0}$ are easy to approximate using divided differences.

Differentiating, we have

$$\frac{\partial a_j}{\partial V_i} = \sum_{k=1}^{NP} \frac{e_{jk}}{\nu\sigma_i^2} \cdot \frac{\partial \hat{V}_i}{\partial a_k}\bigg|_{\vec{a}_0}$$

Thus,

$$\sigma_{a_j}^2 = \sum_{i=1}^{NE} \frac{1}{\nu\sigma_i^2} \cdot \sum_{k=1}^{NP}\sum_{m=1}^{NP} e_{jk} \cdot e_{jm} \cdot \frac{\partial \hat{V}_i}{\partial a_k}\bigg|_{\vec{a}_0} \cdot \frac{\partial \hat{V}_i}{\partial a_m}\bigg|_{\vec{a}_0}$$

$$= \sum_{k=1}^{NP}\sum_{m=1}^{NP} e_{jk} \cdot e_{jm} \cdot c_{km} = e_{jj}$$

The result is that the uncertainty in each parameter is given by a diagonal term of the error matrix ($E=C^{-1}$), and it assumes insignificant correlation between parameters.[28] This is reflected in the form of the linear expansion of the fitting function near the minimum. When this assumption is valid, one-parameter confidence regions may be calculated from {163}:

$$a_j^{min} - \sqrt{NP \cdot t_{1-\alpha}(NP,\nu) \cdot \chi_\nu^2(min) \cdot e_{jj}} \leq a_j \leq a_j^{min} + \sqrt{NP \cdot t_{1-\alpha}(NP,\nu) \cdot \chi_\nu^2(min) \cdot e_{jj}}$$

where $t_{1-\alpha}(\nu)$ is the $1-\alpha$ point of the Student's t-distribution with $\nu(=NE-NP)$ degrees of freedom. The interpretation of these confidence regions is that in many repetitions of the parameter estimation from different data measurements, it is expected that $(1-\alpha)\cdot 100\%$ of these repetitions will yield parameter estimates within the specified limits. When significant correlations exist, the one-parameter confidence regions will underestimate the true intervals in which the parameters may lie. In this case support-plane confidence regions should be used {163}:

---

[28] The parameter correlations r_{ij} are given by $e_{ij}/(\sqrt{e_{ii}} \cdot \sqrt{e_{jj}})$ {163}. Thus, another way of saying this is that the error matrix is diagonally dominant.

$$a_j^{min} - \sqrt{NP \cdot F_{1-\alpha}(NP,\nu) \cdot \chi_\nu^2(min) \cdot e_{jj}} \leq a_j \leq a_j^{min} + \sqrt{NP \cdot F_{1-\alpha}(NP,\nu) \cdot \chi_\nu^2(min) \cdot e_{jj}}$$

where $F_{1-\alpha}(NP,\nu)$ is the upper $1-\alpha$ point of the variance ratio distribution for NP and ν (=NE-NP) degrees of freedom.

As a rule, the error matrix and both the one-parameter and support-plane confidence regions were calculated for the parameter estimations presented in this thesis. Unless otherwise stated, the confidence regions presented are of the support-plane variety.

4. RESULTS - EVOKED POTENTIAL DATA

4.1 Basic Data Characteristics

4.1.1 Reliability and Controls

Fig. 57a shows average potentials at one electrode position (Channel 25) evoked by pulsed appearance/disappearance (Fig. 11a) of a red left half field (LHF) checkerboard in subject JPA using electrode layout 2, Fig. 18, and a summing reference. Twenty traces are shown, each trace being the average of a run consisting of 150 stimulus repetitions. The hatched region in the plot indicates the stimulus occurrence. These data were taken in the course of 8 experiments in one year and are representative of the long term day-to-day intrasubject variability of the data presented in this thesis. Much of the variation shown in Fig. 57a is attributable to day-to-day changes in amplitude which are not in evidence on a given day (Fig. 57b). However, these variations are similar at most electrodes, such that approximately the same scale factor could be applied to data at all the electrodes on a given day to make them nearly the same as data from another day. This means that potential distribution shapes are not highly variable from day-to-day, but their amplitudes may vary significantly from day-to-day. This is fortunate for the purposes of this work, since equivalent source positions and orientations are highly sensitive to distribution shape, but independent of absolute amplitude.

Figs. 57c and 57d show examples of two controls which were performed for the experiments reported here. Fig. 57c is the evoked potential waveform which resulted on the same electrode as in Figs. 57a and 57b and under the same conditions with the exception that a diffuser

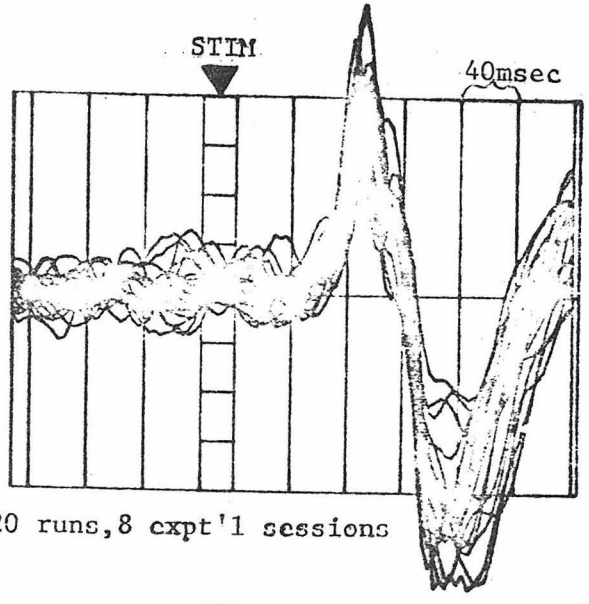

57a - 20 runs, 8 expt'l sessions

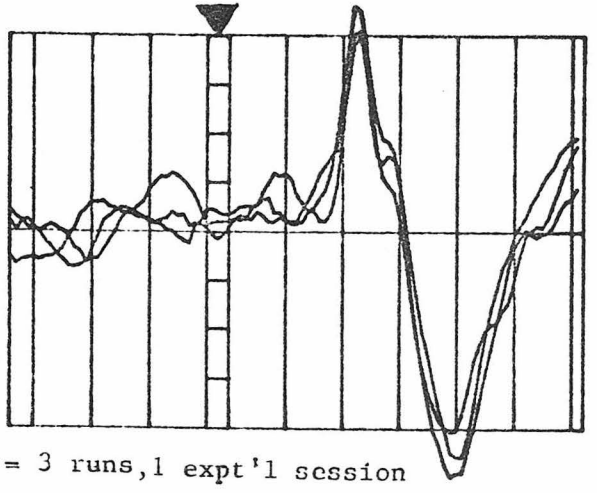

57b = 3 runs, 1 expt'l session

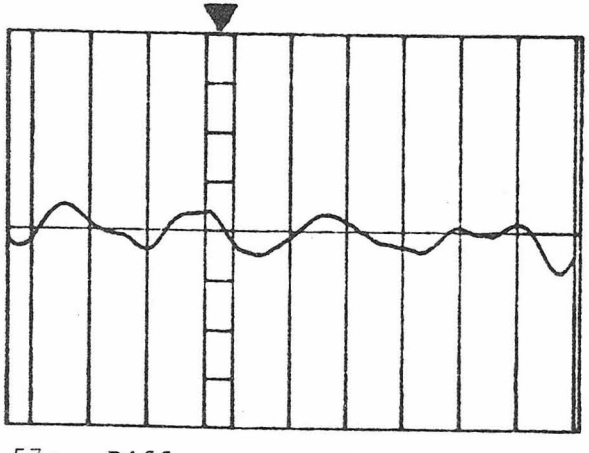

57c - Diffuser over stimulus

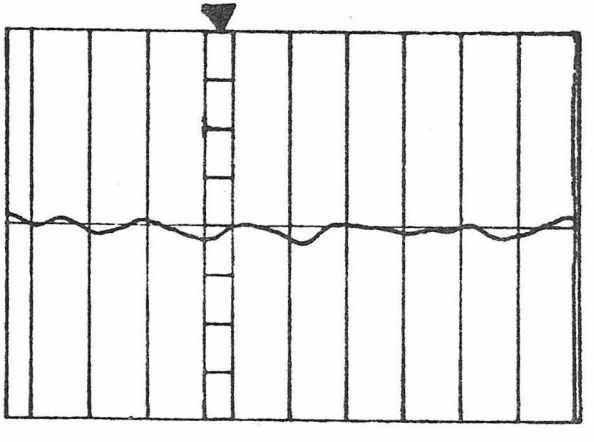

57d - Stimulus occluded

Fig. 57 - Mean evoked potentials, subject JPA, channel 25, A/D left half field

was placed over the stimulus. Fig. 57d is also recorded from the same electrode and same stimulus condition, with the exception that the stimulus was occluded so that the subject could not see it. These tests gave responses which were below the noise level[29] and served to check that the stimulus was balanced and that there were no stray light artifacts synchronized with the stimulus events. They also ensure that the responses (Figs. 57ab) resulted from the visual stimulation and were not contaminated by some equipmental artifact or response arising from another sense (e.g. auditory response arising from the subject hearing shutter movements).

As may be seen in Figs. 57, the response is sampled for a fairly substantial amount of time before the stimulus. This period is not 'contaminated' by sensory responses and, as mentioned above, may be used to assess the inherent noise level on a given electrode. This information is essential in estimating data reliability and determining a baseline against which to measure potential fluctuations.

Fig. 58 shows average EP's for all 40 electrodes under the conditions of Fig. 57a. The central line in each trace represents the mean of 20 average evoked potentials collected over the course of one year on the same subject. The upper and lower lines indicate plus and minus one standard deviation of the mean. All potentials are referred to an average reference electrode. The reliability of these data may be taken as representative of all the data in this thesis, except as otherwise noted. Note that responses on many of the electrodes are obviously highly correlated. The implications of this will be discussed in section 4.4.

---

[29]The noise level may be estimated from the prestimulus data.

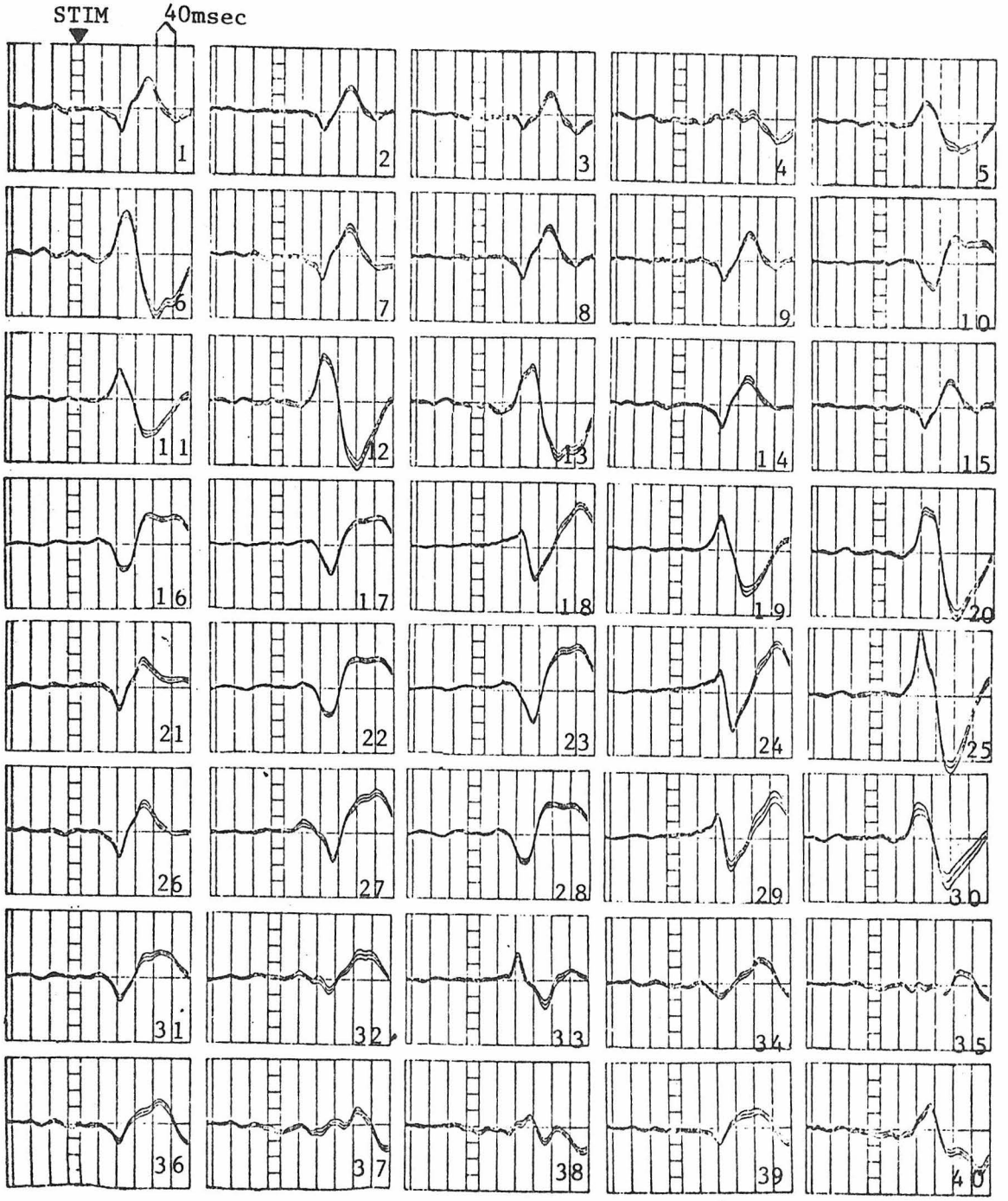

Fig. 58 - 40 channel evoked potentials ±1 sdev.of the mean, for subject JPA with an appearance/disappearance LHF stimulus and using electrode layout 2, Fig. 18.

Since equipotential maps are much more revealing of the topographical nature of the EP, the data in this thesis will generally be displayed as such. However, EP waveform plots are useful in assessing reliability and noise levels, as well as for investigating the origin of unusual features in equipotential maps and rejecting bad electrodes. They are also useful for comparisons with the work of other investigators who do not (or cannot) plot their data as equipotential maps. Plots such as those of Fig. 58 were made for all of the data presented in this thesis prior to the plotting of equipotential maps.

Equipotential maps of the data in Fig. 58 are show in Fig. 59. The contours on these maps denote 11 levels spanning the minimum and maximum of the entire time series, thus facilitating comparisons of maps at different times. The times associated with each plot denote time elapsed since stimulus offset. The maps reemphasize how highly correlated the signals are on the various electrodes. Figs. 60 and 61 are plots of data taken on the same subject in two experiments with one month intervening. Note their striking similarity, especially at those times when the peaks are highest. The conditions of the two experiments were identical to those described for Fig. 57a with the exception that the data shown in Fig. 61 were taken with a diffuse white background surrounding the stimulus (see section 3.1 for description). The similarity of Figs. 60 and 61 indicates that there is little if any dependence of the responses on the presence of an adapting surround over a large range of surround luminances. Thus, the data of Figs. 58 and 59 include both of these types of data (the surround was used in 2 of the 8 experiments).

Fig. 59 - Equipotential map series for the data of the previous figure

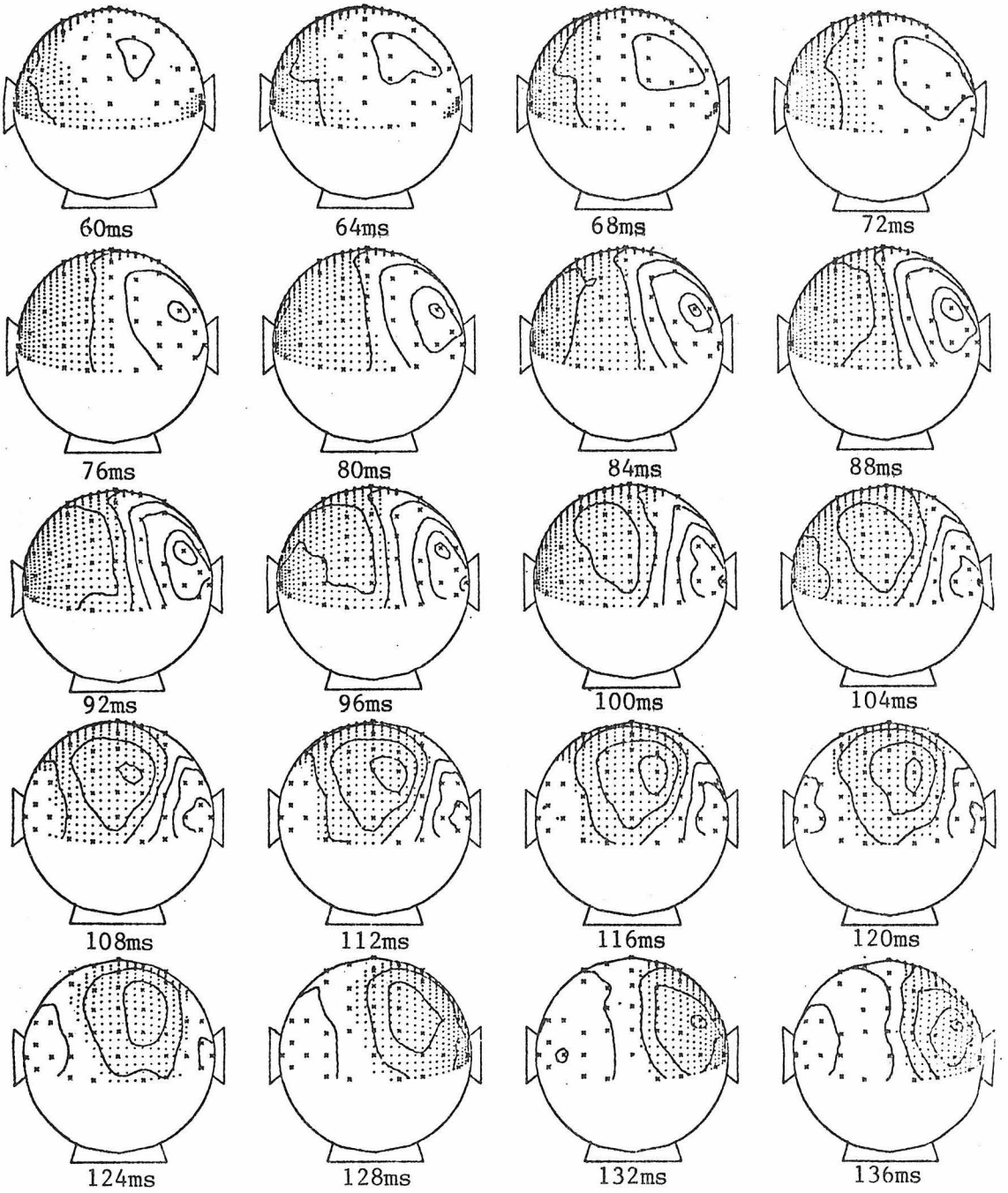

Fig. 59 (continued)

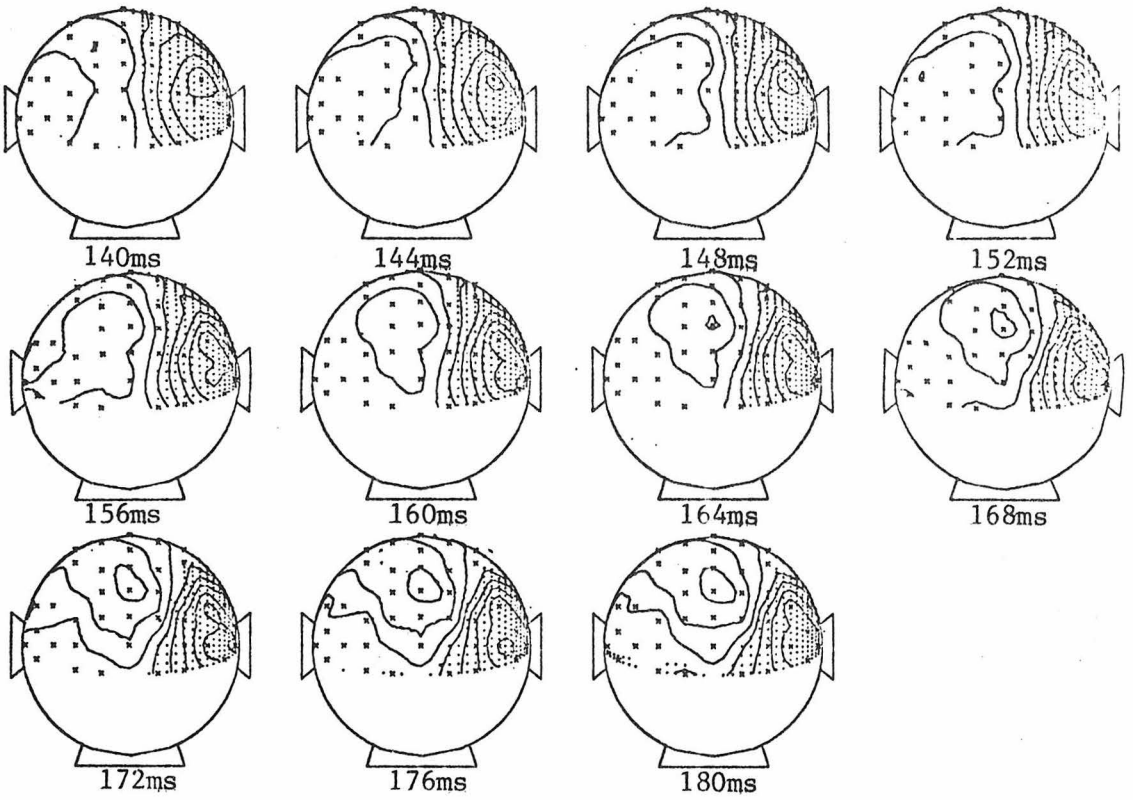

Fig. 60 - One day series for subject JPA left half field stimulation

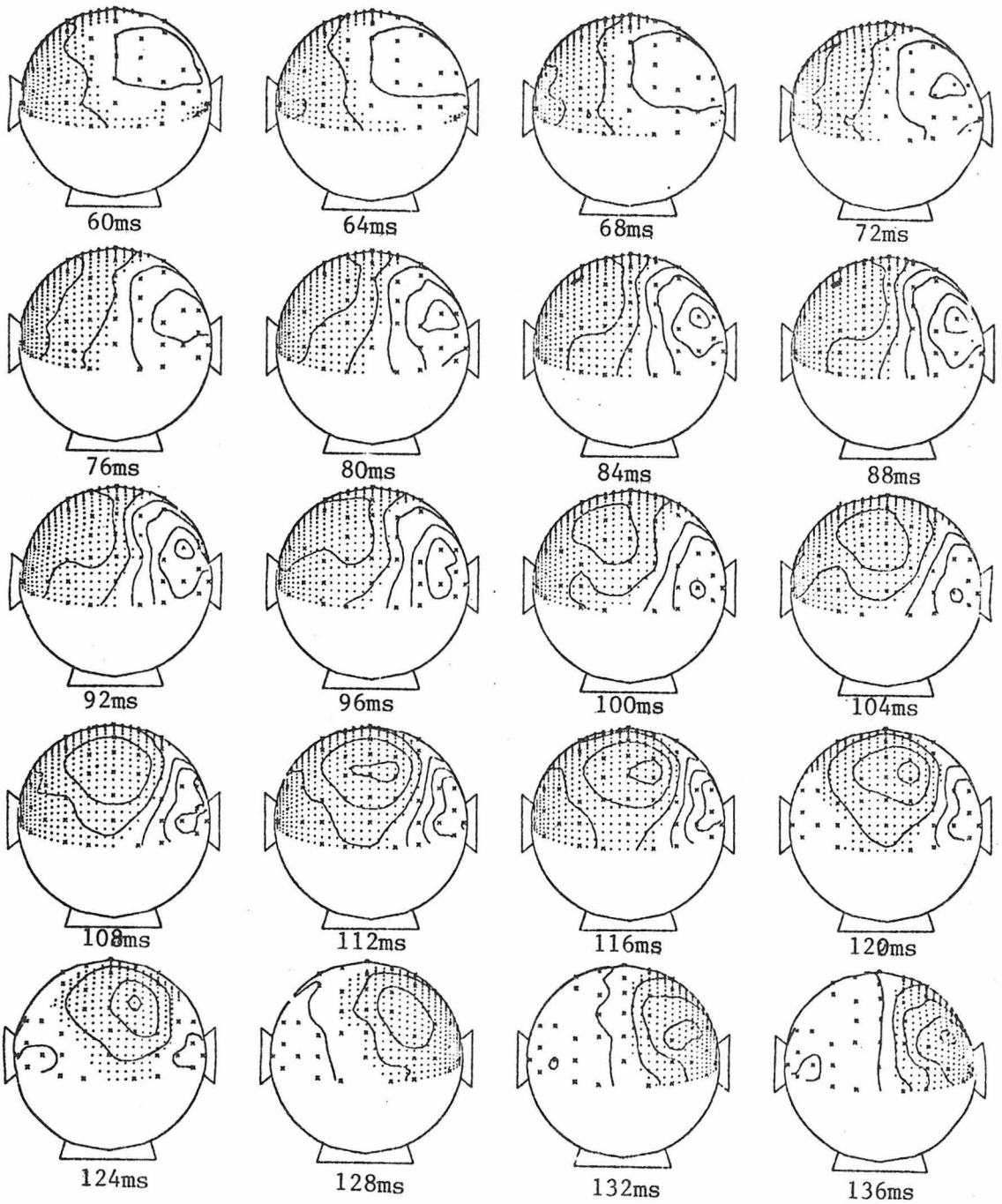

Fig. 60 (continued)

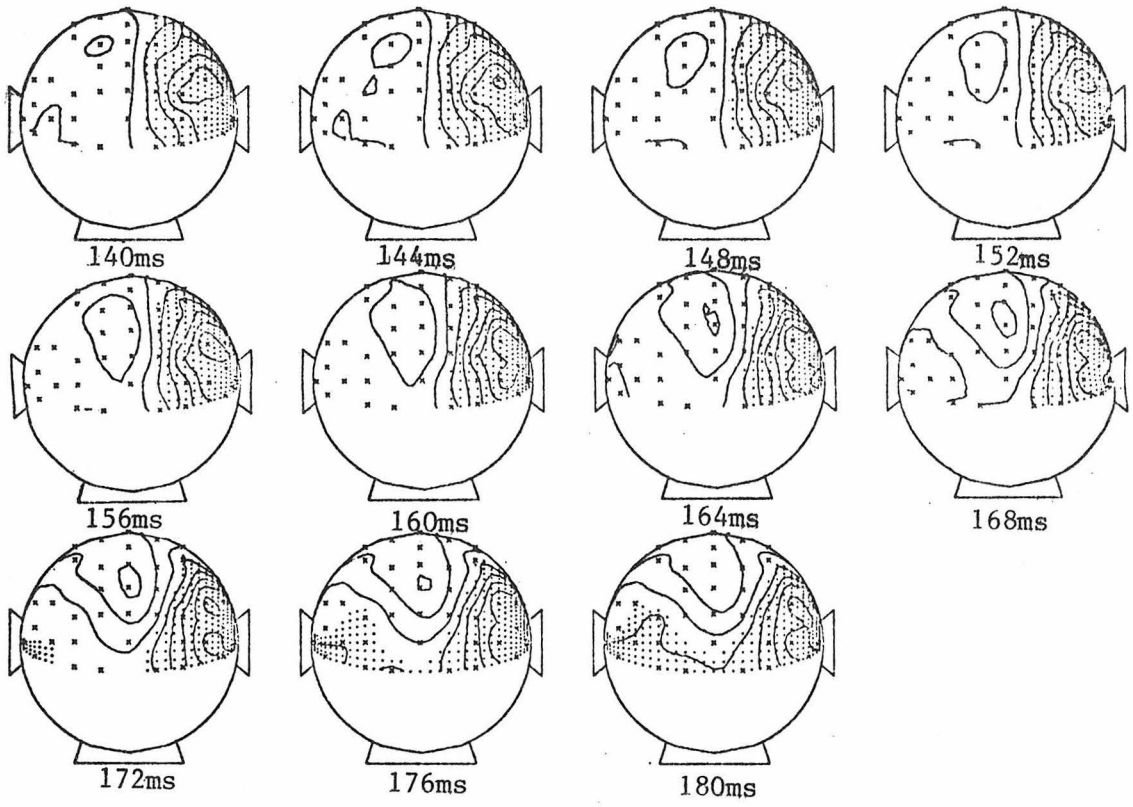

Fig. 61 - Another one day series for subject JPA left half field stimulation (with surround)

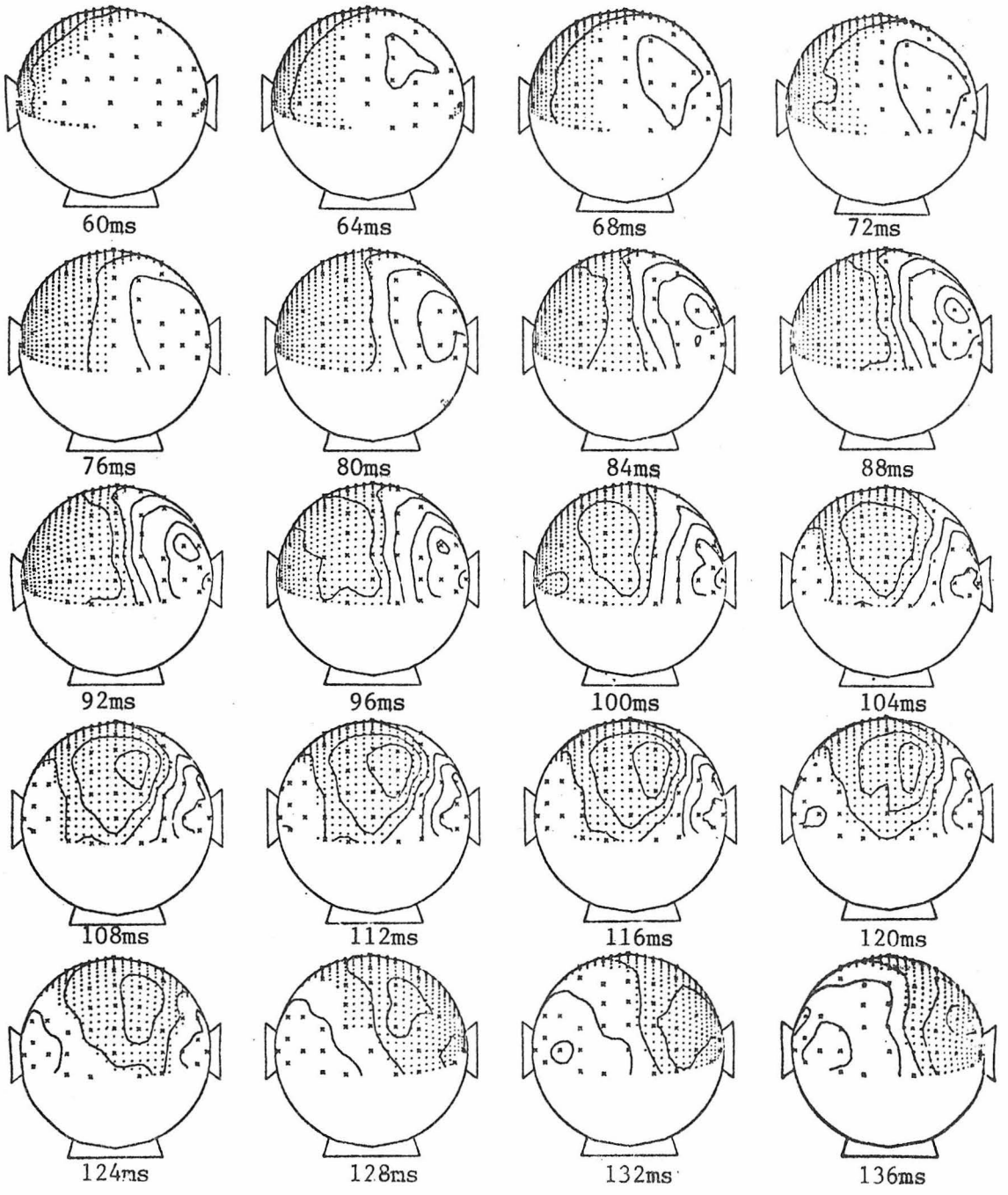

Fig. 61 (continued)

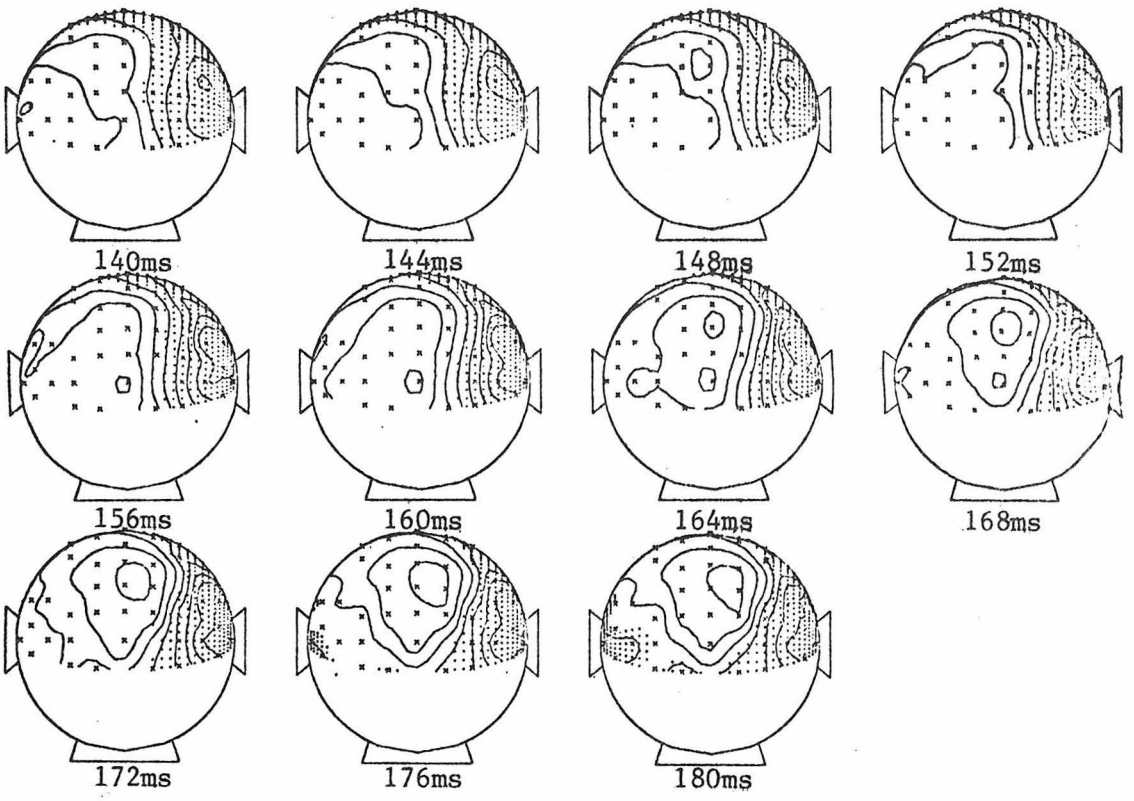

4.1.2 Referencing and Bandwidth Dependence

Figs. 62 and 63 show EP waveforms and equipotential maps which resulted from pulsed appearance/disappearance right half field (RHF) stimulation of subject JPA using electrode layout 1 (Fig. 17) and a summing reference electrode. Figs. 64 and 65 show EP waveforms and equipotential maps under identical conditions with the exception that a monopolar reference electrode was used. The monopolar reference electrode was placed frontally 4 cm above the nasion on the midline. From Figs. 63 and 65 it can be seen that the choice of reference did not markedly affect the potential distribution shapes, but that there are differences in the location of the zero line at various times, especially in the 152 to 180 msec range.[30] Also, comparison of Figs. 62 and 64 show a greater inherent noise level in the monopolar case, more so on occipital electrodes than electrodes more frontal on the head (i.e. nearer the reference). This is probably due to the increasing inequality of extraneous signals (e.g. alpha waves) on the reference and active electrodes with increasing separation (see section 3.2.2). On the basis of its lower inherent noise level, the summing reference was used in the rest of the experiments reported here.

Fig. 66 shows the effect of varying the bandwidth of the recording amplifiers. These waveforms resulted from right half field (RHF) stimulation of subject PDP using electrode layout 2 (Fig. 18) and a summing reference. Three waveforms are shown for each electrode and

---

[30] As discussed in section 3.2.2, such shifts do not affect the locus and orientation of equivalent sources, which depend only on gradient information.

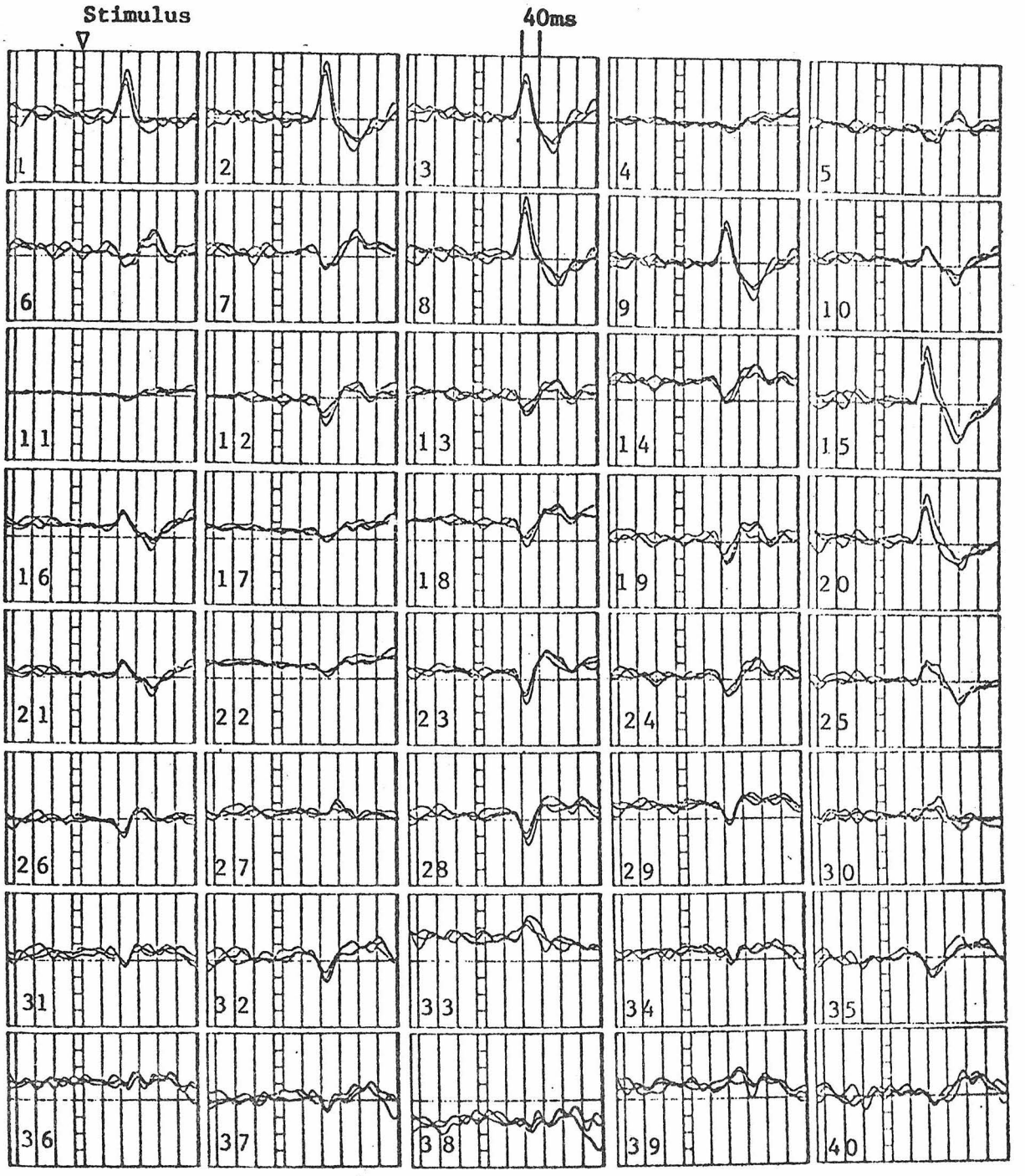

Fig. 62 - 3 average EPs for right half field appearance/disappearance stimulation of subject JPA using electrode layout 1 (Fig. 17) and a summing reference

Fig. 63 - Equipotential maps of the data in the previous figure

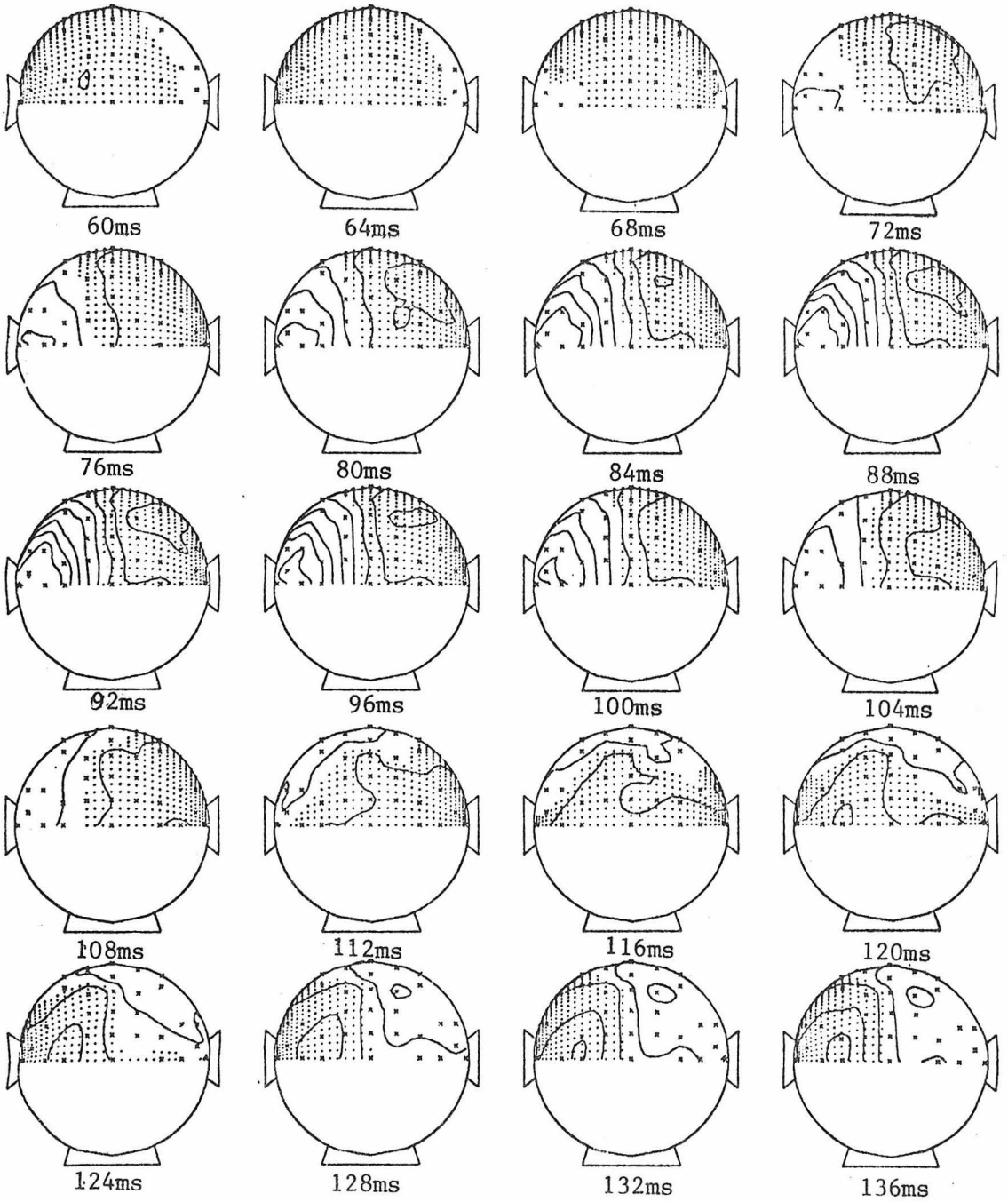

Fig. 63 (continued)

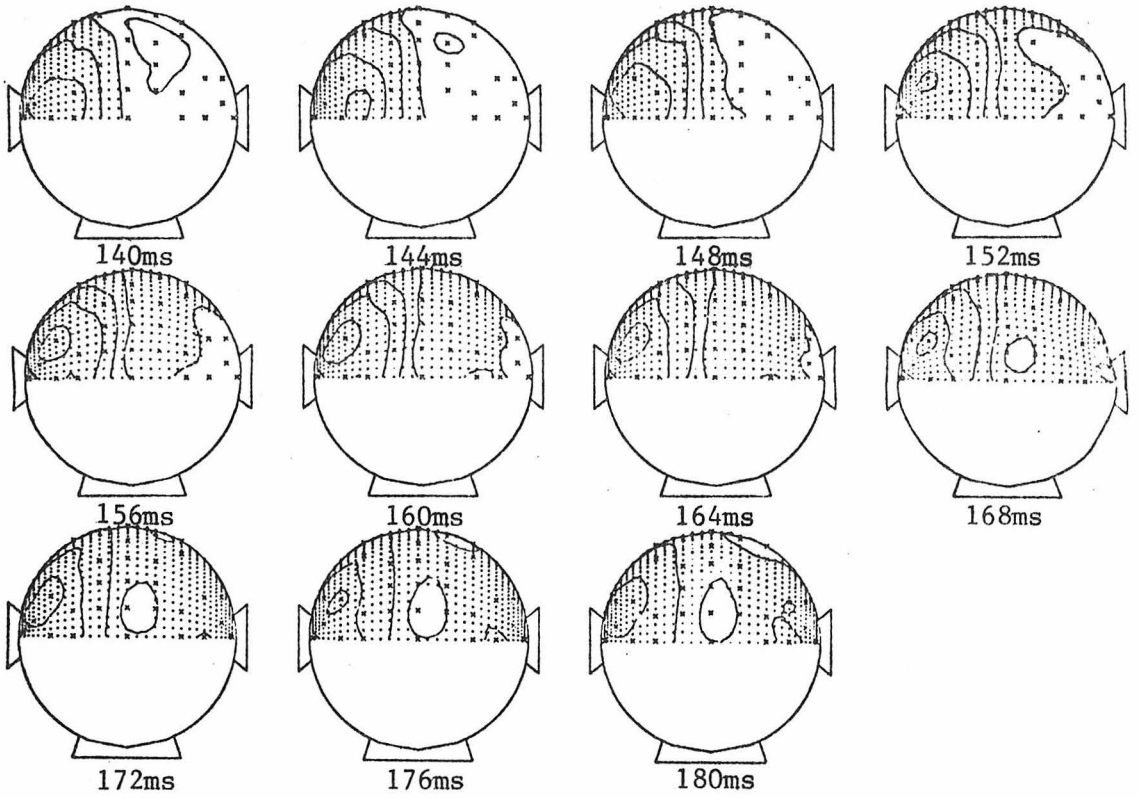

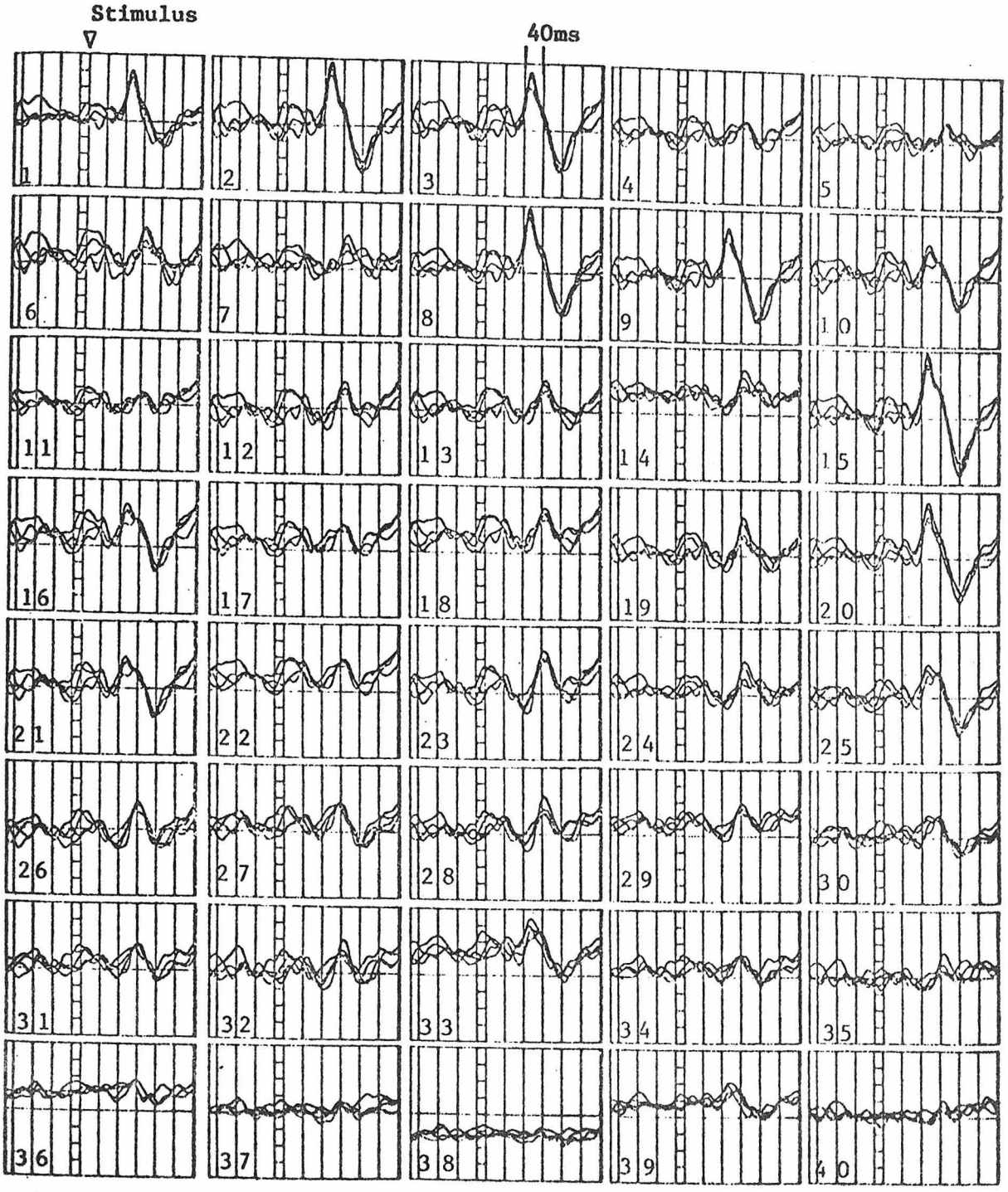

Fig. 64 - 4 average EPs for right half field appearance/disappearance stimulation of subject JPA using electrode layout 1 (Fig. 17) and a frontal monopolar reference

Fig. 75 - Equipotential maps of the data in the previous figure

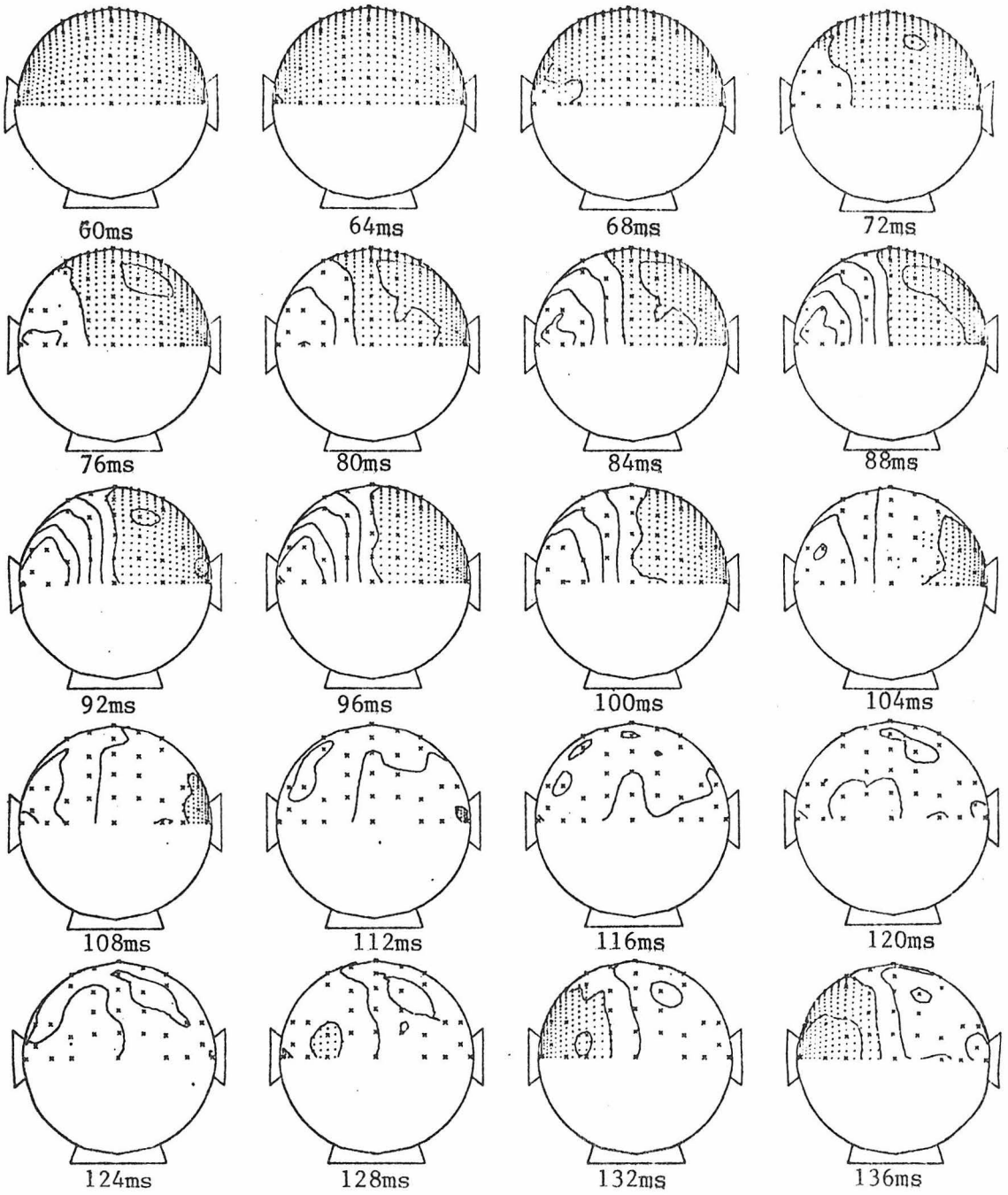

Fig. 65 (continued)

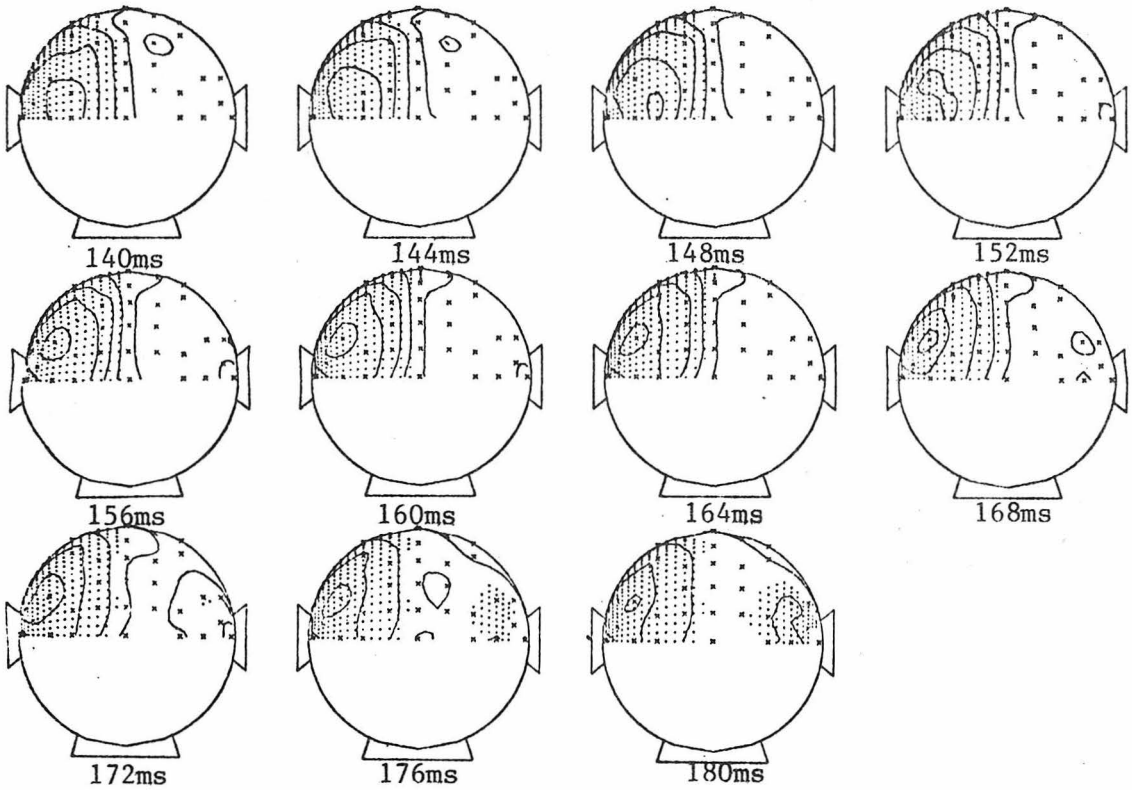

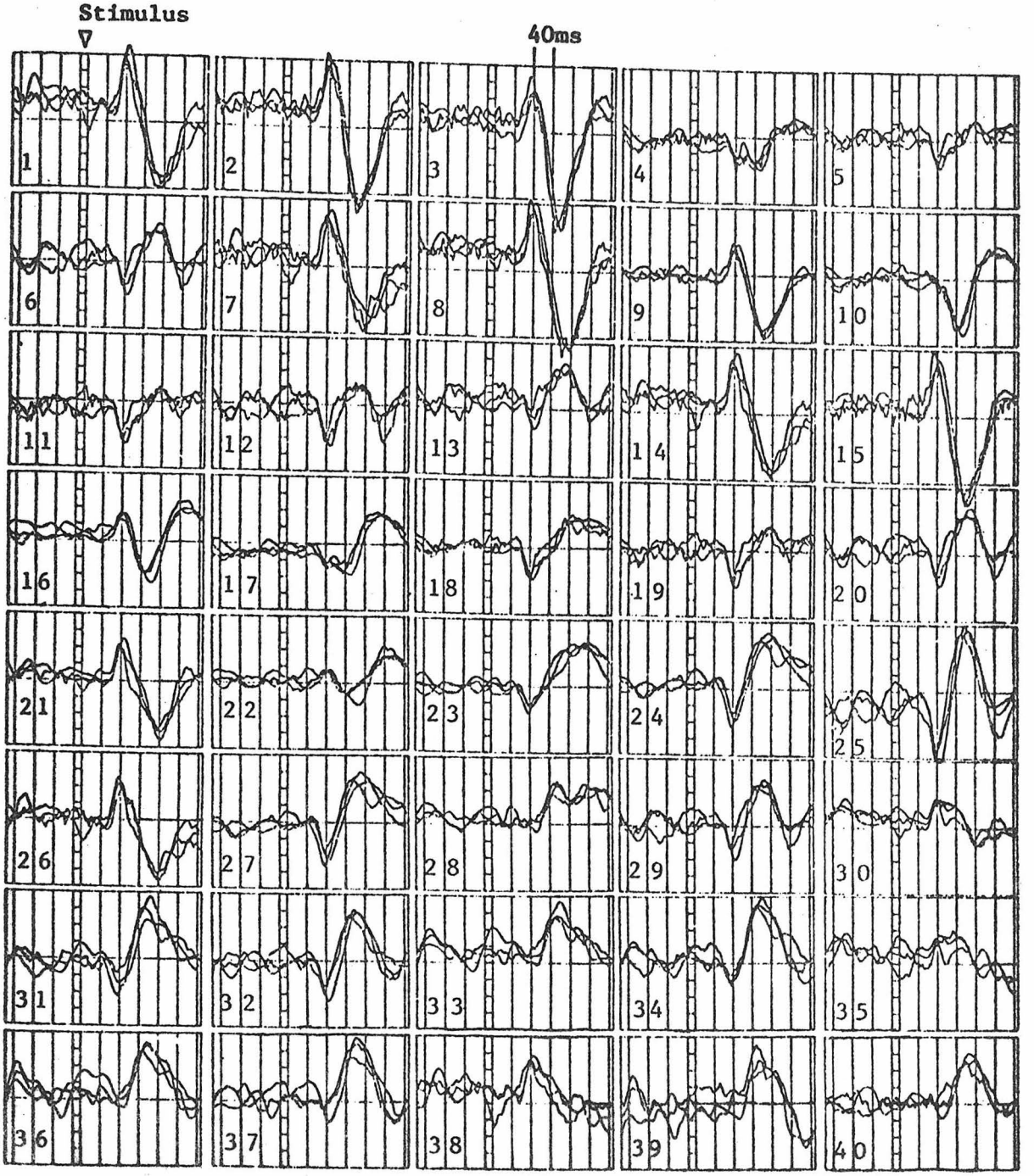

Fig. 66 - Average EPs for right half field appearance/disappearance stimulation of subject PDP using electrode layout 2 (Fig. 18) and three different amplifier bandwidths (30,60,90 Hz)

each is an average EP from a different bandwidth (the three bands have corner frequencies of 30, 60 and 90 Hz as described in section 3.2.3). The result is that the differences between the responses are negligible for the purposes of this study. Closer inspection reveals small differences in latency and amplitude, but these are so small that the three bands were deemed equivalent. This was further evidenced by the fact that their equipotential map series were unaffected by the choice of band. In light of these facts, the 30 Hz band was arbitrarily chosen for the experiments reported here.

4.2 Partial Field Data

4.2.1 Effect of Stimulus Locus on Spatio-Temporal EP's

The following pages show time series (from 60 msec to 180 msec after stimulus offset in 4 msec intervals) of equipotential maps on subject JPA using electrode layout 2 (Fig. 18) for each of 8 appearance/disappearance stimuli. Figs. 67-74 show responses for whole field (WF), right half field (RHF), upper half field (UHF), bottom half field (BHF), bottom left quadrant (BLQ), bottom right quadrant (BRQ), upper left quadrant (ULQ) and upper right quadrant (URQ) stimuli, respectively. The response for left half field (LHF) stimulation has already been shown in Fig. 59. Various octant stimuli were also attempted, but reliable data was not obtained and thus will not be presented here.

The most striking feature which these series have in common other than obviously high correlations between electrodes is an initial positive topography in the equipotential map which is maximum in the 88 to 96 msec range and whose peak locations depend systematically on stimulus locus in the visual field. The peak locations and shapes of these equipotential maps remain more or less the same for a period of 20 to 30 msec, with their amplitude rising and decaying in this interval. As shall be seen in Chapter 5, this is indicative of a source (or sources) which is stable in position and orientation, but which varies in magnitude over time.

The WF response (Fig. 67) shows an initial bilateral topography with peak locations which are symmetric about the midline and located a little above the level of the inion. This is more or less what one would expect, since each hemisphere of the brain is known (see sections

Fig. 67 - Map series for whole field (WF) stimulation (#runs=11)

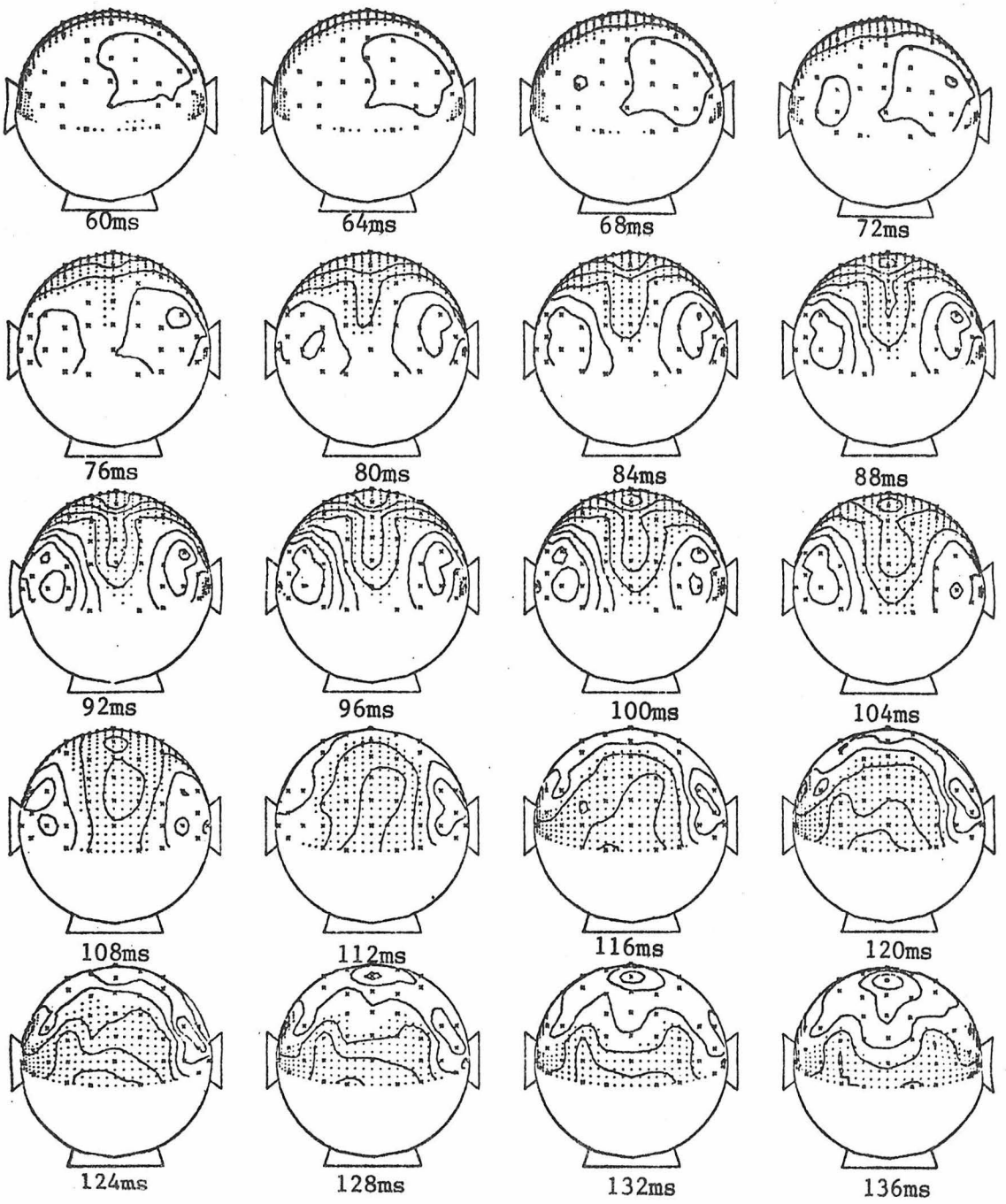

Fig. 67 (continued)

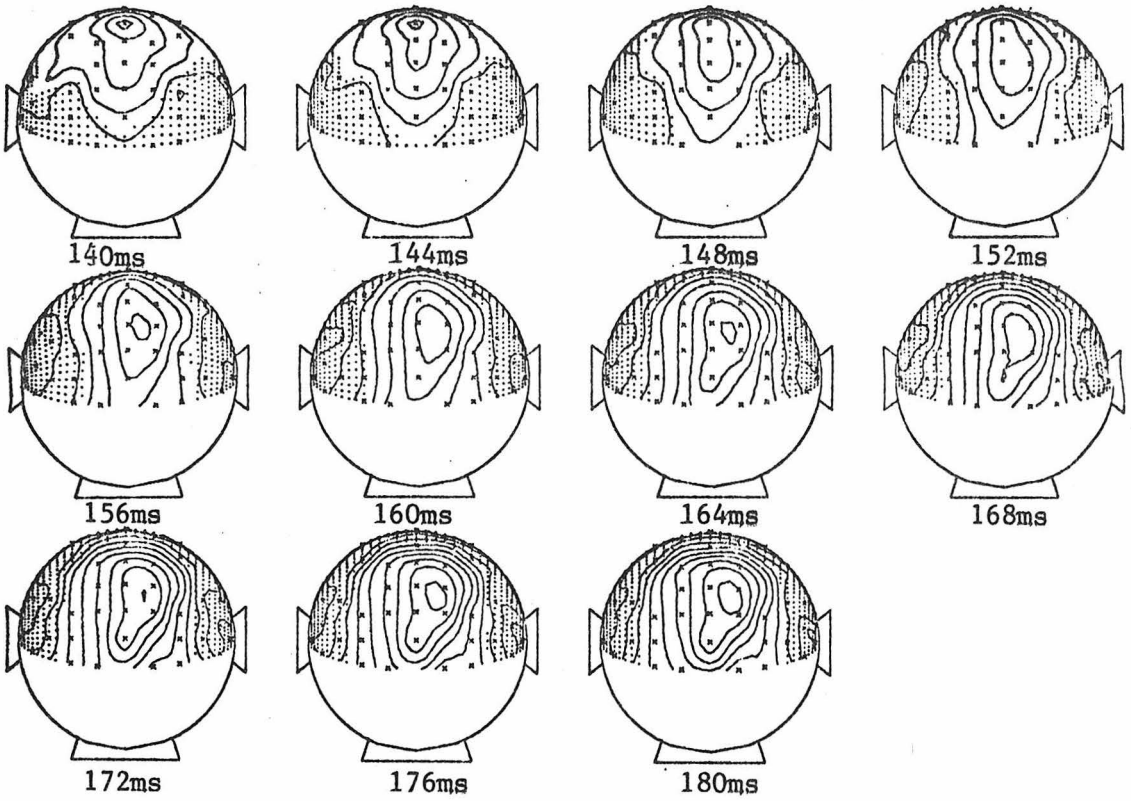

Fig. 68 - Map series for right half field (RHF) stimulation (#runs=13)

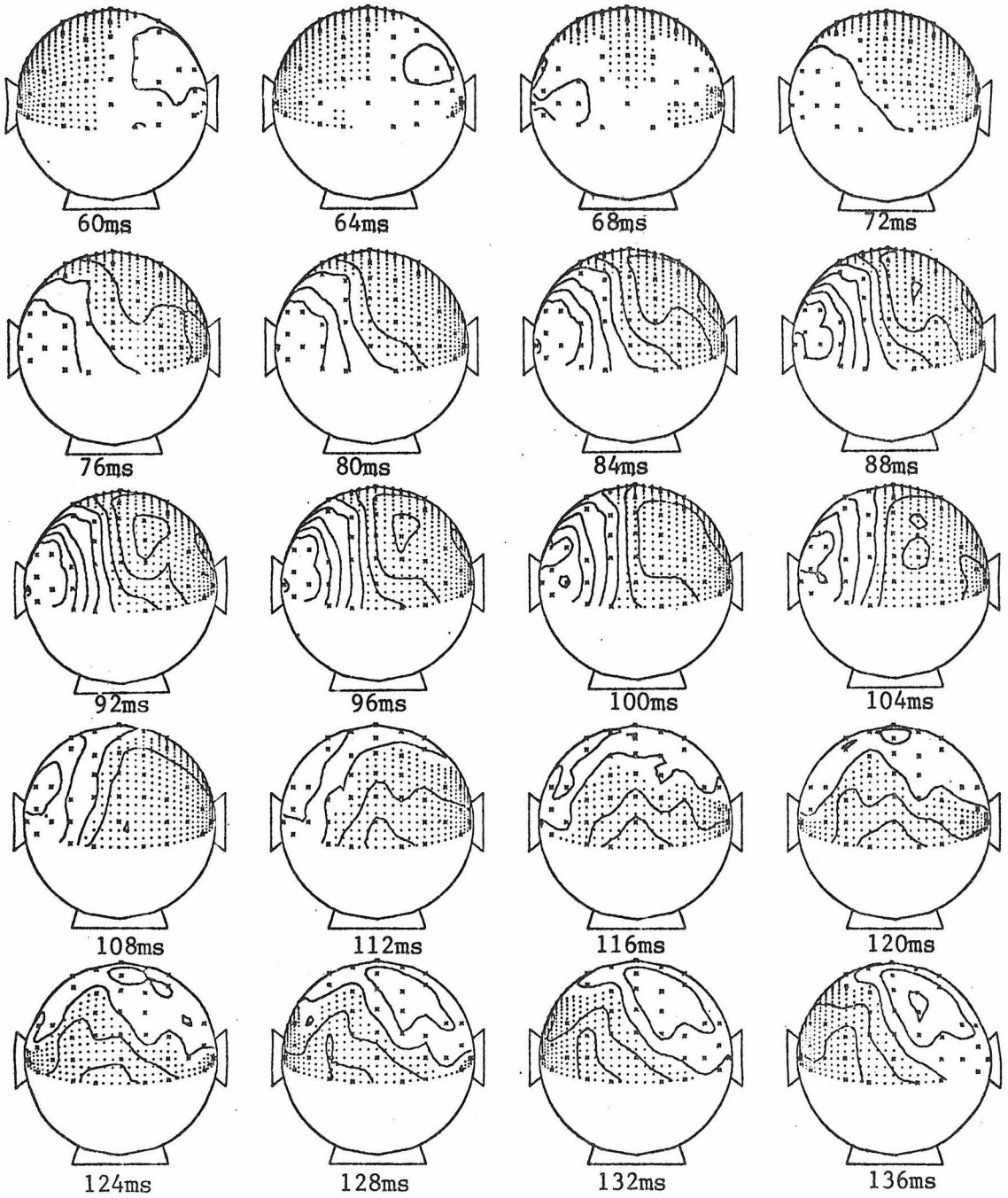

Fig. 68 (continued)

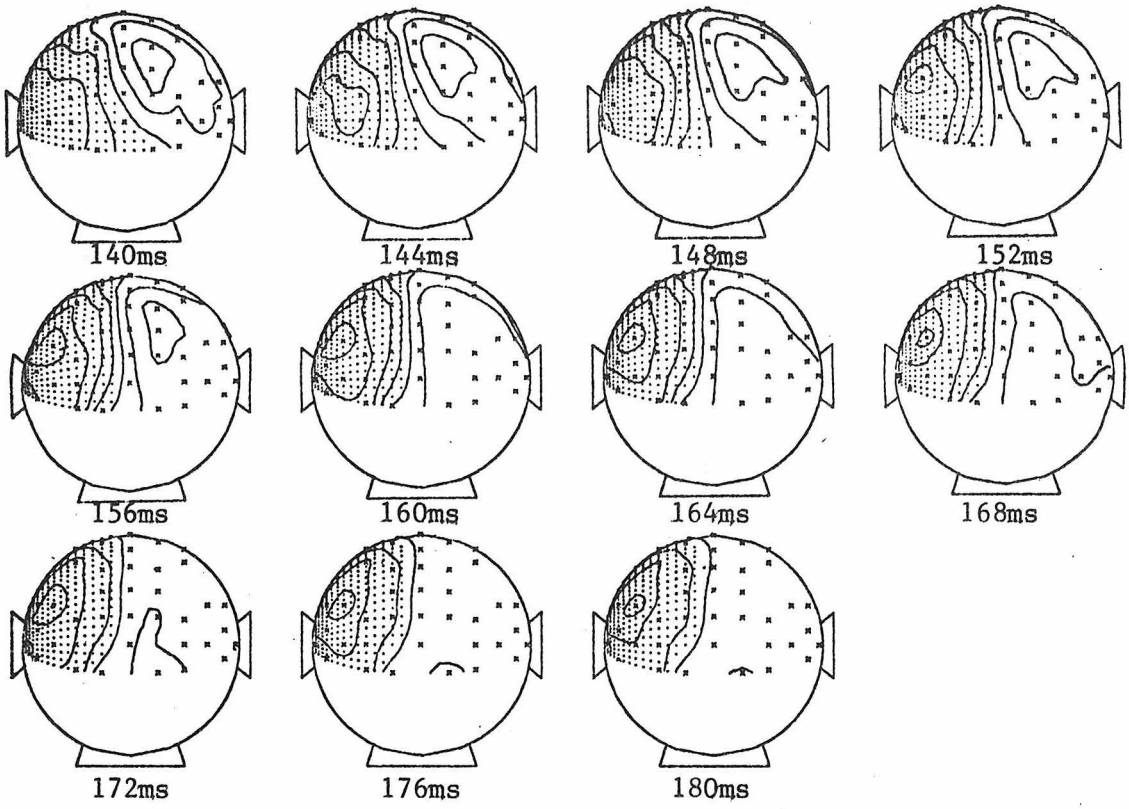

Fig. 69 - Map series for upper half field (UHF) stimulation (#runs=11)

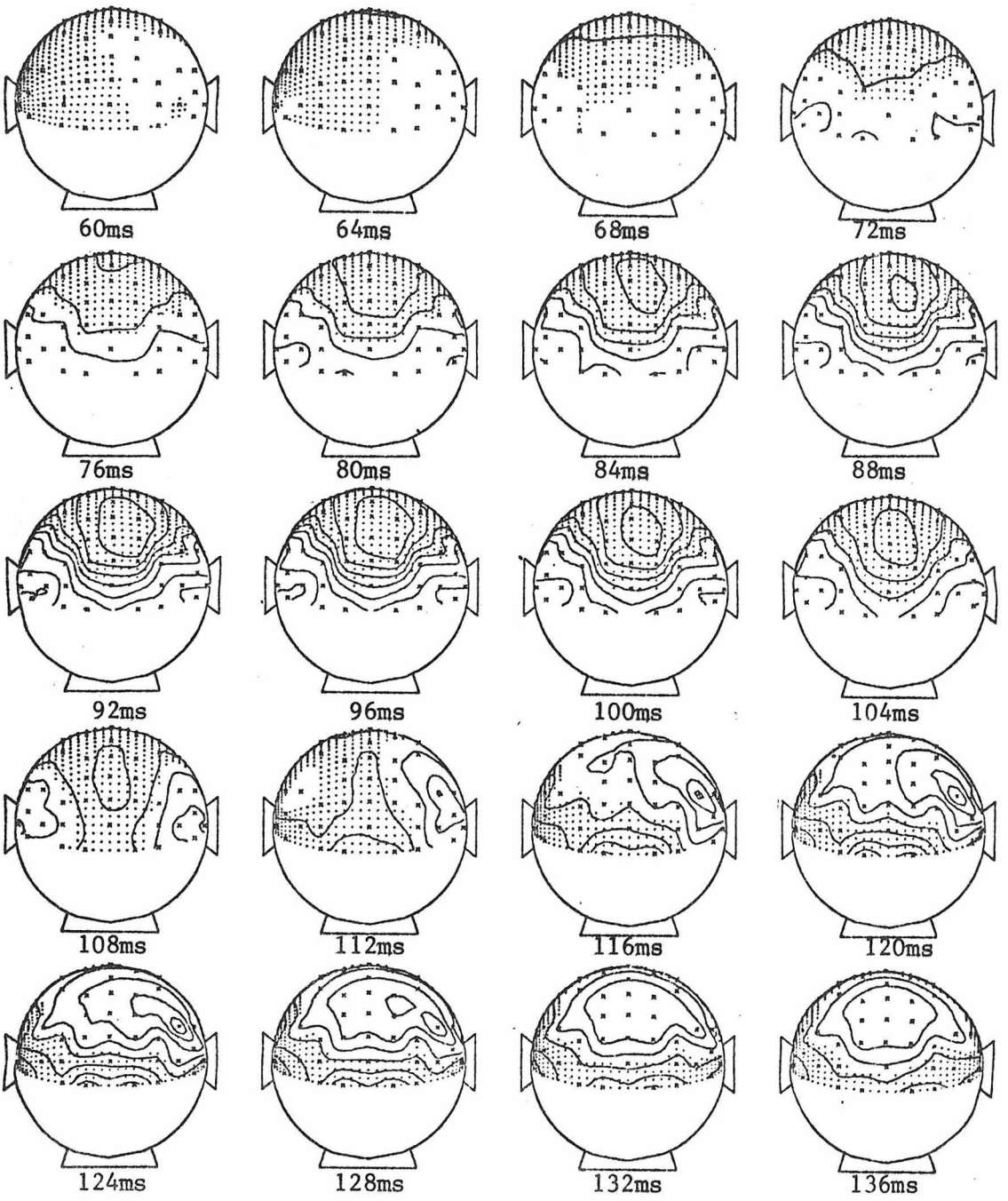

Fig. 69 (continued)

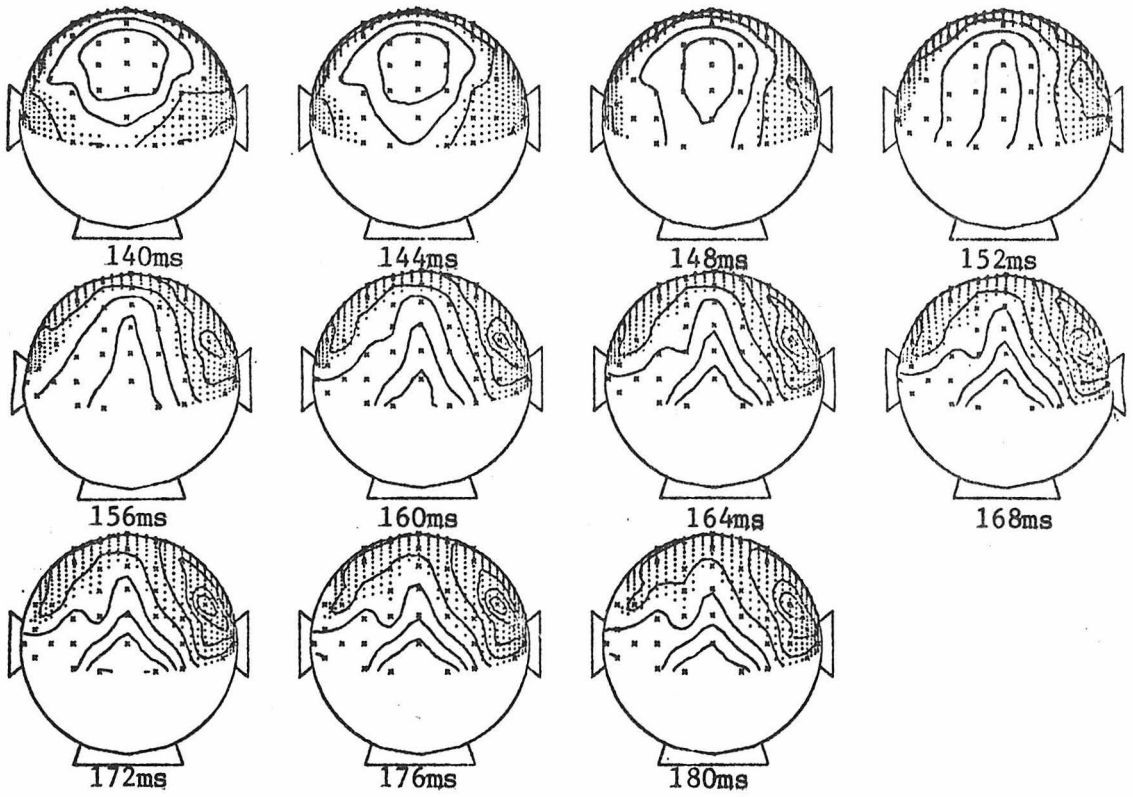

Fig. 70 - Map series for bottom half field (BHF) stimulation (#runs=12)

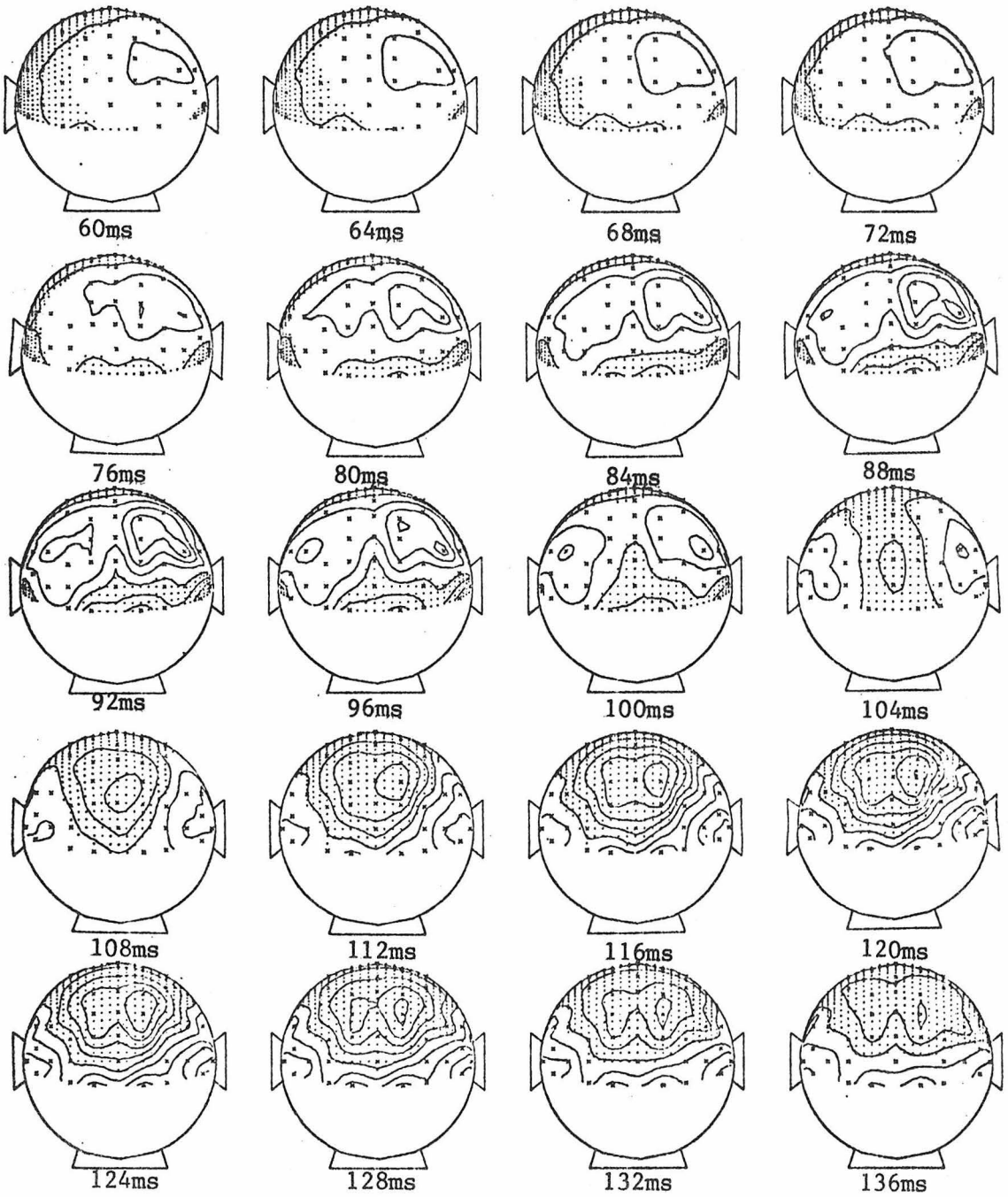

Fig. 70 (continued)

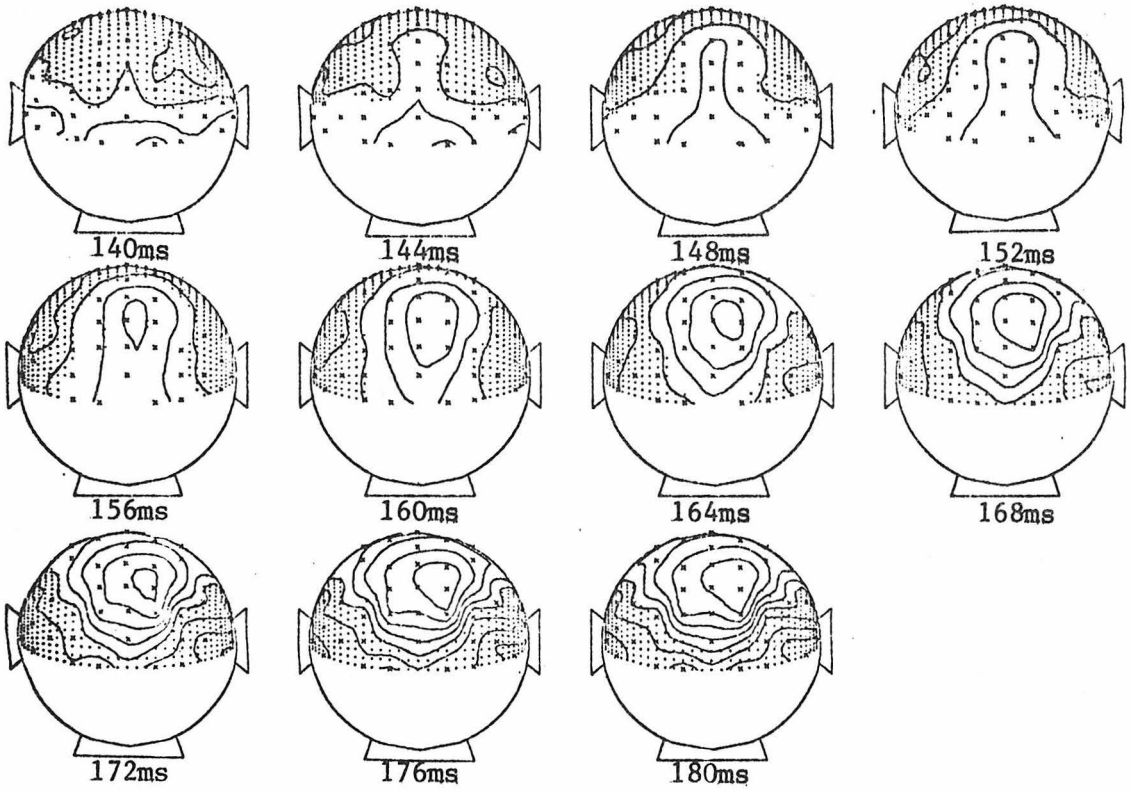

Fig. 71 - Map series for bottom left quadrant (BLQ) stimulation (#runs=8)

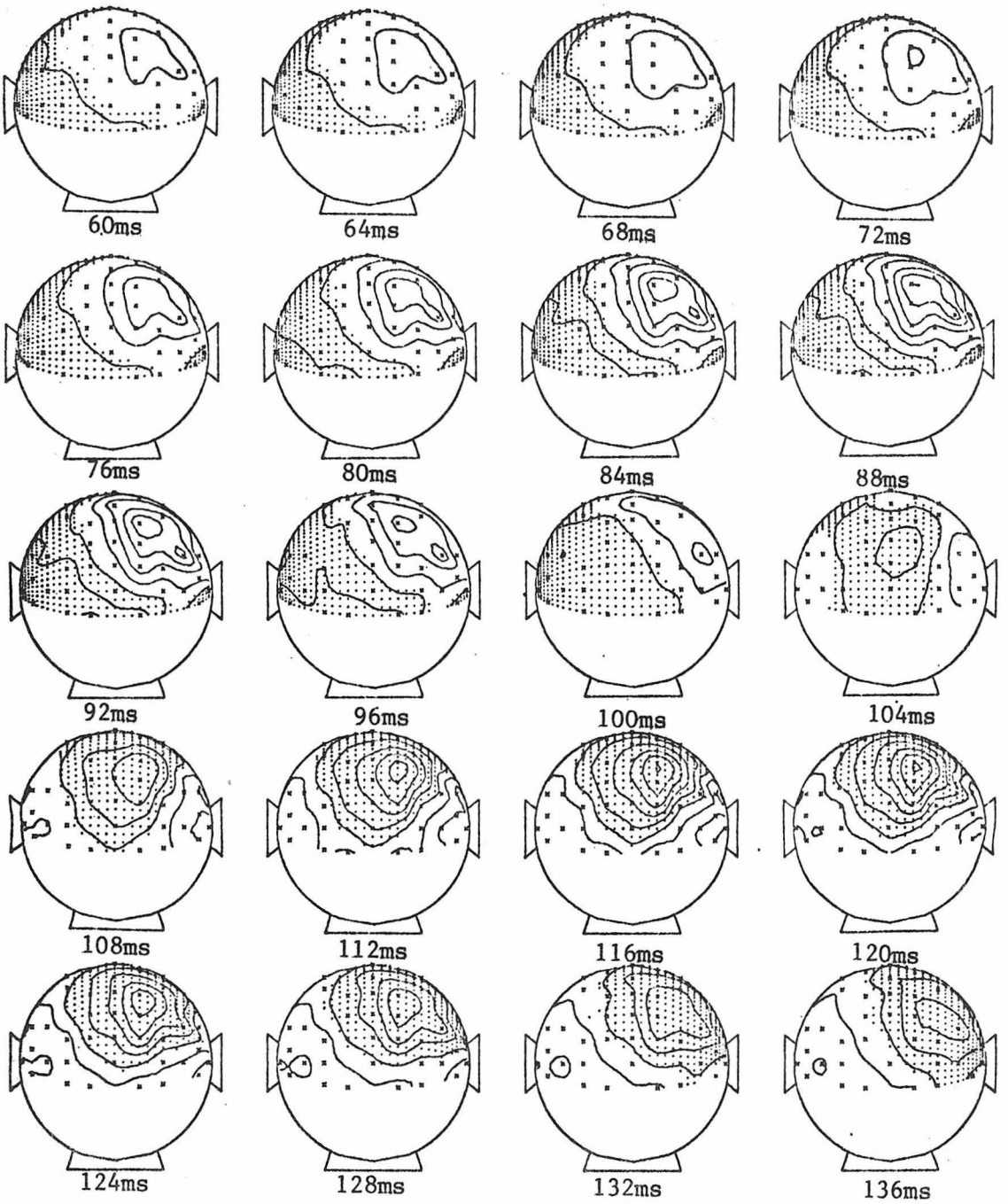

Fig. 71 (continued)

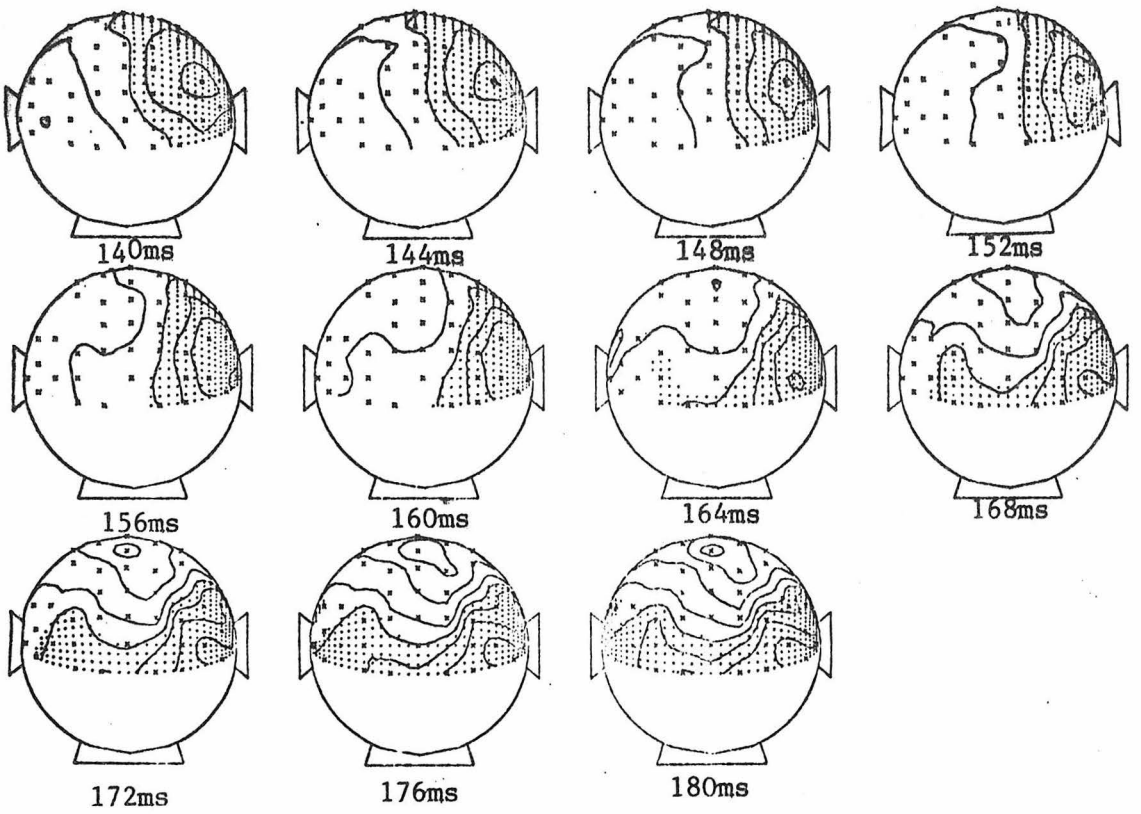

Fig. 72 - Map series for bottom right quadrant (BRQ) stimulation (#runs=7)

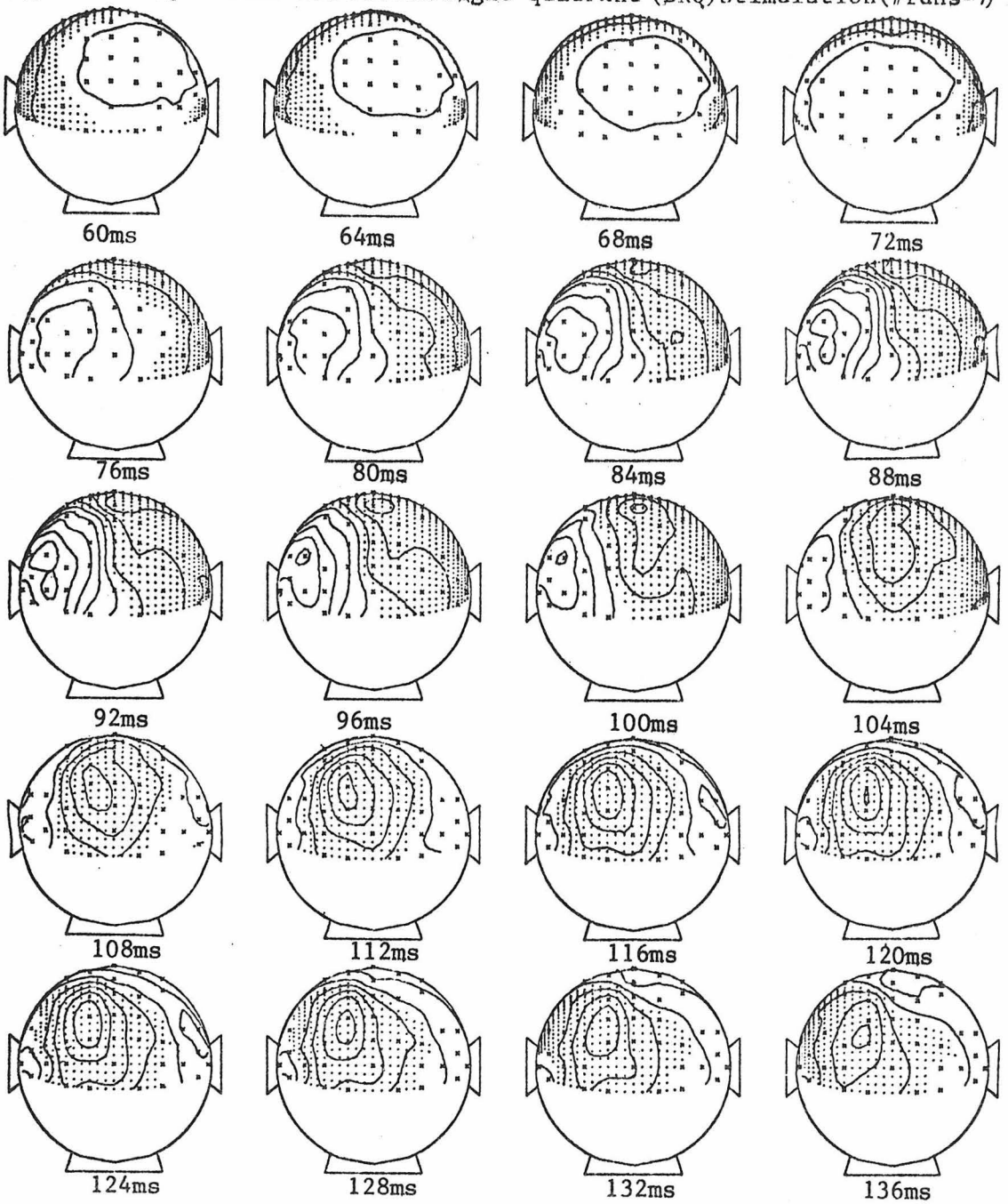

Fig. 72 (continued)

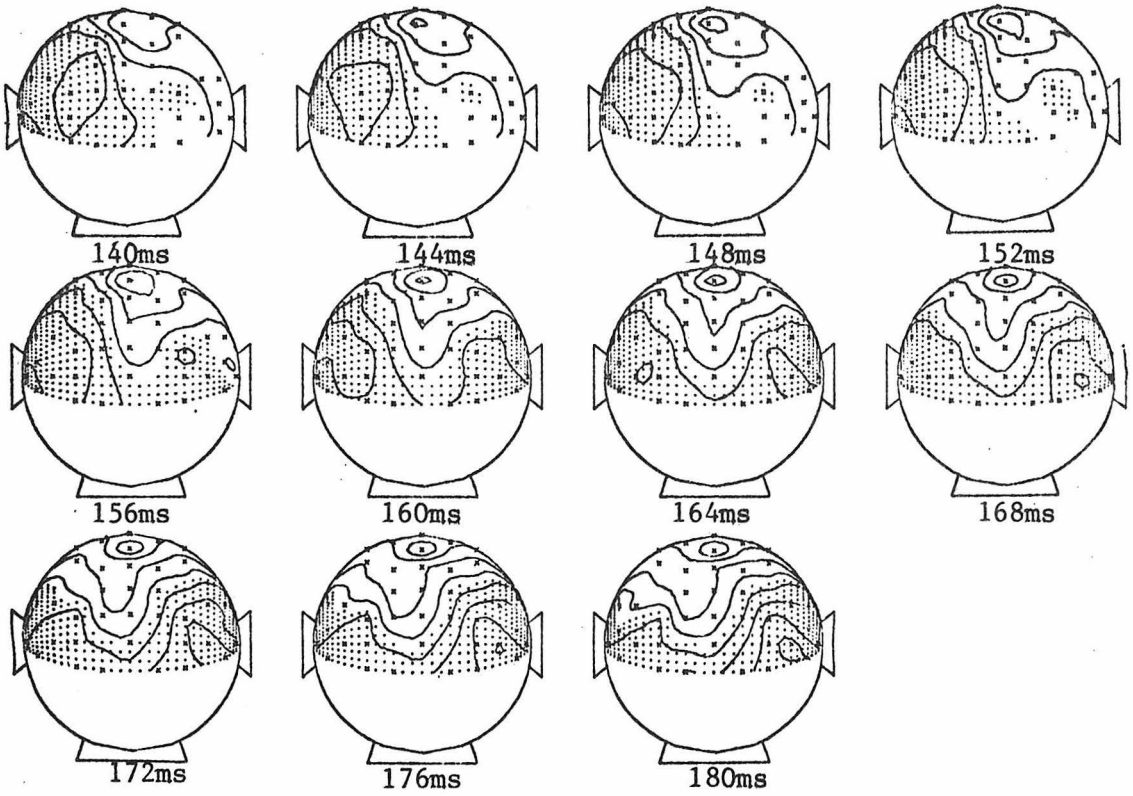

Fig. 73 - Map series for upper left quadrant (ULQ) stimulation (#runs=9)

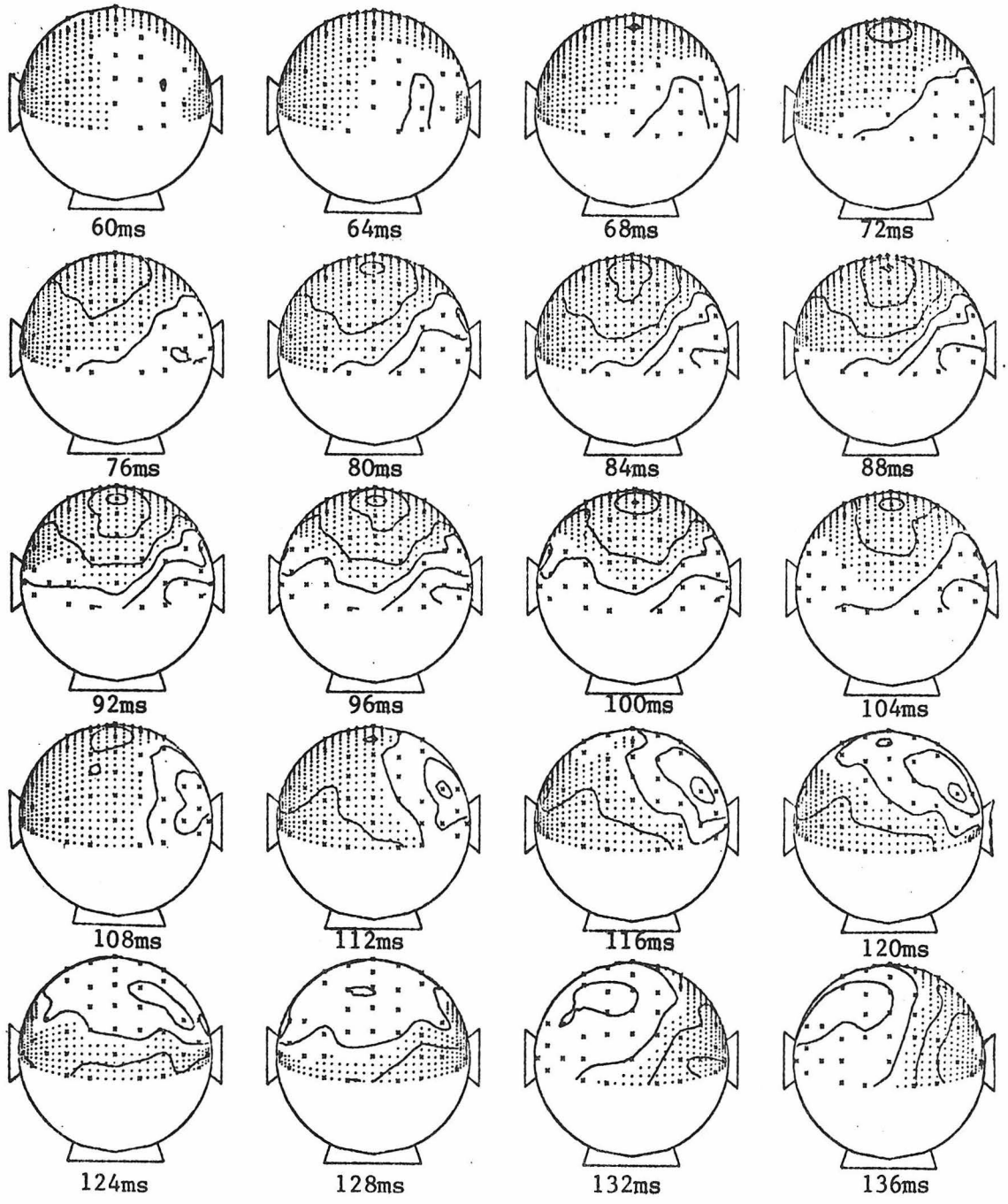

Fig. 73 (continued)

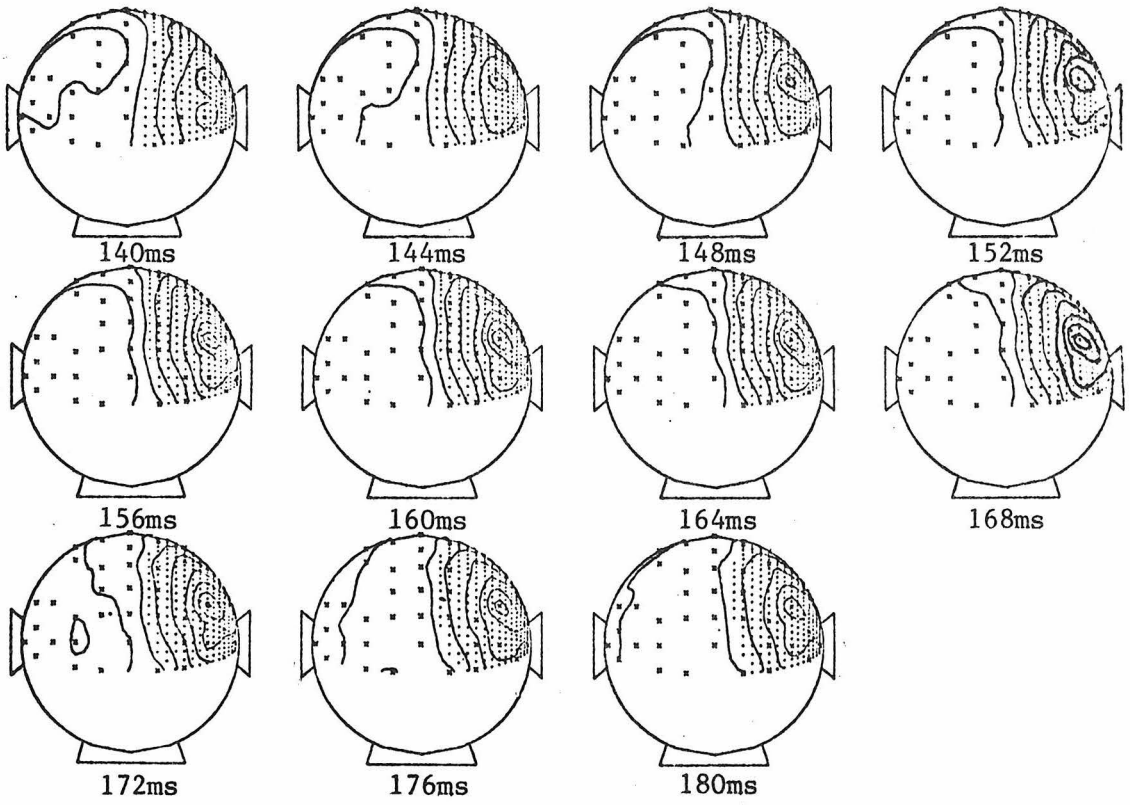

Fig. 74 - Map series for upper right quadrant (URQ) stimulation (# runs=9)

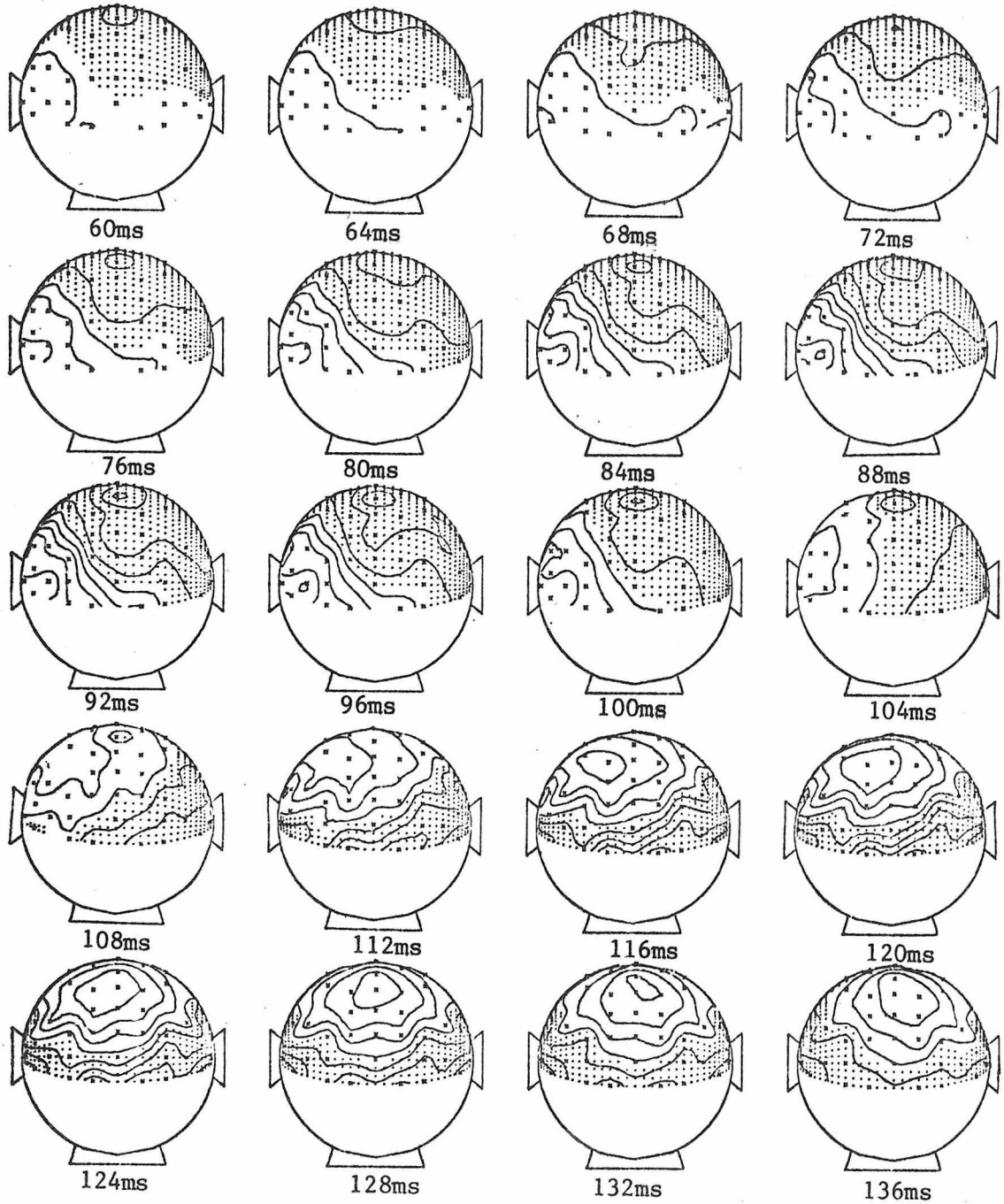

Fig. 74 (continued)

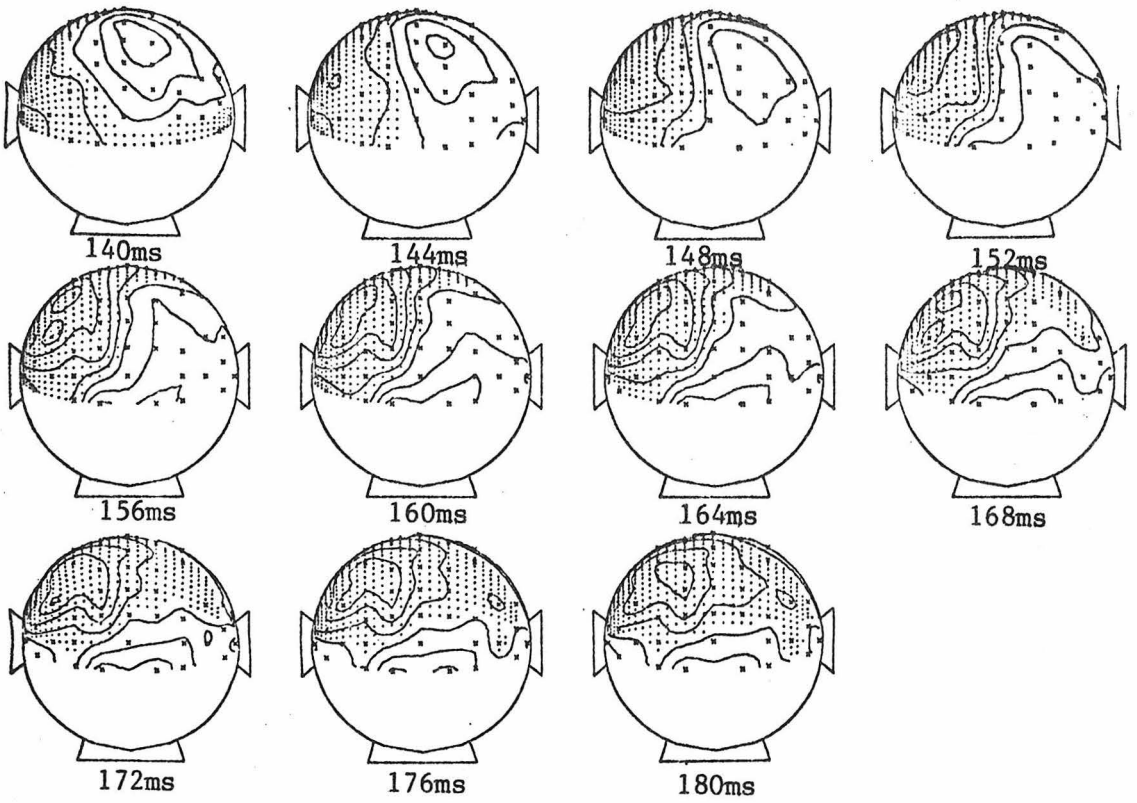

2.2.3 and 2.2.6) to receive projections from the contralateral half of the visual field. The LHF response (Fig. 59) shows a unilateral initial topography which peaks to the right of the midline and a little above the level of the inion, while the RHF response (Fig. 68) shows an initial topography peaking to the left of the midline at about the level of the inion. The lateralization of these initial peaks is in conformity with the contralateral projections of the visual field. Note also that the WF initial topography appears to be a mere composite or superposition of the LHF and RHF initial topographies. This notion will be tested and discussed in section 4.3.

The UHF response (Fig. 69) shows an initial bilateral topography whose peaks are symmetric about the midline a little below the level of the inion. Again this does not conflict with anatomical predictions, since the upper half of the visual field is presumed to project bilaterally to visual cortex below the level of the calcarine fissure. The BHF response (Fig. 70) also shows a bilateral initial topography which peaks symmetrically about the midline well above the level of the inion. The amplitude of the two peaks in this case are not as close as in the WF and UHF cases.

The BLQ response (Fig. 71) shows an initial topography which peaks to the right of the midline and well above the inion level, while the BRQ response (Fig. 72) shows an initial topography which peaks to the left of the midline and above the inion level. Correspondingly, the ULQ response (Fig. 73) shows an initial topography which peaks to the right of the midline and a little below the level of the inion, while the URQ response (Fig. 74) shows an initial topography which peaks to the

left of the midline and a little below the level of the inion. These are again in keeping with expectations. Note again that various half field initial topographies appear to be composites or superpositions of the initial topographies of their constituent quadrants.

As may be seen in Figs. 59 and 67-74, the initial positive topographies are followed by negative topographies which are located on the scalp in the proximity of the initial positive peaks. The latencies at which they are minimum, however, differ among the stimuli. This occurs in the 120 msec to 160 msec range and there may be one or more such deflections. The quadrants (except ULQ) and vertical half fields (UHF, BHF) generally have their minima earlier than do the lateral half fields (LHF, RHF) and whole field (WF). Fig. 75 helps to illustrate this point and the previous discussion of the initial peaks. It shows that all 9 stimuli result in an initial positive deflection in the 88 to 96 msec range, but that the following negative deflection has a latency variation. Fig. 75 shows a mean evoked potential waveform (± one standard deviation of the mean) for each positive peak of the potential distribution in each of the 9 stimulus conditions. The waveform shown in each case is taken from a single electrode which is representative of the response on electrodes in the vicinity of an initial positive peak. Indeed, in most cases this waveform is representative of waveforms over a fairly large area of the scalp. By representative, it is meant to say that electrodes in the vicinity have similar waveshapes, but differ by a scale factor (positive or negative constant) depending on their location. This appears to be true at least in a piecewise sense, i.e. in the time

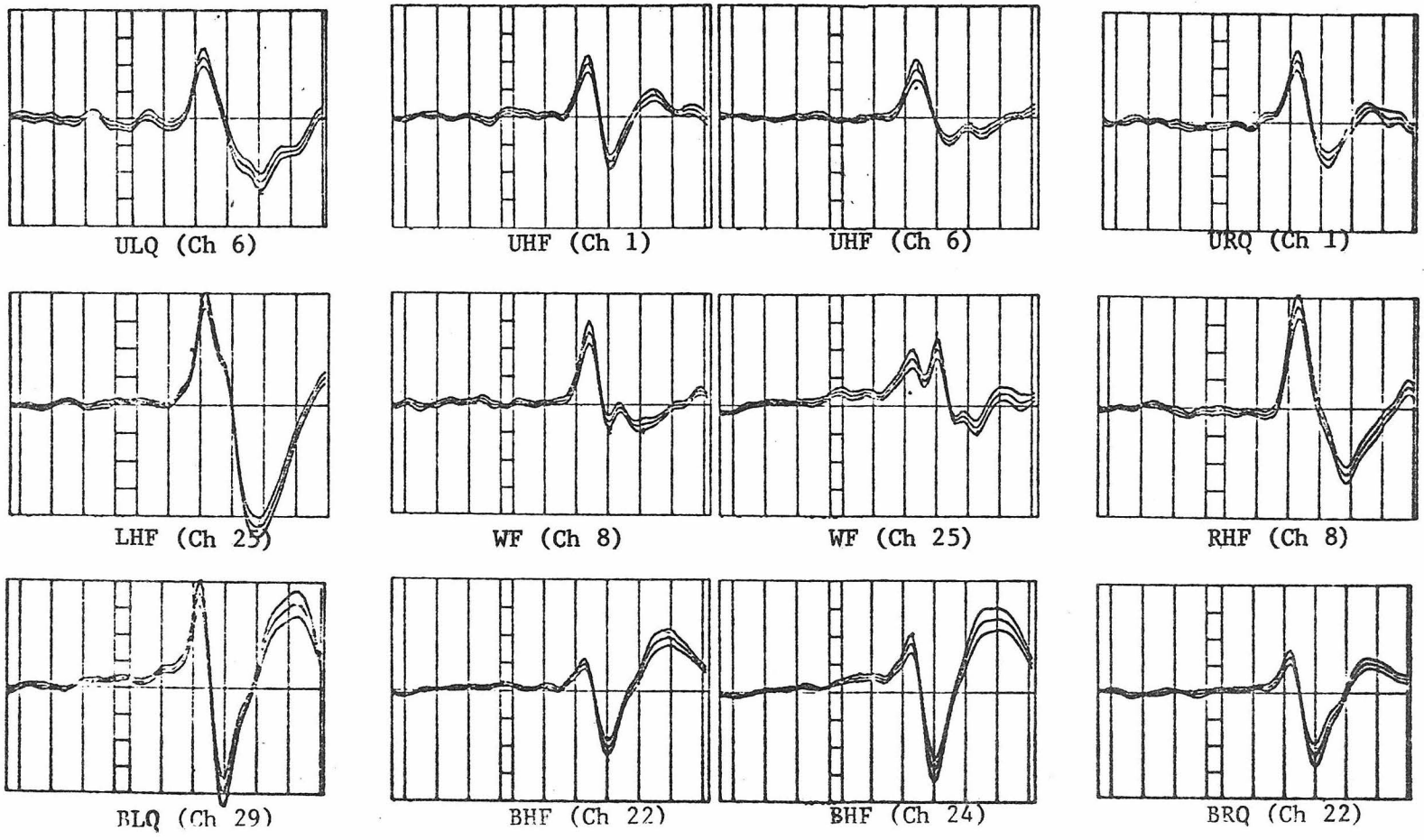

Fig. 75 - Mean EPs on representative electrodes (± 1 sdev. of the mean) for subject JPA appearance/disappearance stimulation and electrode layout 2 (Fig. 18)

ranges of 20 to 50 msec which the different map peaks occur.

The meaning of the latency variation is unclear, but it appears possible that there are actually 3 activities occurring over longer time intervals and that the surface field of the second activity is electrically cancelled out in the case of the lateral half field responses. Obviously, if there is cancellation occurring in the lateral half field responses, it would probably also appear in the whole field response. This notion will be considered further in section 4.3, where measured responses will be compared with responses predicted from the superposition of responses to constituent parts of the visual field.

4.2.2 Intersubject and Intrasubject Dependence of EP Topographies on Stimulus Locus

Figures 76 and 77 show selected mean appearance/disappearance evoked potential waveforms analogous to those of Fig. 75, for subjects PDP and RML, respectively. It may be noted that the initial positive deflection in the 88 to 96 msec time period is common to all three subjects for all 9 stimuli and that the latency of the following negative deflection is variable as previously discussed.

Figures 78, 79 and 80 show the stimulus dependence of the initial topography of the responses in each of the three subjects: JPA, PDP, and RML, respectively. In this case the maps are all plotted with 11 contour levels to accentuate detail. Note that subjects JPA and PDP have very similar responses, but that subject RML is quite different. Although this aspect of the data is initially somewhat disappointing to look at, it will be seen that subject RML reveals some very important clues regarding the cortical origin of these evoked potentials.

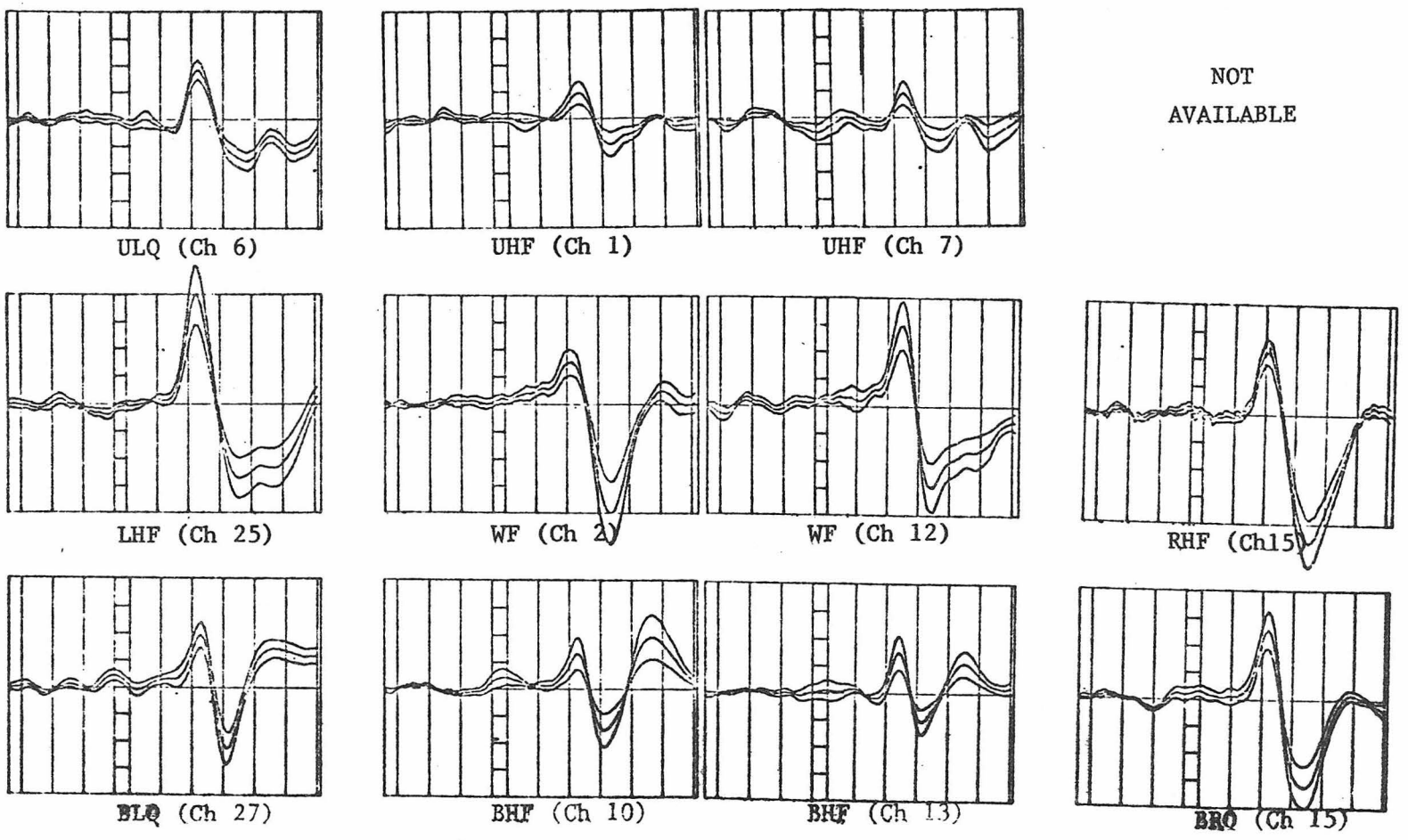

Fig. 76 - Mean EPs on representative electrodes (± 1 sdev. of the mean) for subject PDP appearance/disappearance stimulation and electrode layouts 1 (UHF,BHF) and 2 (WF,LHF,RHF,ULQ,BLQ,BRQ)

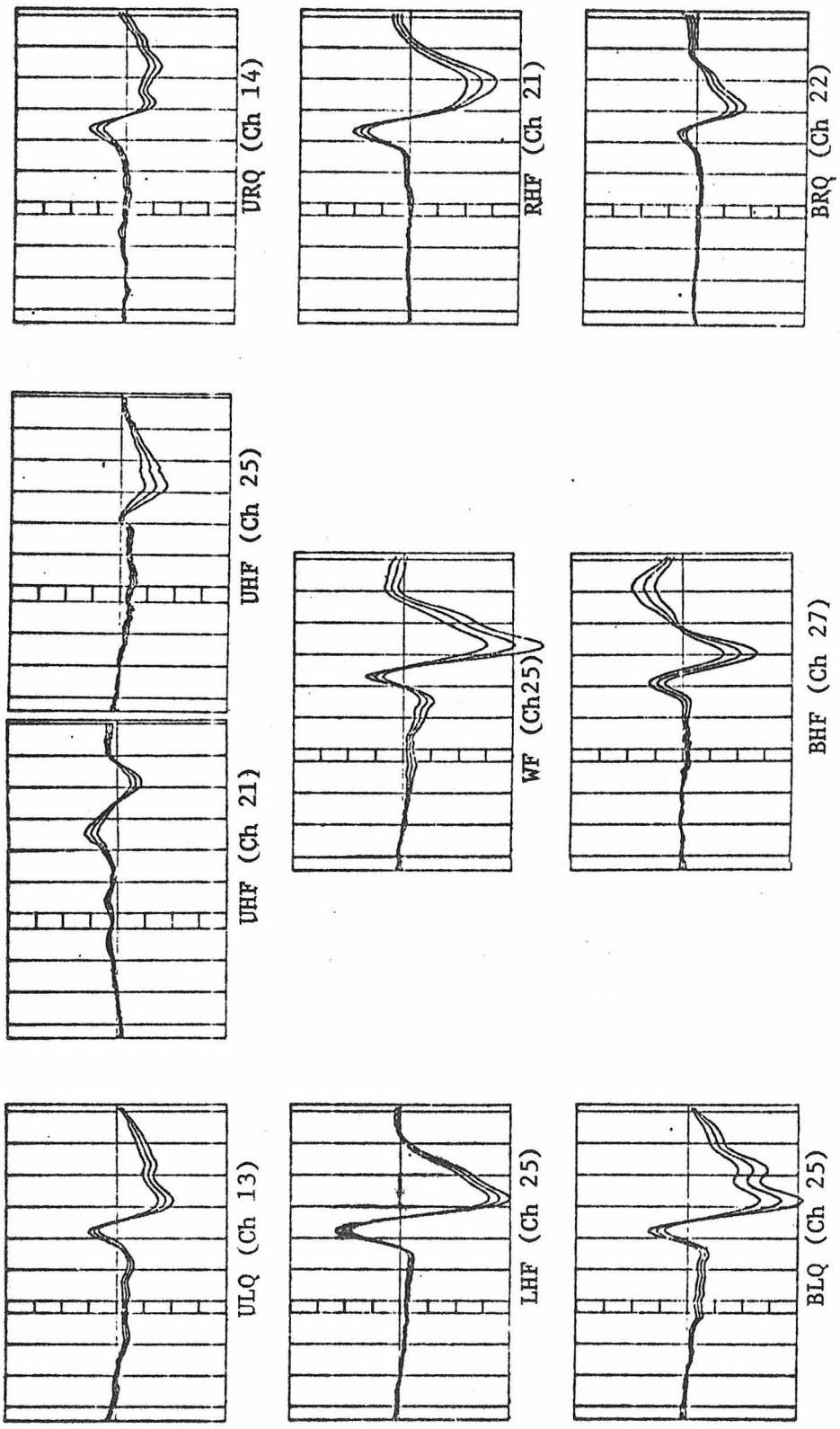

Fig. 77 - Mean EPs on representative electrodes (± 1 sdev. of the mean) for subject RML appearance/disappearance stimulation and electrode 2 (Fig. 18)

Fig. 78 - Initial peaks of various partial field appearance/disappearance responses in subject JPA

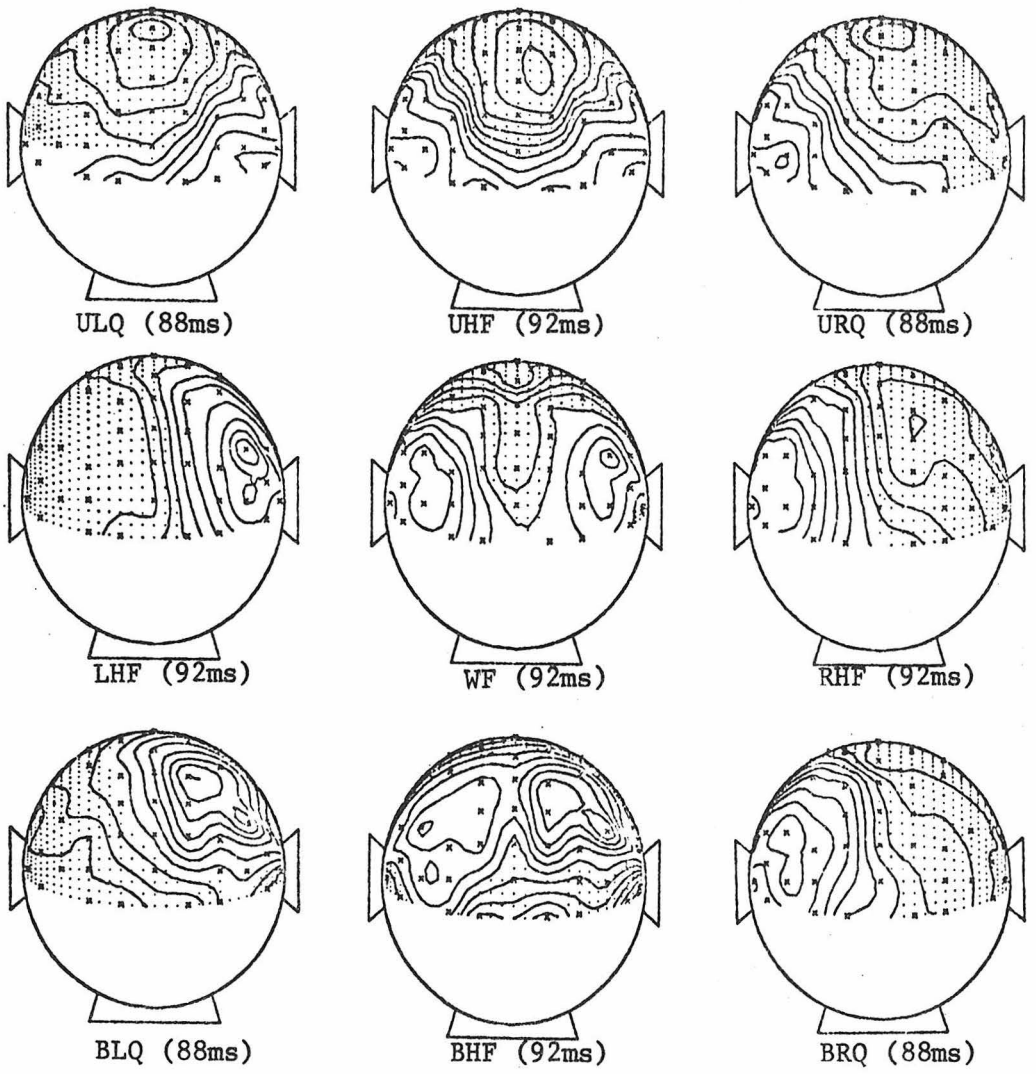

Fig. 79 - Initial peaks of various partial field appearance/disappearance responses in subject PDP

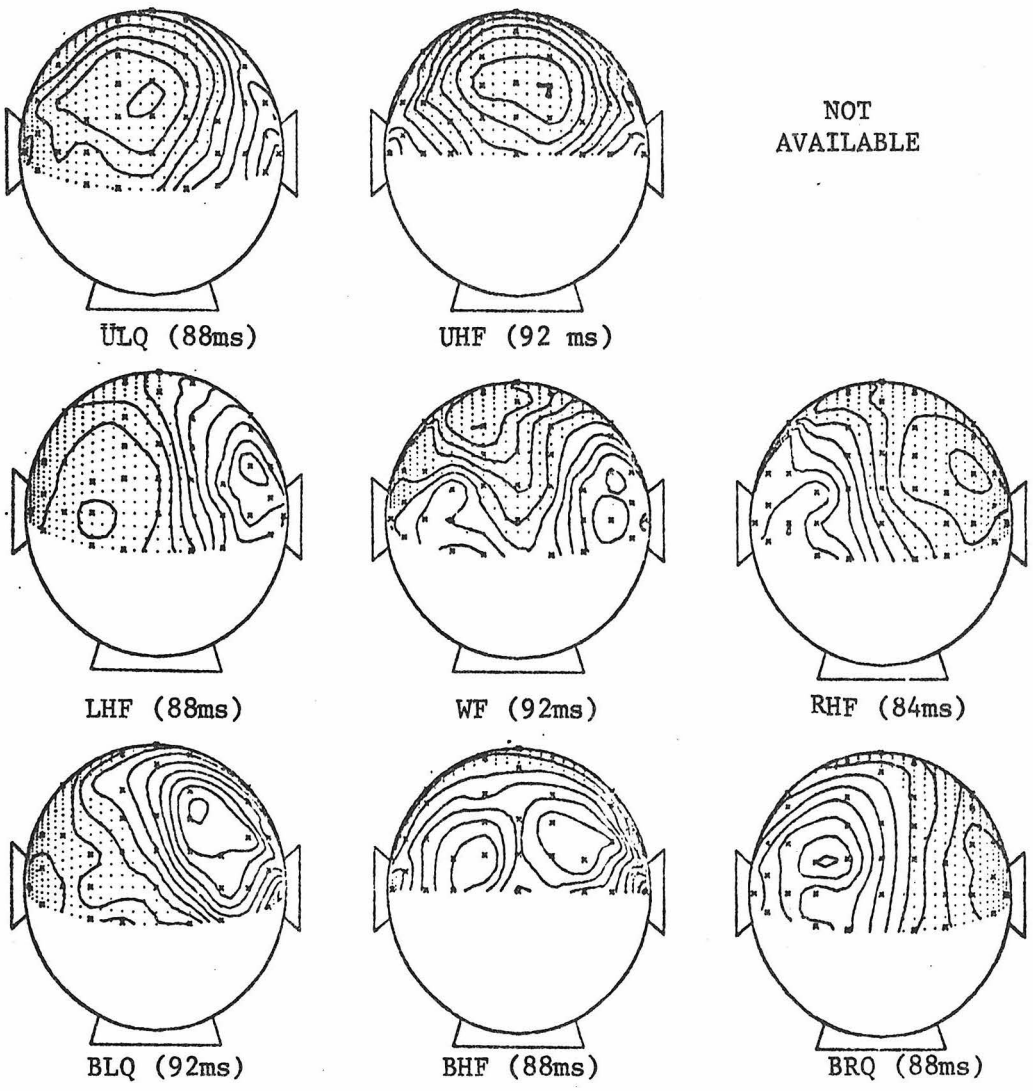

Fig. 80 - Initial peaks of various partial field appearance/disappearance responses in subject RML

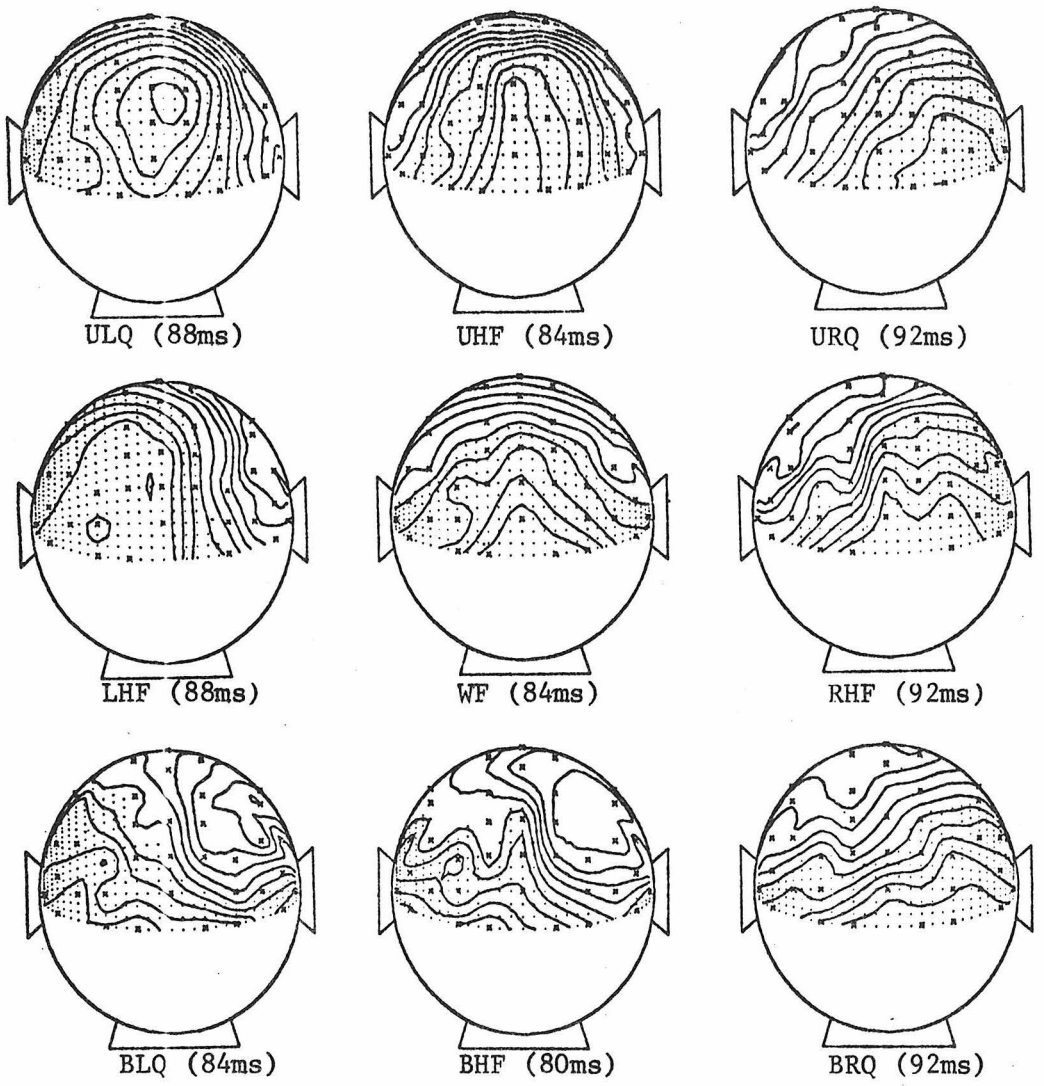

Also, it should be noted that such variations are compatible with the known variability in the topography or folding of cortex (section 2.2.6) and the hypothesis of this thesis that variations in EP's reflect changes in the cerebral location and orientation of their source (or sources) more than changes in the generative process. Note, however, that the initial topography of subject RML does have several aspects in common with subjects JPA and PDP, and which meet with expectations based on the projections of the visual field to visual cortex. For example, the lateral half field (LHF, RHF) responses again have peaks which are appropriately lateralized to opposite sides of the midline. The scalp locations of these peaks are, however, much further up on the head than in the other two subjects. Again the WF topography looks as though it might be the superposition of the LHF and RHF topographies. Also the relative vertical (i.e. parallel to midline) locations of the peaks in the quadrant responses are above and below the locations of the peaks of the lateral half fields, in conformity with the two other subjects. For example, the scalp location of the ULQ peak is below the location of the LHF peak, which is, in turn, below the location of the BLQ peak. Also note (Figs. 75-77) that the waveshapes of the responses of all three subjects are similar, especially with respect to the first positive deflection. The likely explanation for this is that subject RML has the same generative processes as the other subjects, but has a different cortical topography.

Figures 81, 82 and 83 show the stimulus dependence of the initial negative topography of the responses in each of the three subjects

Fig. 81 - Secondary peaks of partial field appearance/disappearance responses in subject JPA

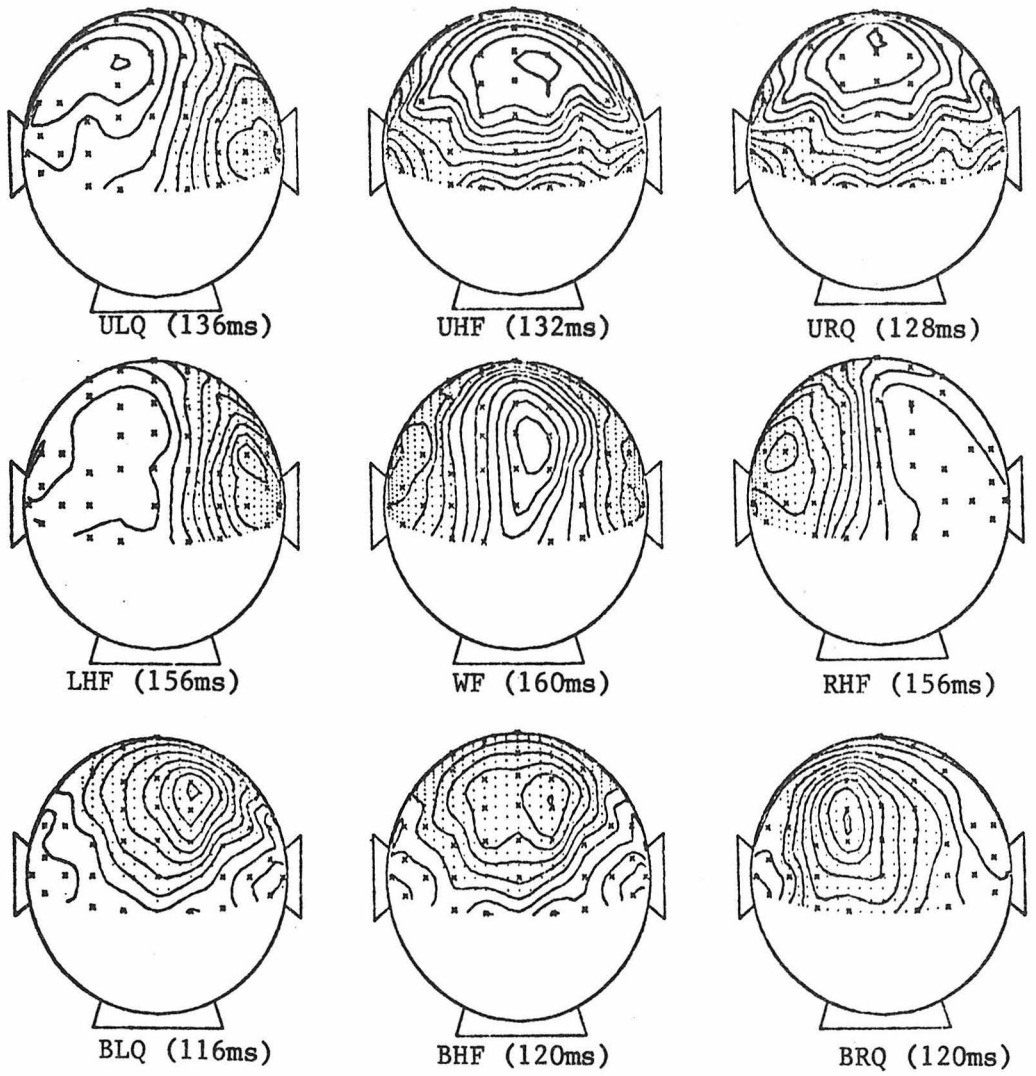

Fig. 82 - Secondary peaks of partial field appearance/disappearance responses in subject PDP

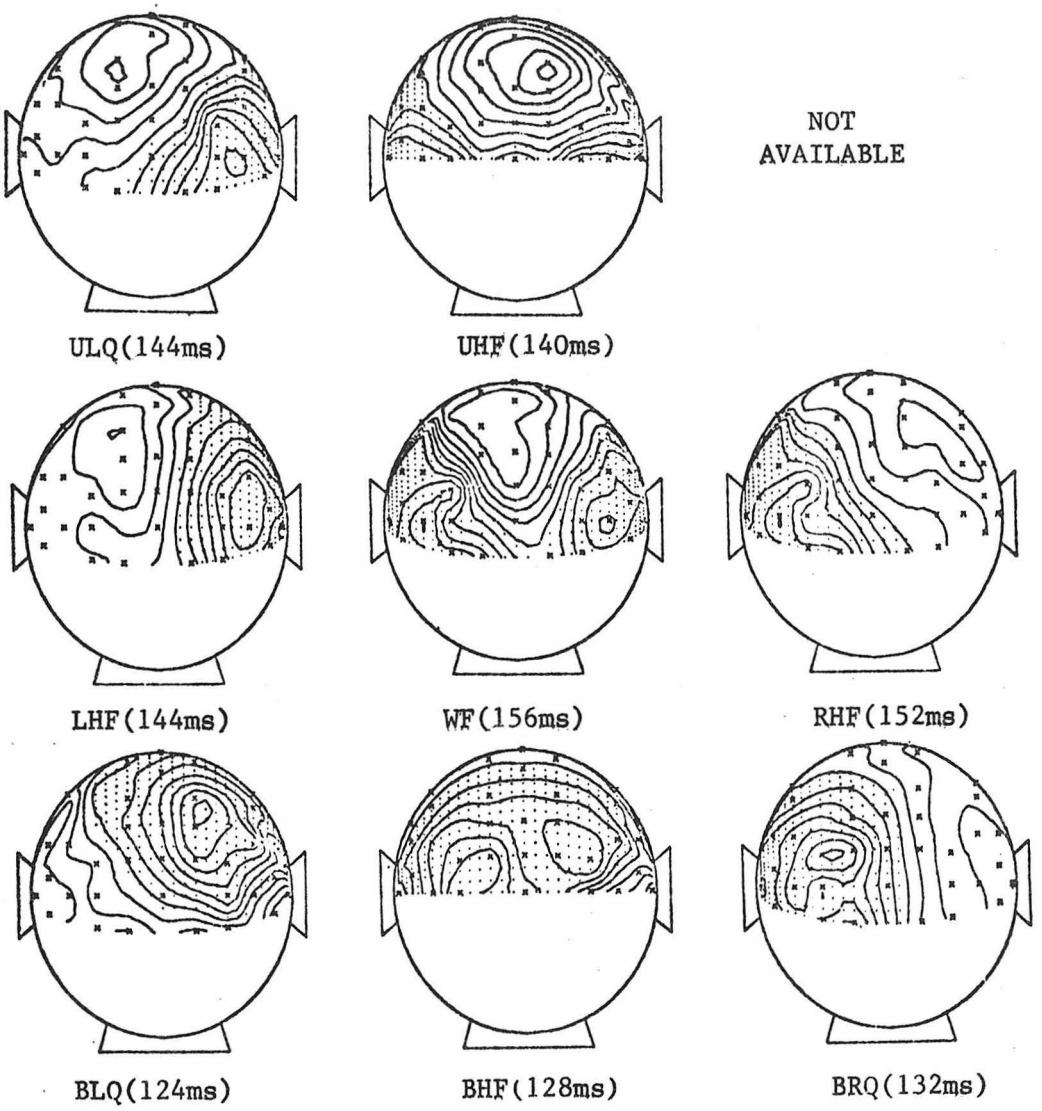

Fig. 83 - Secondary peaks of partial field appearance/disappearance responses in subject RML

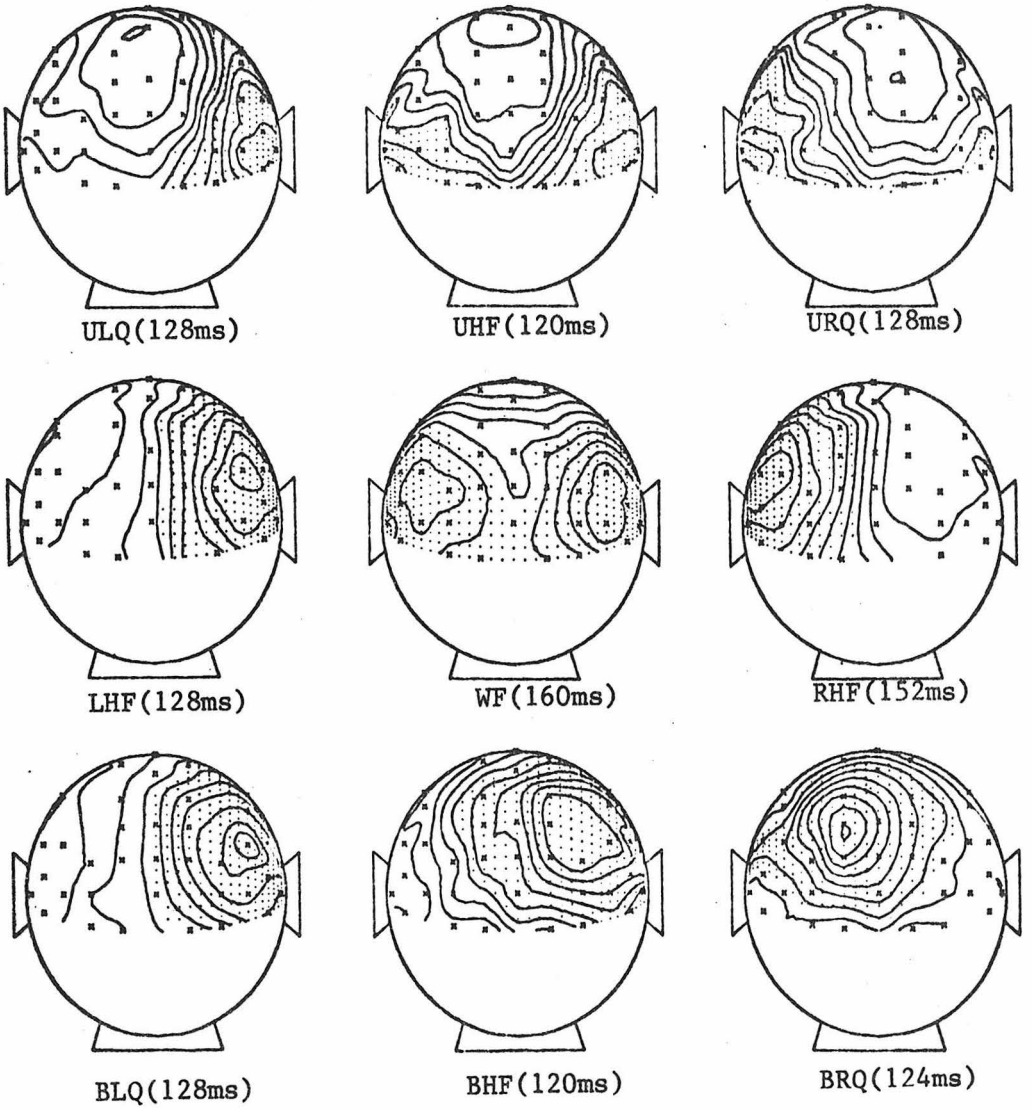

JPA, PDP and RML, respectively. Note that the responses of all three subjects are very similar in this case and that the locations of the peaks are in conformity with expectations based on cortical projections of the visual field. The radical difference in subject RML between the topographies of the initial positive and negative activities, as opposed to the subtle changes in topography in subjects JPA and PDP, is significant. It suggests that the first two parts of the response might be coming from two different locations in the brain, whose topography is different in one subject for the first part, but nearly the same in all subjects for the second part. Differences in the orientation of cortical tissues would be the most likely topographic changes, since surface fields are much more sensitive to source orientation changes than position changes (see section 3.4).

4.2.3 The Effect of Stimulus Color on EP Components

As mentioned in Footnote 22 on p. 89, subject RML was discovered to be color anomalous (unable to distinguish red and green). This was verified by subjecting RML to the Davidson and Hemmendinger Color Rule Test as described by Biersdorf {165} to screen for color anomalies. This test was also done on subjects JPA and PDP, who proved color normal. Since a red stimulus was being used for these experiments, it was conjectured that the difference in the initial topography of subject RML's responses might be attributable in some way to his color anomaly. Since Ary {69} has reported a dependence of pattern EP's on stimulus color, a scheme was devised to test if RML's initial difference was a color effect. Ary {69} reported that red and blue checkerboards gave identical responses in normal subjects. Since subject RML's red/green

system is likely somewhat different functionally than that of the other two subjects, while his blue/yellow system is likely the same functionally, it was speculated that this might be revealed in a comparison of responses to equiluminant red and blue checkerboards. If RML's initial activity was similar to that of the other subjects when a blue stimulus was used, then his initial topography would surely be a color effect. If he were to give identical responses to both red and blue checkerboards, then some other explanation would have to be invoked (such as variation in cortical topography).

Figures 59 and 84-86 are examples of the results of this investigation. It is seen that the responses to both red and blue left half field checkerboards are quite similar in both the ' normal' subject (JPA,Figs. 59 and 84) and the 'abnormal' subject (RML,Figs. 85 and 86). The results were the same for other partial field stimili, and on this basis the possibility of a color effect was rejected. These data do, however, confirm the results of Ary {69} that red and blue checkerboards give similar responses.

Fig. 84 - Map series for left half field (Blue LHF) stimulation (#runs=3) subject JPA

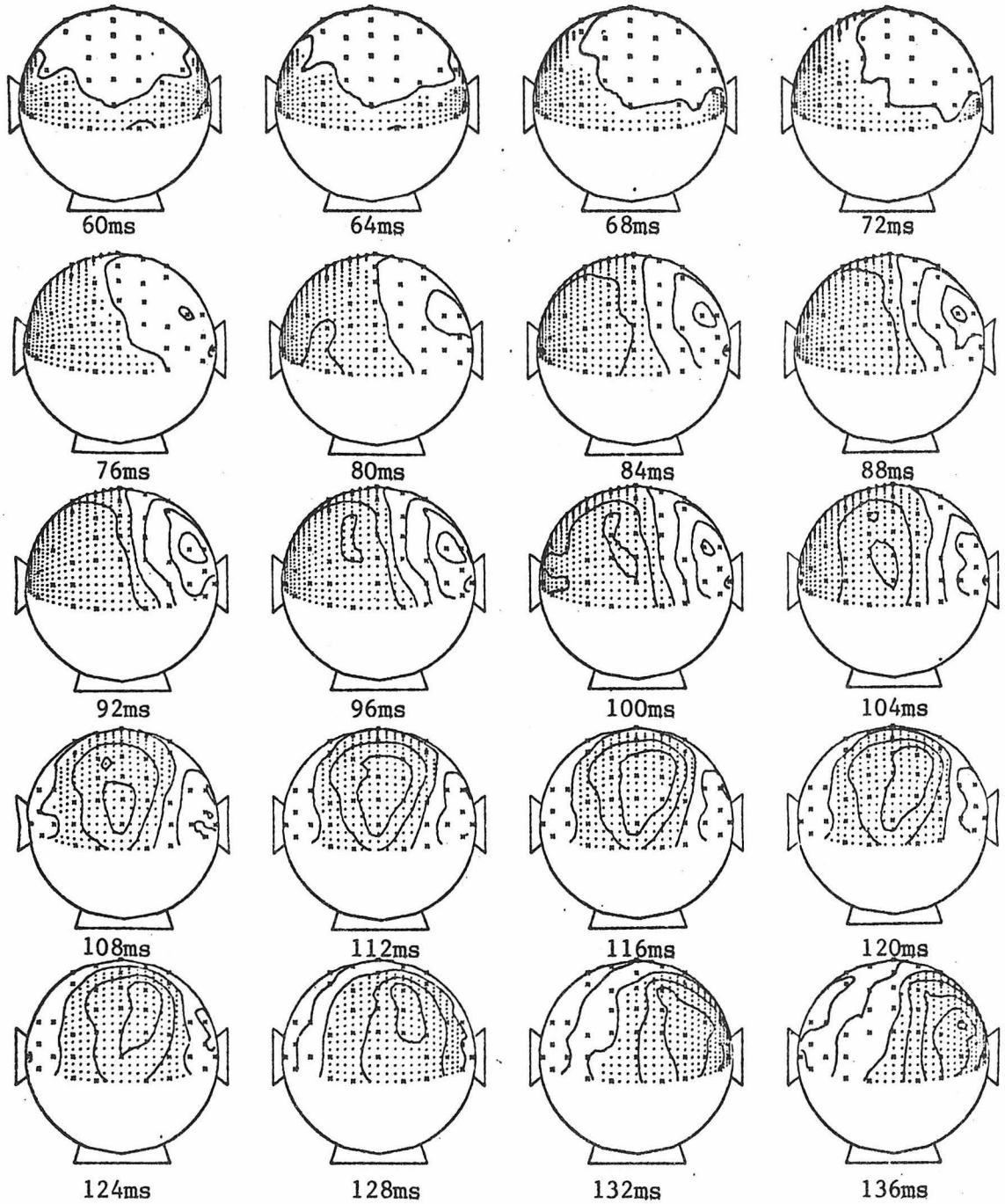

Fig. 84 (continued)

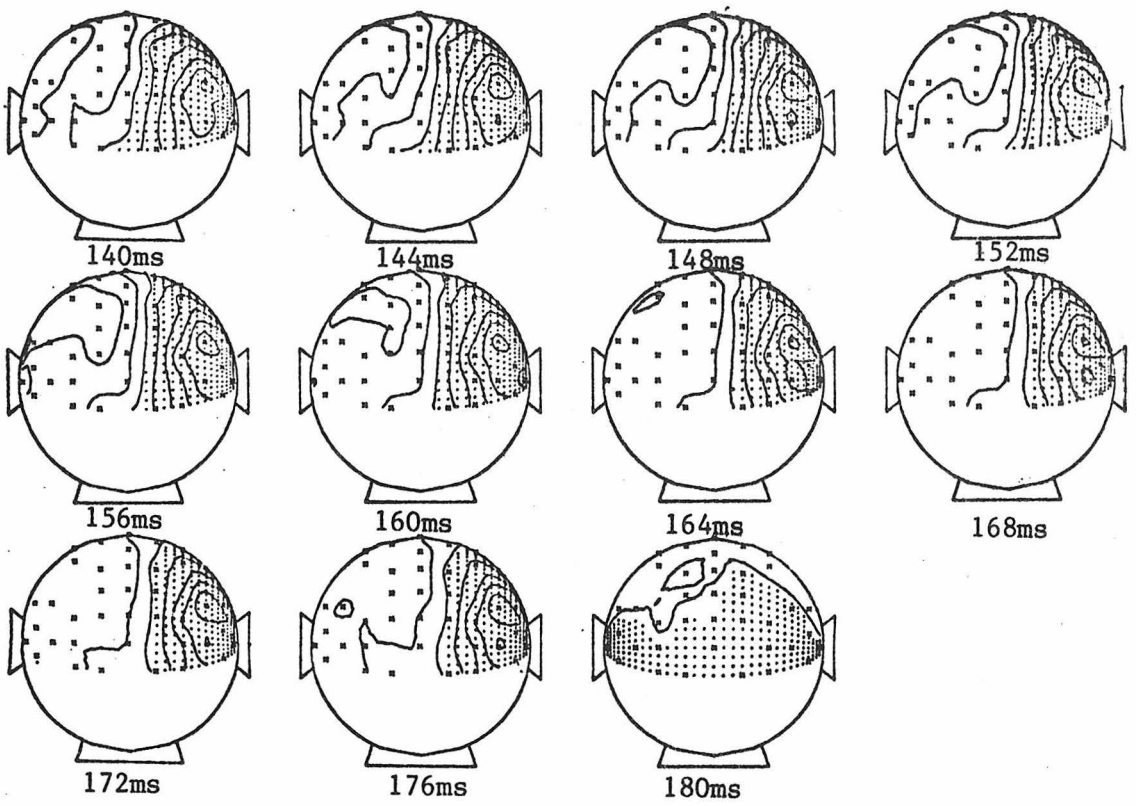

Fig. 85 - Map series for left half field (Red LHF) stimulation (#runs=11) subject RML

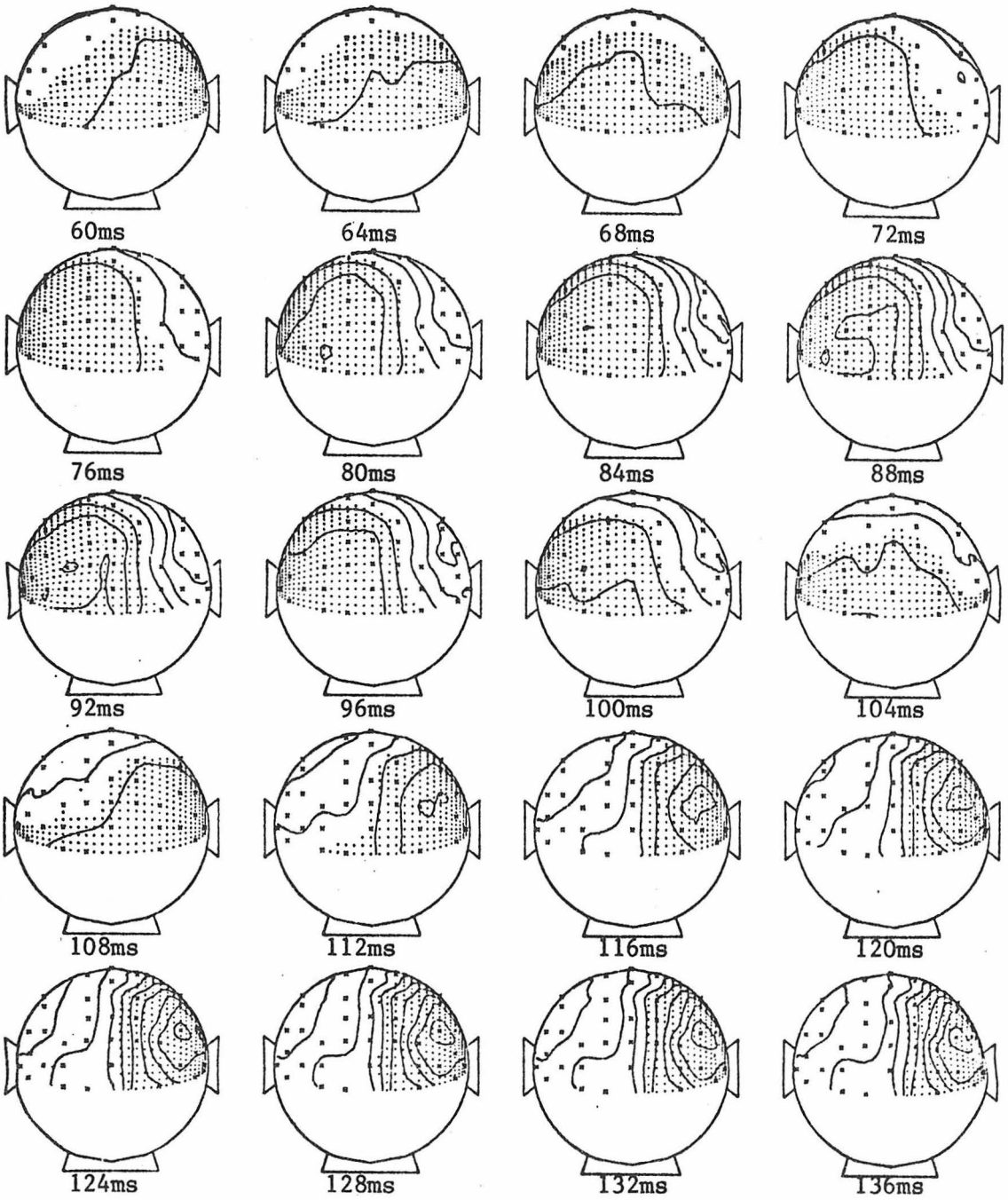

Fig. 85 (continued)

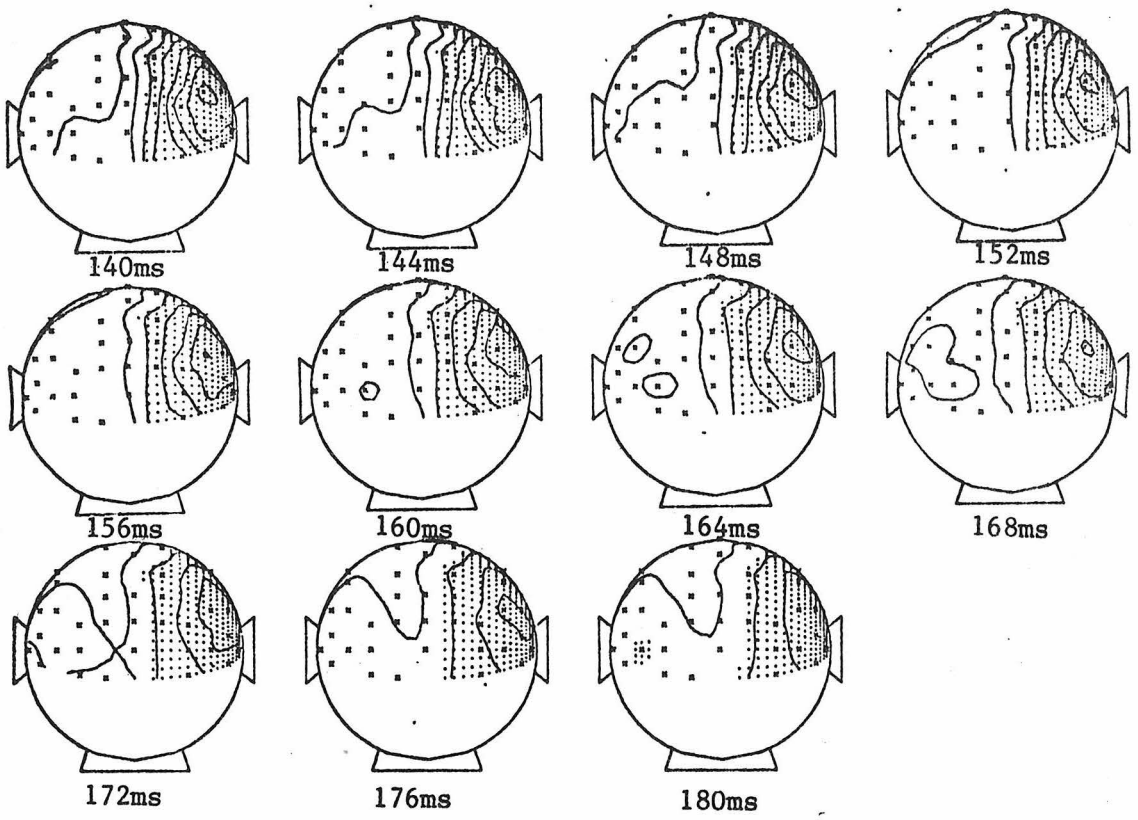

Fig. 86 - Map series for left half field (Blue LHF) stimulation (#runs=3) subject RML

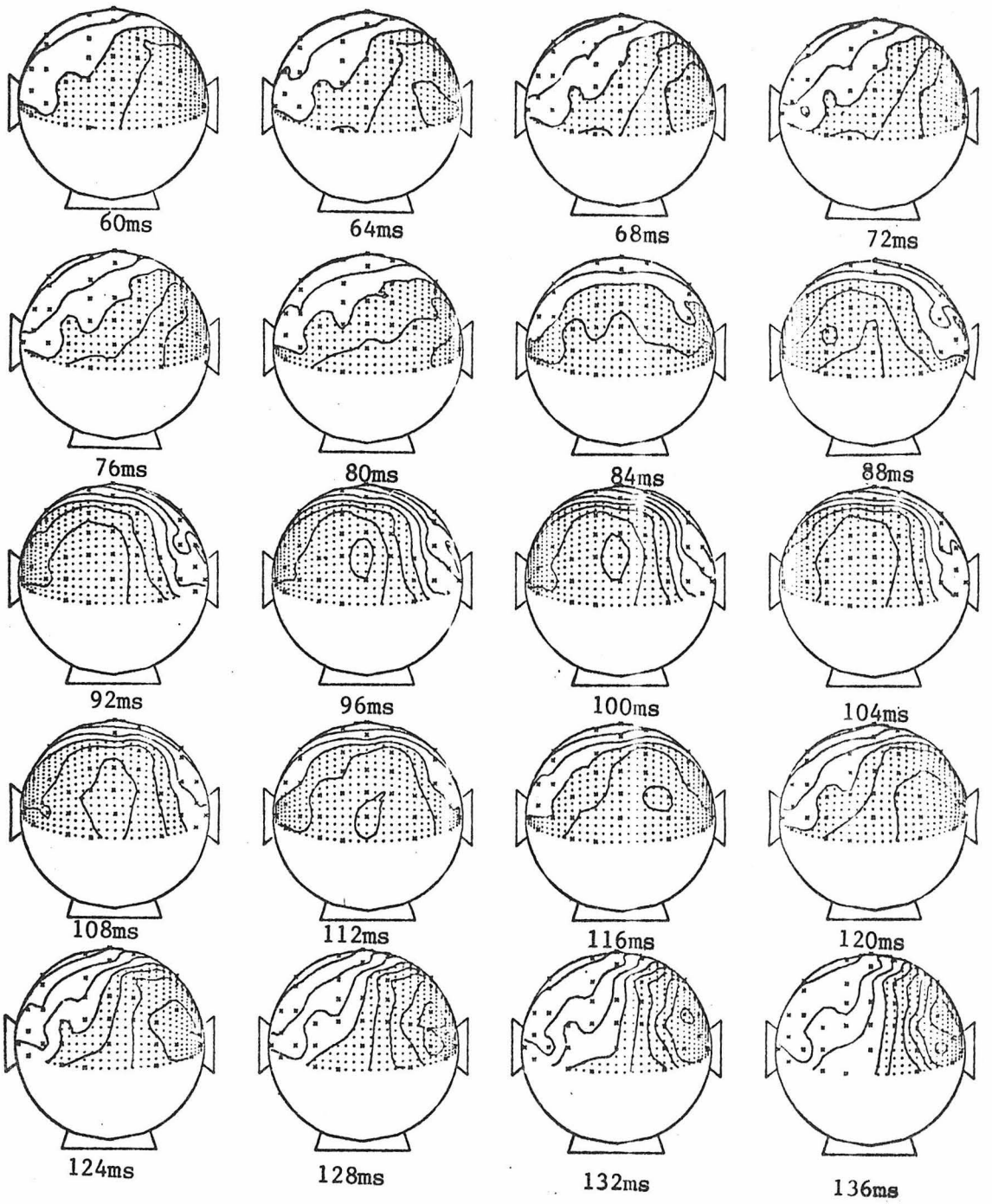

Fig. 86 (continued)

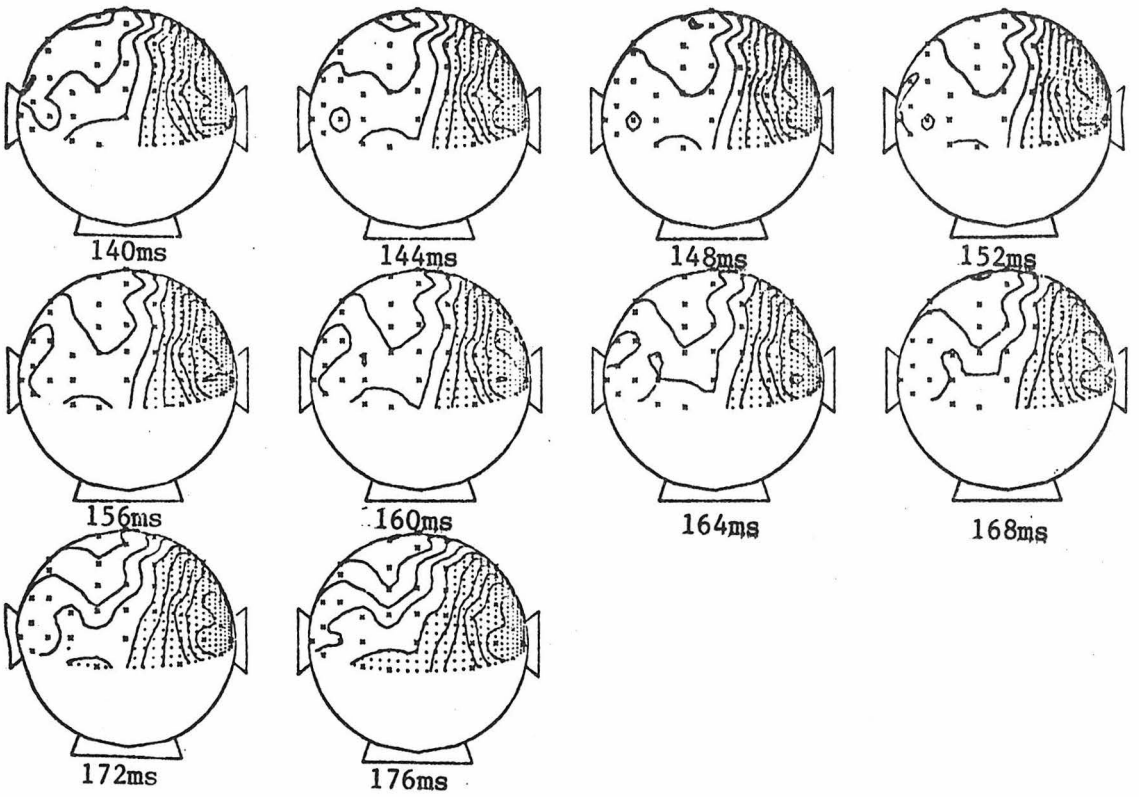

4.3 Superposition and the Independence of Different Areas of the Visual Field

As mentioned in the preceding discussion, the measured response for a given partial field stimulus often appears to be a composite or superposition of responses from stimuli which are subelements of the given stimulus. For example, the LHF (Fig. 59) response may be the sum of the BLQ (Fig. 71) and ULQ (Fig. 73) responses, while the WF (Fig. 67) response appears to be the sum of the LHF (Fig. 59) and RHF (Fig. 68) responses. This section tests this notion by considering the results of calculated superpositions of responses and comparing them with appropriate measured responses. The implication of a result which showed that strict superposition applied (linear independence) would be that the cortical projections of the different areas of the visual field (at least to the quadrant level) are acting independently in their production of evoked potentials. This result is expected at least at layer IV of striate cortical level, where local areas of the visual field project to local areas in cortex (see sections 2.2.3 and 2.2.5).

Fig. 87 shows quadrant superposition (BLQ + ULQ) predictions of EP's on 40 electrodes for subject JPA LHF appearance/disappearance stimulation. These compare favorably with the measured LHF responses shown in Fig. 58. Fig. 88 shows a corresponding series of equipotential maps, which compares favorably with the measured series shown in Fig. 59. Figs. 89-91 show evoked potential map predictions of the initial positive activity for each of the three subjects. These are comparable to the measured maps in Figs. 78-80. Figs. 92-94 show similar predictions of the initial negative activity for comparison with the measured maps

Fig. 87 - Computed evoked potentials for upper and lower left quadrant (ULQ+URQ) superposition

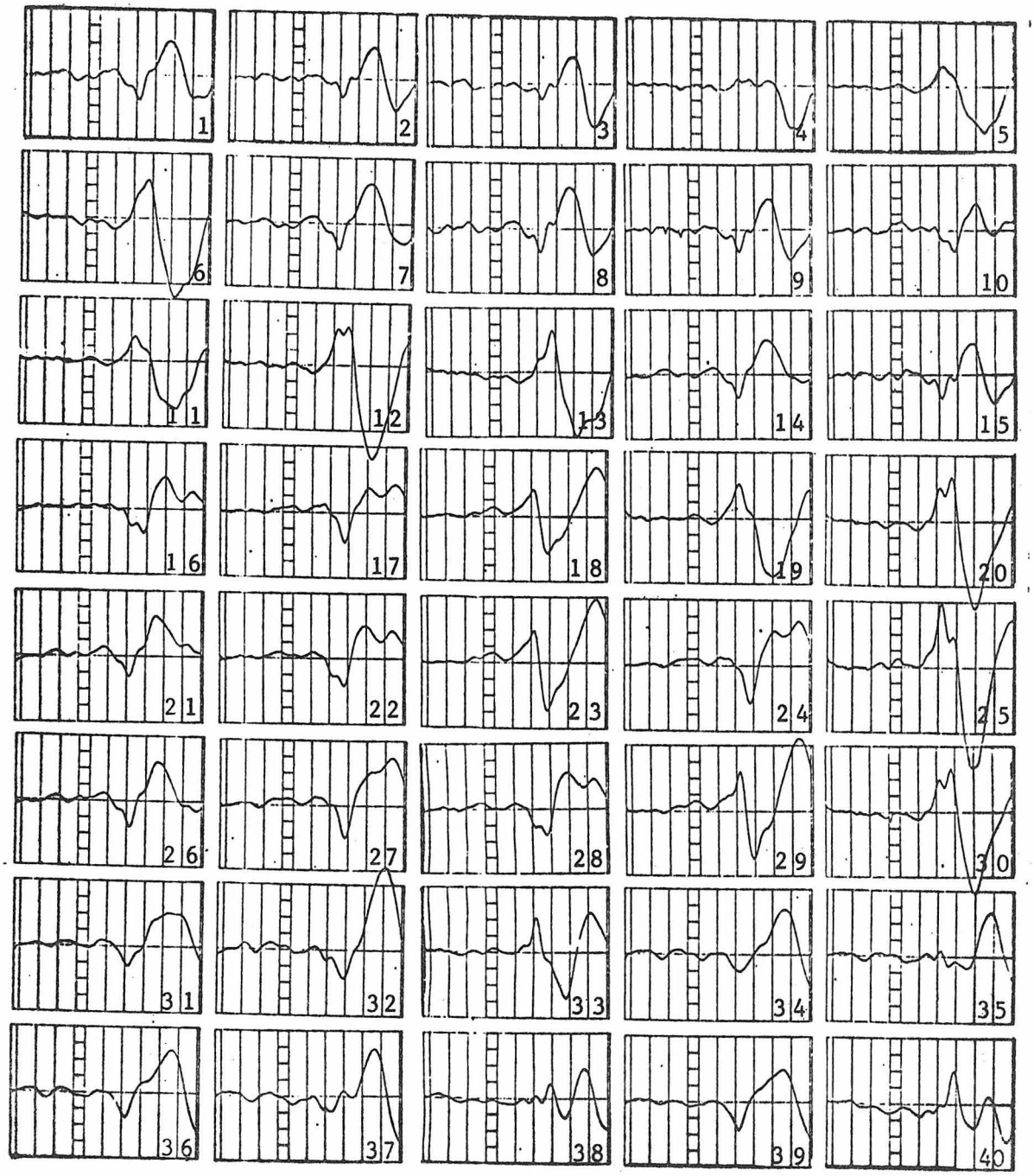

Fig. 88 - Computed map series for upper and lower left quadrant (ULQ+BLQ) superposition

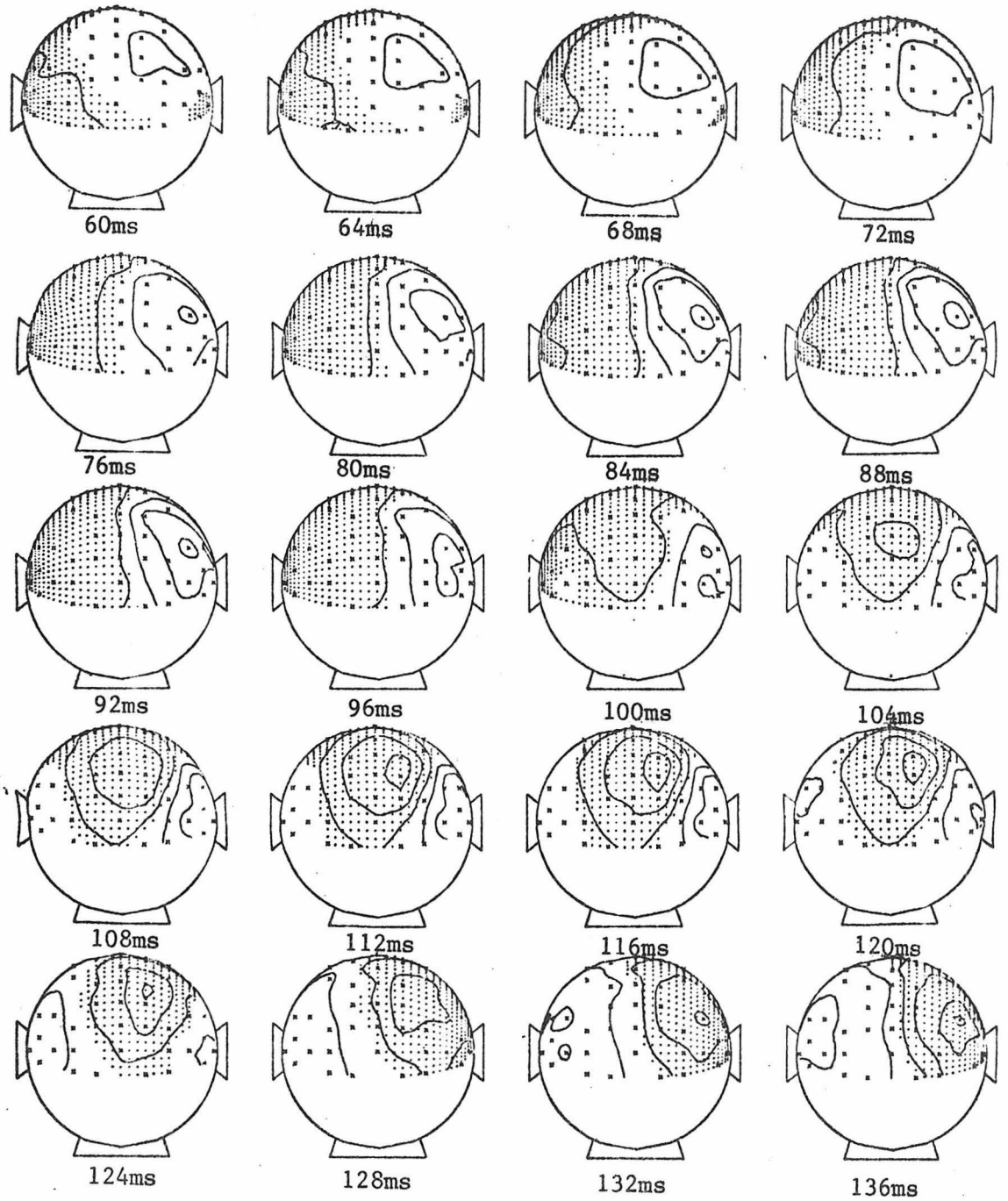

Fig. 88 (continued)

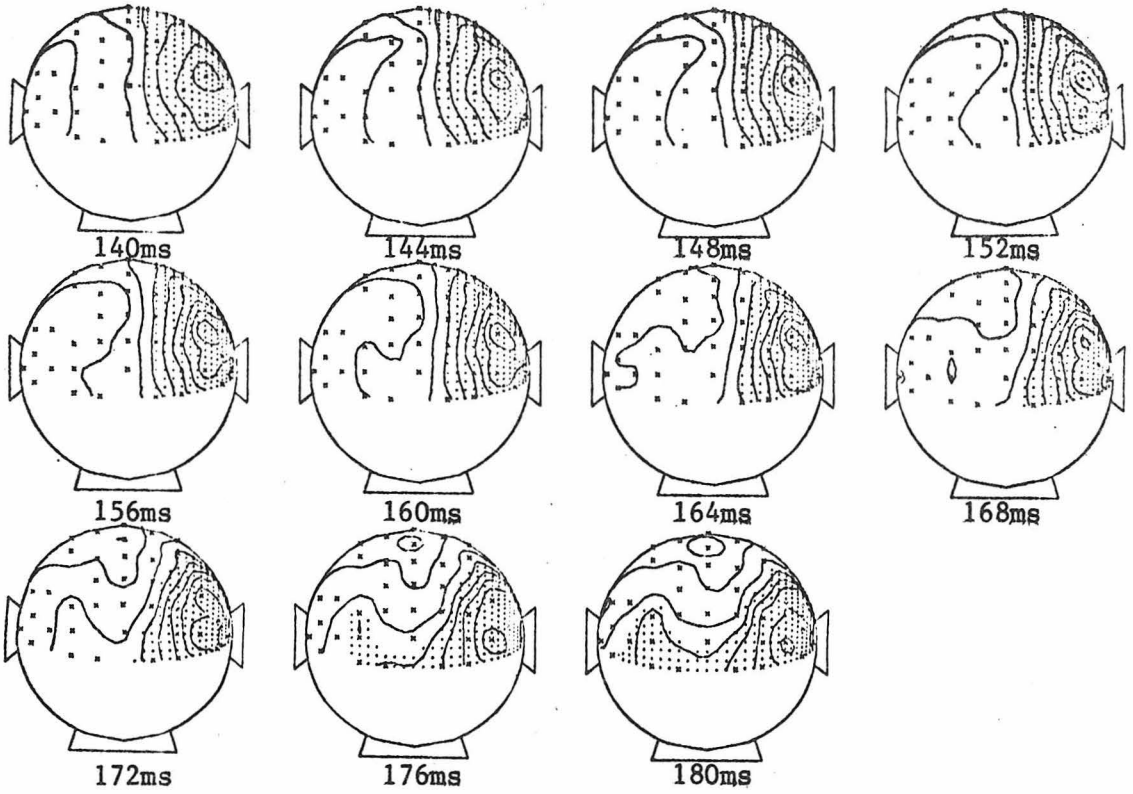

Fig. 89 - Computed superposition for subject JPA initial peaks

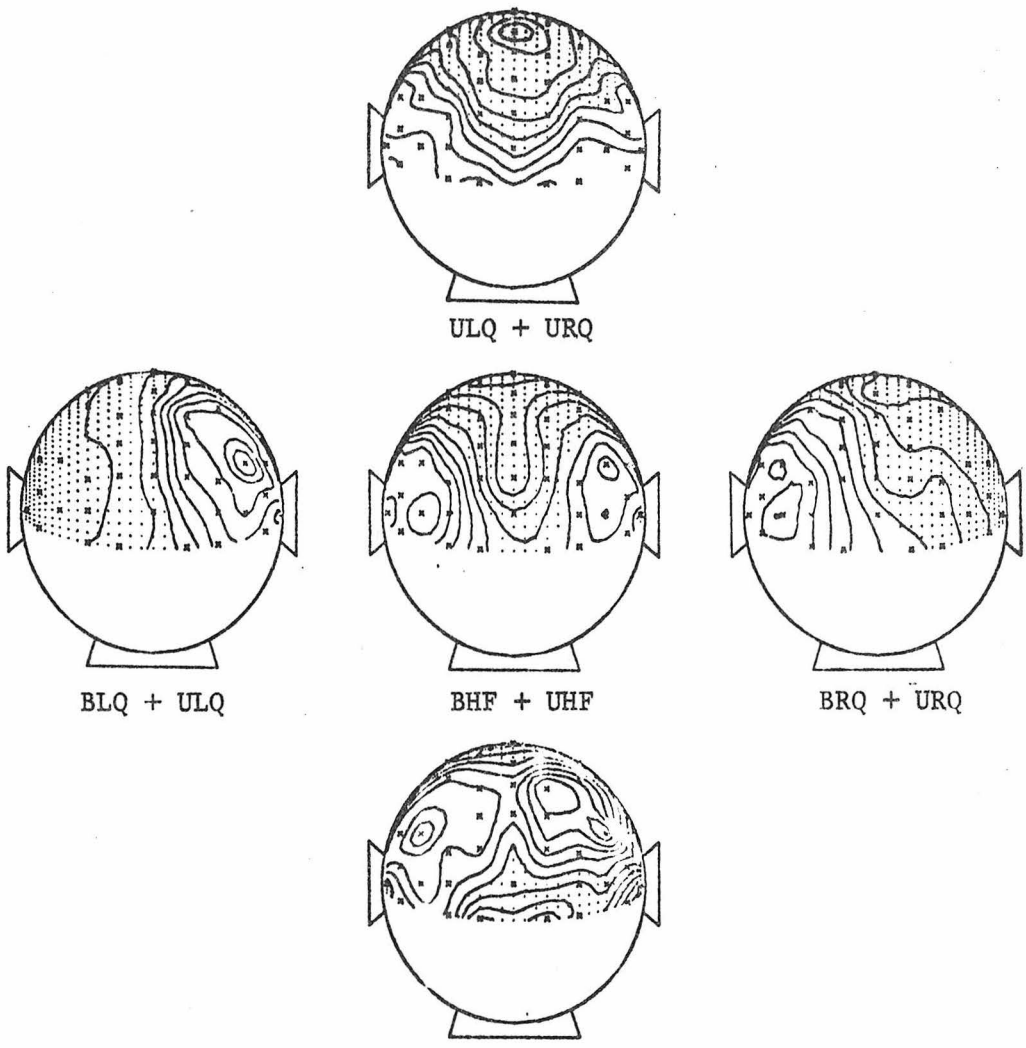

Fig. 90 - Computed superposition for subject PDP initial peaks

NOT
AVAILABLE

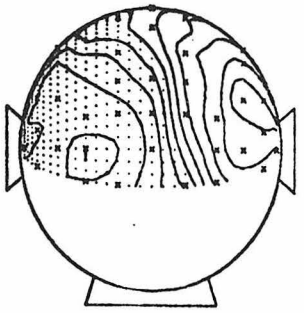

BLQ + ULQ

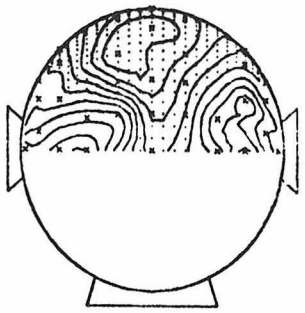

BHF + UHF

NOT
AVAILABLE

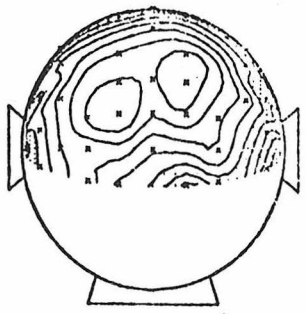

BLQ + BRQ

Fig. 91 - Computed superposition for subject RML initial peaks

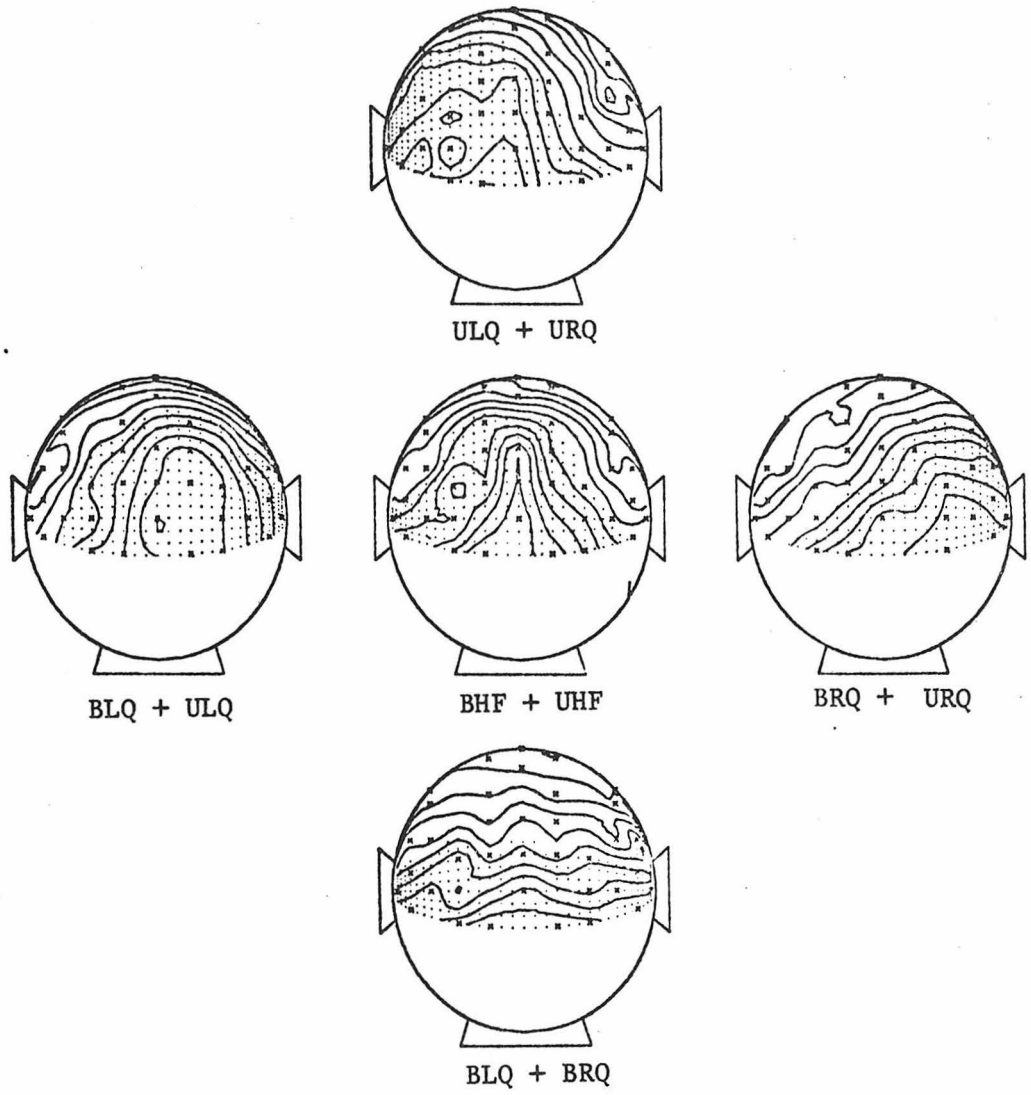

Fig. 92 - Computed superposition for subject JPA secondary peaks

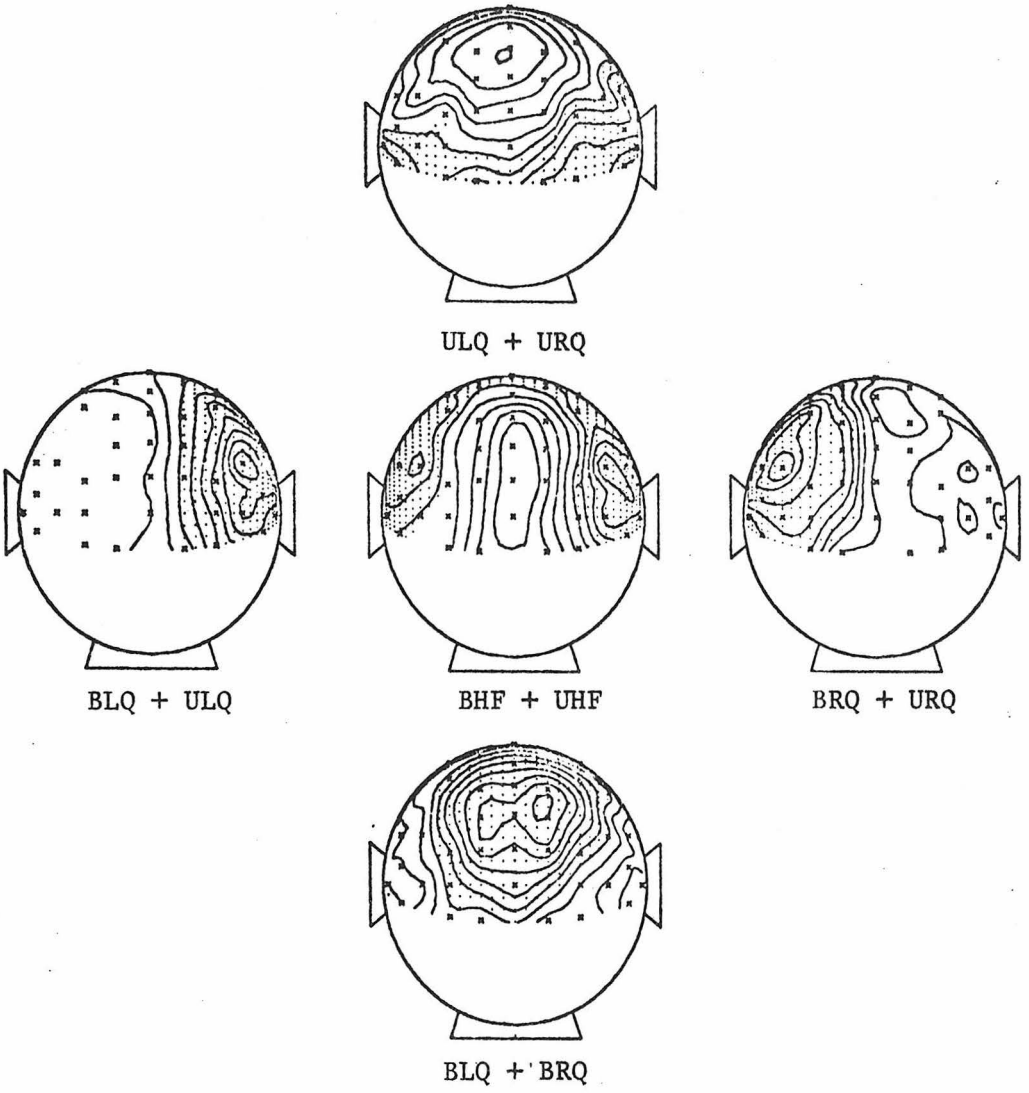

Fig. 93 - Computed superposition for subject PDP secondary peaks

NOT
AVAILABLE

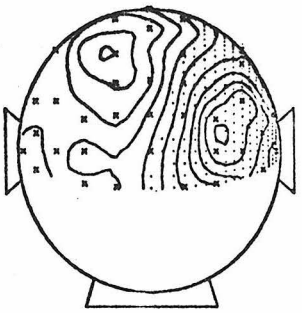

BLQ + ULQ

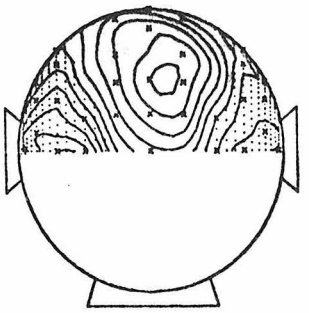

BHF + UHF

NOT
AVAILABLE

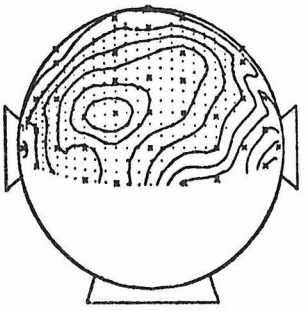

BLQ + BRQ

Fig. 94 - Computed superposition for subject RML secondary peaks

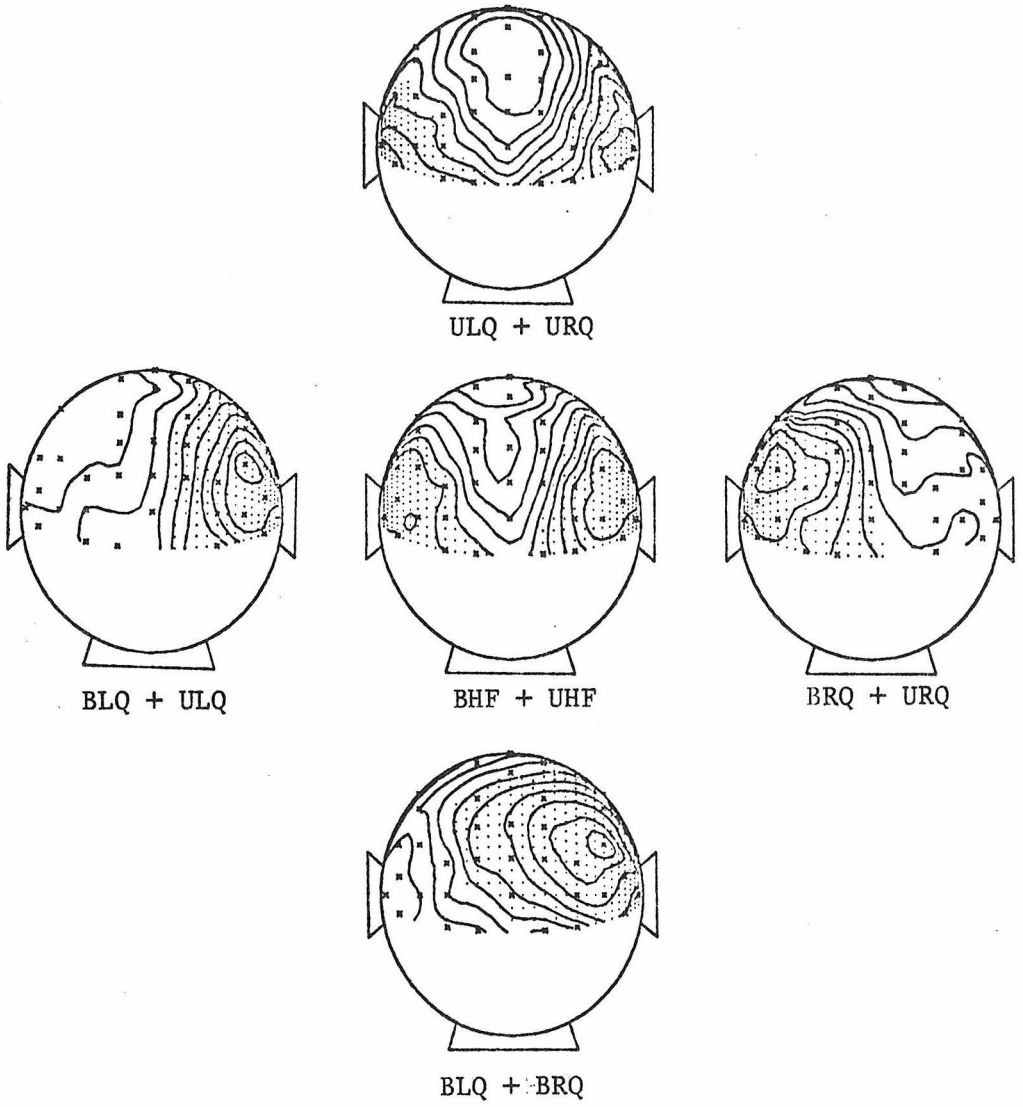

in Figs. 81-83. From a qualitative standpoint, it appears that the superposition notion is a valid one.

4.4 Summary and Discussion

From the preceding it is clear that in the 3 subjects studied[31] pattern EP topographies depend systematically on stimulus locus. It is also clear that this dependence does not conflict with expectations based on the assumed projections of the visual field on visual cortex and the notion that EP's reflect the topography of the tissues which produce them. Stimuli which should project to both hemispheres give bilateral topographies, while stimuli which should project to one hemisphere, give appropriate unilateral topographies. The peak latency of the initial positive topography is very nearly the same in all subjects for all stimuli. The initial negative topography is very similar in all subjects. The distributions are independent of stimulus color (red or blue), the presence or absence of an adapting surround and the choice of reference electrode.

For a given stimulus, there are extended time periods (corresponding to EP waveform deflections) of 20-30 msec in which the peak locations and shapes of the EP topography remain more or less the same, with their amplitude rising and decaying in this time interval, indicative of sources which are stable in terms of position and orientation, but which vary in magnitude over time.

---

[31] The author is aware of the fact that the subject space here is quite small and that further work on a larger group of subjects is necessary. However, owing to the difficulties inherent in setting up and keeping subjects for these experiments, it was decided to concentrate mainly on intrasubject results insofar as statistical significance is concerned. On the matter of intrasubject variability, a very complete study has been done. As for intersubject variability, there are indications that this may be considerable, although the 3 subjects have most features in common when the data are viewed as equipotential maps.

The signals on many electrodes over a very large area of the scalp are highly correlated both in space and time. This is compelling evidence for the notion that these evoked potentials are volume conducted field effects arising from a small number of electrical sources in the head {14}. Indeed, it is very difficult to conceive of any other explanation. The suggestion {25} that evoked potentials arise mostly from the surface of the brain would have difficulty explaining these data, since it is implausible that there could be a single widespread surface cortex activity or, alternatively, a widespread number of highly correlated surface cortex sources.

Finally, there appears to be approximate linear independence of the different areas of the visual field in terms of the EP distributions which they produce. The EP distributions of hemifield and whole field stimuli are predictable from the superposition of EP distributions of their constituents. This is further evidence for volume conduction since its theory states that the potential fields of multiple sources or source distributions are merely the linear sum of the potential fields produced by the various individual sources acting alone. Further, this result does not dispute the general belief (at least at the striate cortical level) that there is a point-to-point mapping between the visual field and visual cortex and that different areas of cortex are independent in terms of which areas of the visual field they represent.

5. EQUIVALENT SOURCE MODELING

5.1 Multiple Sources and Constraints

Three different source models were applied in the analysis of most of the evoked potential data in this thesis: single dipole (6 parameters), two dipoles (12 parameters) and two dipoles with symmetry constraint (7 parameters). The latter model was introduced because of instabilities which sometimes arose in applications of the unconstrainted two dipole model and involves an assumption of mirror-image symmetry in the two sources. Two versions were available: midline mirror-image symmetry (assuming sources in opposite hemispheres were mirror-images) and calcarine fissure mirror-image symmetry (assuming sources above and below the calcarine fissure were mirror-images). The 7 parameter model forced mirror-image position and orientation, but allowed each dipole to vary in individual magnitude. The parameters of the 3 models are as follows:

(1) single dipole - (x,y,z,P_x,P_y,P_z)

(2) two dipole - $(x_1,y_1,z_1,P_{x_1},P_{y_1},P_{z_1},x_2,y_2,z_2,P_{x_2},P_{y_2},P_{z_2})$

(3) two dipole with symmetry constraint - (x,y,z,P_x,P_y,P_z,k)

$= (x,y,z,P_x,P_y,P_z,x,y,-z,kP_x,kP_y,-kP_z)$ for midline symmetry

$= (x,y,z,P_x,P_y,P_z,x,-y,z,kP_x,-kP_y,kP_z)$ for calcarine symmetry

5.2 The Application of Equivalent Source Modeling to Evoked Potential Data

5.2.1 Illustration of Equivalent Source Modeling on Selected Evoked Potential Data Sets

The following pages (Fig. 95) show a time series (from 60 to 180 msec after stimulus offset in 4 msec intervals) of measured equipotential maps (LHF appearance/disappearance stimulation of subject JPA), model-generated equipotential maps, three-shell model equivalent dipole sources and corresponding 95% confidence limits.[32] Here and in the accompanying reduced chi-square values it can be seen that single equivalent dipoles give excellent fits to the measured evoked potential data. A discussion of the significance of the behavior of the equivalent sources will be deferred until the next section. Figs. 96,97 illustrate the behavior of equivalent sources computed for the same data set, but using the two-source models discussed in section 5.1. They also show examples of actual and model-generated equipotential maps (92 msec). From these figures it is clear that a single source in the right side of the head is indicated.

Fig. 98 shows a time series of measured equipotential maps (WF appearance/disappearance, subject JPA), model-generated equipotential maps, 3-shell model equivalent dipole source pairs (using the unconstrained 12 parameter model). Here again it can be seen that the model sources give excellent fits to the EP data. Figs. 99,100 show the behavior of

---

[32] It is important to remember that the confidence limits shown are a measure of the reliability in the location parameters of the equivalent source and bear no relation to the volume of tissue which is active. The location parameters identify the center of electrical activity and the moment parameters identify its net orientation.

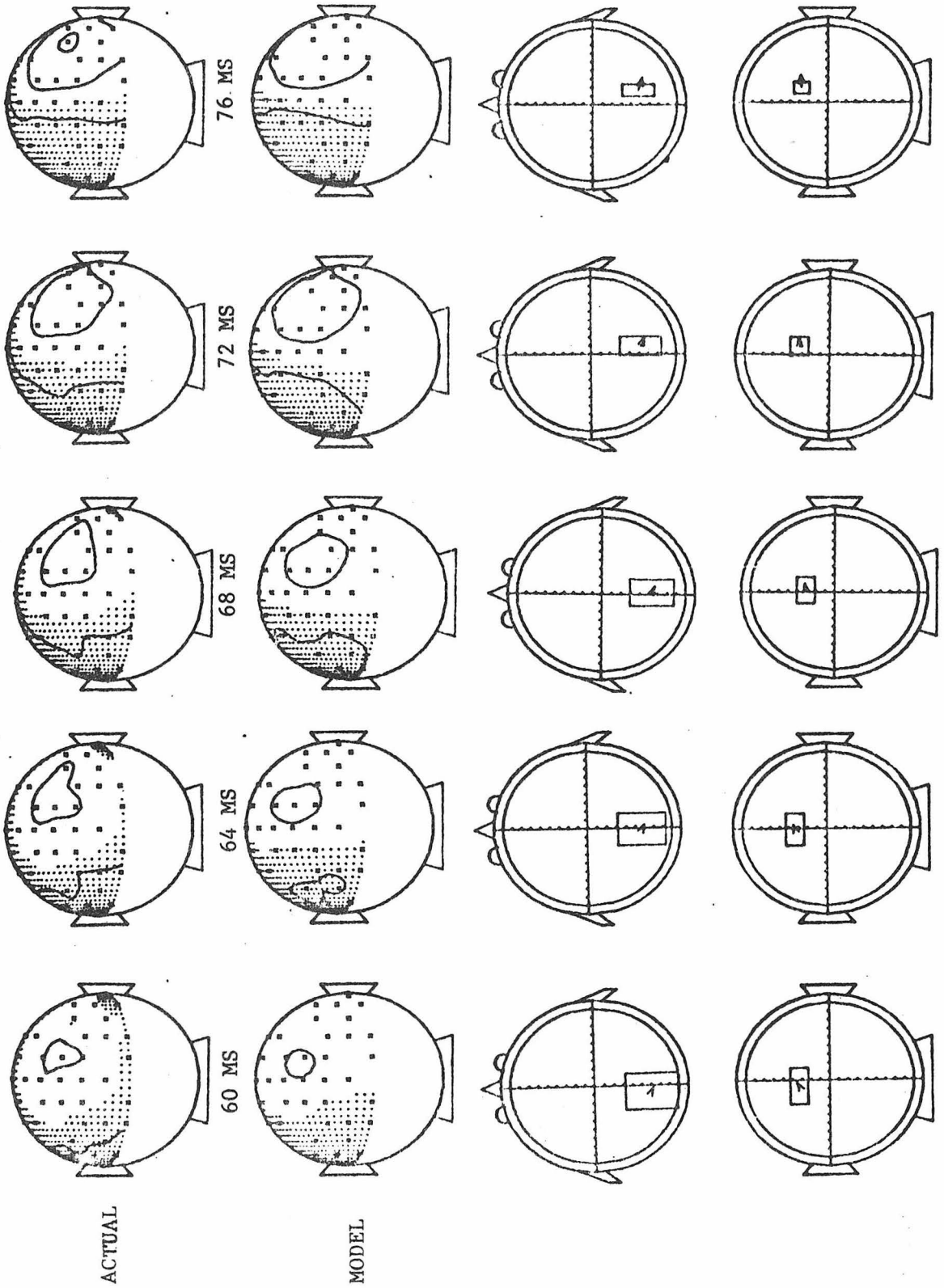

Fig. 95 - Time series of 3-shell model equivalent dipoles for LHF stimulation of subject JPA

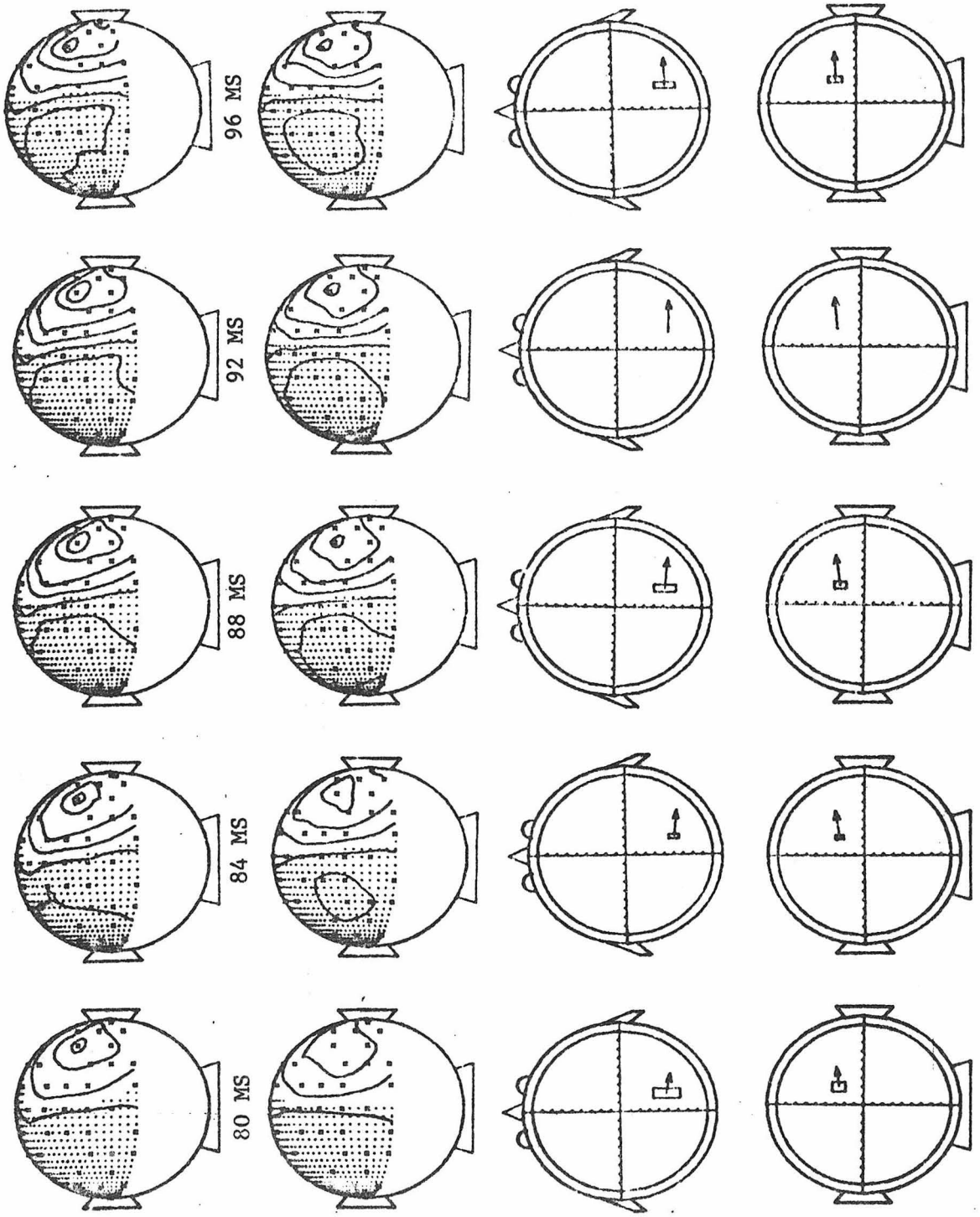

Fig. 95 (continued)

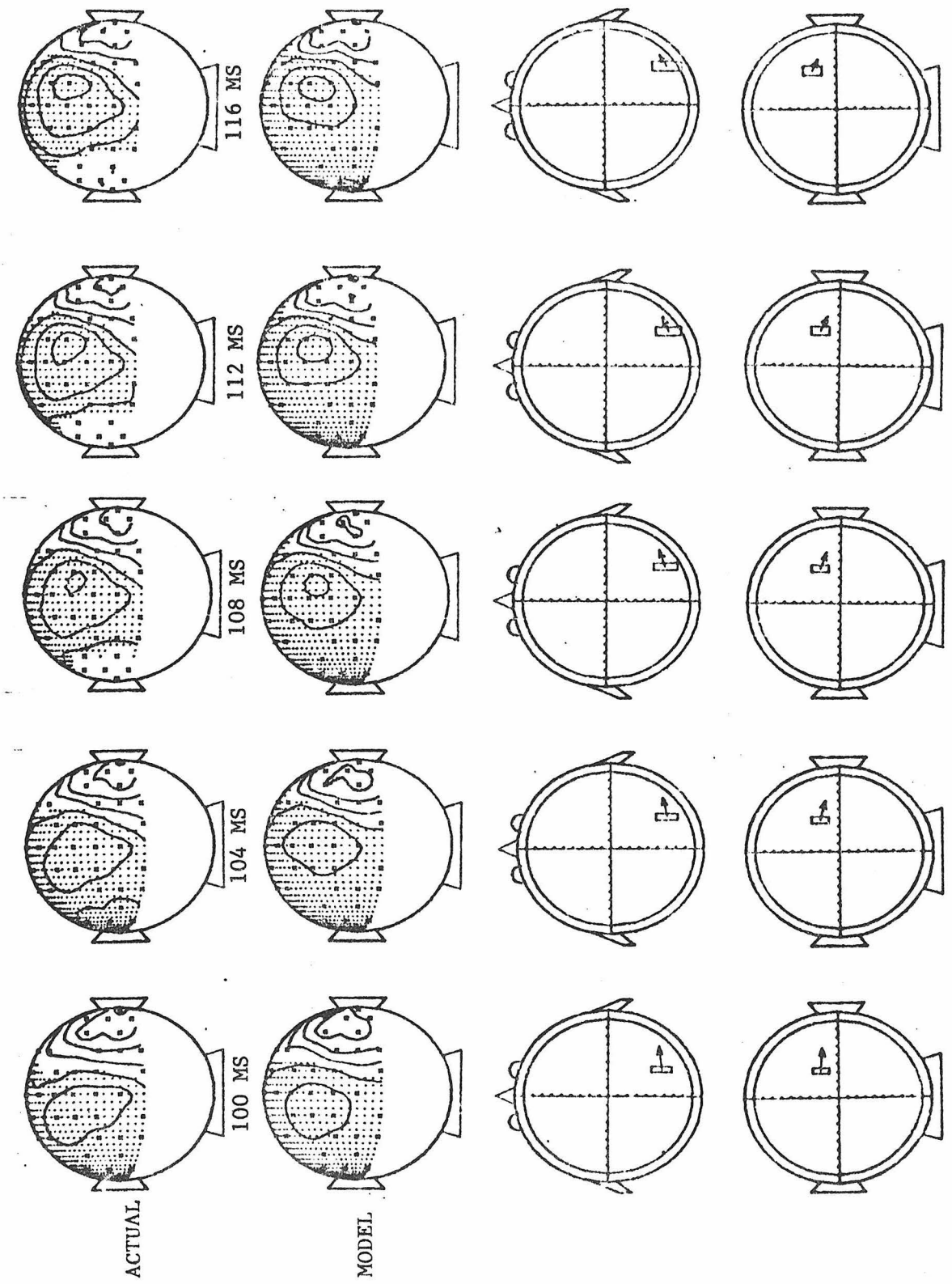

Fig. 95 (continued)

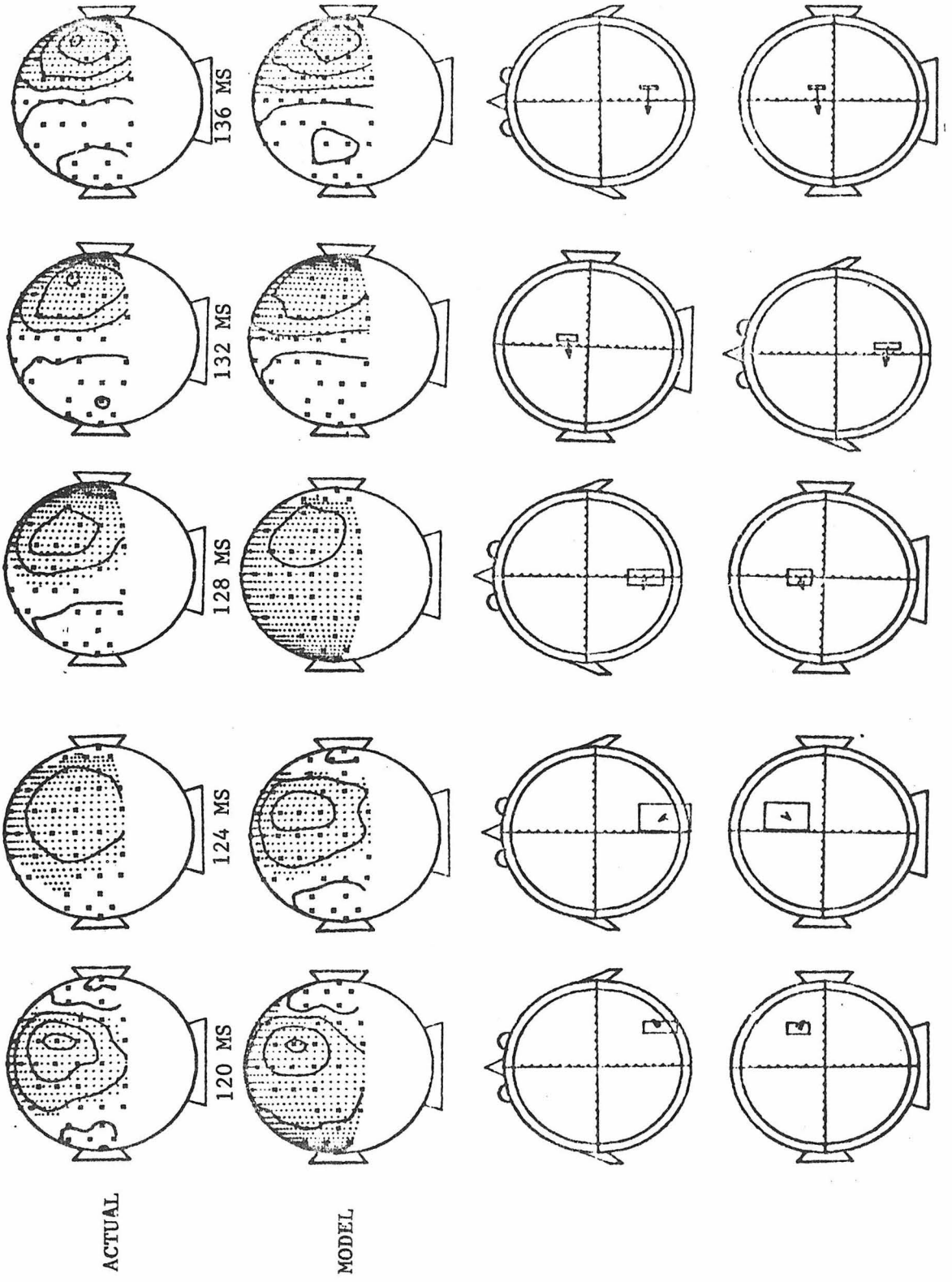

Fig. 95 (continued)

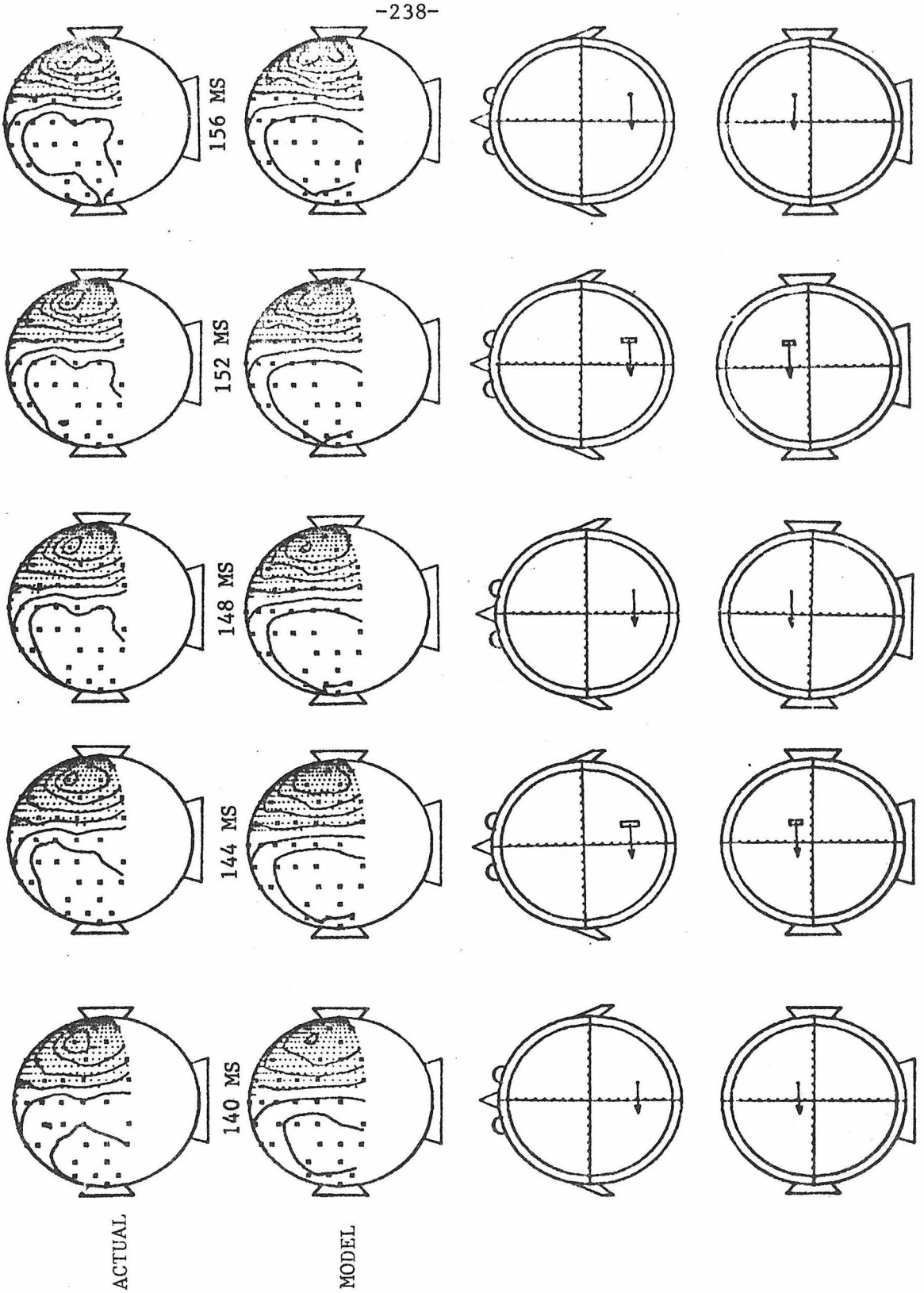

Fig. 95 (continued)

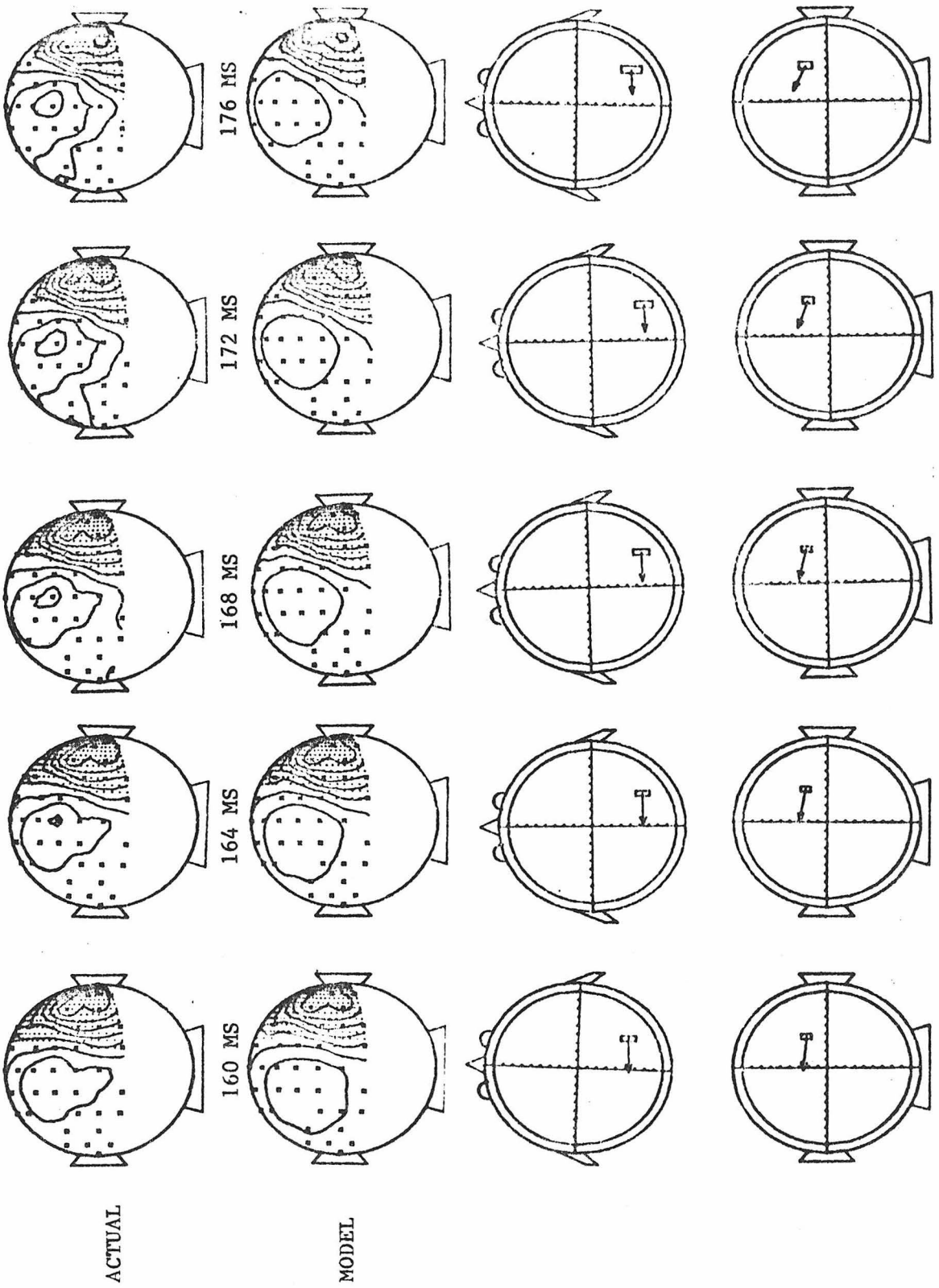

Fig. 95 (continued)

Fig. 95 (continued)

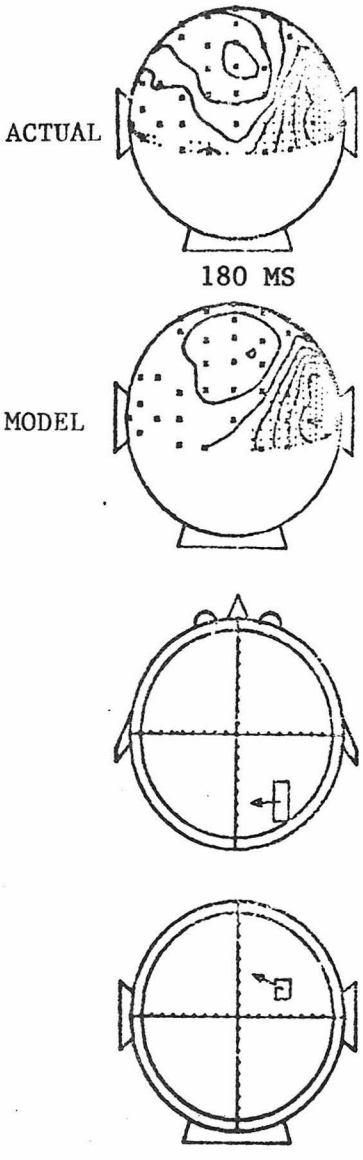

TIME	χ^2_ν
60	.0520
64	.0582
68	.0623
72	.0656
76	.0774
80	.1116
84	.1691
88	.2142
92	.2279
96	.2052
100	.1994
104	.2584
108	.3729
112	.4521
116	.4654
120	.4225

TIME	χ^2_ν
124	.3884
128	.2070
132	.1543
136	.1577
140	.1691
144	.1875
148	.1976
152	.2116
156	.1984
160	.1975
164	.2155
168	.2782
172	.3577
176	.4509
180	.5091

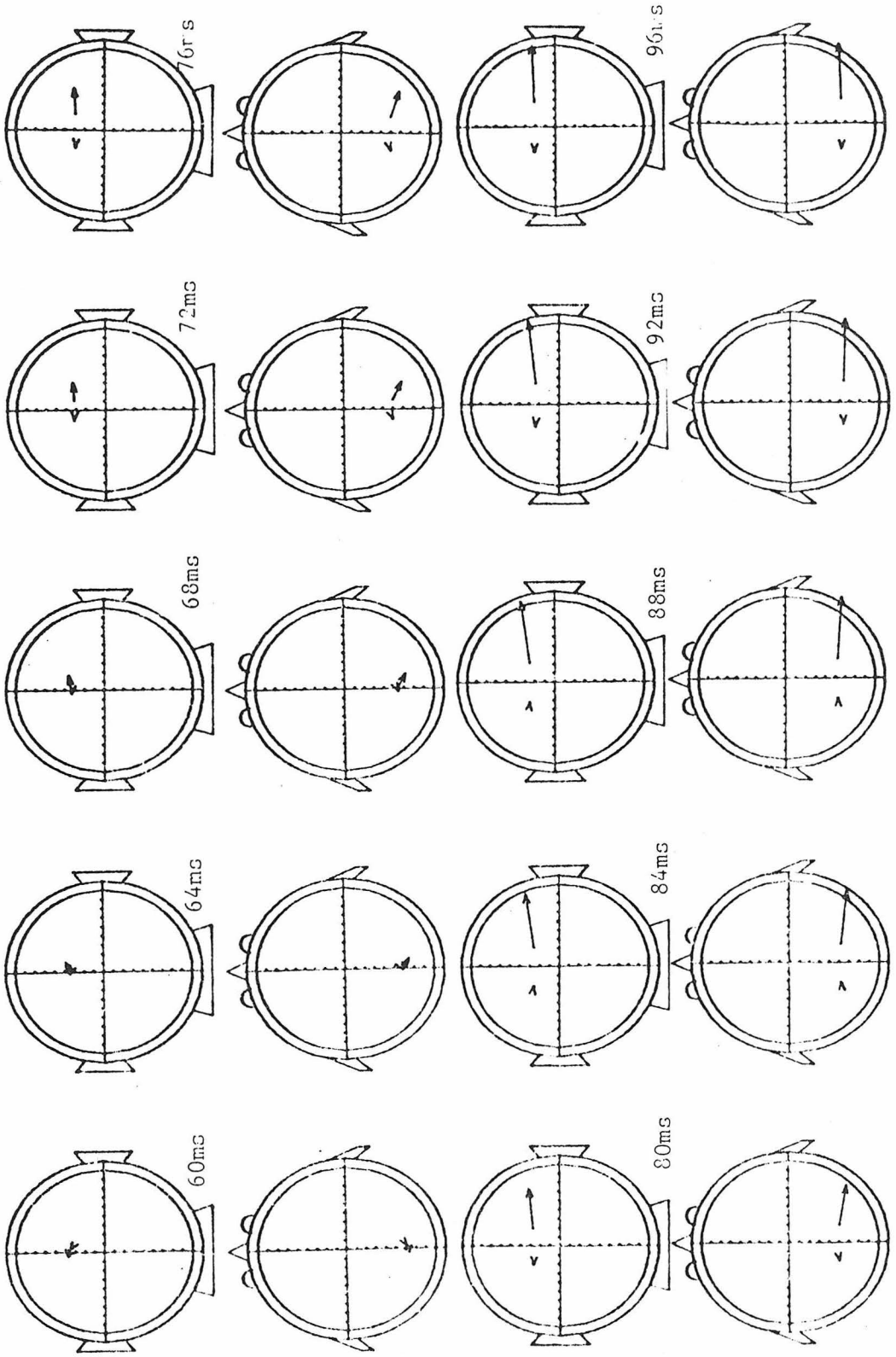

Fig. 96 - 12 parameter 2-dipole fits for subject JTA responses to LHF stimulation. Confidence regions and χ^2_ν values are approximately the same as in Fig. 95.

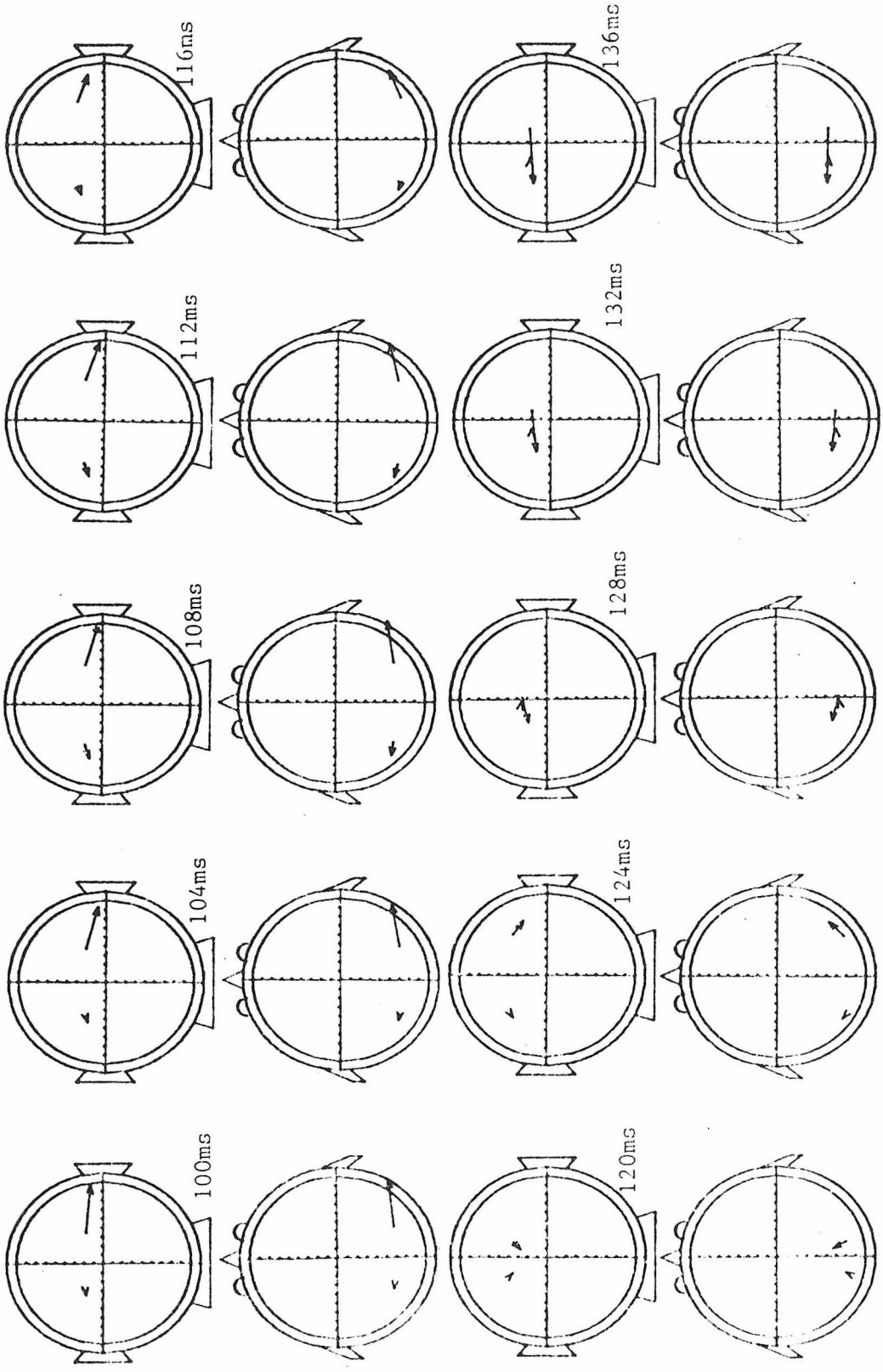

Fig. 96 (continued)

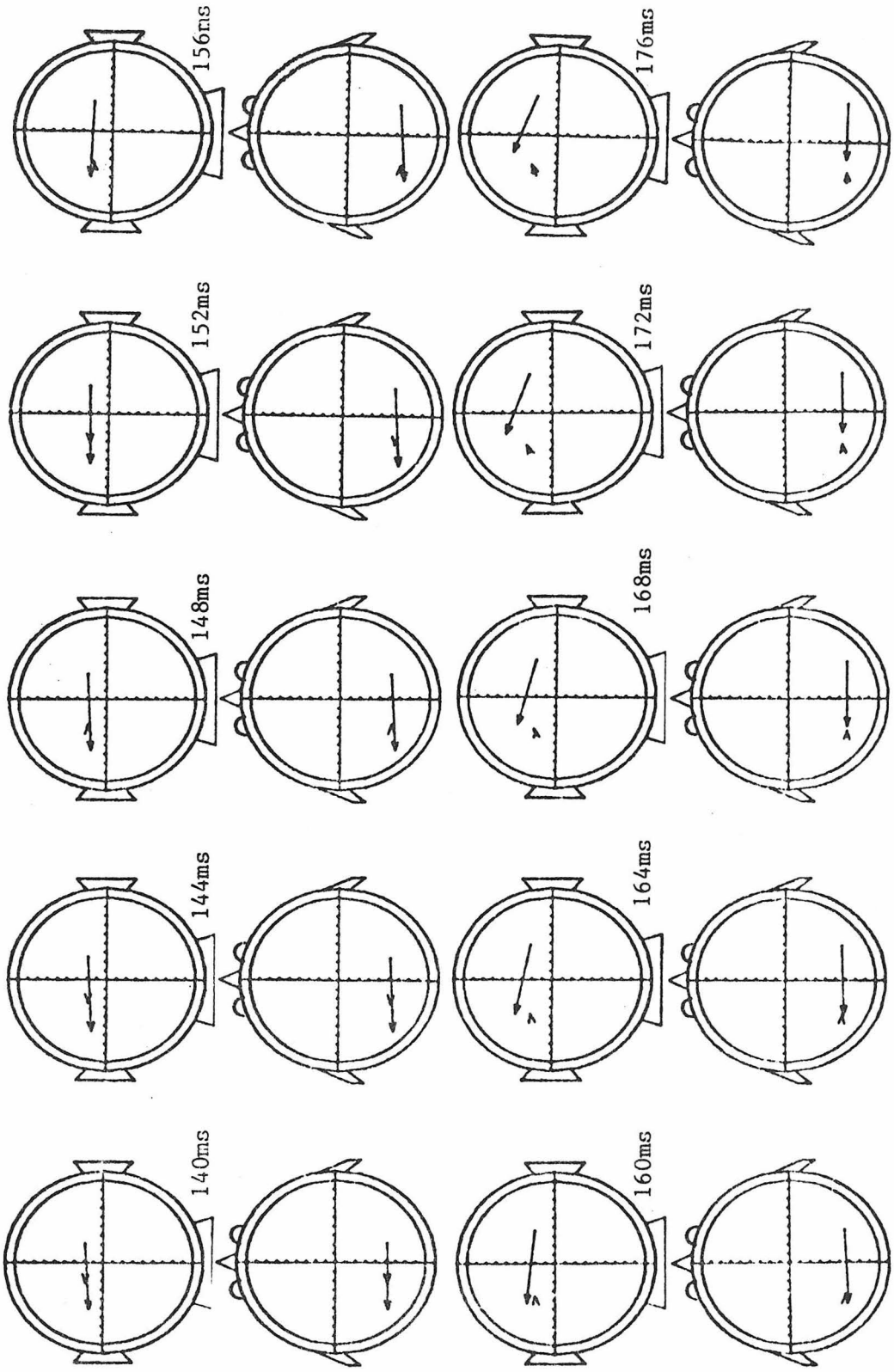

Fig. 96 (continued)

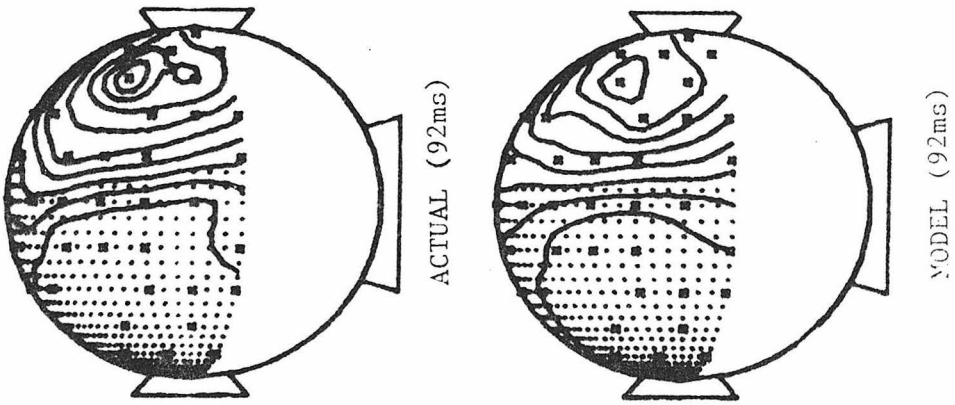

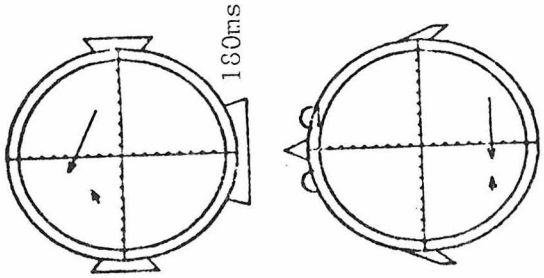

Fig. 96 (continued)

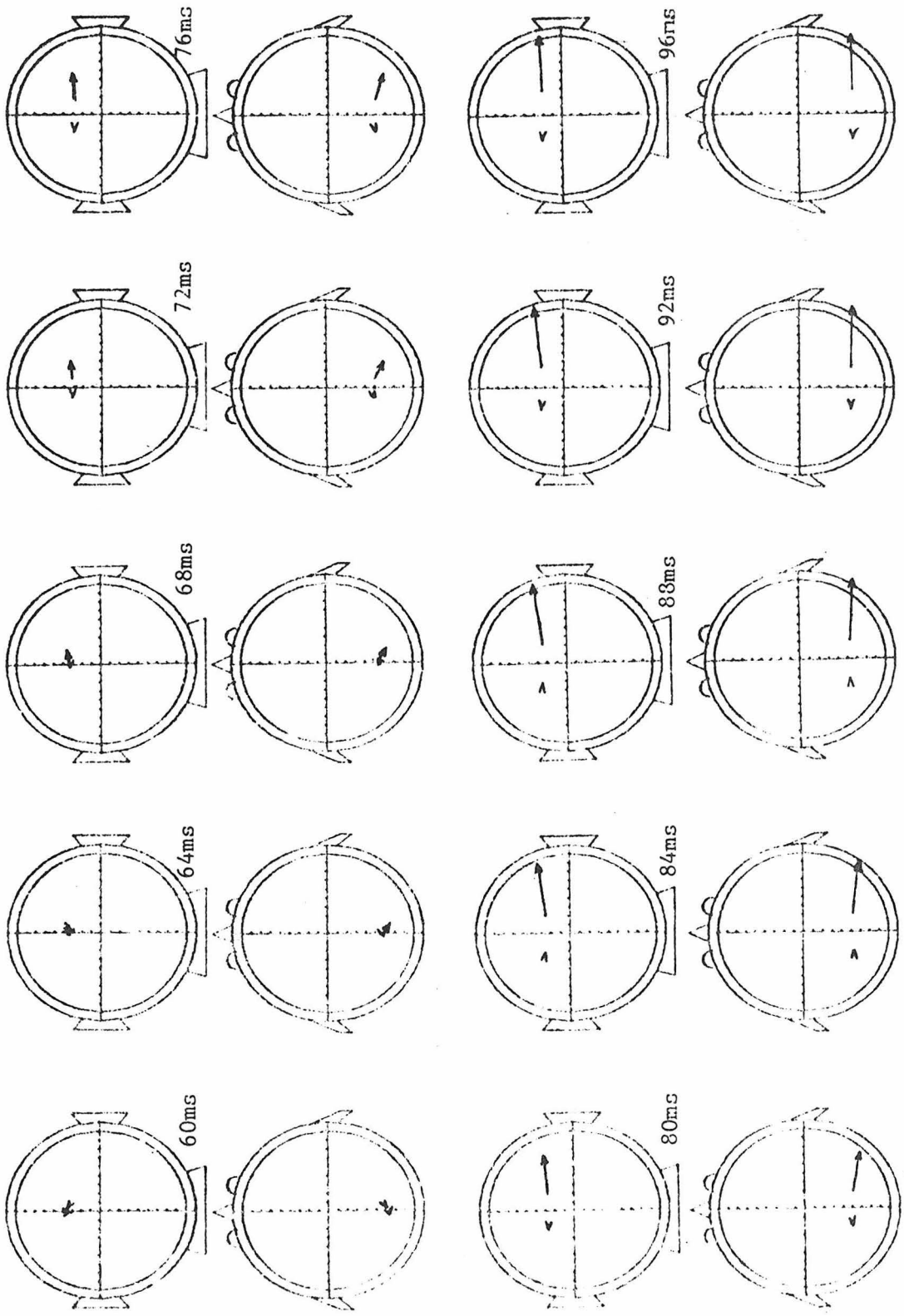

Fig. 97 - Symmetric 2-dipole fits for subject JPA responses to LHF stimulation. Confidence regions and χ^2_ν values are the same as in Fig. 95.

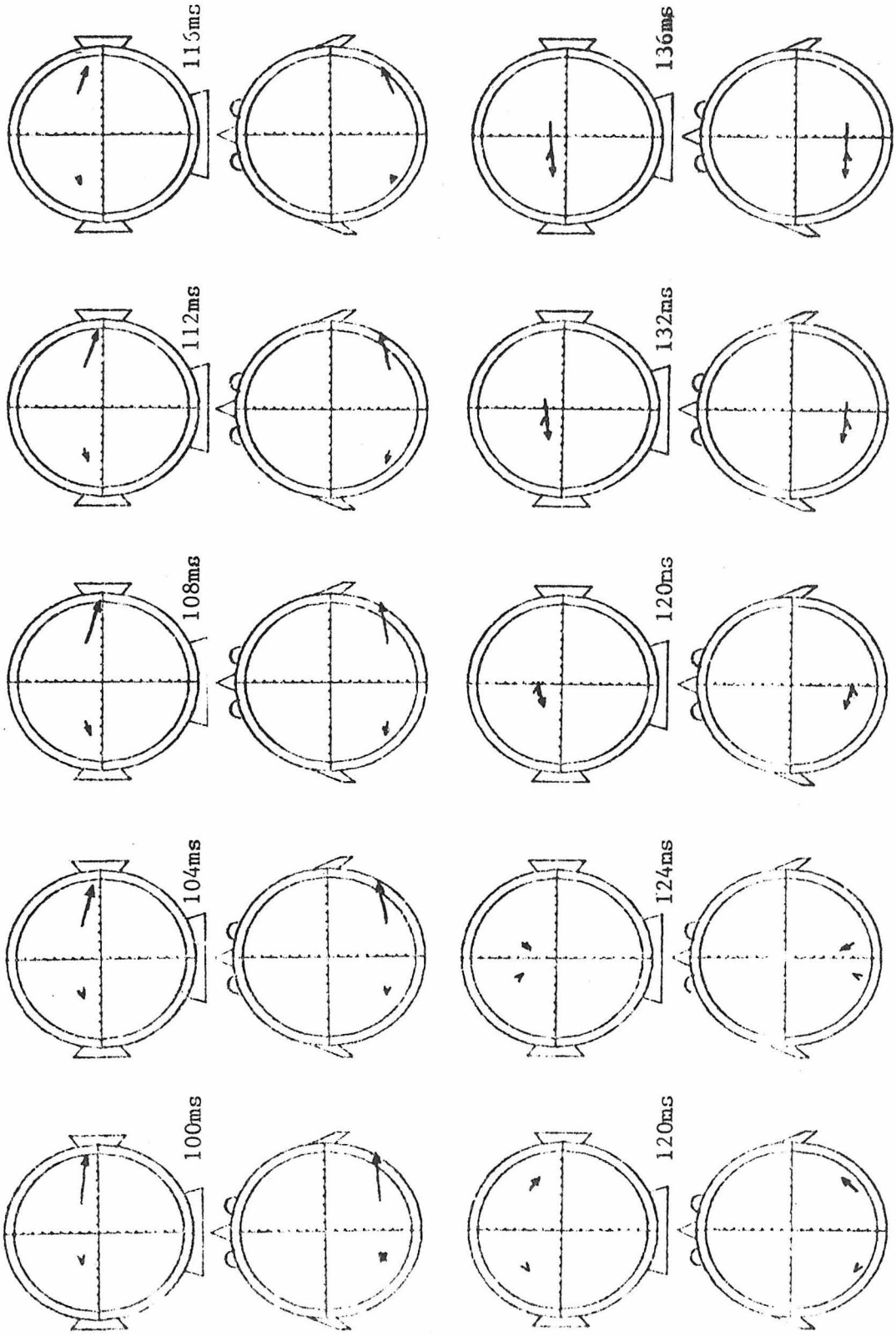

Fig. 97 (continued)

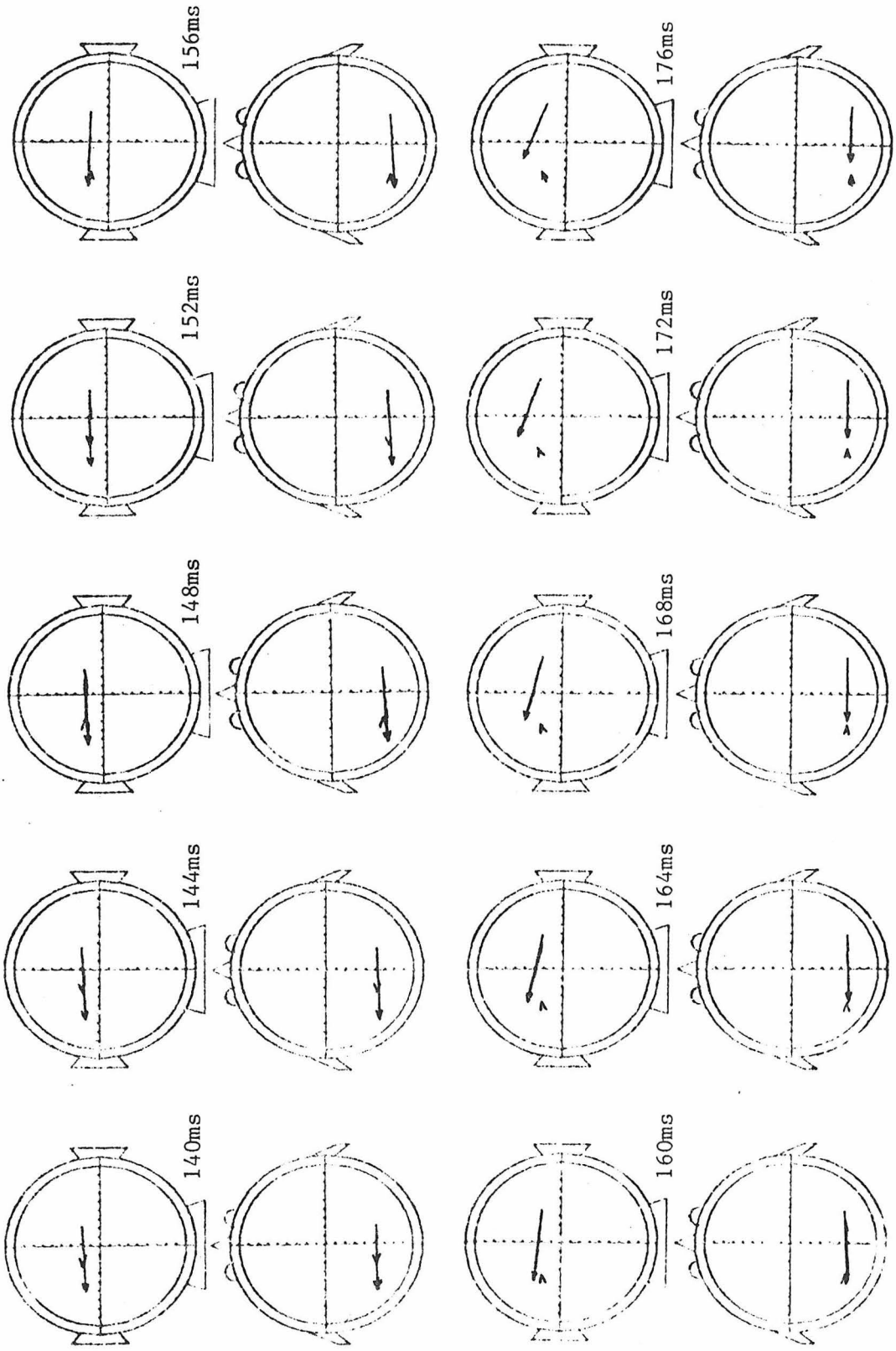

Fig. 97 (continued)

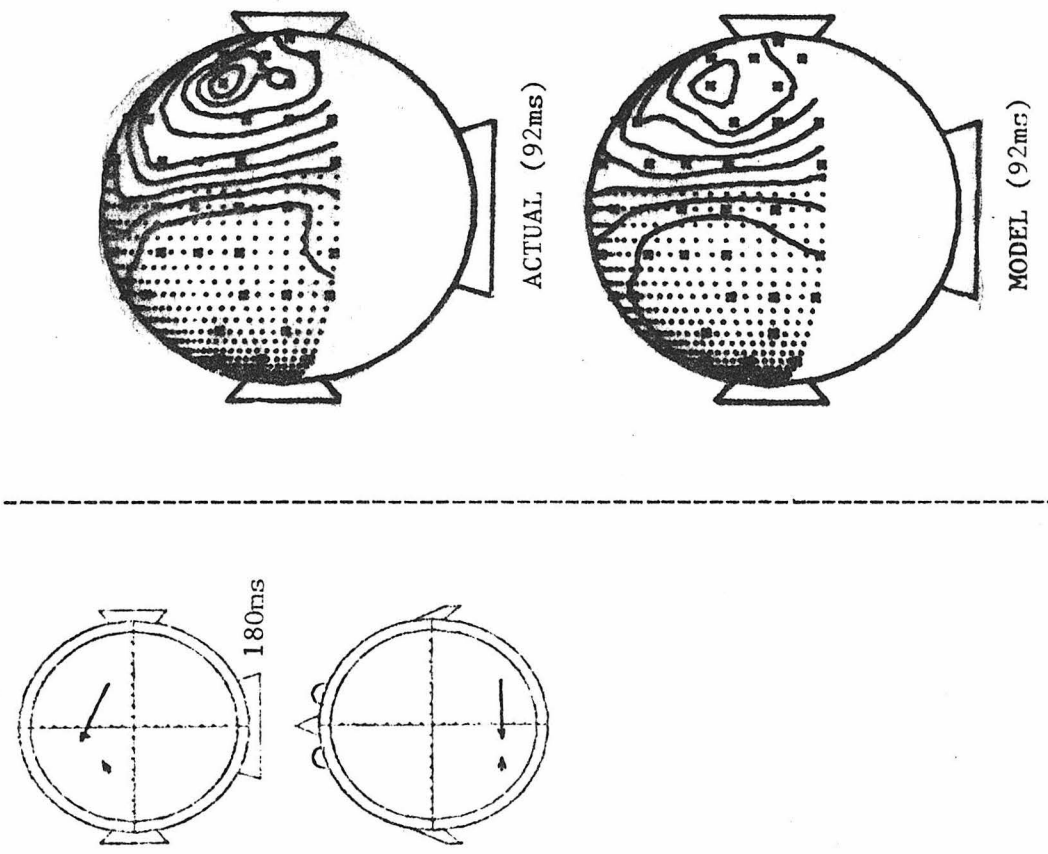

Fig. 97 (continued)

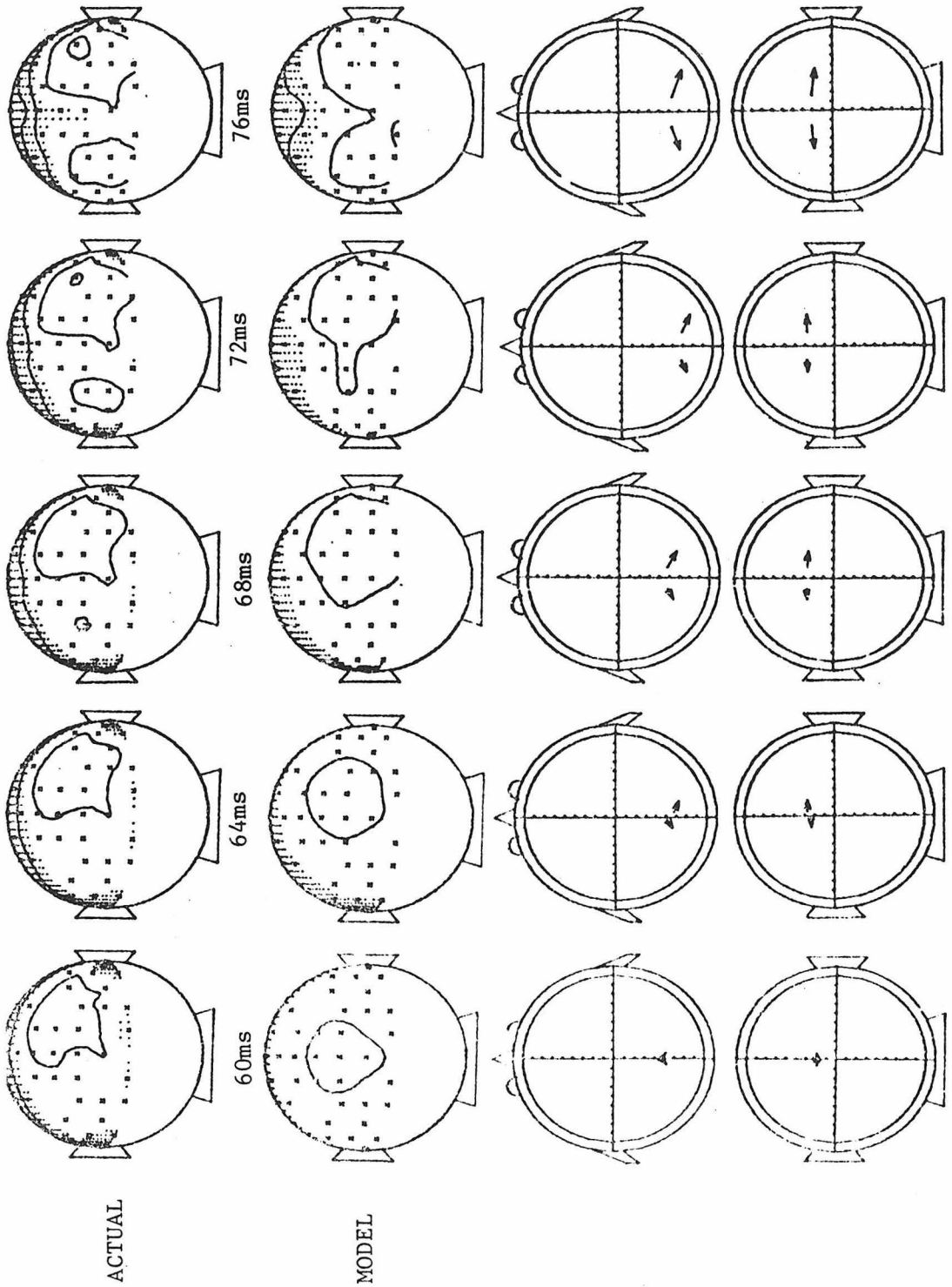

Fig. 98 - Time series of 3-shell model equivalent dipoles for WF stimulation of subject JPA using the 12 parameter model

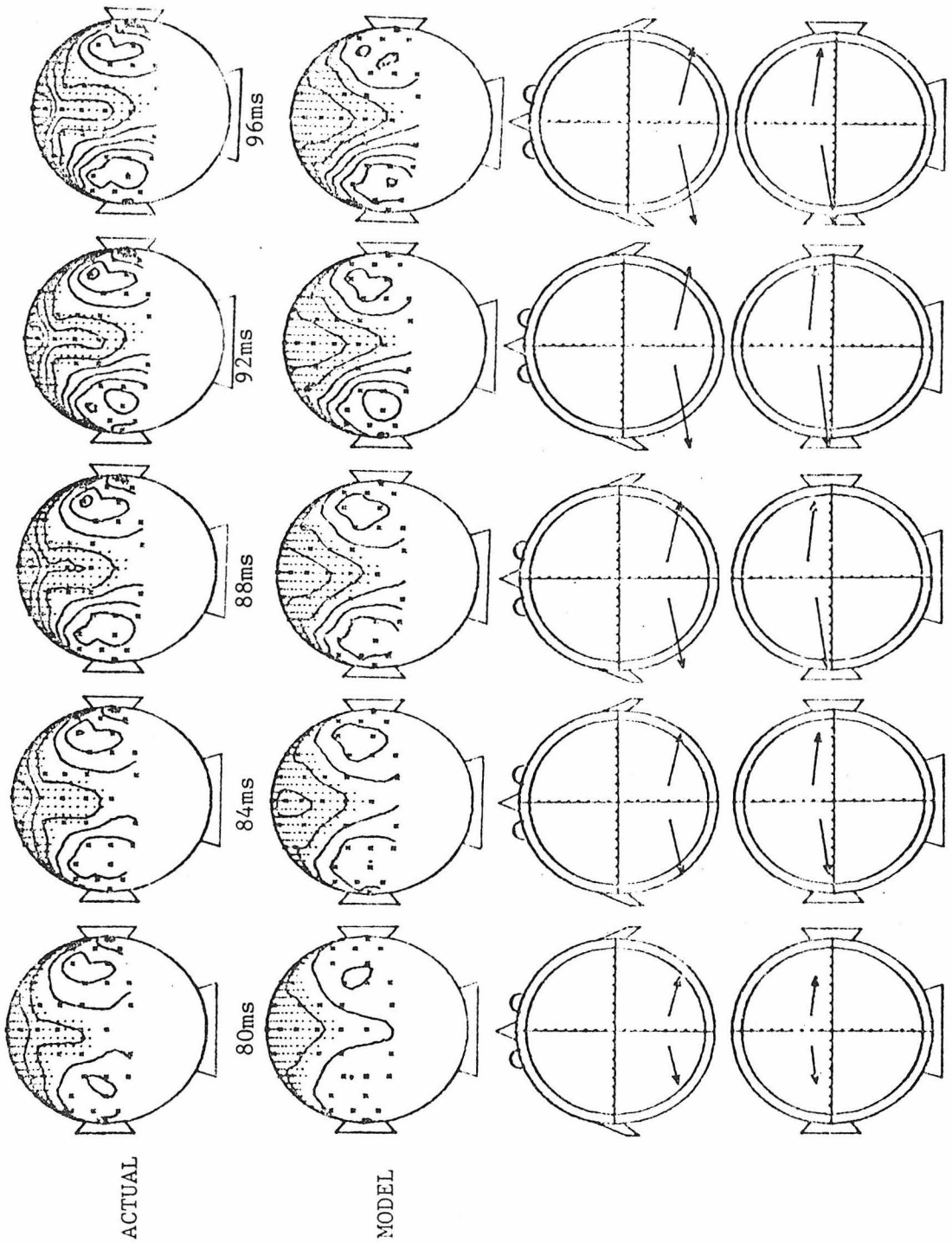

Fig. 98 (continued)

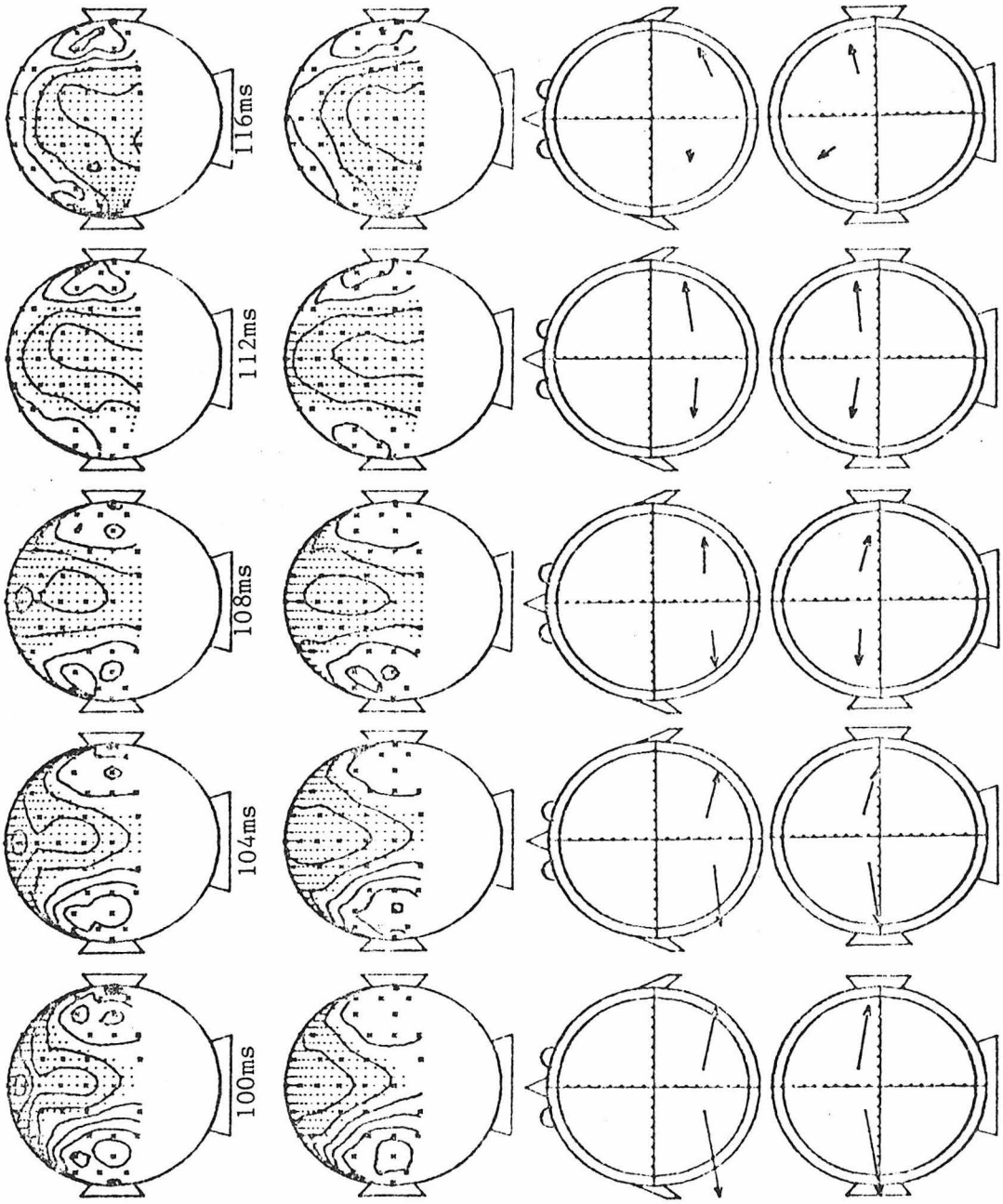

Fig. 98 (continued)

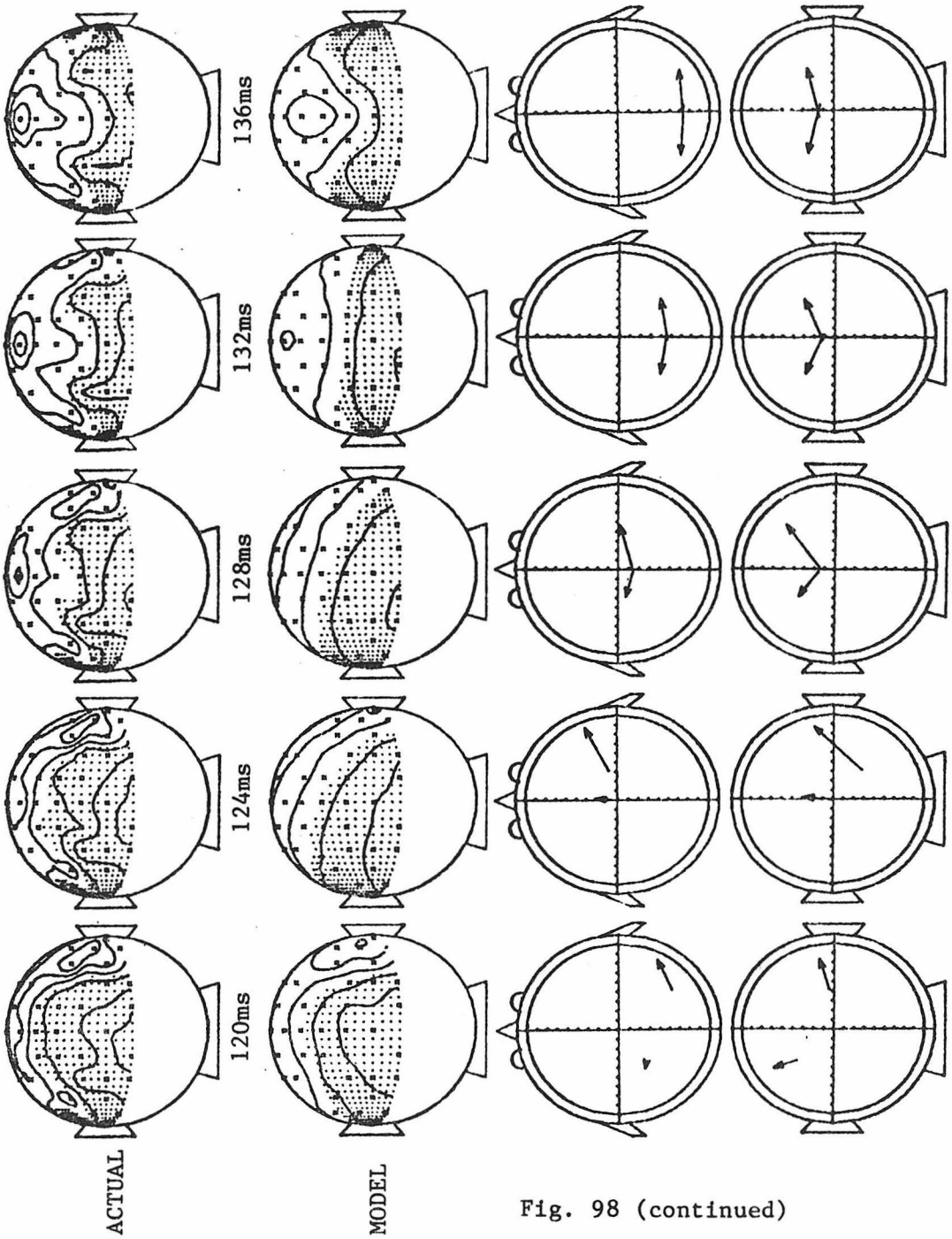

Fig. 98 (continued)

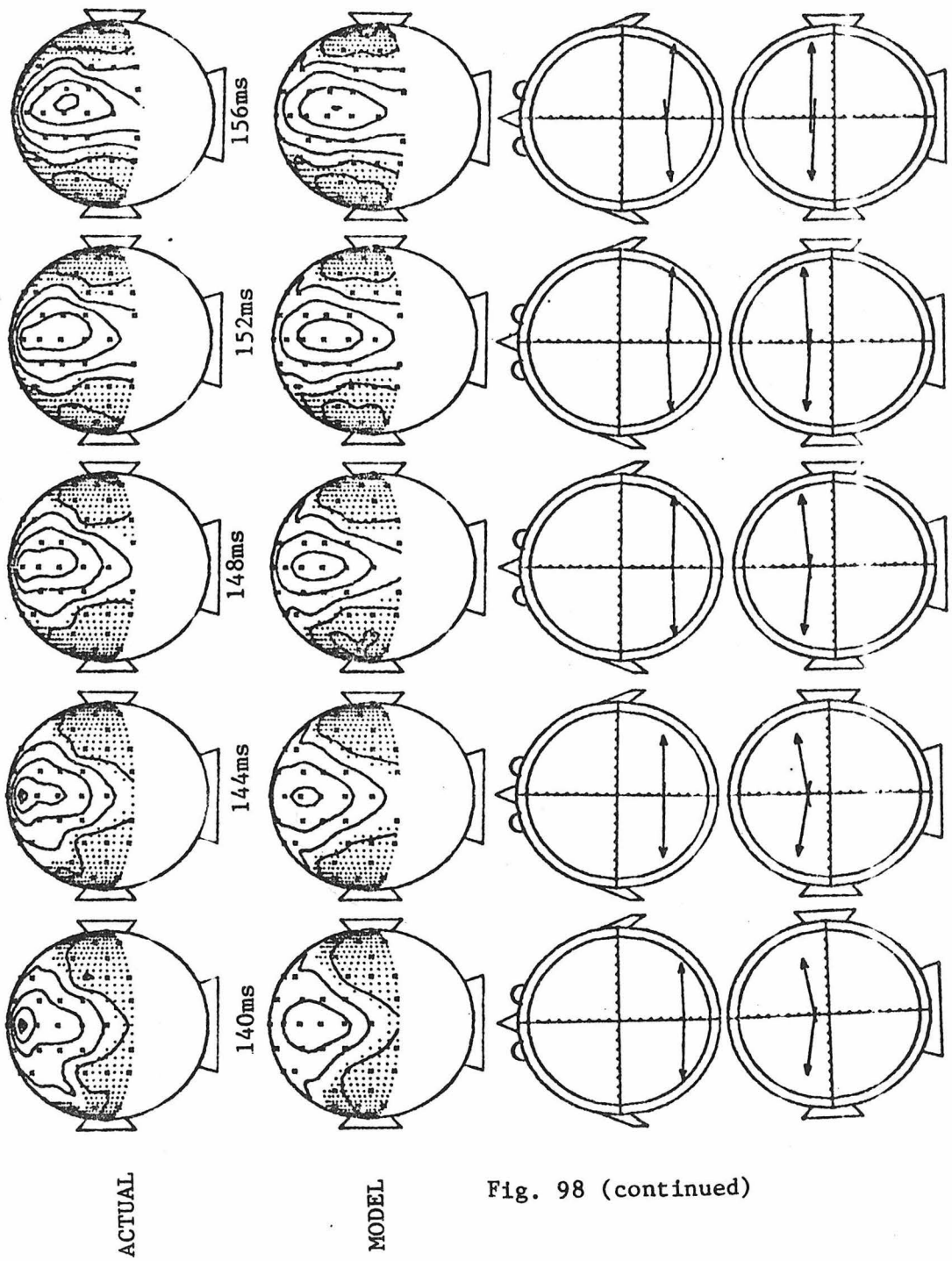

Fig. 98 (continued)

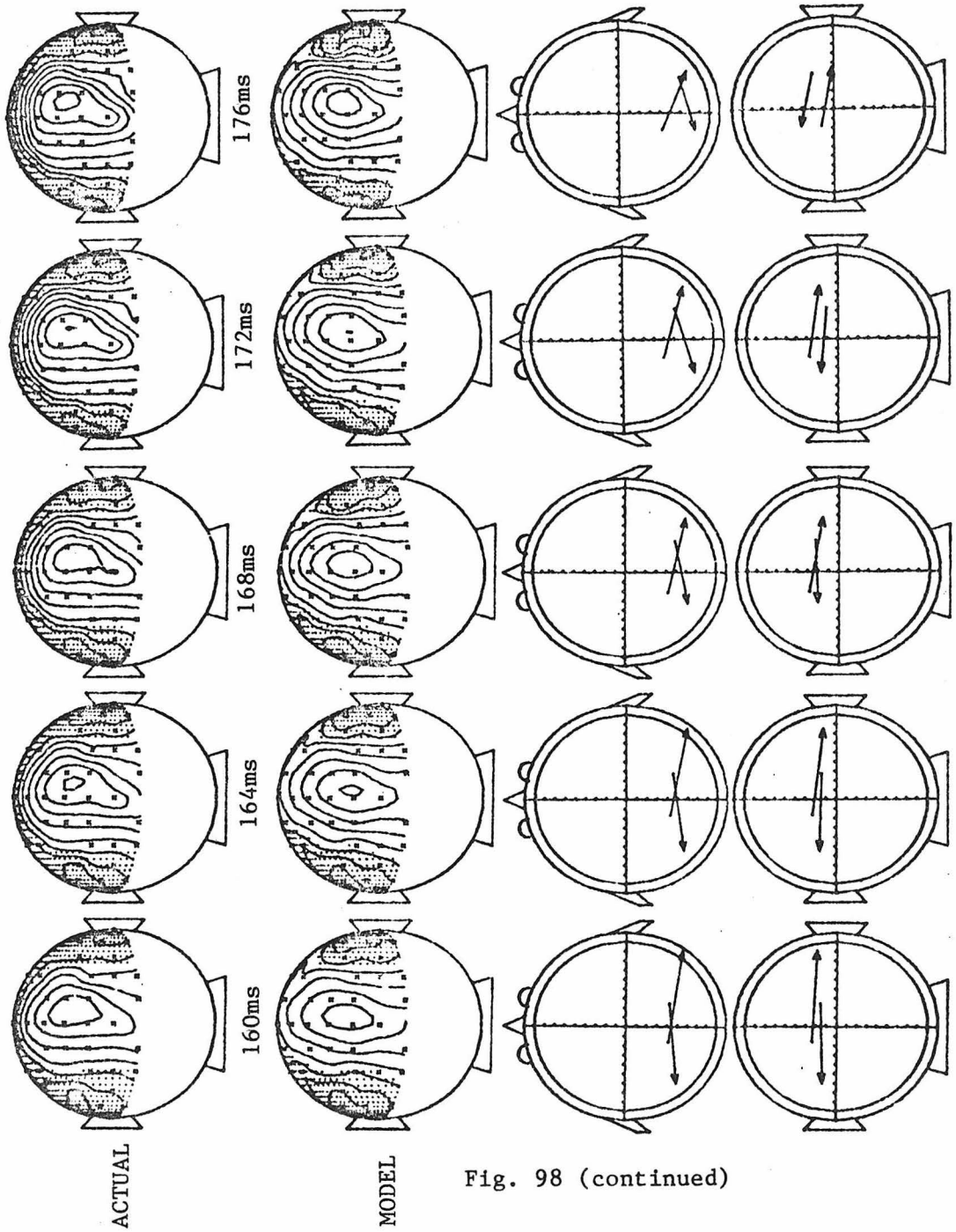

Fig. 98 (continued)

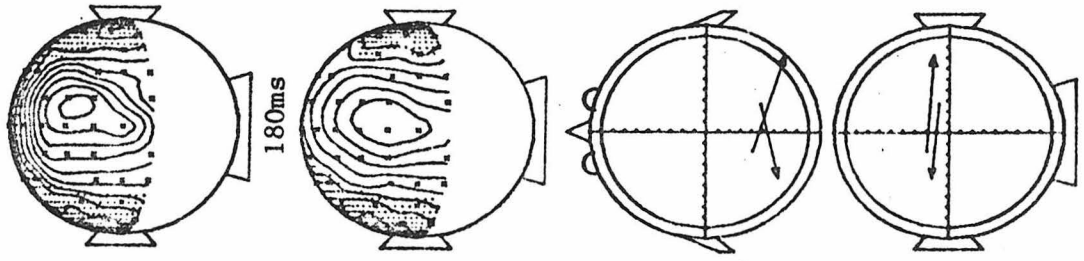

Fig. 98 (continued)

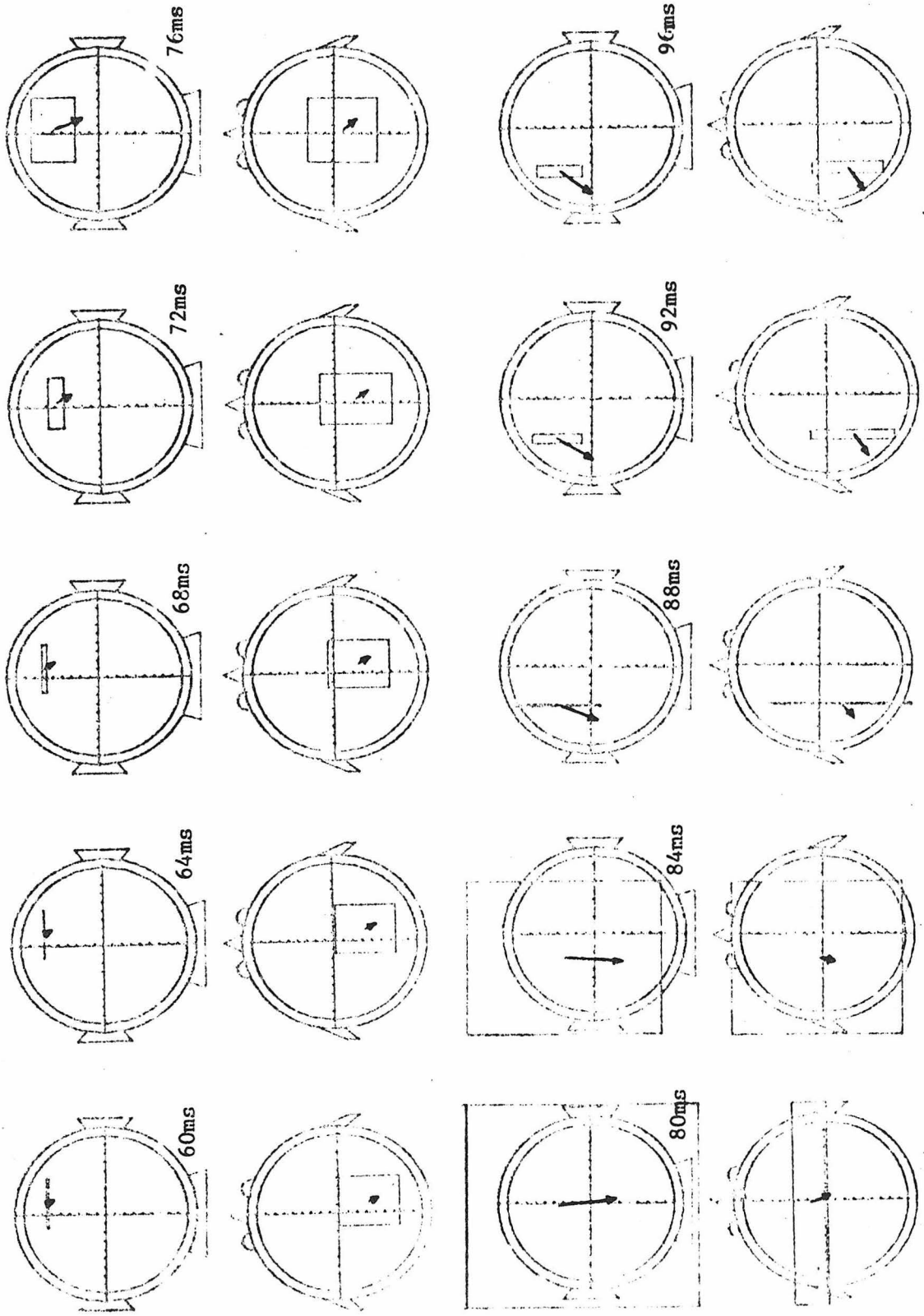

Fig. 99 - 1 dipole fits for subject JPA responses to WF stimulation

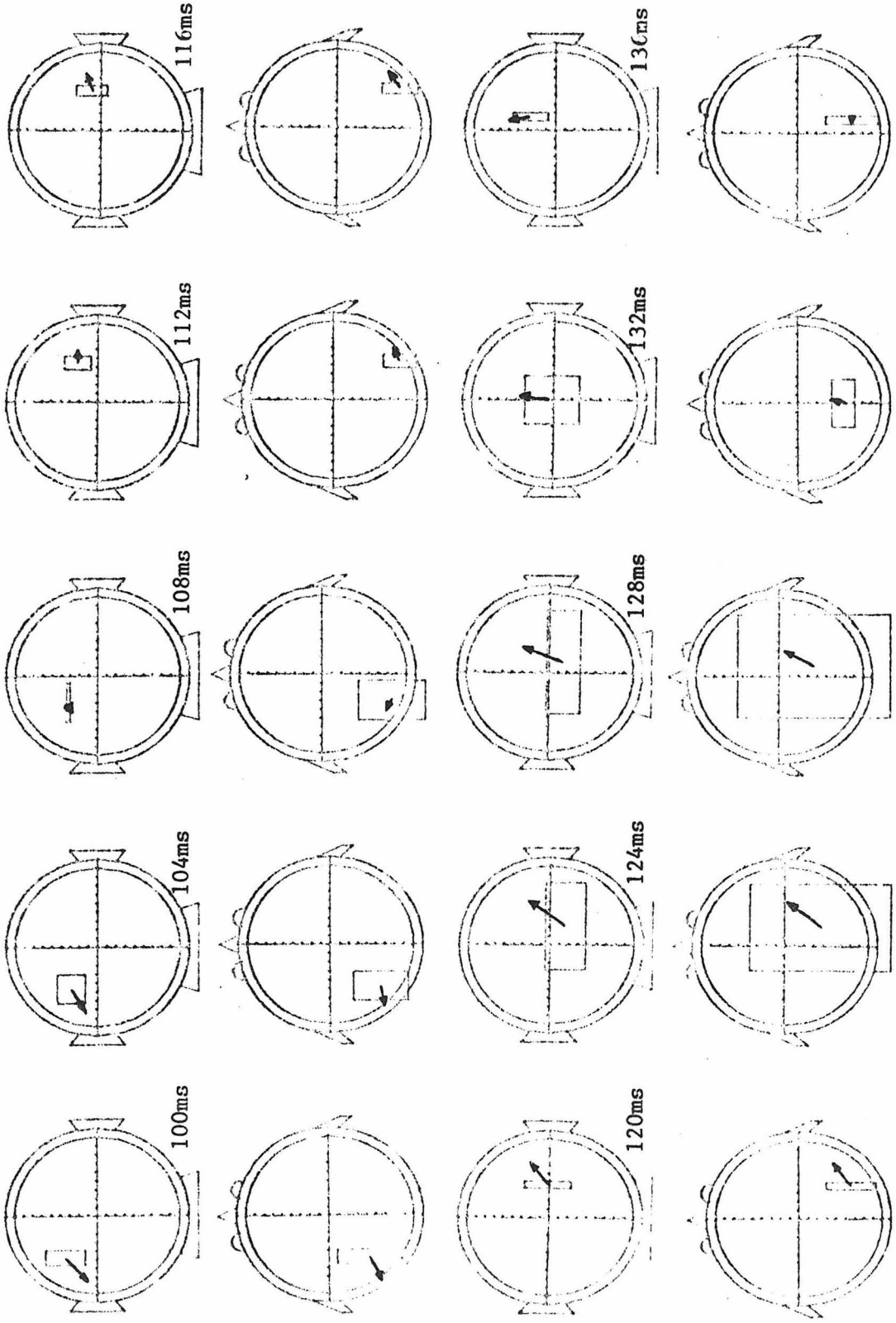

Fig. 99 (continued)

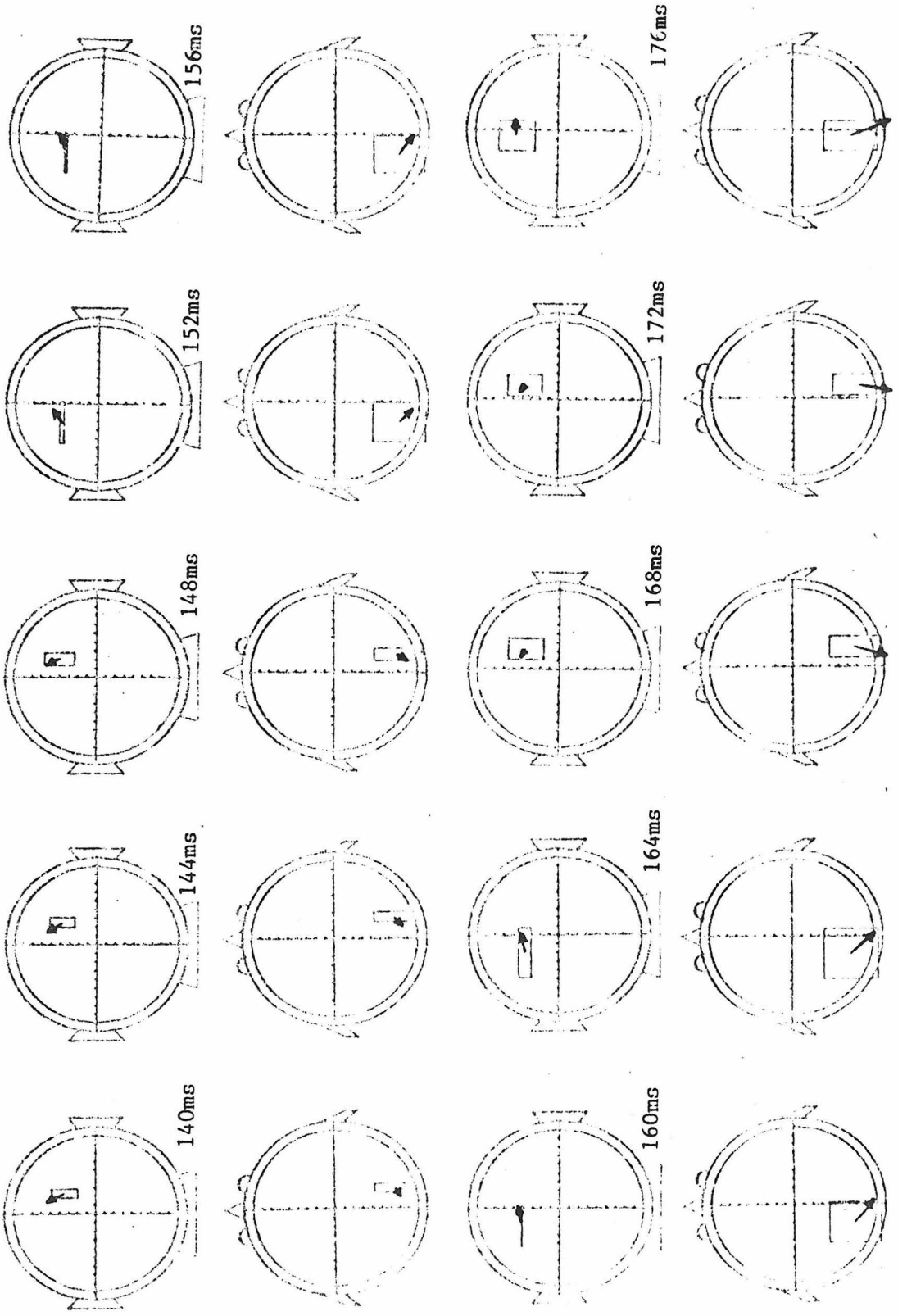

Fig. 99 (continued)

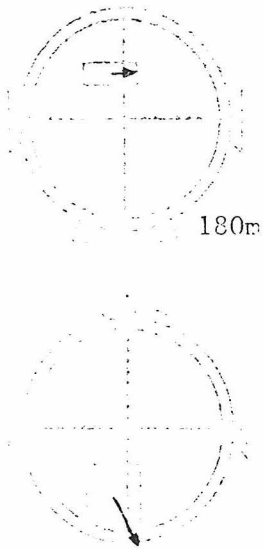

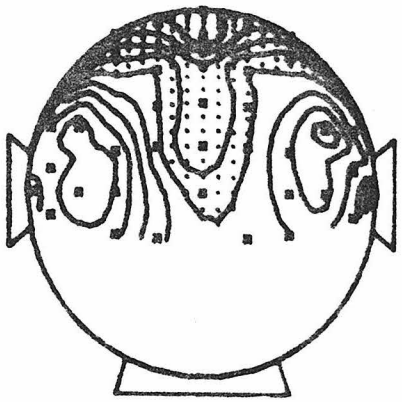

ACTUAL (92ms)

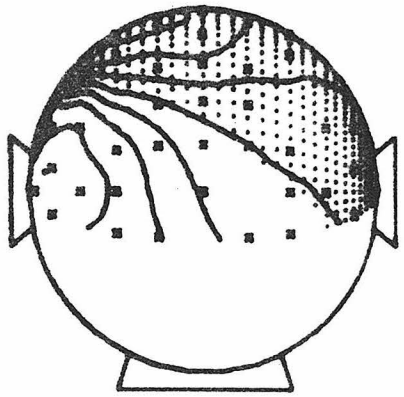

MODEL (92ms)

Fig. 99 (continued)

TIME	χ^2_ν	TIME	χ^2_ν
60	.1543	124	.9215
64	.1695	128	.8165
68	.2089	132	.8359
72	.2787	136	.7524
76	.4693	140	.7612
80	.9698	144	.9023
84	2.0124	148	1.1460
88	3.0804	152	1.4885
92	3.5301	156	1.7567
96	3.4735	160	2.3289
100	2.8396	164	3.0665
104	1.9792	168	3.2762
108	1.2628	172	3.5701
112	.5331	176	3.7339
116	.6142	180	3.5794
120	.8908		

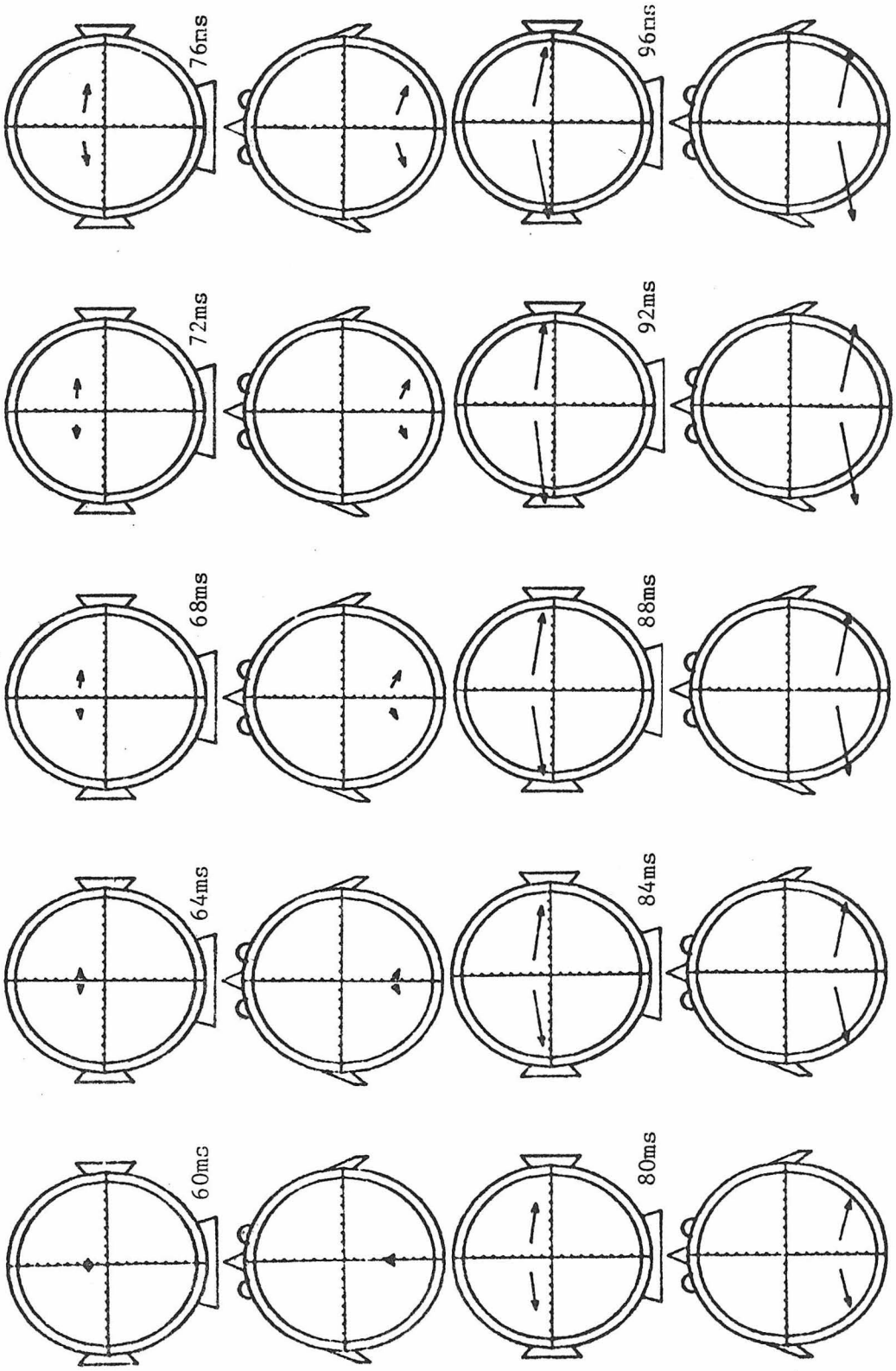

Fig. 100 - 7 parameter 2-dipole fits for subject JPA responses to WF stimulation.

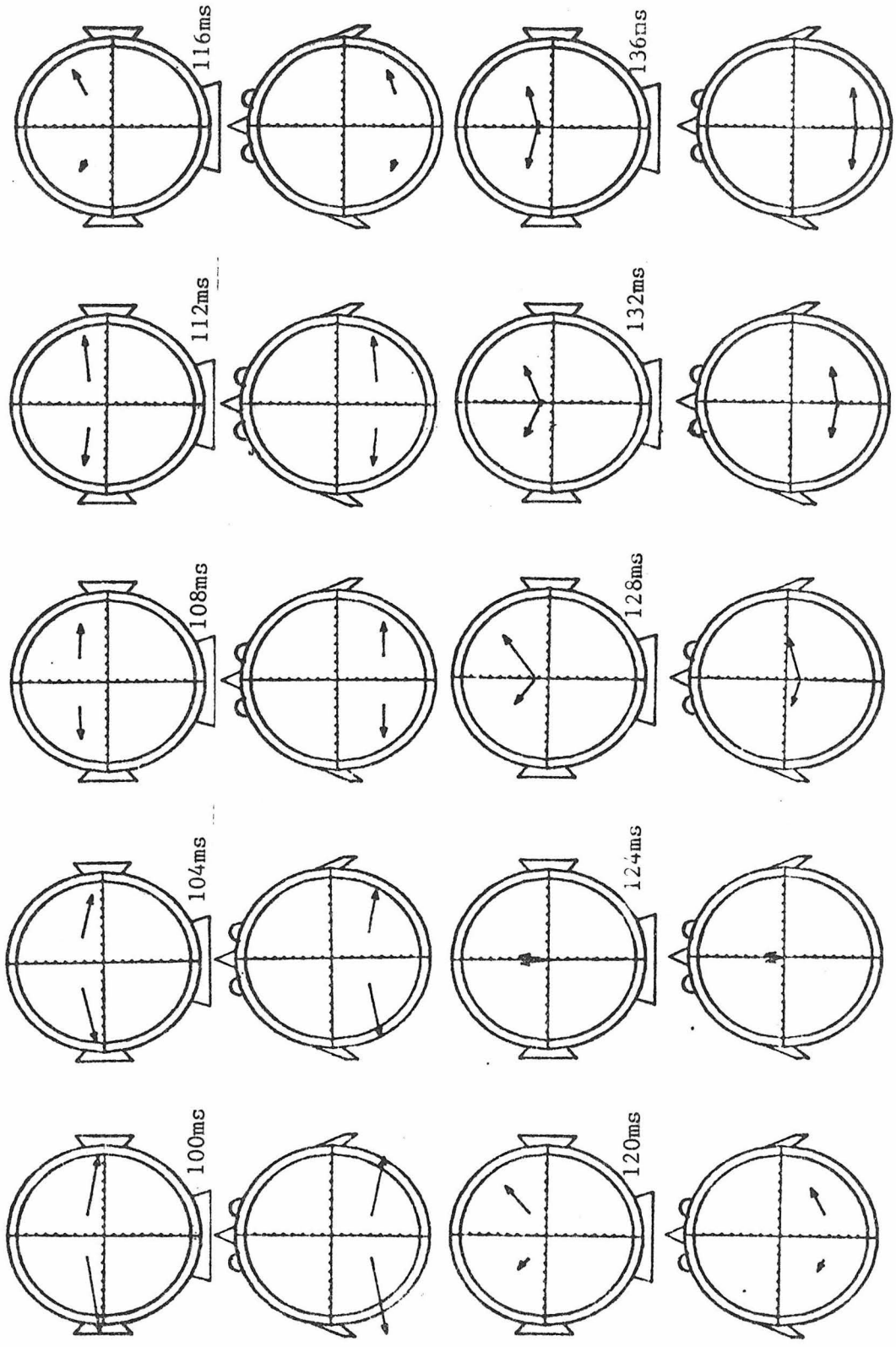

Fig. 100 (continued)

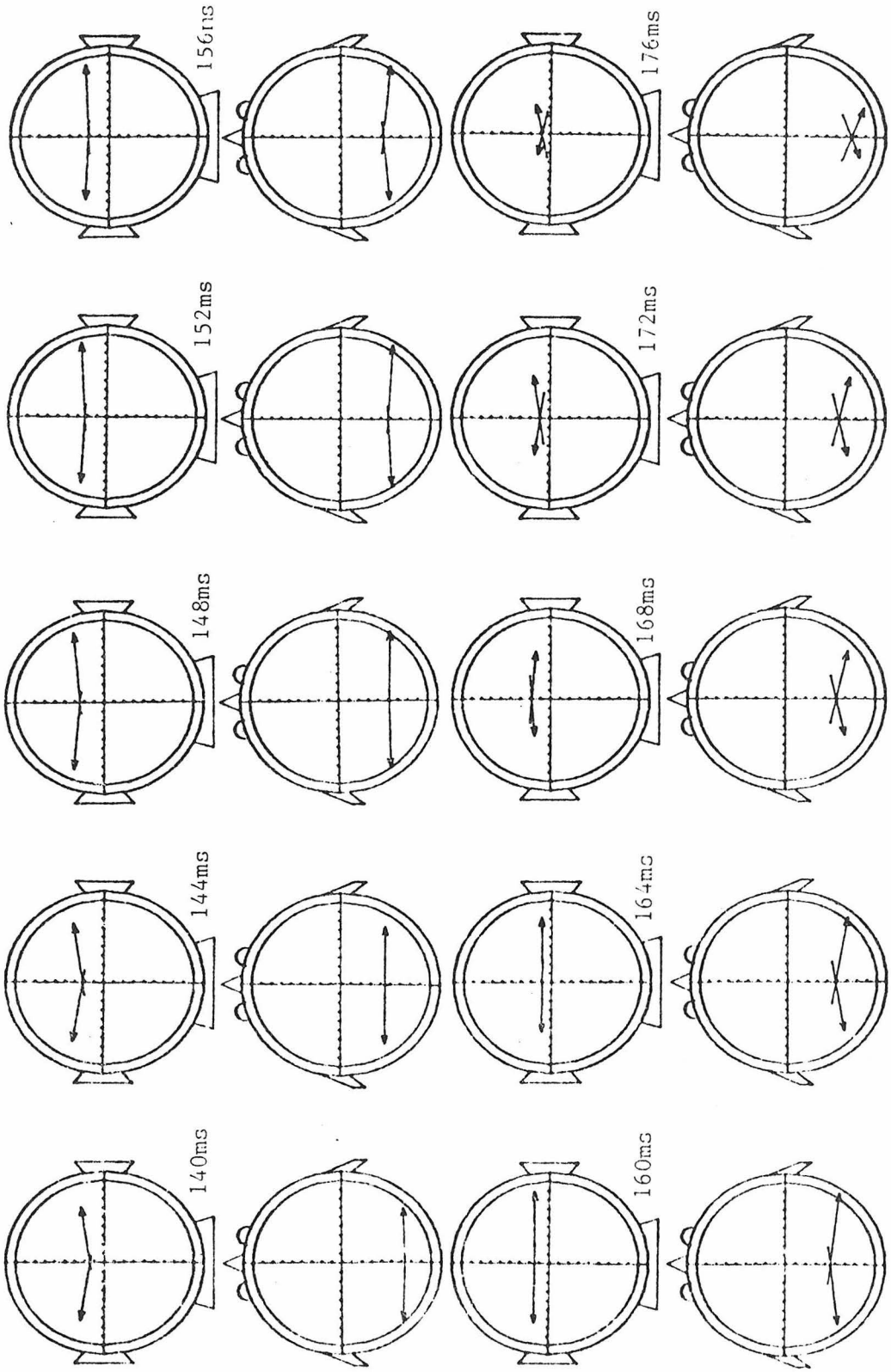

Fig. 100 (continued)

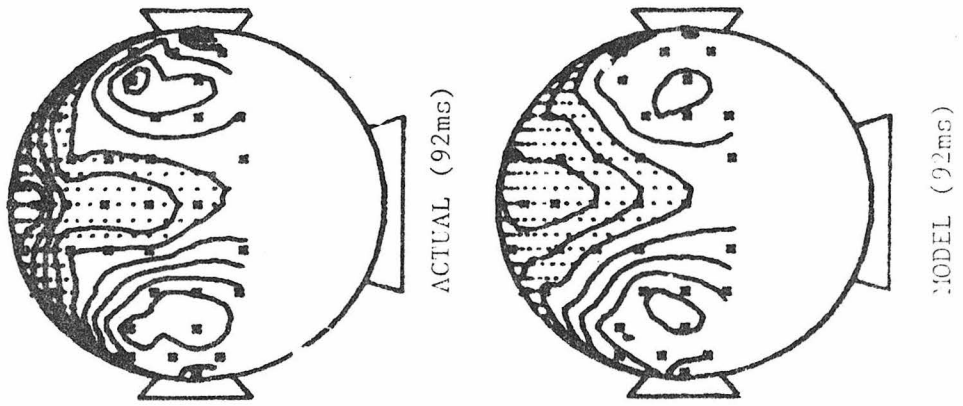

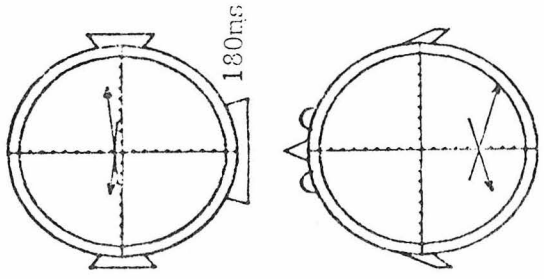

Fig. 100 (continued)

equivalent sources using the single source and the other two source model (7 parameter constrained). The single source model (Fig. 99) does not give a good fit to the data (note the very large confidence regions and poor χ^2_ν values). From these figures it is clear that two sources are indicated, one each in the left and right sides of the head.

The previous examples illustrate an objective process which may be used to decide on the number of equivalent sources which are indicated. However, with little or no experience it is obvious how many sources are indicated. Indeed, multiple sources are indicated when there are multiple peaks on the scalp of the same polarity and of significant size. In the data analyzed in this thesis, only three source multiplicity conditions were encountered: no source, one source and two sources. As a rule, these were quite easy to distinguish.

5.2.2 Effect of Stimulus Locus on Spatio-Temporal Equivalent Sources

The following pages show time series of 3-shell model equivalent sources in 4 msec intervals on subject JPA for each of 9 appearance/disappearance stimuli. Figs. 101-109 show source series for whole field (WF), left half field (LHF), right half field (RHF), upper half field (UHF), bottom half field (BHF), bottom left quadrant (BLQ), bottom right quadrant (BRQ), upper left quadrant (ULQ), and upper right quadrant (URQ), respectively. The location parameters have been separated from the moment parameters for clarity. In situations where one source is indicated (LHF,RHF,BLQ,BRQ,ULQ,URQ), there is one series of positions and one of moment vectors for each view of the head. In those situations where two sources are indicated (WF,UHF,BHF), two series of positions and two of moment vectors are shown for each view of the head.

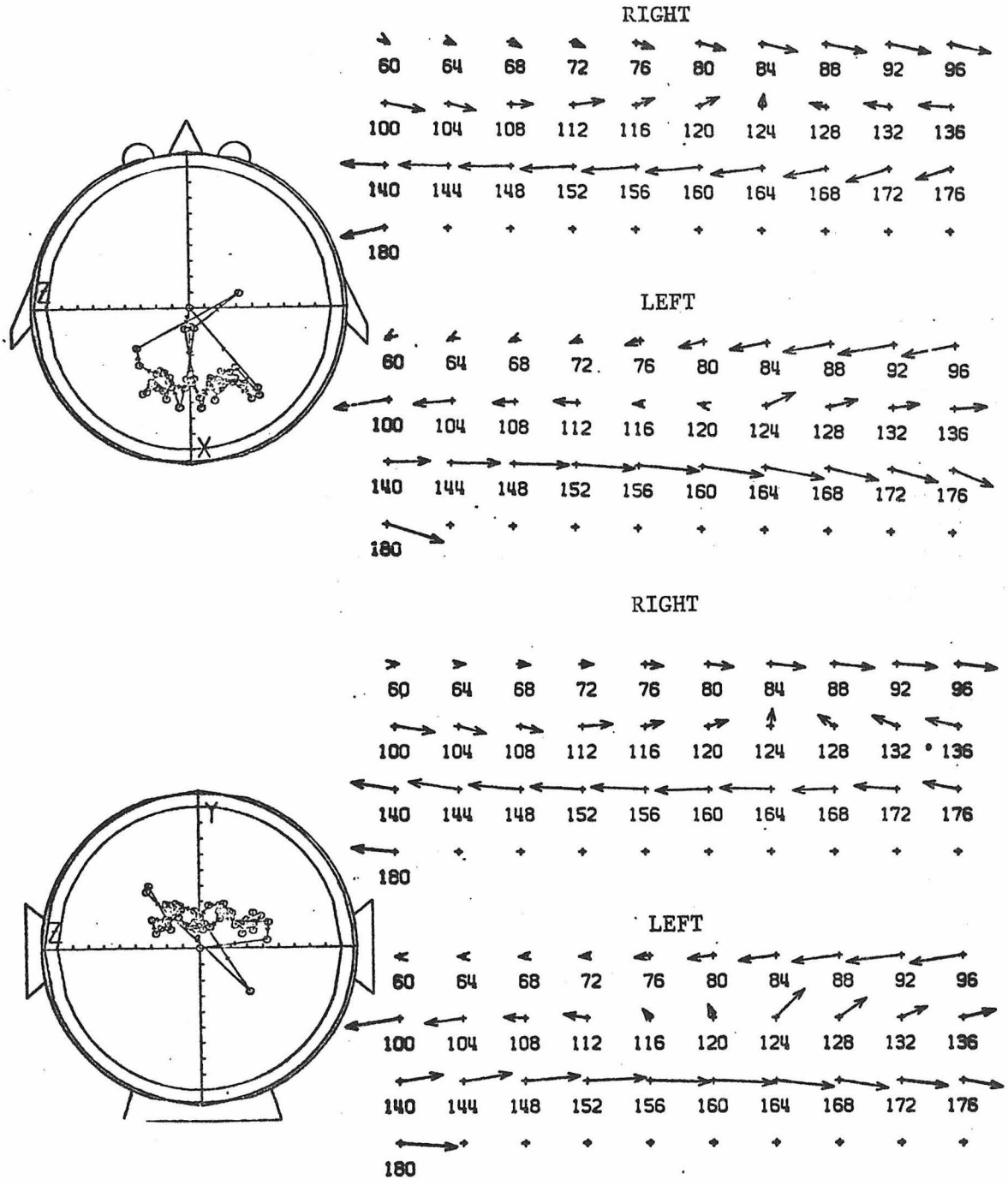

Fig. 101 - 3-shell model equivalent source series for subject JPA WF stimulation

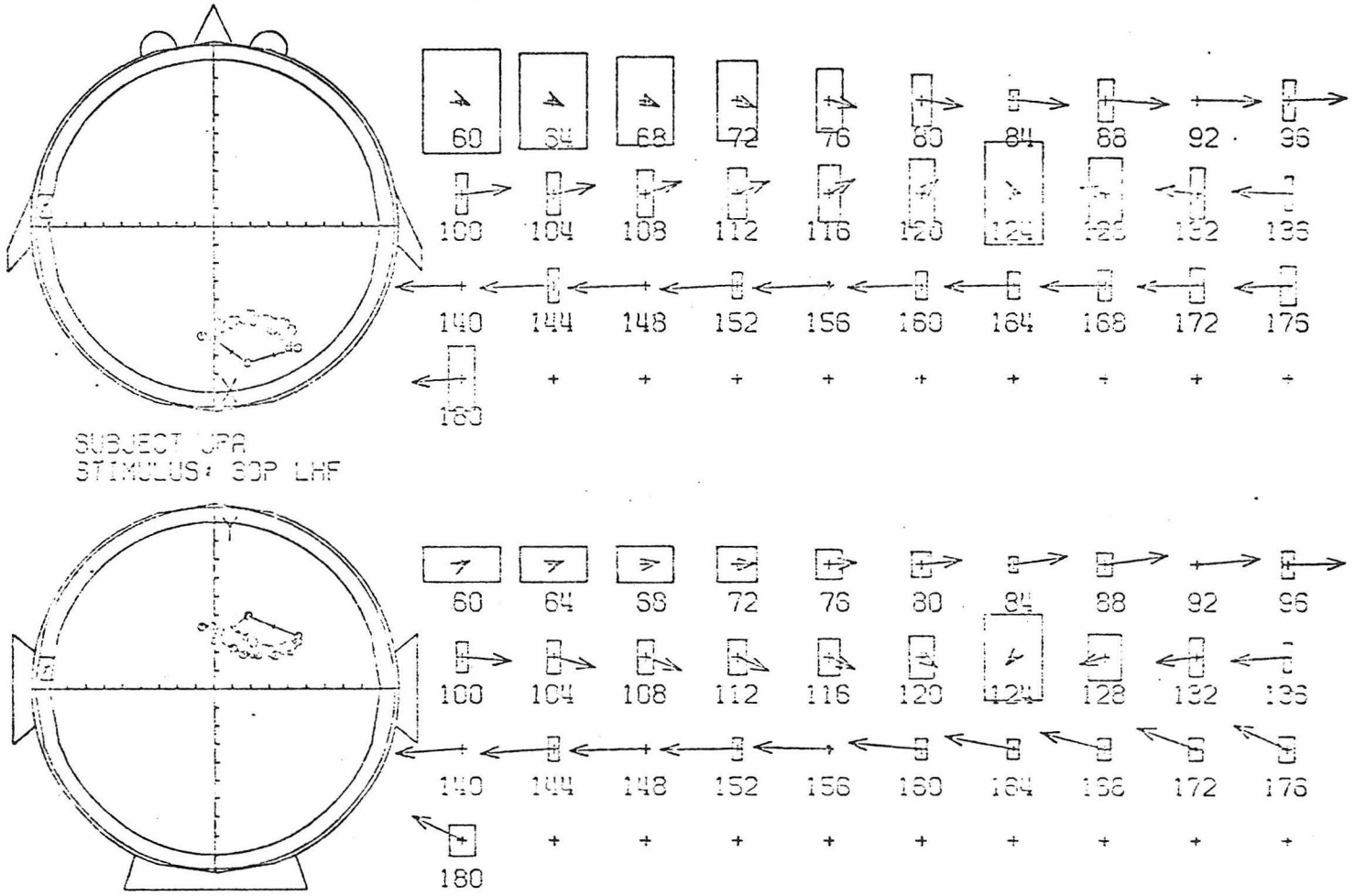

Fig. 102 - 3-shell model equivalent source series and 95% confidence regions for subject JPA LHF stimulation

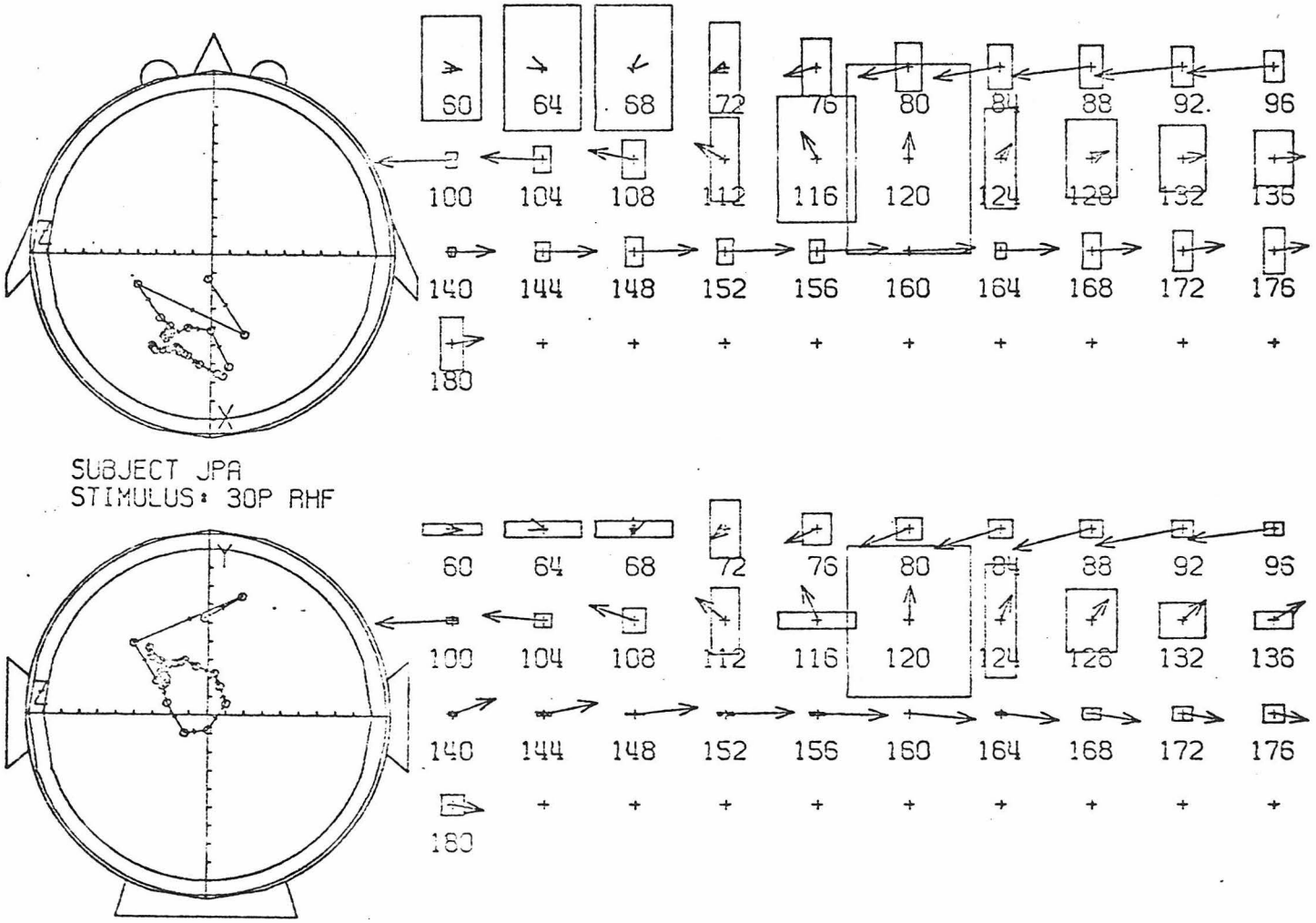

Fig. 103 - 3-shell model equivalent source series and 95% confidence regions for subject JPA RHF stimulation

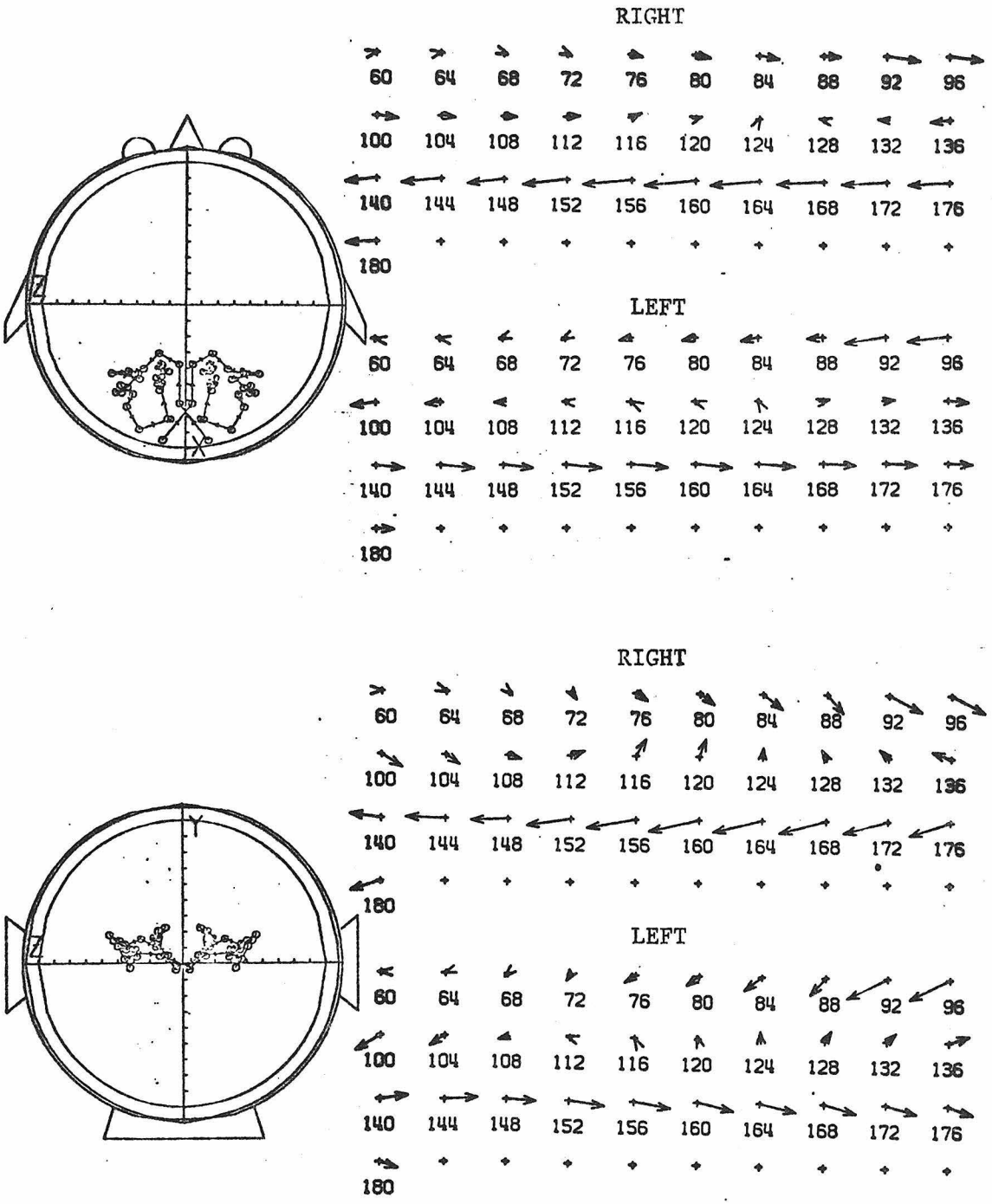

Fig. 104 - 3-shell model equivalent source series for subject JPA UHF stimulation

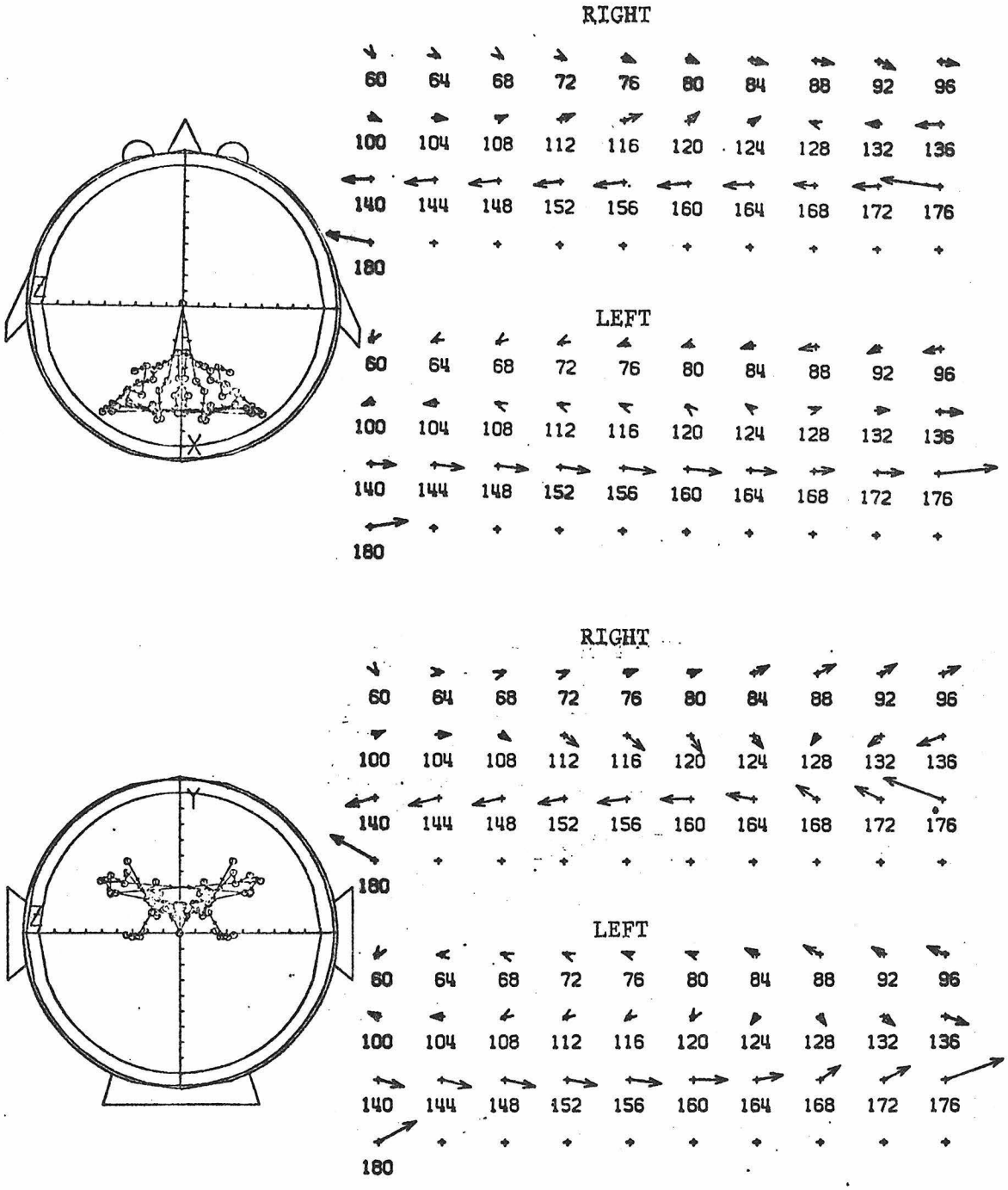

Fig. 105 - 3-shell model equivalent source series for subject JPA BHF stimulation

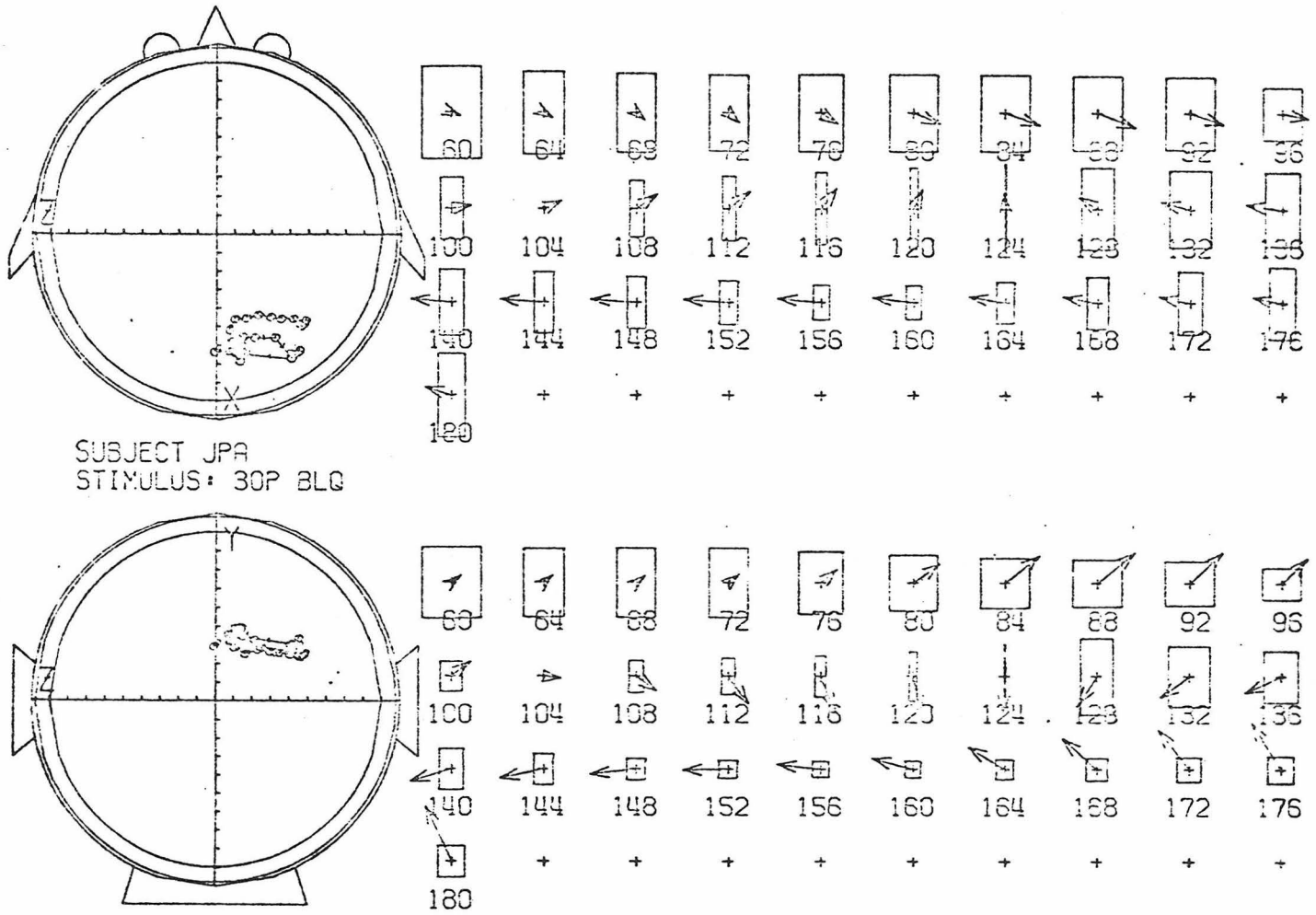

Fig. 106 - 3-shell model equivalent source series and 95% confidence regions for subject JPA BLQ stimulation

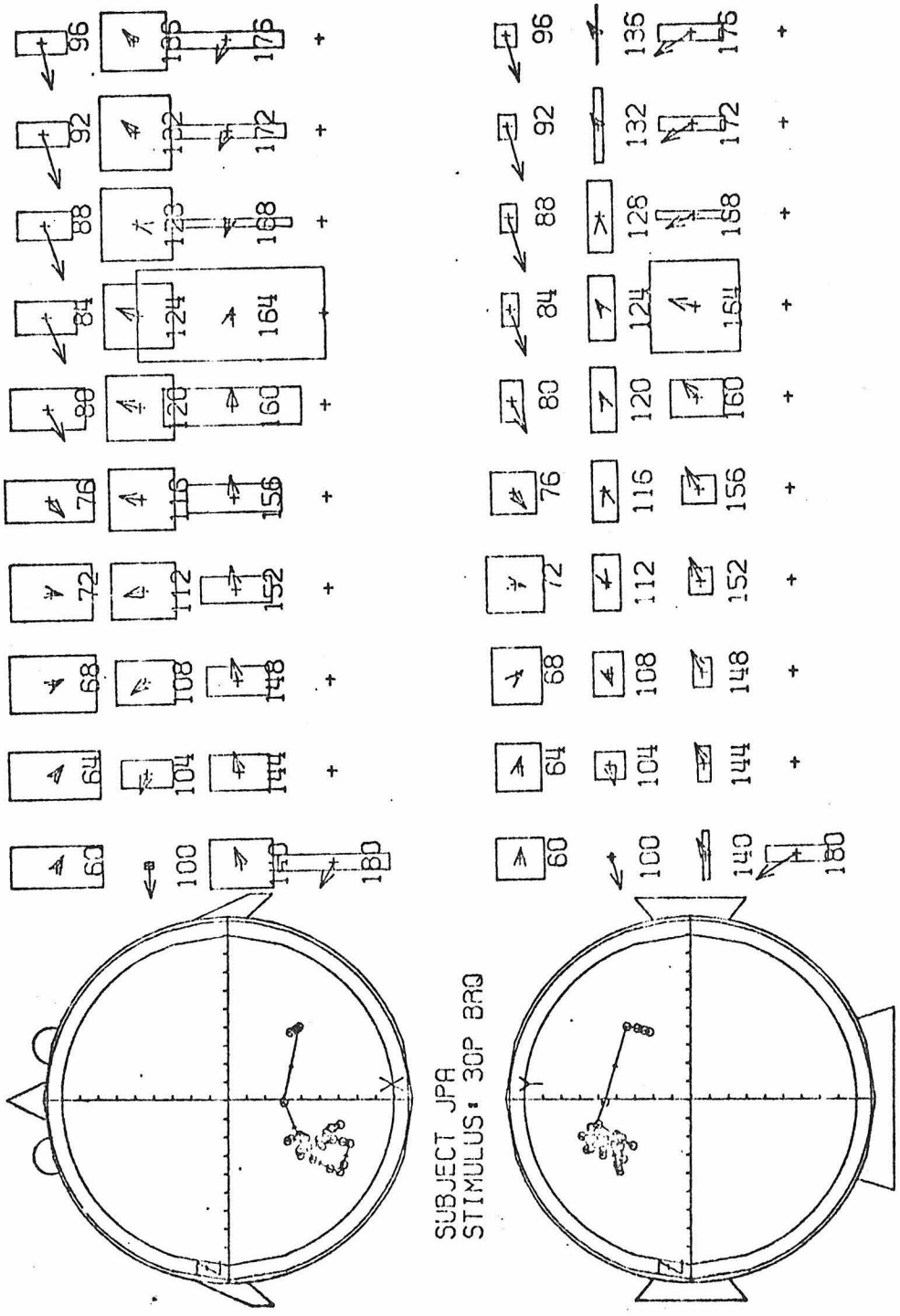

Fig. 107 - 3-shell model equivalent source series and 95% confidence regions for subject JPA BRQ stimulation

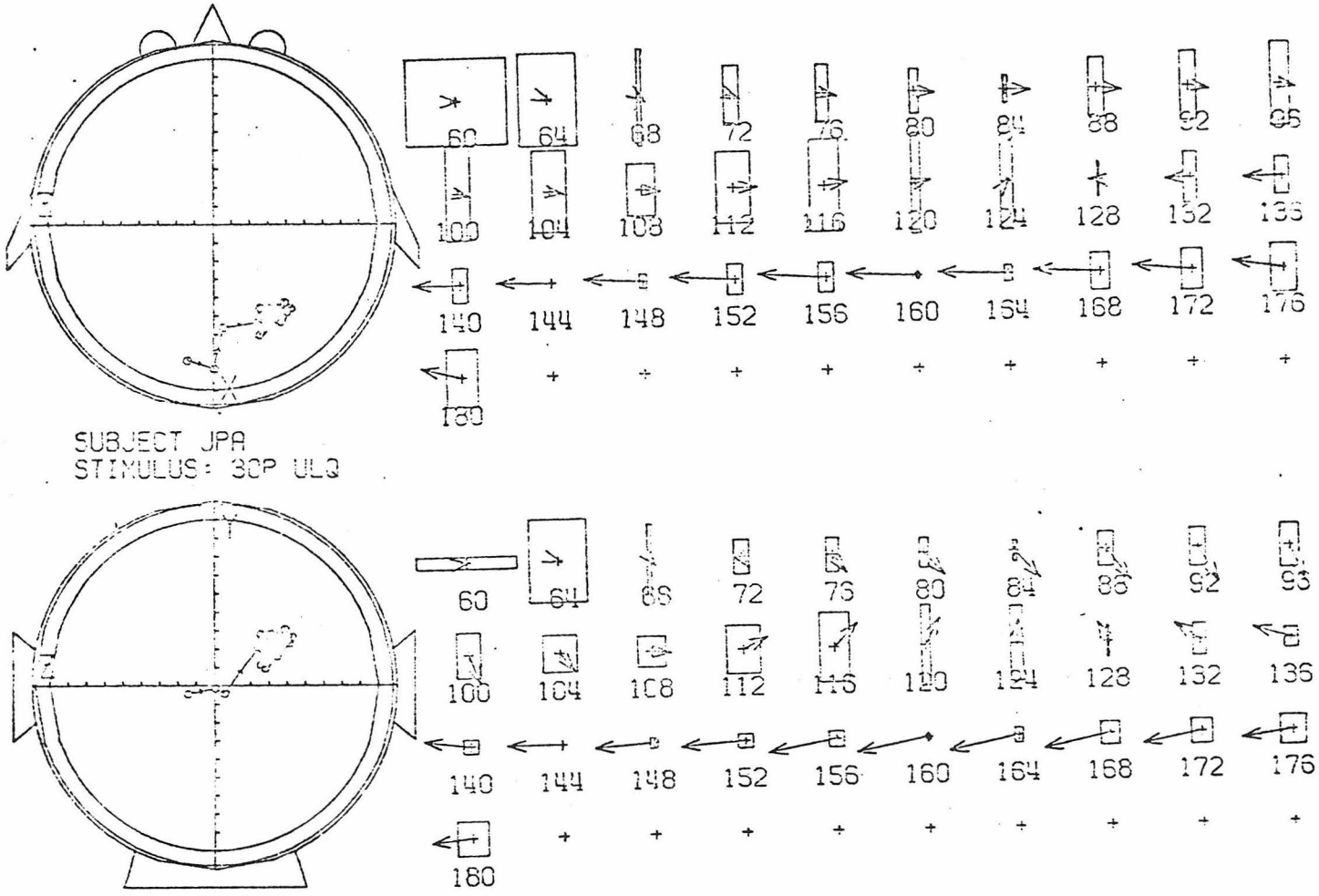

Fig. 108 - 3-shell model equivalent source series and 95% confidence regions for subject JPA ULQ stimulation

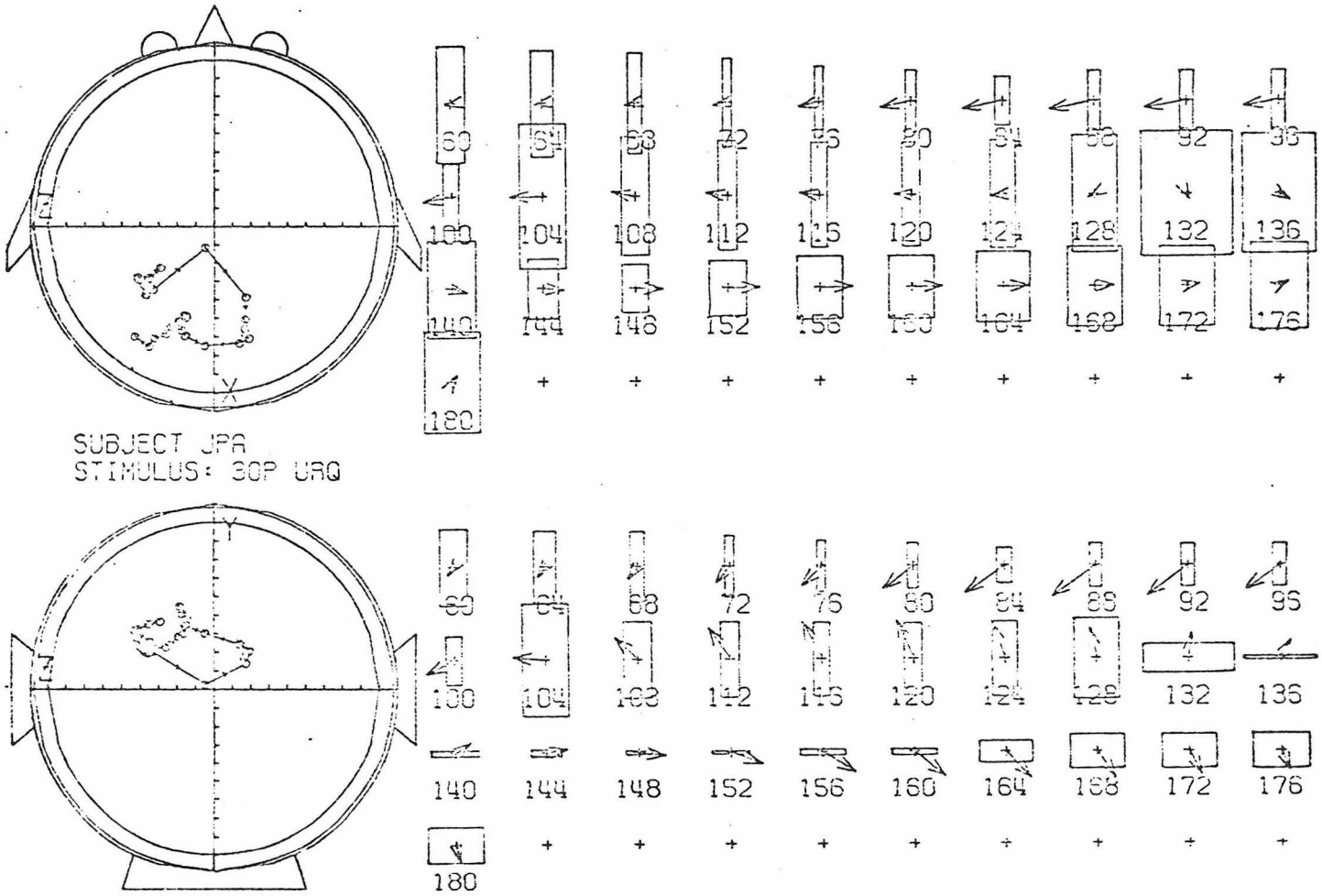

Fig. 109 - 3-shell model equivalent source series and 95% confidence regions for subject JPA URQ stimulation

The one source series which are shown utilized the 6-parameter dipole model, while the two source series utilized the 12-parameter two dipole model. Several of these figures show 95% confidence regions in location parameters around the series of moment vectors.

In Figs. 101-109 it can be seen that the location parameters of the model do a considerable amount of wandering, but that the equivalent sources are generally confined to the contralateral hemisphere fairly near the midline and near the back of the head. However, much of this wandering is accounted for by low-reliability equivalent sources at times when the scalp activity is irregular or non-existent (very early in the time sequence or at the transition between components, e.g. LHF 124 msec). Also it can be seen that the orientation(s) of the source(s) depends very much on the stimulus used. Two sources are always indicated for stimuli which ought to project to two hemispheres (WF,UHF,BHF) and one contralateral source indicated for stimuli which ought to project to one hemisphere. When two sources are indicated, they very often appear to be mirror images about the midline in both position and orientation (e.g. UHF). There are long periods of time (20-30 msec) when the sources remain stable in position and orientation, but grow and decay in magnitude over time in correspondence with the growth and decay of evoked potential components (Chapter 4) and often reverse direction at about 120-124 msec. Also the sizes of the confidence regions vary inversely with the magnitude of the source, as the locus is more accurately identified when the activity is strongest.

The dependence of source orientation on stimulus locus is pretty much consistent with the modified cruciform model (section 2.2.6).

Fig. 110 illustrates this fact by showing superimposed equivalent sources and 95% confidence regions for each of the 9 stimuli in the range of 80 to 100 msec. Paired sources (WF,UHF,BHF) are connected by dashed lines. By looking at the rear view of the head, it can be plainly seen that there is a hierarchy of orientations for equivalent sources in each hemisphere and that this hierarchy is consistent with the modified cruciform model. For example, the rear view of the LHF equivalent sources shows a horizontally directed group of dipoles in the right hemisphere. This is expected since a LHF stimulus activates all of posteriolateral and portions of medial and intracalcarine striate cortex in the right hemisphere. Intracalcarine cancellation is expected (section 2.2.6), leaving only the medial and posteriolateral portions, a horizontally directed surface. The ULQ and BLQ stimuli produce equivalent sources in the right hemisphere which, when viewed from the rear, point down and to the right, and up and to the right, respectively. These are also expected since these stimuli should activate posteriolateral, medial and intracalcarine cortex unilaterally above (lower quadrant) or below (upper quadrant) or below the level of the calcarine fissure. The degree of inclination of a single source equivalent to the surface representing a particular quadrant would depend on the relative amounts of medial (horizontally directed surface) and intracalcarine (vertically directed surface) tissues which are activated. As may be seen in the similar but less dramatic hierarchy of right visual field stimuli (RHF,URQ,BRQ), these relative amounts are probably variable.

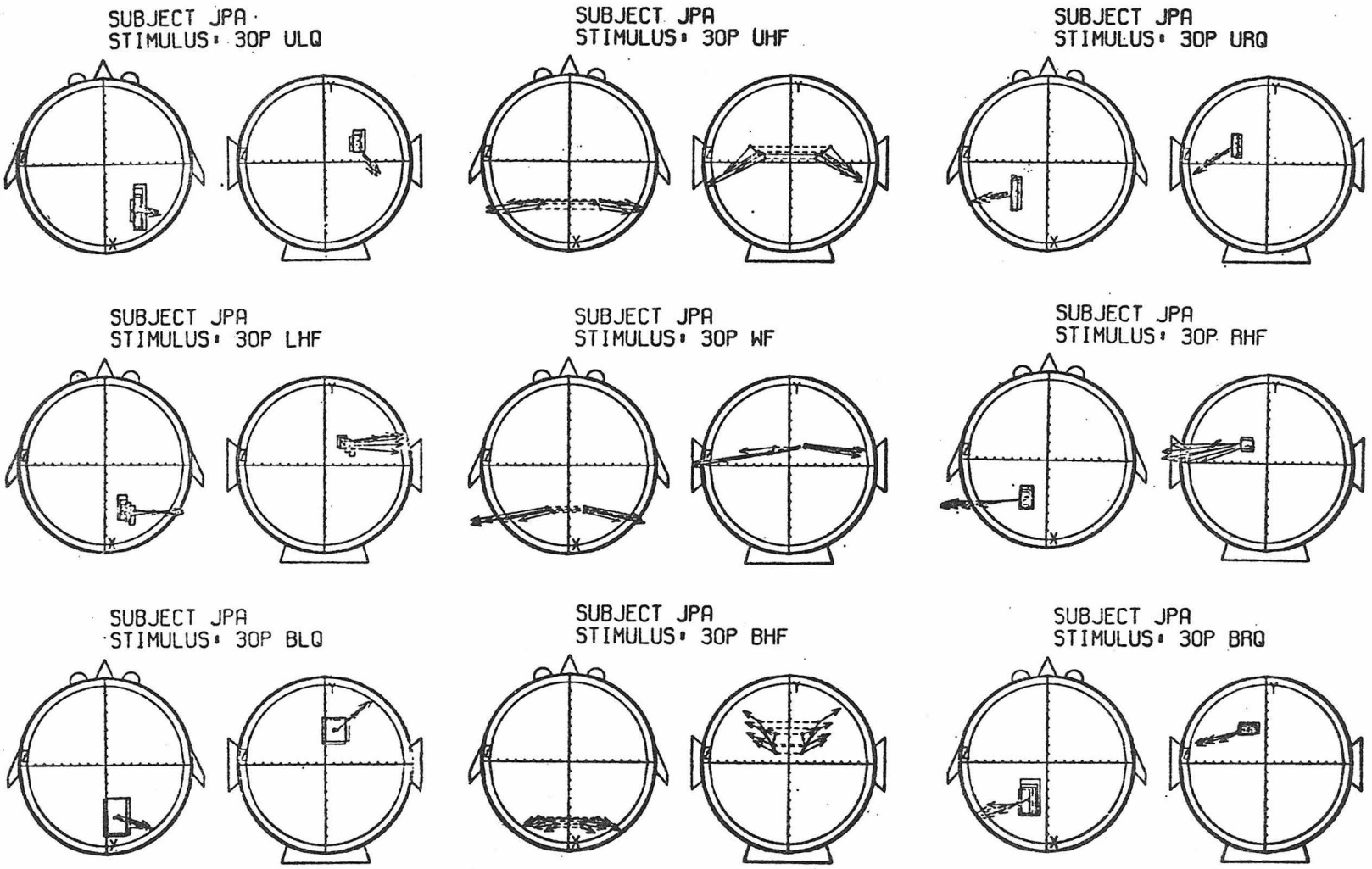

Fig. 110 - Behavior of subject JPA equivalent sources in the range of 80-100 msec.

In addition to the preceding, Fig. 110 illustrates that in the 80 to 100 msec interval, neither the location nor the orientation parameters change a great deal, but the source magnitude varies. This is true of the secondary component as well.

5.2.3 Intersubject and Intrasubject Dependence of Equivalent Sources on Stimulus Locus

The following pages (Figs. 111-116) show the stimulus dependence of equivalent sources (Figs. 111,113,115) and the potential distributions predicted by these sources (Figs. 112,114,116) computed for the initial peak (88-96msec) in the appearance/disappearance response in each of the three subjects. The potential distributions are plotted with 11 contours to accentuate detail. In these figures it can be seen that with the sole exception of PDP BHF stimulation, equivalent dipoles give good fits to the measured evoked potential data. It can also be seen that all subjects give contralateral equivalent sources in the rear of the head near the midline in all of the stimulus conditions (excepting PDP BRQ which is slightly ipsilateral) and that stimuli which project to both hemispheres give bilateral equivalent sources. The previously described orientation hierarchies are present in all three subjects, with lower visual field stimuli (BHF,BLQ,BRQ) always producing equivalent sources with inclinations which are greater than or equal to the inclinations of the lateral and whole field equivalent sources, which are in turn greater than or equal to the inclinations of upper visual field stimuli (UHF,ULQ,URQ). By a greater inclination we mean here that dipole points more nearly upward (i.e. in the y direction). In terms of equivalent sources, the three subjects

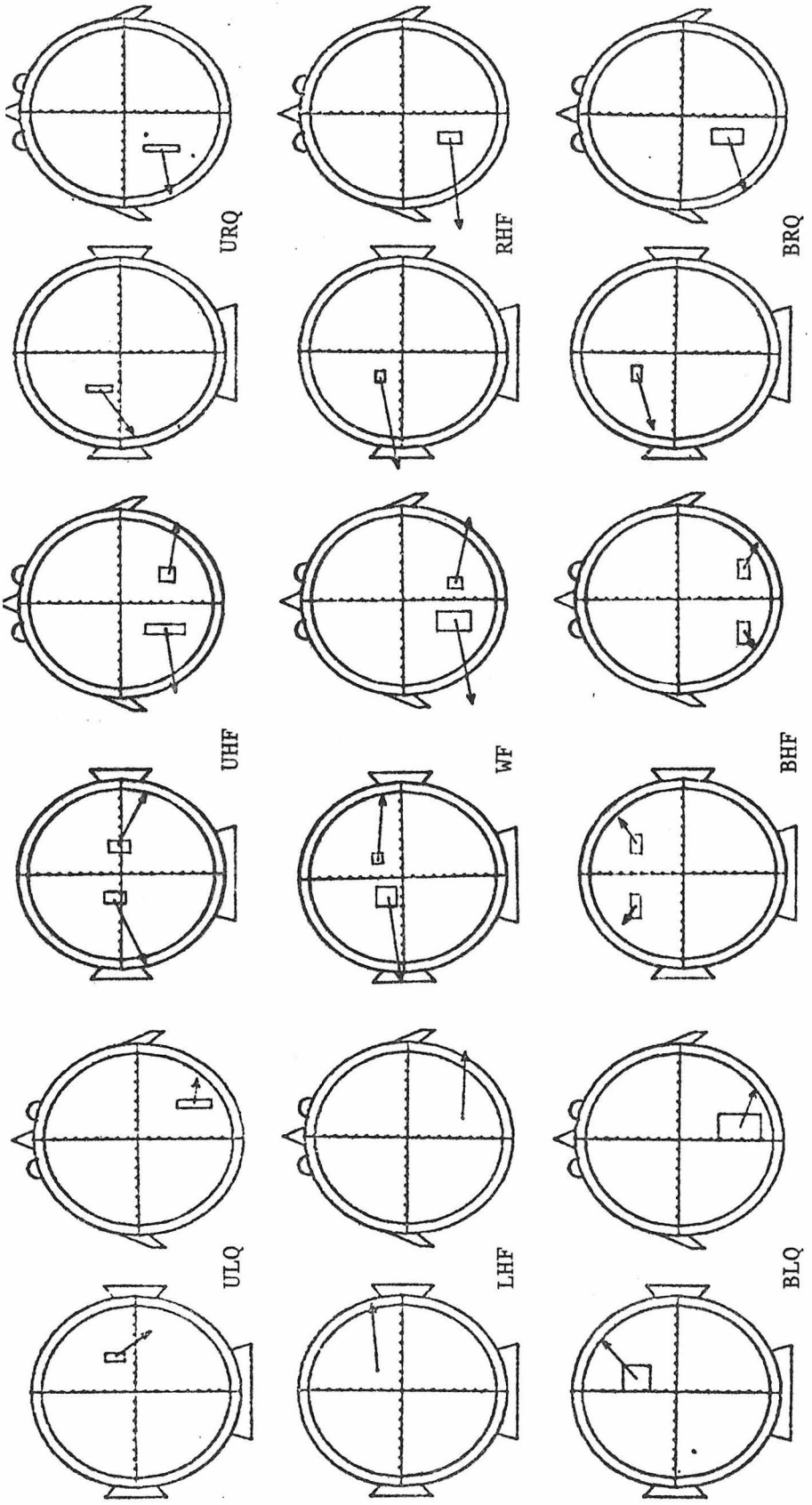

Fig. 111 · 3-shell equivalent dipoles for subject JPA initial peak

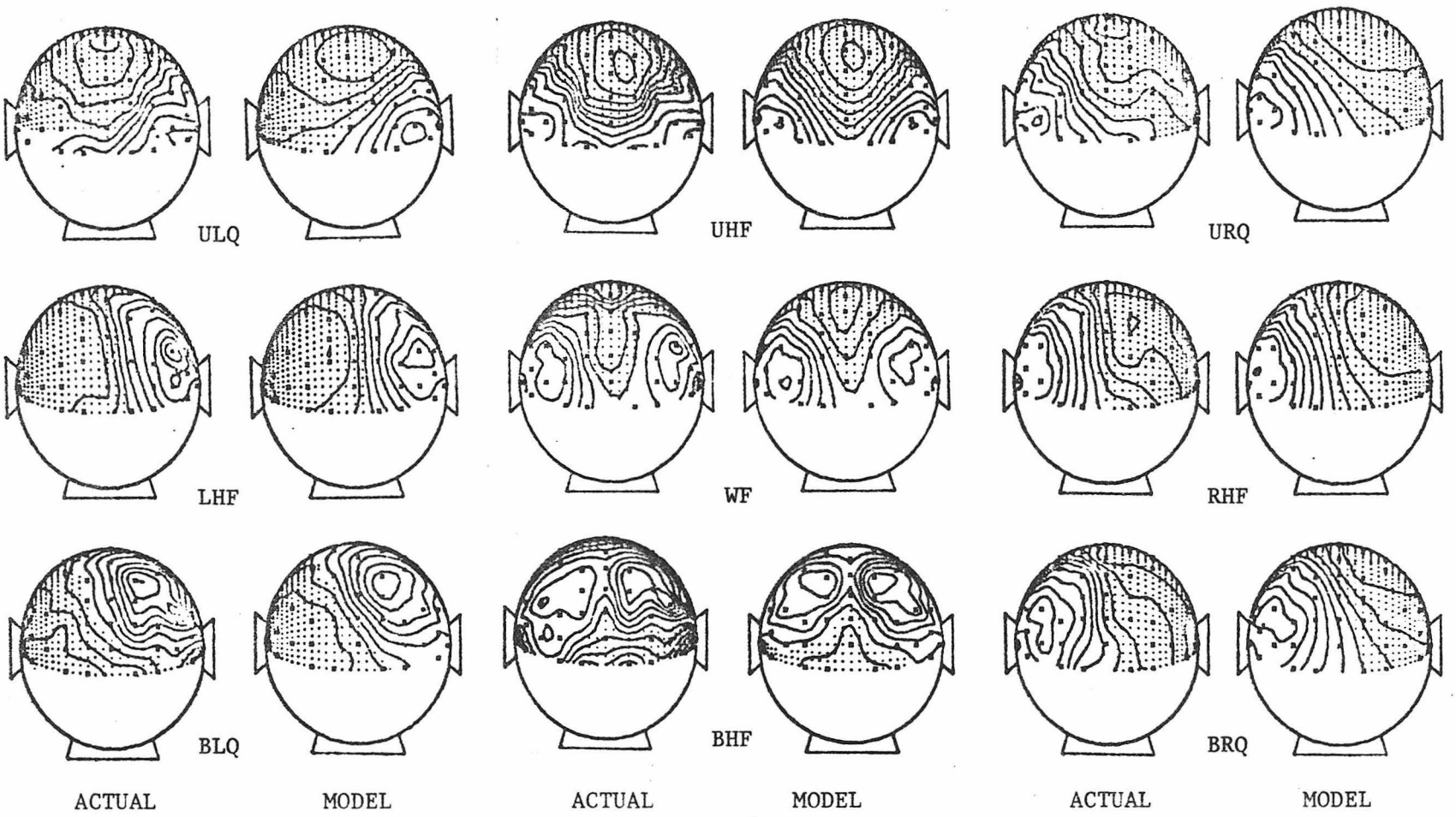

Fig. 112 - Actual and model fields for subject JPA initial peak

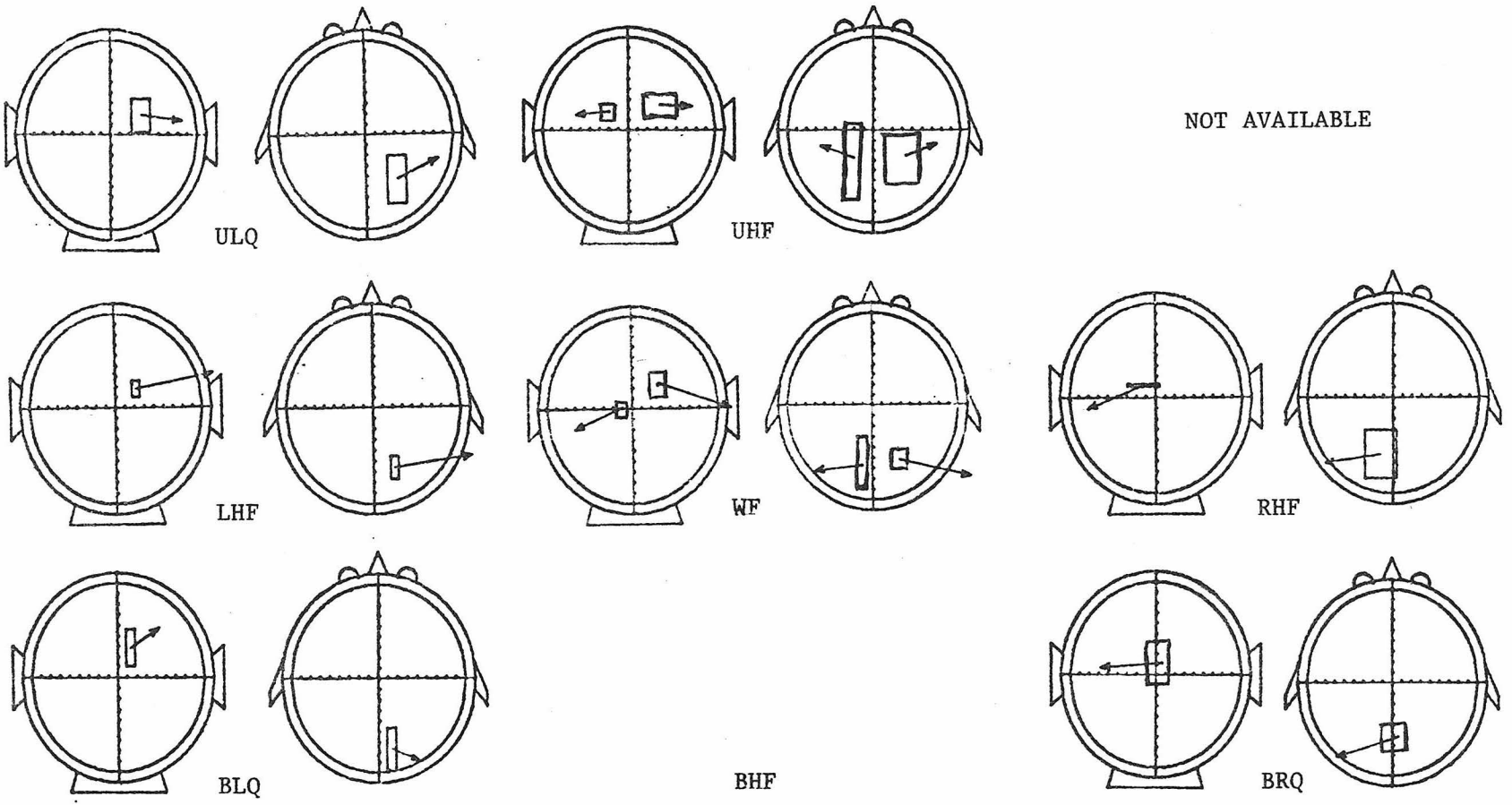

Fig. 113 - 3-shell equivalent dipoles for subject PDP initial peak

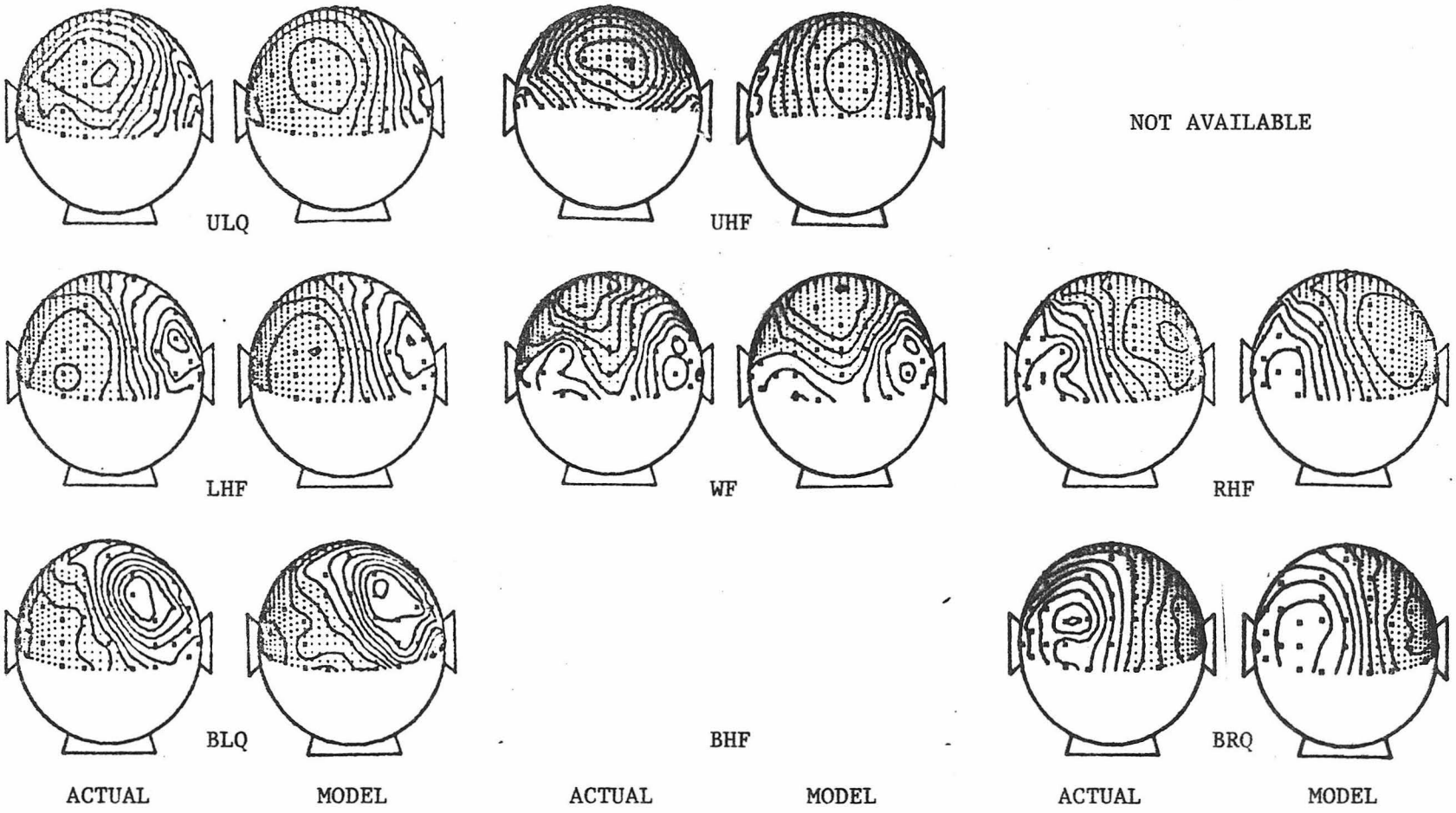

Fig. 114 - Actual and model fields for subject PDP initial peak

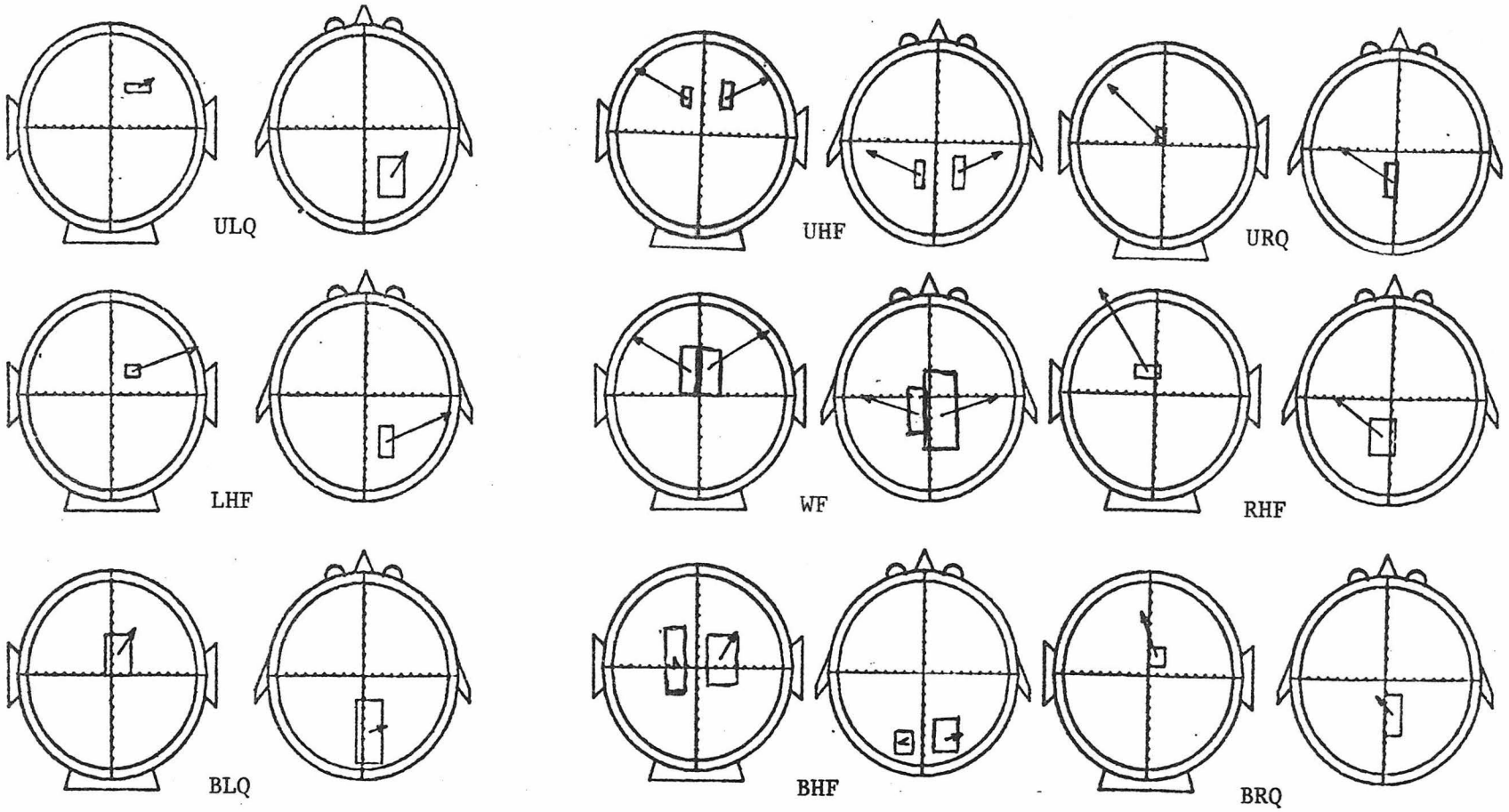

Fig. 115 - 3-shell equivalent dipoles for subject RML initial peak

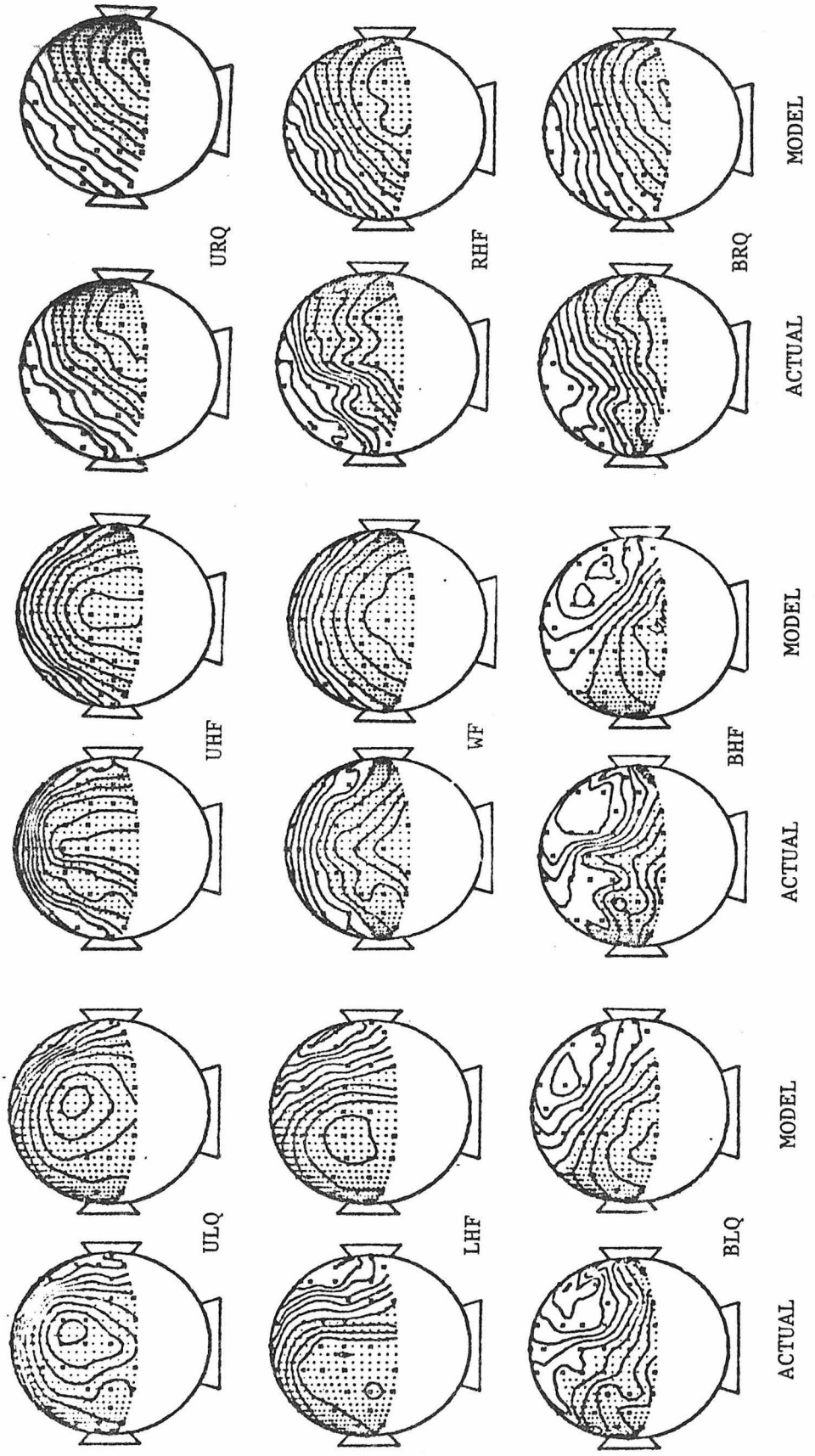

Fig. 116 - Actual and model fields for subject RML initial peak

are much more nearly alike than one would expect on the basis of their evoked potentials.

Figs. 117-122 show the stimulus dependence of equivalent sources (Figs. 117,119,121) and the potential distributions predicted by these sources (Figs. 118,120,122) computed for the secondary peak (120-160msec) in the appearance/disappearance response in each of the three subjects. Here again it can be seen that equivalent dipoles give good fits to the measured evoked potential data and all sources are contralateral (with the exception of JPA URQ). Many of the equivalent sources are located in the same place as the initial peak equivalent sources were located, while their moment vectors point in opposite directions. However, the exceptions to this are ample enough to reject this as a general rule. At any rate, the orientations of the sources generally change a great deal, often by as much as 180 degrees.

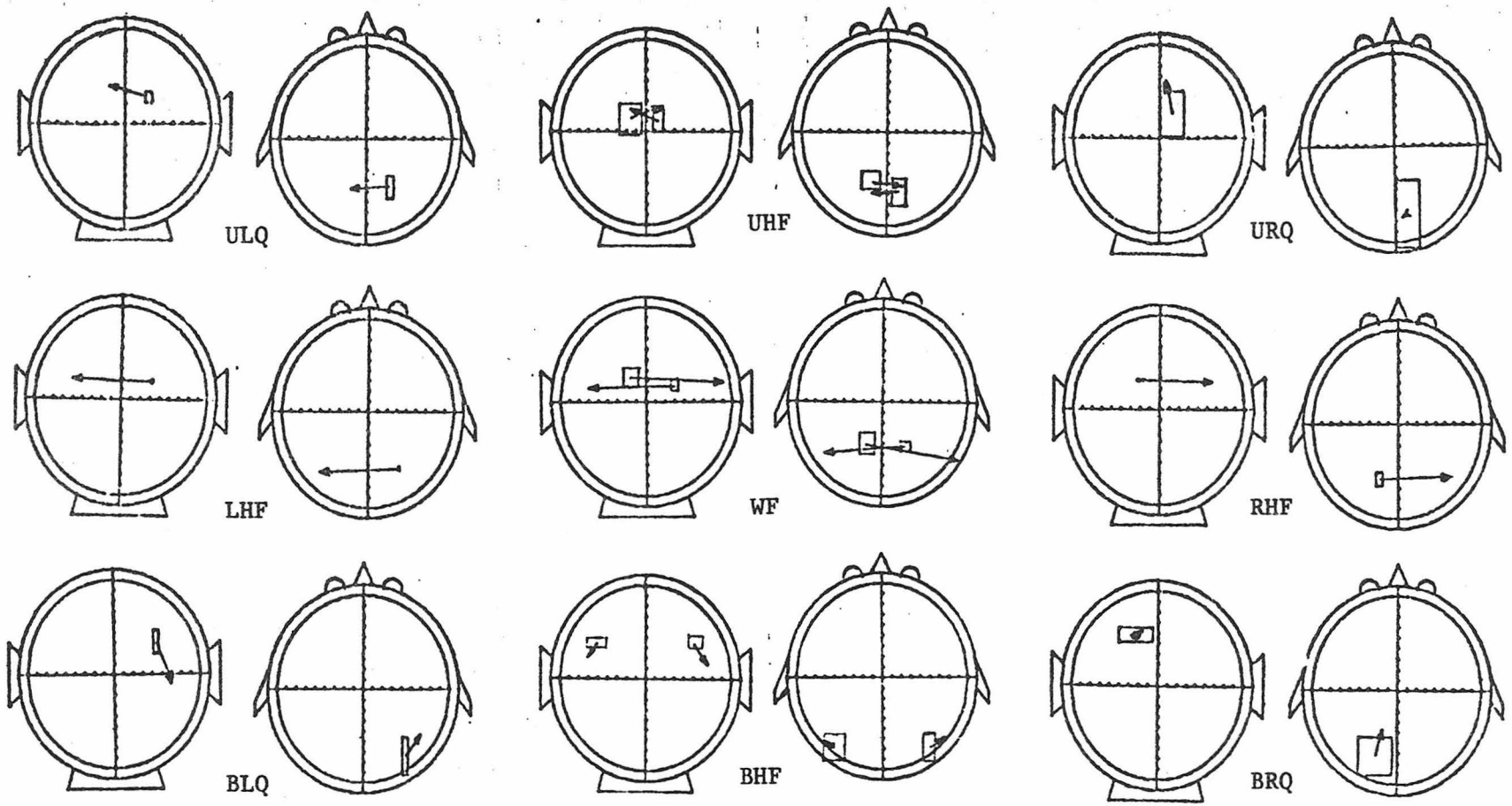

Fig. 117 - 3-shell equivalent dipoles for subject JPA secondary peak

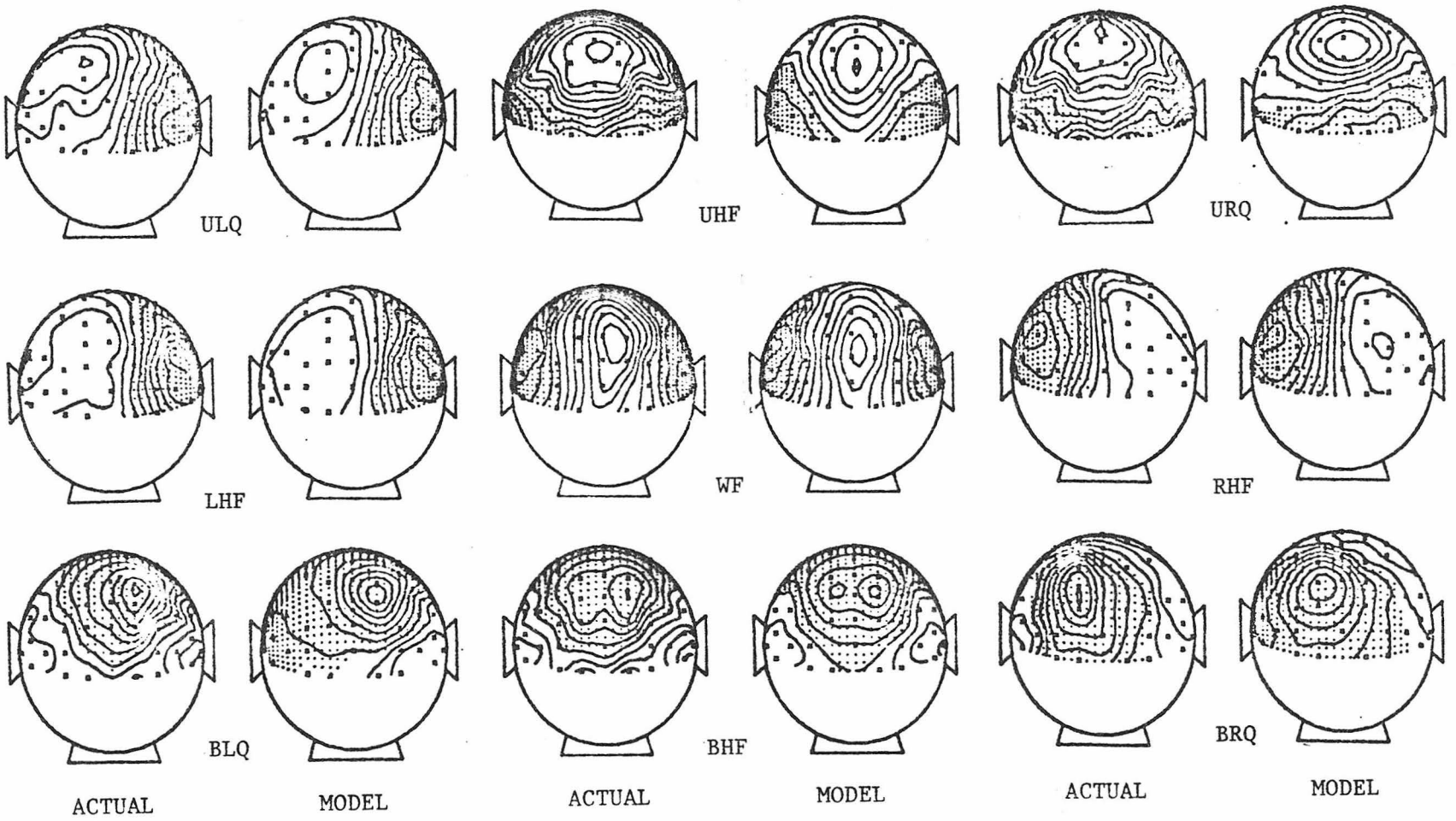

Fig. 118 - Actual and model fields for subject JPA secondary peak

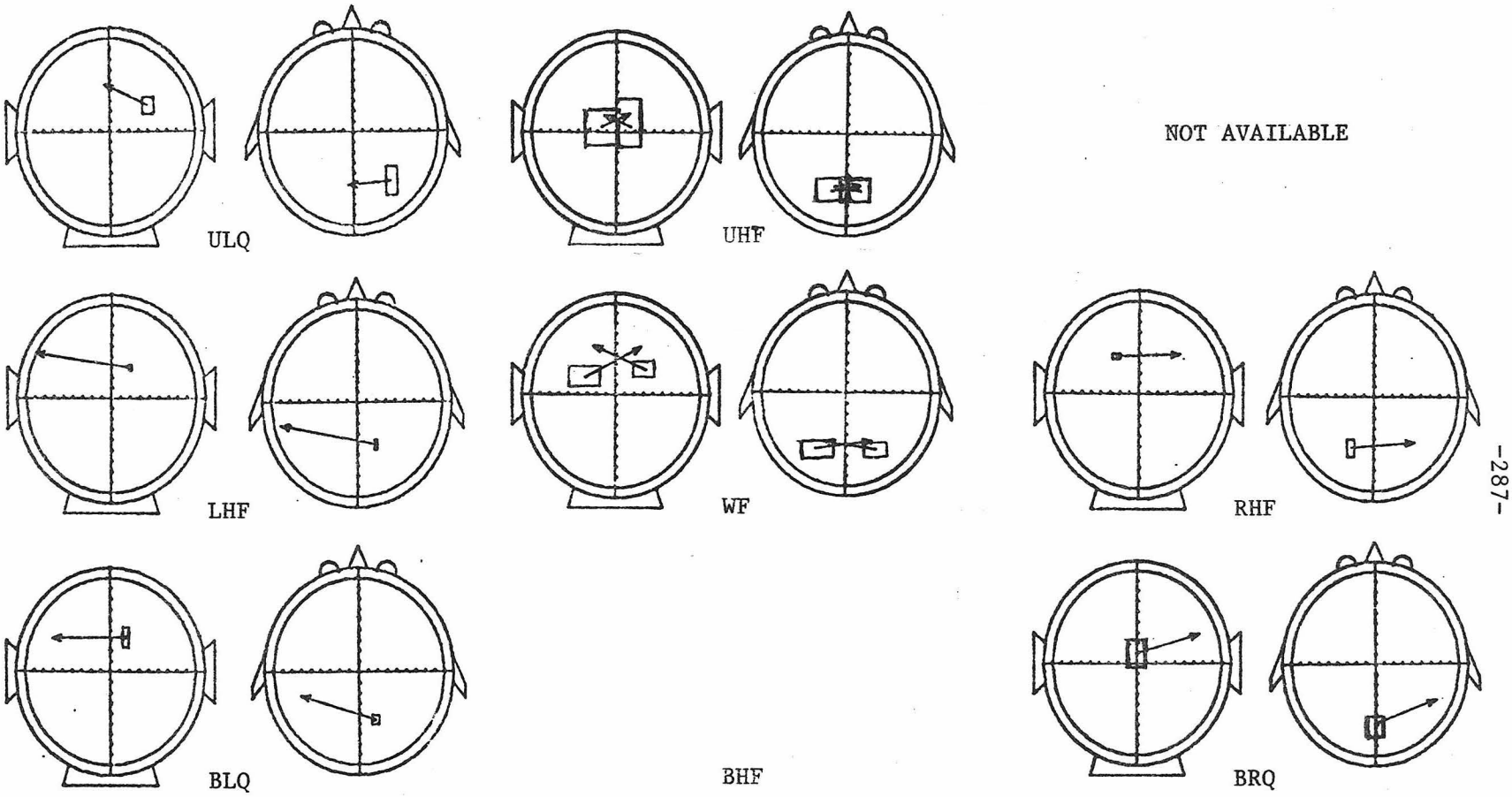

Fig. 119 - 3-shell equivalent dipoles for subject PDP secondary peak

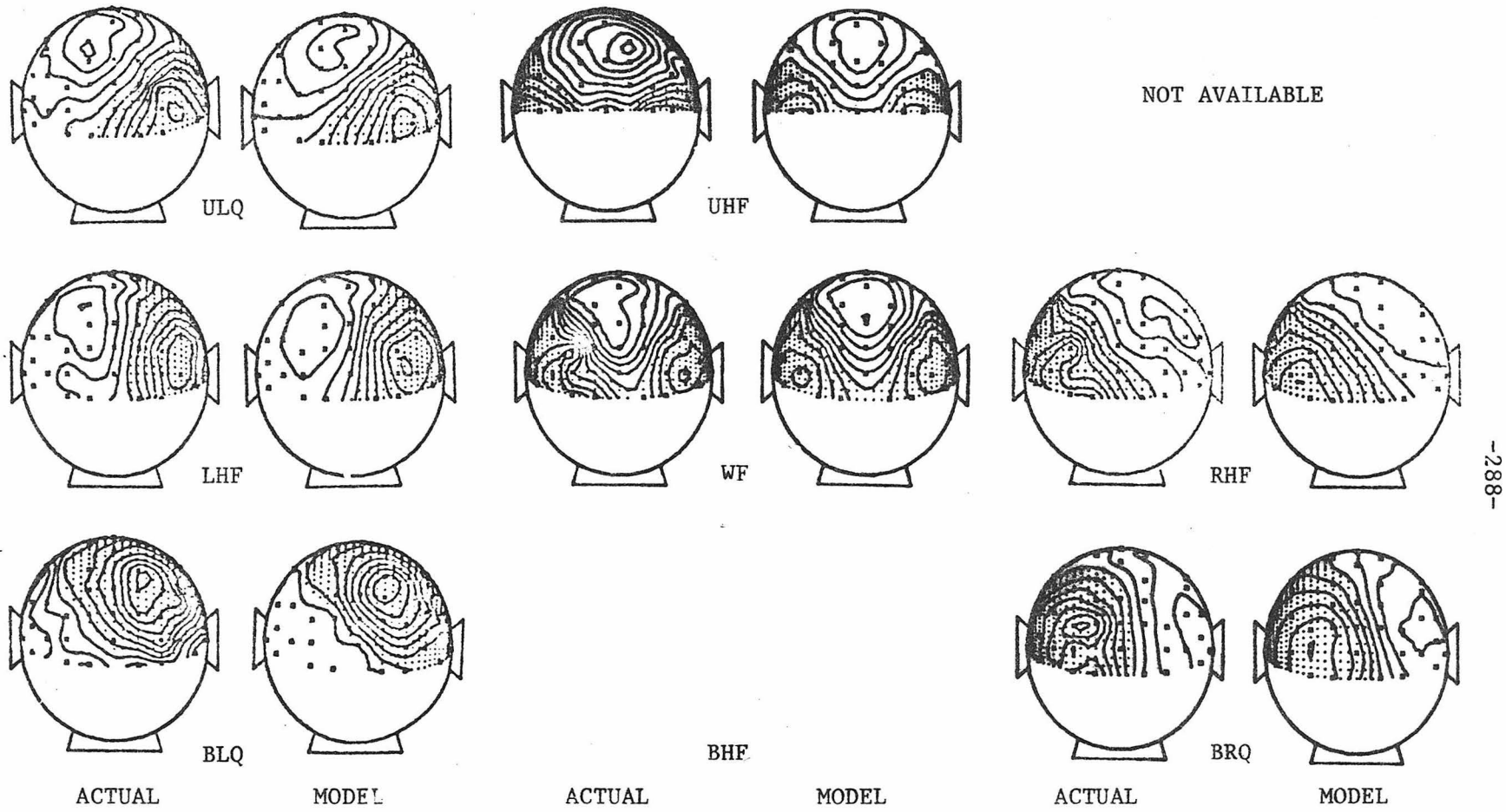

Fig. 120 - Actual and model fields for subject PDP secondary peak

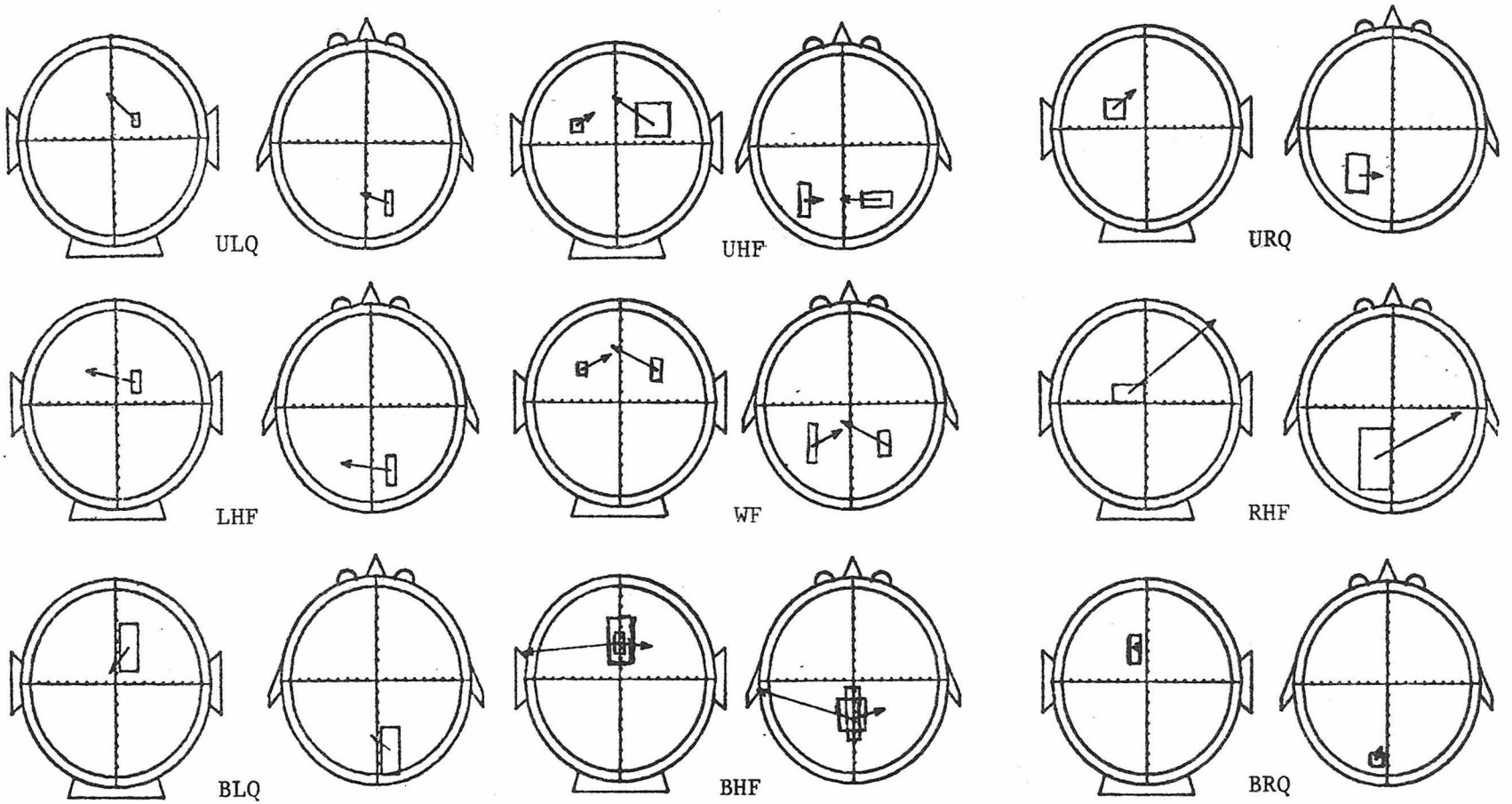

Fig. 121 - 3-shell equivalent dipoles for subject RML secondary peak

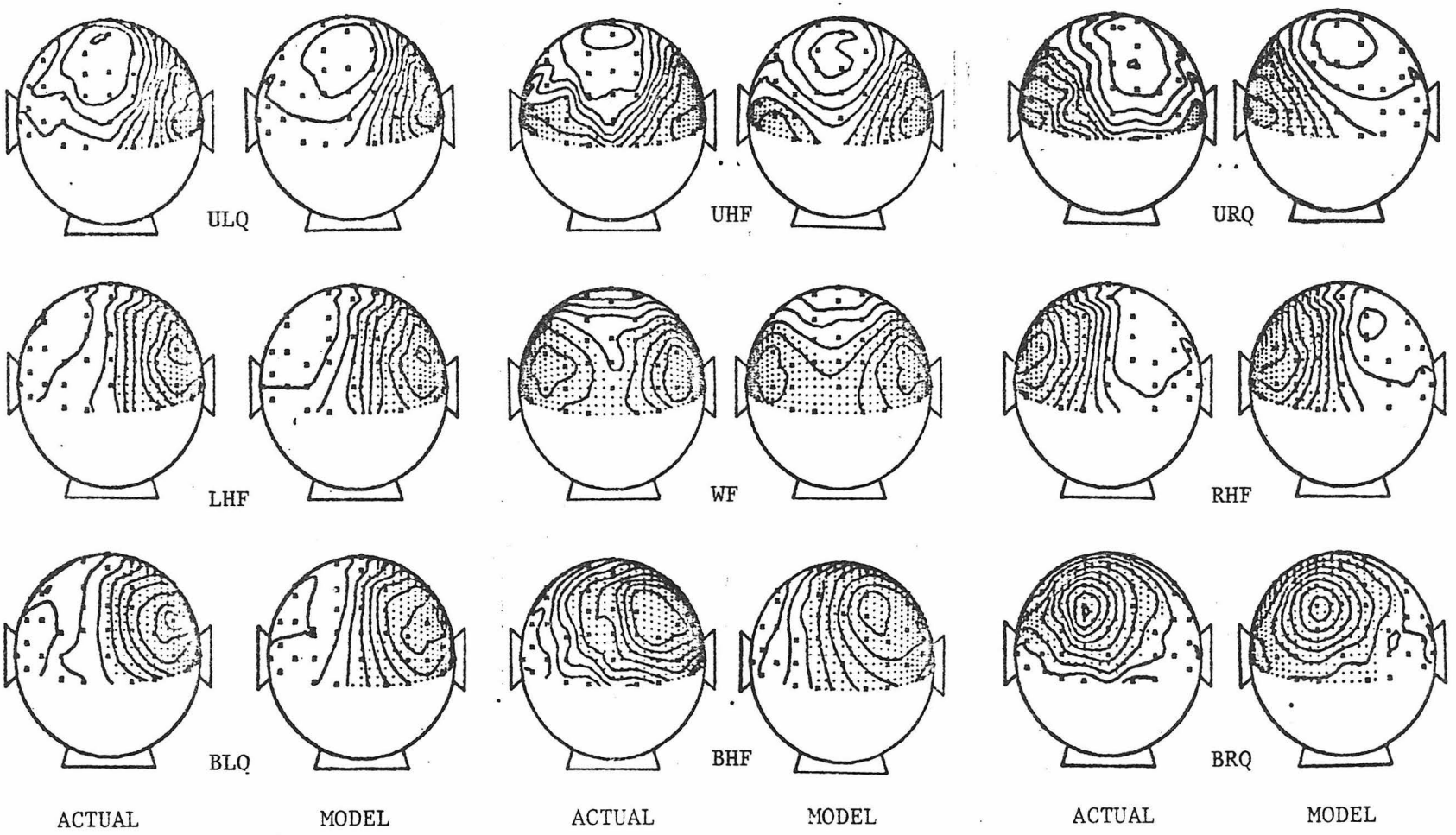

Fig. 122 - Actual and model fields for subject RML secondary peak

5.3 Summary and Discussion

From the preceding it is clear that in the 3 subjects studied equivalent dipole sources depend systematically on stimulus locus. It is also clear that this dependence does not conflict with expectations based on the assumed projections of the visual field on visual cortex and the notion that EP's reflect the topography of the tissues that produce them. Stimuli which should project to both hemispheres give bilateral equivalent sources, while stimuli which should project to one hemisphere give one contralateral source. The decision as to the number of sources indicated can be made objectively, since in all cases either one or the other (but not both) of two models gives a very good fit to the measured data. One and two dipole equivalent source models are adequate for modeling the data in all cases except one (PDP BHF).

The different stimuli give equivalent sources of varying orientation in the rear of the head fairly near the midline. This would not be obvious from the study of evoked potential waveforms or the equipotential maps. For a given stimulus, there are extented periods of time (20-30 msec) in which the position and orientation of the equivalent dipoles remains the same, with their magnitude rising and falling in this time interval. Changes in position or orientation come rather suddenly. This sort of dynamics may be indicative of slow synapto-dendritic processing in one area of the brain followed by rapid axonal transmission to another area.

In considering the first component of the EP, it is seen that there is a hierarchy of orientations for equivalent sources in each hemisphere when the models are viewed from the rear. These are fairly consistent with the cruciform model of striate cortex. Although one subject (RML) differs greatly in absolute orientations, his relative orientations are the same as those of the other two subjects. This may be consistent with known variations in cortical topography. The expected degree of inclination of the equivalent sources is postulated to be that of the surfaces which they are intended to represent. For quadrant stimulation this would depend on the relative amounts of medial (horizontally directed tissue) and intracalcarine (vertically directed tissue) surfaces which contribute. Of course, the same considerations apply to the relative amounts of posteriolateral and medial surfaces, which would presummably affect the orientation of the equivalent source as viewed from above.

Although what is being refered to as the secondary component is often very large and adequately modeled by equivalent dipoles, it is not clear what these may be reflecting, especially in terms of their relationship to the first component. They are indeed contralateral and bilateral when expected and are very often in the same location and 180 degree opposite orientation to those of the first component. Subject RML violates this principle, although his secondary component is very much like that of the other two subjects. Directly opposite orientations would be consistent with the two components having the same origin, for it is quite conceivable that the same tissue could be activated with

processes of opposite polarity at successive times. Subject RML is problematic, since it has been assumed that surface fields are mostly determined by the orientations of the tissues that produce them. One proposal is that the two components come from different but nearby areas, in which it is possible that these areas have the same orientation in one subject and a different orientation in another. Another possibility is that the two components are coming from the same area but from different layers whose distributions of activity differ amongst subjects. In particular, it could be that with respect to the first component, the vertical meridian of the visual field contributes less in subject RML than in the other two subjects, leading to the more'vertically' oriented source seen in subject RML's first component.

In conclusion, it does appear that in spite of the inherent limitations imposed by theoretical non-uniqueness (section 2.1.1), useful information about the origin of VESP's is obtainable from the determination of equivalent dipole sources. The behavior of the equivalent sources does not conflict with expectations based on our knowledge of anatomy and electrophysiology. Both in theory (sections 2.1.5,3.4.6, 3.4.7) and in practice (Chapter 5), the dipole is a good model for the far field potentials which are measureable as VESP's. The method is quantitative and yields information which would be difficult to obtain by other methods. The method is hampered by the lack of a means for assessing individual topographic differences in the intact human. It is, however, quite feasible that computed tomography (CAT Scans) will begin to yield such information in the near future.

REFERENCES

{1} BRENNER, D., WILLIAMSON, S. J. and KAUFMAN, L. Visually evoked magnetic fields of the human brain. Science, 1975, 190:480-481.

{2} BRINDLEY, G. S. Physiology of the Retina and Visual Pathway. Edward Arnold Ltd., London, 1970, pp. 132-138.

{3} JULESZ, B. Foundations of Cyclopean Perception. Univ. of Chicago Press, Chicago, 1971, 406 p.

{4} HELMHOLTZ, H. Uber einige Gesetze der Verthei lung elektrischer Strome in korperlichen Leitern, mit Anwendung auf die thierischelektrischen Versuche. Ann. de Phys. u. Chem., 1853, 29:211-233, 353-377.

{5} WILSON, F. N. and BAYLEY, R. H. The electric field of an eccentric dipole in a homogeneous spherical conducting medium. Circulation, 1950, 1:84-92.

{6} MCFEE, R. and BAULE, G. M. Research in electrocardiography and magnetocardiography. Proc. IEEE, 1972, 60(3):290-321.

{7} PLONSEY, R. Limitations on the equivalent cardiac generator. Biophysic. J., 1966, 6:163-173.

{8} KLEIN, S. Personal communication, 1978.

{9} SMYTHE, W. R. Static and Dynamic Electricity. McGraw-Hill, New York, 1968, 623 pp.

{10} FORSYTHE, G. E. and WASOW, W. R. Finite-Difference Methods for Partial Differential Equations, Wiley, New York, 1960, 444 pp.

{11} MACKAY, D. M. Evoked brain potentials as indicators of sensory information processing. Neurosciences Res. Prog. Bull., 1969, 7(3):189-191.

{12} KELLY, D. L., Jr., GOLDRING, S. and OLEARY, J. L. Average evoked somatosensory responses from exposed cortex in man. Arch. Neurol., 1965, 13:1-9.

{13} SANCES, A., Jr. and LARSON, S. J. Evoked potential recordings an adjunct to human stereotatic surgery. IEEE Trans. bio-med. Engng., 1967, BME-14:162-166.

{14} LEHMANN, D., KAVANAGH, R. N. and FENDER, D. H. Field studies of averaged visually evoked EEG potentials in a patient with a split chiasm. Electroenceph. clin. Neurophysiol., 1969, 26:193-199.

{15} JEWETT, D. L., ROMANO, M. N. and WILLISTON, J. S. Human auditory evoked potentials: possible brainstem components detected on the scalp. Science, 1970, 167:1517-1518.

{16} HOSEK, R. S., SANCES, A., Jr., JODAT, R. W. and LARSON, S. J. The contributions of intracerebral currents to the EEG and evoked potentials. IEEE Trans. bio.-med. Engng., 1978, BME-25:405-413.

{17} VAUGHAN, H. G., Jr. The relationship of brain activity to scalp recordings of event-related potentials. In E. Donchin and D. B. Lindsley (Eds.), Average Evoked Potentials: Methods, Results, Evaluations. Washington D. C.: National Aeronautics and Space Administration, NASA SP-191, 1969, pp. 45-94.

{18} MORRELL, F. and MORRELL, L. Computer aided analysis of brain electrical activity. In L. D. Proctor and W. R. Adey (Eds.), The Analysis of Central Nervous System and Cardiovascular Data Using Computer Methods. Washington D. C.: NASA, 1965, pp. 441-478.

{19} SCHWAN, H. P. and KAY, C. F. The conductivity of living tissues. Ann. N. Y. Acad. Sci., 1957, 65:1007-1013.

{20} PLONSEY, R. and HEPPNER, D. B. Considerations of quasi-stationarity in electrophysiological systems. Bull. Math Biophys., 1967, 29:657-664.

{21} MACKAY, pp. 199-204.

{22} HOLSHEIMER, J. and FEENSTRA, B. W. Volume conduction and EEG measurements within the brain: A quantitative approach to the influence of electrical spread on the linear relationship of activity measured at different locations. Electroenceph. clin. Neurophysiol., 1977, 43:52-58.

{23} GELERNTER, H. L. and SWIHART, J. C. A mathematical-physical model of the genesis of the electrocardiogram. Biophys. J., 1964, 4:285-301.

{24} HAVSTAD, J. W. Personal communication, 1977.

{25} CHILDERS, D. G., MESA, W. and HALPENY, O. S. A neuronal model for and simulation of spatio-temporal evoked EEG's. IEEE Trans. Syst., Man, and Cybern., 1973, SMC-3:336-348.

{26} FREEMAN, W. J. Mass Action of the Nervous System. Academic Press, New York, 1975, pp. 177-180.

{27} ABRAHAM, K. and AJMONE-MARSON, C. Patterns of cortical discharge and their relation to routine scalp electrencephalography. Electroenceph. clin. Neurophysiol., 1958, 22:378-380.

{28} COBB, W. and SEARS, T. A. A study of the trasmission of potentials after hemispherectomy. Electroenceph. clin. Neurophysiol., 1960, 12:371-383.

{29} RAYPORT, M., VAUGHAN, H. G., Jr., and ROSENGART, C. L. Simultaneous recording of visual averaged evoked response to flash from scalp and calcarine cortex in man. Electroenceph. clin.

Neurophysiol., 1964, 17:608.

{30} COOPER, R., WINTER, A. L., CROW, H. J. and WALTER, W. G. Comparison of subcortical and scalp activity using chronically indwelling electrodes in man. Electroenceph. clin. Neurophysiol., 1965, 18:217-228.

{31} HEATH, R. G. and GALBRAITH, G. C. Sensory evoked responses recorded simultaneously from human cortex and scalp. Nature, 1966, 212:1535-1537.

{32} CORLETTO, F., GENTILOMO, A., ROSADINI, G., ROSSI, G. F. and ZATTONI, J. Visual evoked potentials as recorded from the scalp and from the visual cortex before and after surgical removal of the occipital pole in man. Electroenceph. clin. Neurophysiol., 1967, 22:378-380.

{33} CREUTZFELDT, O. D. and KUHNT, U. Visual evoked potentials in animals. In R. Jung (Ed.), Handbook of Sensory Physiology - Vol. 7/3B - Central Processing of Visual Information, Springer-Verlag, New York, 1973, pp. 595-646.

{34} REGAN, D. Evoked Potentials in Psychology, Sensory Physiology and Clinical Medicine. Wiley & Sons, New York, 1972, pp. 18-25.

{35} COWAN, J.D. Stochastic models of neuroelectric activity. Unknown reference, pp. 109-127.

{36} BONIN, G. VON, GAROL, H. W. and MCCULLOCH, W. S. The functional organization of the occipital lobe. Biol. Symposia, 1942, 7: 165-192.

{37} EBNER, F. F. and MEYERS, R. E. Distribution of corpus callosum and anterior commissure in cat and raccoon. J. comp. Neurol., 1965, 124:353-375.

{38} GRECO, E. C., Jr. and CLARK, J. W., Jr. The field from an isolated nerve in a volume conductor. IEEE Trans. bio-med. Engng., 1977, BME-24:18-23.

{39} RALL, W. Electrophysiology of dendritic neuron model. Biophysics J., 1962, 2:145-167.

{40} FREEMAN, pp. 202-249.

{41} BISHOP, G. H. Potential phenomena in thalamus and cortex. Electroenceph. clin. Neurophysiol., 1949, 1:421-436.

{42} CLARK, W. E. Le Gros. Observation on the association fiber system of the visual cortex and central representation of the retina. J. Anat., 1941, 75:225-235.

{43} LANDAU, W. M. Evoked potentials. In G. C. Quarton, T. Melnechuk and F. O. Schmitt (Eds.), The Neurosciences - A Study Program, Rockefeller Univ. Press, New York, 1967, pp. 469-482.

{44} CREUTZFELDT, O. D., ROSINA, A., ITO, M. and PROBST, W. Visual evoked response of single cells and of the EEG in primary visual area of the cat. J. Neurophysiol., 1969, 32:127-139.

{45} WITWER, J. G., TREZEK, G. J. and JEWETT, D. L. The effect of media inhomogeneities upon intracranial electrical fields. IEEE Trans. bio-med. Engng., 1972, BME-19:352-362.

{46} HAVSTAD, J. W. Measurement of cellular and extracellular parameters of cerebral cortex by analysis of cortical impedance. Paper presented at Seventh Annual Meeting of the Society for Neuroscience, Anaheim, California, 1977.

{47} NICHOLSON, P. W. The specific impedance of cerebral white matter. Expt'l. Neurol., 1965, 13:386-401.

{48} RUSH, S. and DRISCOLL, D. A. Current distribution in the brain from surface electrodes. Anesthesia and Analgesia - Current Researches, 1968, 47(6):717-723.

{49} RUSH, S. and DRISCOLL, D. A. EEG electrode sensitivity - An application of reciprocity. IEEE Trans. bio-med. Engng., 1969, BME-16:15-22.

{50} ARTHUR, R. M. and GESELOWITZ, D. B. Effect of inhomogeneities on the apparent location and magnitude of a cardiac dipole source. IEEE Trans. bio-med. Engng., 1970, BME-17:141-146.

{51} SCHNEIDER, M. Effect of inhomogeneities on surface signals coming from a cerebral dipole source. IEEE Trans. bio-med. Engng., 1974, BME-21:52-54.

{52} HENDERSON, C. J., BUTLER, S. R. and GLASS, A. The localization of the equivalent dipoles of EEG sources by the application of electric field theory. Electroenceph. clin. Neurophysiol., 1975, 39:117-130.

{53} VAUGHAN, H. G., Jr. The analysis of scalp-recorded brain potentials. In R. F. Thompson and M. M. Patterson (Eds.), Bioelectric Recording Techniques (Part B), 1974, pp. 157-207, Academic Press, New York, Chapter 4.

{54} BRAZIER, M. A. B. A study of the elctrical field at the surface of the head. Electroenceph. clin. Neurophysiol., 1949, 2(Suppl): 38-52.

{55} SHAW, J. C. and ROTH, M. Potential distribution analysis. II. A theoretical consideration of its significance in terms of electric field theory. Electroenceph. clin. Neurophysiol., 1955, 7:285-292.

{56} GEISLER, C. D. and GERSTEIN, G. L. The surface EEG in relation to its sources. Electroenceph. clin. Neurophysiol., 1961, 13: 927-934.

{57} FOURMENT, A., JAMI, L., CALVET, J. et SCHERRER, J. Comparaison de l'EEG recueilli sur le scalp avec l'activité élémentaire des dipoles corticaux radiares. Electroenceph. clin. Neurophysiol., 1965, 19:217-229.

{58} RISTANOVIC, D. The human visual cortex as a system of four generators. Acta Med. Iug., 1971, 25:379-395.

{59} RISTANOVIC, D. Four dipole mathematical model of visual cortex electrogenesis. Periodicum Biologorum, 1972, 74:9-20.

{60} VAUGHAN, H. G., Jr., COSTA, L. D. and RITTER, W. Topography of the human motor potential. Electroenceph. clin. Neurophysiol., 1968, 25:1-10.

{61} VAUGHAN, H. G., Jr., and RITTER, W. The sources of auditory evoked responses recorded from the human scalp. Electroenceph. clin. Neurophysiol., 1970, 28:360-367.

{62} HALLIDAY, A. M. and MICHAEL, W. F. Changes in pattern-evoked responses in man associated with the vertical and horizontal meridians of the visual field, J. Physiol., 1970, 208:499-513.

{63} MICHAEL, W. F. and HALLIDAY, A. M. Differences between the occipital distribution of upper and lower field pattern-evoked responses in man. Brain Res., 1971, 32:311-324.

{64} JEFFREYS, D. A. and AXFORD, J. G. Source locations of pattern-specific components of human visual evoked potentials. I. Component of striate cortical origin. Exp. Brain Res., 1972 a, 16:1-21.

{65} JEFFREYS, D. A. and AXFORD, J. G. Source locations of pattern-specific components of human visual evoked potentials. II. Component of extrastriate cortical origin. Exp. Brain Res., 1972 b, 16:22-40.

{66} NAKAMURA, F. and BIERSDORF, W. R. Localization of the human visual evoked response. Early components specific to visual stimulation. Amer. J. Ophth., 1971, 72:988-997.

{67} BIERSDORF, W. R. and NAKAMURA, F. Localization studies of the human visual evoked response. Xth ISCERG Symposium, Doc. Ophth. Proc., 1973, Ser. 2:137-144.

{68} BIERSDORF, W. R. Cortical evoked responses from stimulation of various regions of the visual field. XIth ISCERG Symposium, Doc. Ophth. Proc., 1974, Ser. 3:249-259.

{69} ARY, J. P. The effect of color on the localization of the sources of the human visual evoked response. Ph. D. Dissertation, Ohio State University, 1976, 101 p.

{70} SCHNEIDER, M. et GERIN, P. Une méthode de localisation des dipôles cérébaux. Electroenceph. clin. Neurophysiol., 1970, 28:69-78.

{71} SCHNEIDER, M. A multistage process for computing virtual dipolar sources of EEG discharges from surface information. IEEE Trans. bio-med. Engng., 1972, BME - 19:1-12.

{72} HENDERSON, C. J., BUTLER, S. R. and GLASS, A. Abstract of presentation given at EEG Society meeting in London on 15 Jan. 1977.

{73} KAVANAGH, R. N. Localization of sources of human evoked responses. Ph.D. Dissertation, California Institute of Technology, 1972, 280 p.

{74} TEUBER, H.-L., BATTERSBY, W. S. and BENDER, M. B. Visual Field Defects After Penetrating Missile Wounds of the Brain. Harvard Univ. Press, Cambridge, Mass., 1960, 143 p.

{75} SZENTÁGOTHAI, J. Neuronal and synaptic architecture of the lateral geniculate nucleus. In R. Jung (Ed.) Handbook of Sensory Physiology - Vol. 7/3B - Central Processing of Visual Information, Springer-Verlag, New York, 1973, pp. 141-176.

{76} ALLMAN, J. Evolution of the visual system in early primates. In J. Sprague and A. Epstein (Eds.), Progress in Physiological Psychology, Academic Press, 1977, in press, 88 p.

{77} WILSON, M. E. and CRAGG, B. G. Projections of the lateral geniculate nucleus in the cat and monkey. J. Anat., 1967, 101:677-692.

{78} FREUND, H.-J. Neuronal mechanisms of the lateral geniculate body. In R. Jung (Eds.) Handbook of Sensory Physiology - Vol. 7/3B - Central Processing of Visual Information, Springer-Verlag, New York, 1973, pp. 177-246.

{79} SPRAGUE, J. M., BERLUCCHI, G. and RIZZOLATTI, G. The role of the superior colliculus and pretectum in vision and visually guided behavior. In R. Jung (Ed.) Handbook of Sensory Physiology - Vol. 7/3B - Central Processing of Visual Information, Springer-Verlag, New York, 1973, pp. 27-101.

{80} DOTY, R. W. Ablation of visual areas of the central nervous system. In R. Jung (Ed.), Handbook of Sensory Physiology - Vol. 7/3B - Central Processing of Visual Information, Springer-Verlag, New York, 1973, pp. 483-541.

{81} SCHILLER, P. Personal communication, 1978.

{82} SCHWARTZ, E. L. Spatial mapping in the primate sensory projection: Analytic structure and relevance to perception. Biol. Cybernetics, 1977, 25:181-194.

{83} HUBEL, D. H. and WIESEL, T. N. Sequence regularity and geometry of orientation columns in the monkey striate cortex. J. comp. Neurol., 1974a, 158:267-293.

{84} HUBEL, D. H. and WIESEL, T. N. Uniformity of monkey striate cortex: A parallel relationship between field size, scatter and magnification factor. J. comp. Neurol., 1974b, 158:295-302.

{85} ZEKI, S. M. Functional specialization in the visual cortex of the rhesus monkey. Nature, 1978, 274:423-428.

{86} SPALDING. J. M. K. Wounds of the visual pathway. J. Neurol. Neurosurg. Psychiat., 1952, 15:99-109, 15:169-183.

{87} BRINDLEY, G. S. Sensory effects of electrical stimulation of the visual and paravisual cortex in man. In R. Jung (Ed.), Handbook of Sensory Physiology-Vol. 7/3B - Central Processing of Visual Information, Springer-Verlag, New York, 1973, pp. 583-594.

{88} BRINDLEY, G. S., DONALDSON, P. E. K., FALCONER, M. A. and RUSHTON, D. N. The extent of the region of occipital cortex that when stimulated gives phosphenes fixed in the visual field. J. Physiol., 1972, 225:57P-58P.

{89} MARG, E. Recording from single cells in the human visual cortex. In R. Jung (Ed.), Handbook of Sensory Physiology - Vol. 7/3B - Central Processing of Visual Information, Springer-Verlag, New York , 1973, pp. 441-449.

{90} BRINDLEY, G. S. The variability of human striate cortex. J. Physiol., 1972, 225:1P-3P.

{91} POLYAK, S. The Vertebrate Visual System. Univ. of Chicago Press, Chicago, 1957, pp. 460-466.

{92} DUKE ELDER, S. and WYBAR, K. C. The Anatomy of the Visual System Vol. II, Henry Kimpton, London, 1961, p. 657.

{93} MORRELL, F. Electrical signs of sensory coding. In G. C. Quarton, T. Melnechuk and F. O. Schmitt (Eds.), The Neurosciences-A Study Program, Rockefeller Univ. Press, New York, 1967, pp. 452-469.

{94} CHATRIAN, G. E., BICKFORD, R. G. and UIHLEIN, A. Depth electrographic study of a fast rhythm evoked from the human calcarine region by steady illumination. Electroenceph. clin. Neurophysiol., 1960, 12:167-176.

{95} PEREZ-BORJA, C., CHATRIAN, G. E., TYCE, F. A. and RIVERS, M. H. Electrographic patterns of the occipital lobe in man: A topographic study based on use of implanted electrodes. Electroenceph. clin. Neurophysiol., 1962, 14:171-182.

{96} HIRSCH, J. F., PERTUISET, B., CALVET, J., BUISSON-FEREY, J., FISCHGOLD, H. et SCHERRER, J. Étude des résponses électrocorticales obtenues chez l'homme par des stimulations somesthétiques et visuelles. Electroenceph. clin. Neurophysiol., 1961, 13:411-424.

{97} VAUGHAN, H. G., Jr. The perceptual and physiologic significance of visual evoked responses recorded from the scalp in man. In H. M. Burian and J. H. Jacobson (Eds.), Clinical Electroretinography, Pergamon Press, New York, 1966, pp. 203-223.

{98} VAUGHAN, H. G., Jr. and KATZMAN, R. Evoked response in visual disorders. Ann N. Y. Acad. Sci., 1964, 112:305-319

{99} KOOI, D. A., GUVENER, A. M. and BAGGHI, B. K. Visual evoked responses in lesions of the high optic pathways. Neurology, 1965, 15:841-854.

{100} WEISKRANTZ, L. and COWEY, A. Striate cortical lesions and visual acuity in the rhesus monkey. J. Comp. Physiol., 1963, 53(2): 225-231.

{101} BRINDLEY, G. S., GAUTIER-SMITH, P. C. and LEWIN W. Cortical blindness and the functions of the non-geniculate fibers of the optic tracts. J. Neurol. Neurosurg. Psychiat., 1969, 32:259-264.

{102} REGAN, p. 169.

{103} KOOI, K. A. and SHARBROUGH, F. W. Electrophysiological findings in a case of cortical blindness - A report of a case. Electroenceph. clin. Neurophysiol., 1966, 20:260-263.

{104} SPEHLMANN, R., GROSS, R., HO, S., LEESTMAN, J. and NORCROSS, K. Visual evoked responses and postmortem findings in a case of cortical blindness. Ann. Neurol, 1977, 1:509.

{105} BODIS-WOLLNER, I., ATKIN, A., RAAB, E. and WOLKSTEIN, M. Visual association cortex and vision in man: Pattern-evoked occipital potentials in a blind boy. Science, 1977, 198:629-631.

{106} VAUGHAN, H. G., Jr. and GROSS, C. G. Cortical responses to light in unanesthetized monkeys and their alteration by visual system lesions. Exp. Brain Res., 1969, 8:19-36.

{107} COHN, R. Visual evoked responses in the brain injured monkey. Arch. Neurol., 1969, 21:321-329.

[108] BOYNTON, R. M. Stray light and the human electroretinogram. J. Opt. Soc. Am., 1953, 43:442-449.

[109] JACOBSON, J. H., KAWASAKI, K. and HIROSE, T. The human electroretinogram and occipital potential in response to focal illumination of the retina. Invest. Ophthal., 1969, 8(5):545-556.

[110] REGAN, pp. 52-65.

[111] HUBEL, D. H. and WIESEL, T. N. Receptive fields, binocular interaction and functional architecture of the cats visual cortex. J. Physiol, 1962, 160:106-154.

[112] HUBEL, D. H. and WIESEL, T. N. Receptive fields and functional achitecture of two non-striate visual areas (18 and 19) of the cat. J. Neurophysiol., 1965, 28:1041-1059.

[113] HUBEL, D. H. and WIESEL, T. N. Receptive fields and functional architecture of monkey striate cortex. J. Physiol., 1968, 195:215-243.

[114] COPENHAVER, R. M. and PERRY, N. M., Jr. Factors affecting visually evoked cortical potentials such as impaired vision of varying etiology. Invest. Ophthal., 1964, 3:665-675.

[115] DEVOE, R. G., RIPPS, H. and VAUGHAN, H. G., Jr. Cortical responses to stimulation of the human fovea. Vision Res., 1968, 8:135-147.

[116] REITVELD, W. J., TORDOIR, W. E. M. and DUYUFF, J. W. Contribution of the fovea and parafovea to the visual evoked response. Acta Physiol. Pharmacol. Neerl., 1965, 13:330-339.

[117] EASON, R. G. and WHITE, C. T. Averaged occipital responses to stimulation of sites in the nasal and temporal halves of the retina. Psychon. Sci., 1967, 7(9):309-310.

[118] VAUGHAN, H. G., Jr. and SILVERSTEIN, L. Metacontrast and evoked potentials: A reappraisal. Science, 1968, 160:207-208.

119] JEFFREYS, D. A. in MACKAY, pp. 214-215.

120] SCHREINEMACHERS, H. P. and HENKES, H. E. Relation between localized retinal stimuli and the visual evoked response in man. Ophthalmologica, 1968, 155:17-27.

121] REITVELD, W. J., TORDOIR, W. E. M., HAGENOUW, J. R. B. and VAN DONGEN, W. K. J. Contribution of foveal and extrafoveal quadrants to the visual evoked response. Acta Physiol. Pharmacol. Neerl., 1965, 13:340-347.

[122] NAGATA, M. and JACOBSON, J. Combined ERG and occipital response recording. In H. M. Burian and J. H. Jacobson (Eds.), Clinical Electroretinography, Pergamon Press, New York, 1966, pp. 235-248.

[123] EASON, R. G., GROVES, P., WHITE, C. T. and ODEN, D. Evoked cortical potentials: Relation to visual field and handedness. Science, 1967, 156:1643-1646.

{124] LESÈVRE, N. and RÉMOND, A. Study of the visual field by average evoked potentials. Electroenceph. clin. Neurophysiol., 1968, 25:512.

{125] JEFFREYS, D. A. Cortical source locations of pattern-related visual evoked potentials recorded from the human scalp. Nature, 1971, 229:502-504.

{126] REITVELD, W. J., TORDOIR, W. E. M., HAGENOUW, J. R. B., LUBBERS, J. A. and SPOOR, Th. A. C. Visual evoked responses to blank and to checkerboard patterned flashes. Acta Physiol. Pharmacol. Neerl., 1967, 14:259-285.

{127} COBB, W. A. and MORTON, H. B. Evoked potentials from the human scalp to visual half-field stimulation. J. Physiol., 1970, 208: 39P-40P.

{128} SHAGASS, C. AMADEO, M. and ROEMER, R. A. Spatial distribution of potentials evoked by half-field pattern-reversal and pattern-onset stimuli. Electroenceph. clin. Neurophysiol., 1976, 41: 609-622.

{129} BARRETT, G. BLUMHARDT, L., HALLIDAY, A. M., HALLIDAY, E. and KRISS, A. A paradox in the localization of the visual evoked response. Nature, 1976, 261:253-255.

{130} LEHMANN, D., MELES, H. P. and MIR, Z. Average multichannel EEG potential fields evoked from upper and lower hemi-retina: latency differences. Electroenceph. clin. Neurophysiol., 1977, 43:725-731.

{131} WEISS, G. H. and FISCHMANN, E. J. Effect of surface electrode number on estimates of cardiac dipole moment. IEEE Trans. bio-med. Engng.,1970, BME-17:58-65.

{132} ESTEVEZ, O. and SPEKREIJSE, H. Relationship between pattern appearance-disappearance and pattern reversal responses. Exp. Brain Res., 1974, 19:233-238.

{133} WESTHEIMER, G. The Maxwellian view. Vision Res., 1966, 6: 669-682.

{134} MACKAY, D. M. and JEFFREYS, D. A. Visually evoked potentials and visual perception in man. In R. Jung (Ed.), Handbook of Sensory Physiology - Vol. 7/3B - Central Processing of Visual Information. Springer - Verlag, New York, 1973, p. 665.

{135} REGAN, pp. 59-61.

{136} PLONSEY, R. Current dipole images and reference potentials. IEEE Trans. bio-med. Electronics, 1963, BME-10:3-8.

{137} OSSELTON, J. W. Acquisition of EEG data by bipolar, unipolar and average reference methods: A theoretical comparison. Electroenceph. clin. Neurophysiol., 1965, 19:527-528.

{138} SOKOL, S. Visual evoked potentials: theory, techniques and clinical applications. Survey of Ophthalmology, 1976, 21(1):18-44.

{139} GOLDMAN, D. The clinical use of the "average" reference electrode in monopolar recording. EEG Clin. Neurophysiol., 1950, 2:211-214.

{140} OFFNER, F. F. The EEG as potential mapping: the value of the average monopolar reference. EEG Clin. Neurophysiol., 1950, 2: 215-216.

{141} LEHMANN, D. Multichannel topography of human alpha EEG fields. Electroenceph. clin. Neurophysiol., 1971, 31:439-449.

{142} ARY, J. P. A head-mounted 24-channel evoked potential preamplifier employing low-noise operational amplifiers. IEEE Trans. bio-med. Engng., 1977, BME-24:293-297.

{143} TOBY, G. E., GRAEME, J. G. and HUELSMAN, L. P. (Eds.). Operational Amplifiers: Design and Applications. McGraw-Hill, New York, 1971, 473 p.

{144} REGAN, pp. 244-246.

{145} PAPOULIS, A. Probability, Random Variables, and Stochastic Processes. McGraw-Hill, New York, 1965, 583 p.

{146} BRAZIER, M. A. B. Evoked responses recorded from the depths of the human brain. Ann. N. Y. Acad. Sciences, 1964, 112:33-59.

{147} VIDAL, J. J. Real time detection of brain events in EEG. Proc. IEEE, 1977, 65:633-641.

{148} RUCHKIN, D. S. An analysis of average response computations based upon aperiodic stimuli. IEEE Trans. bio-med. Engng., 1965, BME-12: 87-94.

{149} BORDA, R. P. and FROST Jr., J. D. Error reduction in small sample averaging through the use of the median rather than the mean. Electroenceph. clin. Neurophysiol., 1968, 25:391-392.

{150} WALTER, D. O. Two approximations to the median evoked response. Electroenceph. clin. Neurophysiol., 1971, 30:246-274.

{151} ERTL, J. P. Evoked potential recovery from tape recorded zero crossings of the EEG. Electroenceph. clin. Neurophysiol., 1967, 22:387-388.

{152} RUCHKIN, D. S. Comparison of statistical errors of the median and average evoked responses. IEEE Trans. bio-med. Engng., 1974, BME-21:54-56.

{153} PIERCE, J. R. Personal Communication, 1976.

{154} RUCHKIN, D. S. and WALTER, D. O. A shortcoming of the median evoked response, IEEE Trans. bio-med. Engng., 1965, BME-22:245.

{155} REGAN, pp. 218-222.

{156} GOFF, N. R. Human average evoked potentials: procedures for stimulating and recording. In R. F. Thompson and M. M. Patterson (Eds.), Bioelectric Recording Techniques (Part B), 1974, pp. 101-156, Academic Press, New York, Chapter 4.

{157} GESELOWITZ, D. B. and ISHIWATARI, H. A theoretical study of the effect of the intracavity blood mass on the dipolarity of an

equivalent heart generator. Proc. Long Island Jewish Hospital Symposium Vectorcardiography, North Holland Pub. Company, 1966, pp. 393-402.

{158} KLEE, M. and RALL, W. Computed potentials of cortically arranged populations of neurons. J. Neurophysiol., 1977, 40(3):647-666.

{159} BEVINGTON, P. R. Data Reduction and Error Analysis for the Physical Sciences, McGraw-Hill, New York, 1969, 336p.

{160} NELDER, J. A. and MEAD, R. A simplex method for function minimization. Computer J., 1969, 7:308-313.

{161} O'NEILL, R. Function minimization using a simplex procedure. Applied Statistics, 1971, 20(3):338-345.

{162} MARQUARDT, D. W. An algorithm for least-squares estimation of nonlinear parameters. J. Soc. Industr. Appl. Math, 1963, 11(2): 431-441.

{163} MARQUARDT, D. W. Confidence region calculations. IBM Share Program Catalog No. 3094, 1964, Appendix Exhibit B.

{164} SCHEFFÉ, H. The Analysis of Variance, Wiley and Sons, New York, 1959, 477p.

{165} BIERSDORF, W. R. The Davidson and Hemmendinger color rule test as a color vision screening test. Arch. Ophthalmol., 1977, 95:134-138.